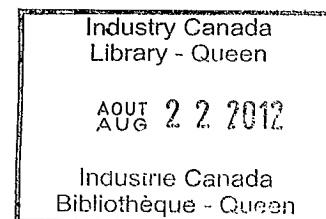# Design of a mounting plate for a low reflection level over a wide range of incidence angles from a profiled lossy dielectric slab

Jasmin E. Roy, Ph.D.

22 May 2008

Canada

CRC

Design of a mounting plate
for a low reflection level
over a wide range of incidence angles
from a profiled lossy dielectric slab

Jasmin E. Roy, Ph.D.

Contents

3

Abstract

This report presents the design and the analysis of a mounting plate for holding an omnidirectional transmitter during radiation pattern measurement. The design achieves a smooth variation of the complex permittivity profile through the plate by means of boring circular cones from the front and the back surfaces of a lossy dielectric slab in a way that achieves near-optimum packing of the cones on both surfaces. The resulting geometry is reminiscent of a honeycomb structure, and is modeled as a uniaxial medium with the optic axis parallel to the normal of the plate. A modified scattering matrix propagator technique was developed to predict the reflection and the transmission coefficients for both the TE and TM polarizations in a way that takes into account explicitly both the effect of the non-uniform wave propagation incurred by the presence of material losses, and the effect of the longitudinal anisotropy incurred by the conical inclusions and extrusions of the plate. A choice of parameters that yields a predicted reflection level of less than about -22 dB over an angular range of 0° to about 50° is presented. Also included is an analysis predicting the error in measuring the radiation pattern in the presence of a reflection from the mounting plate.

Chapter 1

Introduction

Figure 1.1 presents schematically the setup for measuring the far-field radiation pattern of an omnidirectional source along conical cuts of constant θ angular values. The radiating device under test is spun about a horizontal z axis by the roll positioner for scanning the ϕ angular range, and about a vertical axis by the azimuth positioner for scanning the θ angular range. This process, however, requires that the mounting plate for the device under test present a small reflection coefficient in order to avoid corrupting the measurement.

Conceptually, one easy way to achieve a low reflection level from a plate for various incidence angles and for both TE and TM polarizations might be to use the Fabry-Perrot resonance within a single dielectric slab. The resonance frequencies are given by $(2k_z H - \angle S_{11}^{II} - \angle S_{22}^{I}) = 2n\pi$ where n is an integer, H is the thickness of the uniform homogeneous isotropic dielectric slab of relative permittivity ε_r, S_{22}^{I} is the output reflection coefficient of the air-dielectric interface at the input face of the slab, and $\angle S_{11}^{II}$ is the input reflection coefficient of the dielectric-air interface at the output face of the slab. Owing to the fact that $\angle S_{11}^{II} = \angle S_{22}^{I} = 0$ for both TE and TM polarizations, for any θ^i and for any ε_r, the expression[1] for H becomes $H = |n|(\lambda_o/2)/\sqrt{\varepsilon_r - \sin^2 \theta^i}$ for both TE and TM polarizations. Thus, when $\varepsilon_r >>> \sin^2 \theta^i$, H becomes nearly independent of θ^i. The integer n is chosen to obtain a value of H that corresponds to a plate that is thick enough to

---

[1]Rigorously, this is true only if the dielectric plate is of infinite size in the transverse dimensions. Otherwise, diffraction at the edge of a finite-size plate would cause the diffracted waves to modify the overall scattered field of the plate. However, if the finite-size plate is large enough, the overall scattered field would be dominated by the bulk response rather than the edge response. Since the resonance frequencies are not dependent on specific values of $|S_{11}^{II}|$ and $|S_{22}^{I}|$ (although the nulls at resonance frequencies are usually deeper when $|S_{11}^{II}| = |S_{22}^{I}|$), the loss due to diffraction at the edge of the plate might be taken into account as part of S_{11}^{II} and S_{22}^{I}.

ensure the required stiffness. This design approach, however, requires very tight tolerances on the flatness and the parallelism of the interfaces, and on the thickness of the plate specially when ε_r is large. Furthermore, the frequency response has an extremely narrow band because the resonance is very sharp.

Another way to achieve a low reflection level from a plate would be to realize the Uniaxial Perfectly Matched Layer (UPML) that is used in the Finite Difference Time Domain (FDTD) technique to truncate the computational space without incurring reflections from that truncation. According to this concept (see Reference [1]), a Perfect Electrical Conductor (PEC) plate could have a very low level of reflection for any incidence angle and polarization if the PEC surface were covered with the right combination of uniaxial lossy electric and uniaxial lossy magnetic material such that the wave impedance would be that of free space at the input face of the UPML. A wave incident at the input face of the UPML would then be transmitted into the UPML without any reflection, and be gradually absorbed as it propagated within the UPML because of the lossy electric and lossy magnetic media of the UPML. This approach, however, leads to designs that are not physically realizable because the values of the electric and the magnetic conductivities in the direction normal to the absorbing plane are negative, which situation implies the existence of dependent sources within the UPML (see Reference [2]), and because some relative values of permittivity and/or permeability are smaller than 1.

Yet another way to achieve a low reflection level from a plate is to make the plate from a dielectric structure that presents to an incident uniform plane wave propagating in free space, a very gradual variation of the effective complex permittivity as the wave propagates through the mounting plate (see References [3, 54, 55, 56]). This is the approach that is presented in this report. The design for a large mounting plate (see Figures 1.2 and 1.3) was made of a lossy homogeneous dielectric slab that has been machined in the shape of a honeycomb-like plate in order to achieve a specific permittivity profile that provides a low level of reflection over a broad range of incidence angles while also providing mechanical rigidity for mounting a large cylindrical styrofoam jig (see Figure 1.4). The tower to which the mounting plate is attached has been constructed without the use of any metallic part in order to minimize the presence of reflections from the tower itself.

The precise determination of the reflection coefficient of the plate requires that the losses of the dielectric be taken into account. The presence of losses inside a propagation medium introduces an increased complexity in the propagation mechanism as a result of the plane waves being no longer necessarily uniform[2].

---

[2]There are also other complications introduced by the presence of losses. They are:

Chapter 2 presents the Adler-Chu-Fano formulation [4] for treating non-uniform plane waves by taking the propagation vector to be complex-valued as $\vec{\gamma} = (\vec{\alpha} + j\vec{\beta})$, while keeping all propagation angles to be real-valued. Within the Adler-Chu-Fano formulation, this report not only presents a development that is different from that given by Radcliff [6] and Holmes [8] but it also points out a fundamental error that Radcliff made in attempting to generalize Holme's expression from the case of the incident plane wave being uniform to the case of the incident plane wave being non-uniform.

Once the expressions for the propagation constants and the transmission angles are known, the Generalized Scattering Matrix (GSM) for an interface between two lossy media can be written in terms of the generalized Fresnel equations, as presented in Chapter 3. These equations are obtained by generalizing, in the ordinary Fresnel equations that apply at the interface between two lossless media, the expressions of the wave impedances for the TE and the TM polarizations so as to account for the fact that the propagation constant and the permittivity of lossy media are complex-valued. The composite GSM for a cascade of interfaces separated by homogeneous lossy regions can then be computed most expediently by using not the transmission

1. the fields $\vec{E}$ or $\vec{H}$ might no longer be perpendicular to the propagation vector $\vec{\beta}$ of the phase wavefront according to References [75, p. 706] and [84, p. 502] but Reference [4, p. 422] shows that $\vec{E}$ for the $\text{TM}^{(\hat{\alpha} \times \hat{\beta})}$ mode, and $\vec{H}$ for the $\text{TE}^{(\hat{\alpha} \times \hat{\beta})}$ mode, are still perpendicular to $\vec{\beta}$;

2. the Poynting vector no longer lies in the direction of $\vec{\beta}$ (see References [4, pp. 424-425] and [7, pp. 135-142]);

3. the charge density of free charges ρ_{free} in the medium is no longer zero such that the decay of the charge density now presents a non-zero value of relaxation time (see Reference [9, p. 424]);

4. $\vec{E}$ or $\vec{H}$ becomes elliptically polarized (see Reference [75, p. 706]) and the angle between them varies in time over a time period even for a uniform plane wave (see References [4, pp. 411-427] and [77] and [7, pp. 140-141]).

However, the process of taking into account the conductivity σ by means of taking the permittivity ε to become complex-valued effectively replaces the term $\vec{J}_{\text{free}} = \sigma\vec{E}$ by 0 in the curl equation for $\vec{H}$, and replaces, via the continuity equation, the charge density ρ_{free} by 0 in the divergence equation for $\vec{D}$. This leads to $(\vec{\gamma} \cdot \vec{D}) = 0 = (\vec{\gamma} \cdot \vec{H})$ **without** implying that $\vec{\gamma}$ is orthogonal to $\vec{D}$ or $\vec{H}$ because $\vec{\gamma}$, $\vec{D}$ and $\vec{H}$ have now become complex-valued vectors whose real and imaginary vectors point, in general, in different directions (see Reference [4, p. 403]).

In isotropic media, the presence of losses does not prohibit the decomposition of a wave into TE^u and TM^u waves where $\hat{u} = (\hat{\alpha} \times \hat{\beta})$ is the direction for which the fields have no spatial variation. Hence, in general, $H_u = 0$ for TM^u waves, and $E_u = 0$ for TE^u waves, for a total of five non-zero field components for each mode. Under appropriate rotation of the system of coordinates, these five non-zero field components can often be reduced to only three non-zero field components, with $\hat{E} = \hat{u}$ for TM^u waves, and $\hat{H} = \hat{u}$ for TE^u waves, such that the two modes are decoupled (see References [4, pp. 422-423], [85, p. 31, problem 1.3], [76, p. 306] and [77, p. 584]). In such a case, these modes will be referred to as pure modes. Otherwise, they will be referred to as hybrid modes.

matrices but the scattering matrix propagator technique presented in References [10, 11, 12] but corrected as per [13, p. 46]. The reflection coefficient for the mounting plate is obtained as the S_{11} element of the composite GSM for the cascade. The use of the GSM stands in contrast with the invariant imbedding formulation [5, 19, 20, 21] which is a recursive scheme for treating a planar stratified structure[3].

In Chapter 3, the continuous variation of the complex permittivity through the mounting plate is approximated by means of modelling the plate as a cascade of thin homogeneous layers of constant complex permittivity. In practice, this variation of the permittivity is realized by varying the mixture of free space and dielectric material in the longitudinal direction, i.e. the direction normal to the plate. This process results in the complex effective permittivity having a different value in the transverse[4] directions than in the longitudinal direction, and thus the plate becomes a uniaxial medium with the optic axis lying in the longitudinal direction. For such a case, the two eigenwaves (the ordinary and the extraordinary waves) propagate separately through the entire plate without inter-coupling, and thus, the GSM of the plate can be obtained for each eigenwave separately.

Chapter 4 presents the characterization of the complex permittivity profile of the mounting plate as a uniaxial medium. Many references exist on the topic of the propagation in a uniaxial or biaxial medium, and the wave phenomenon at the interface between isotropic and uniaxial or biaxial media. A particularly general treatment that takes into account material losses and optical activity (i.e. the slab can be non-reciprocal), and is based on the tangential electric and magnetic field components rather than the eigenwaves is given in References [22, 23, 24, 25, 26, 27] but the approach results in the existence of some coupling between the TE and TM waves at each interface whereas no such coupling arises between the two eigenwaves. Other treatments, based on the eigenwaves as in Reference [28], or on a TE^y and TM^y decomposition (where $\hat{y}$ was the normal to the incidence plane) as in References [61, 30, 29], dealt with the case of the optic axis being parallel to the interfaces in order to address the applications of polarizers. References [29] and [30] also took into account material losses. Wait [31] and Gedney [1, pp. 285-288] treated in the same way the case of lossy uniaxial

---

[3]In this author's opinion, the expressions given in Reference [21, p. 234-236] are at odds with those given in Reference [20, p. 395], which expressions contain also an error, albeit a small one ($B_{n+1} = 0$ should read $G_{n+1} = 0$).

[4]There are two different references to which the words "transverse" and "longitudinal" can refer in this report:

1. interface between two different media;

2. optic axis of a uniaxial medium.

Unless mentioned otherwise, the terminology of transverse and longitudinal that is used in this report, is synonymous with tangential and normal to the interface, respectively.

stratified media with optic axis perpendicular to the interfaces. Their treatment is simpler than the one presented here but it does not shed much light onto the physics of the phenomenon. Wait's expressions as given in Reference [31, p. 98] will be used for comparison. Finally, Chen [7] treated by a coordinate-free approach, the general case of the planar interface between a lossless isotropic medium and a lossless uniaxial medium whose optic axis was arbitrarily oriented.

Chapter 5 presents the design of the mounting plate in terms of the choice of the design parameters, the resulting performance and a sensitivity analysis showing the performance variation due to the variation of the design parameters. Chapter 6 presents a brief conclusion and Chapter 7 presents the list of references. Appendix A presents the equivalence between the model based on the instantaneous multiple reflections and the model based on the steady state voltage travelling waves, for a system of two cascaded scattering interfaces separated by a uniform homogeneous layer. This development proves the equivalence between Adams' invariant imbedding technique presented in Reference [19, pp. 9-23], and Wait's recursive technique presented in Reference [5, pp. 135,151]. Appendix B presents the mathematical development for the equivalence between a non-uniform plane wave with real-valued propagation angles and a uniform plane wave with complex-valued propagation angles. This development can be used to compare the results given by the method developed herein and the results given by Wait's method in treating the interface between two lossy uniaxial media. Appendix C presents a comparison between Holme's method and the method developed herein for treating the interface between two lossy media. Appendix D presents the development of the expression for the effective relative permittivity as seen by the extraordinary wave propagating in a uniaxial lossy half-space, as well as some generalization to a biaxial lossy half-space with arbitrarily oriented dielectric axes. Appendix E presents the development for the dispersion equation in a lossy biaxial medium. Appendix F presents the Matlab program to obtain the GSM for a free-standing isotropic slab. Appendix G presents a scheme for estimating the error in measuring the radiation pattern of the transmitter under test due to the reflection from the mounting plate. This scheme can be used to compute an error bar for every angle at which measurement was carried out.
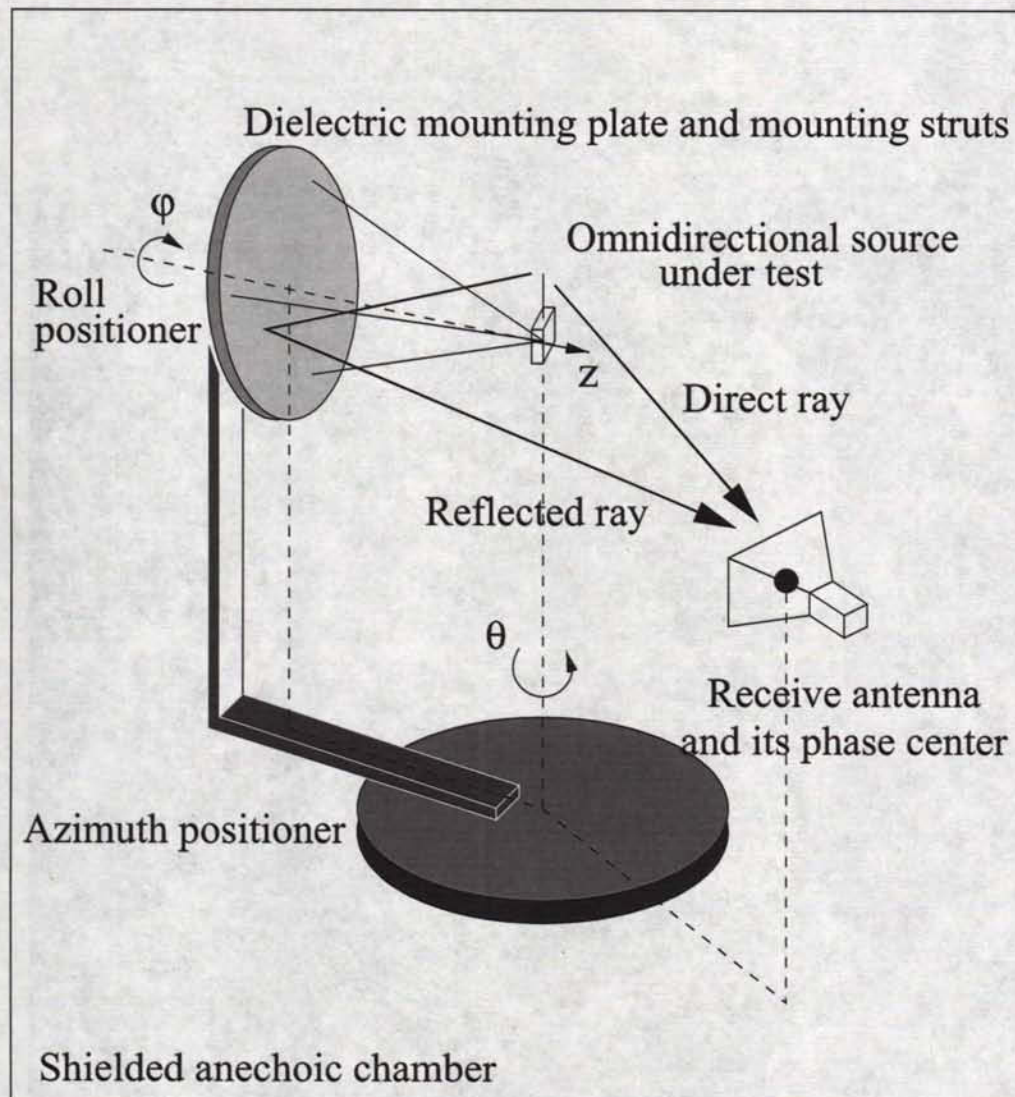
Figure 1.1: Geometry of a test setup for measuring the far field along conical cuts of constant θ values. For convenience of representation, the transmitter is shown here as being mounted with three struts rather than a dielectric styrofoam jig.
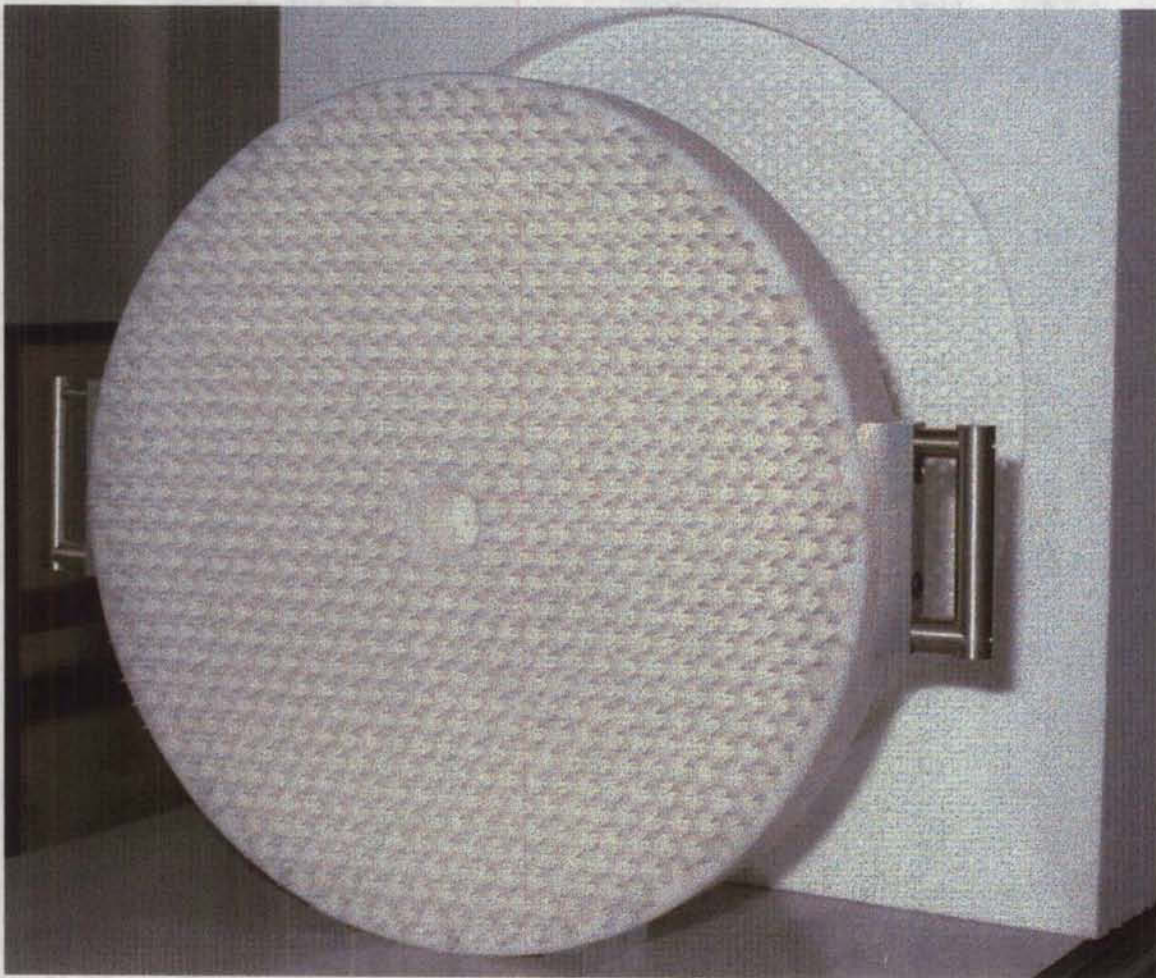
Figure 1.2: Front view of the mounting plate. The two handles are not used during measurement.
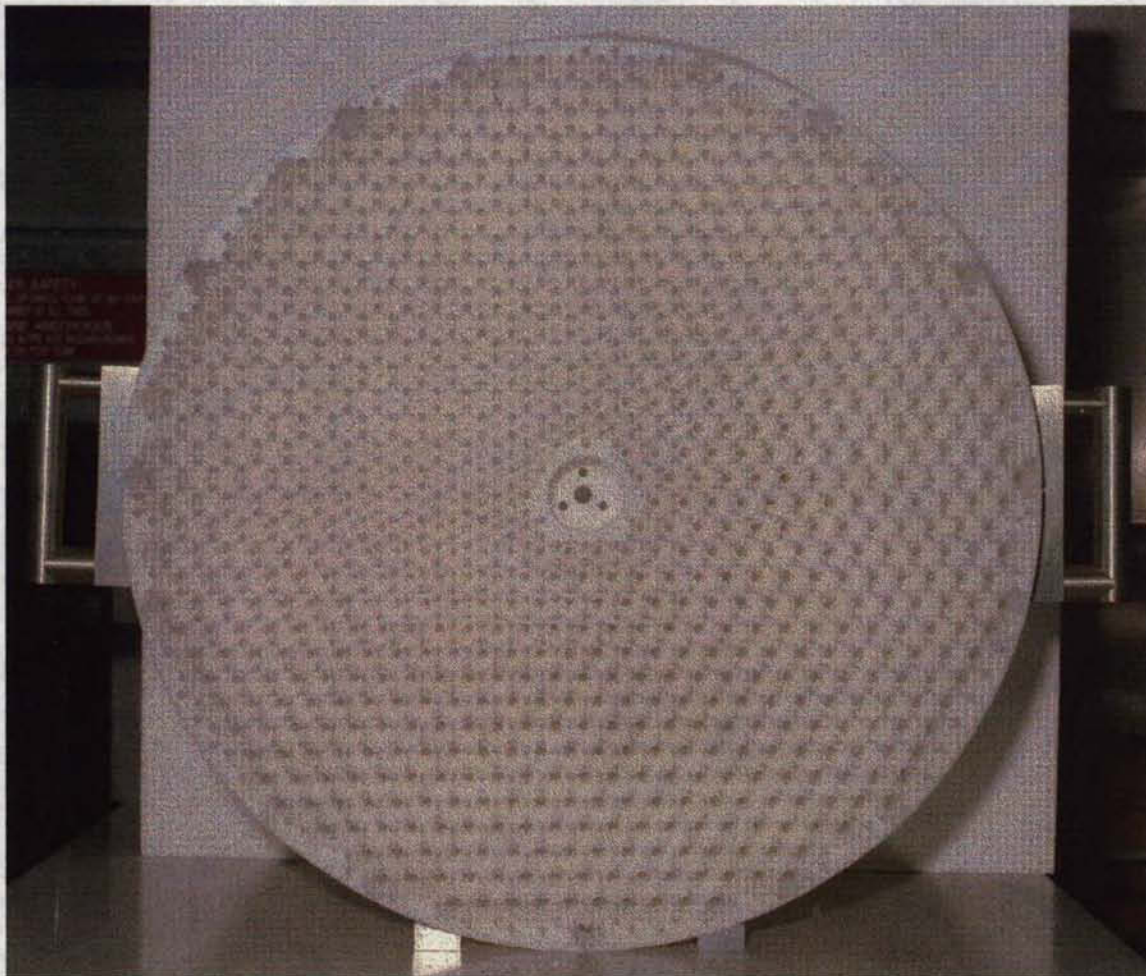
Figure 1.3: Rear view of the mounting plate.
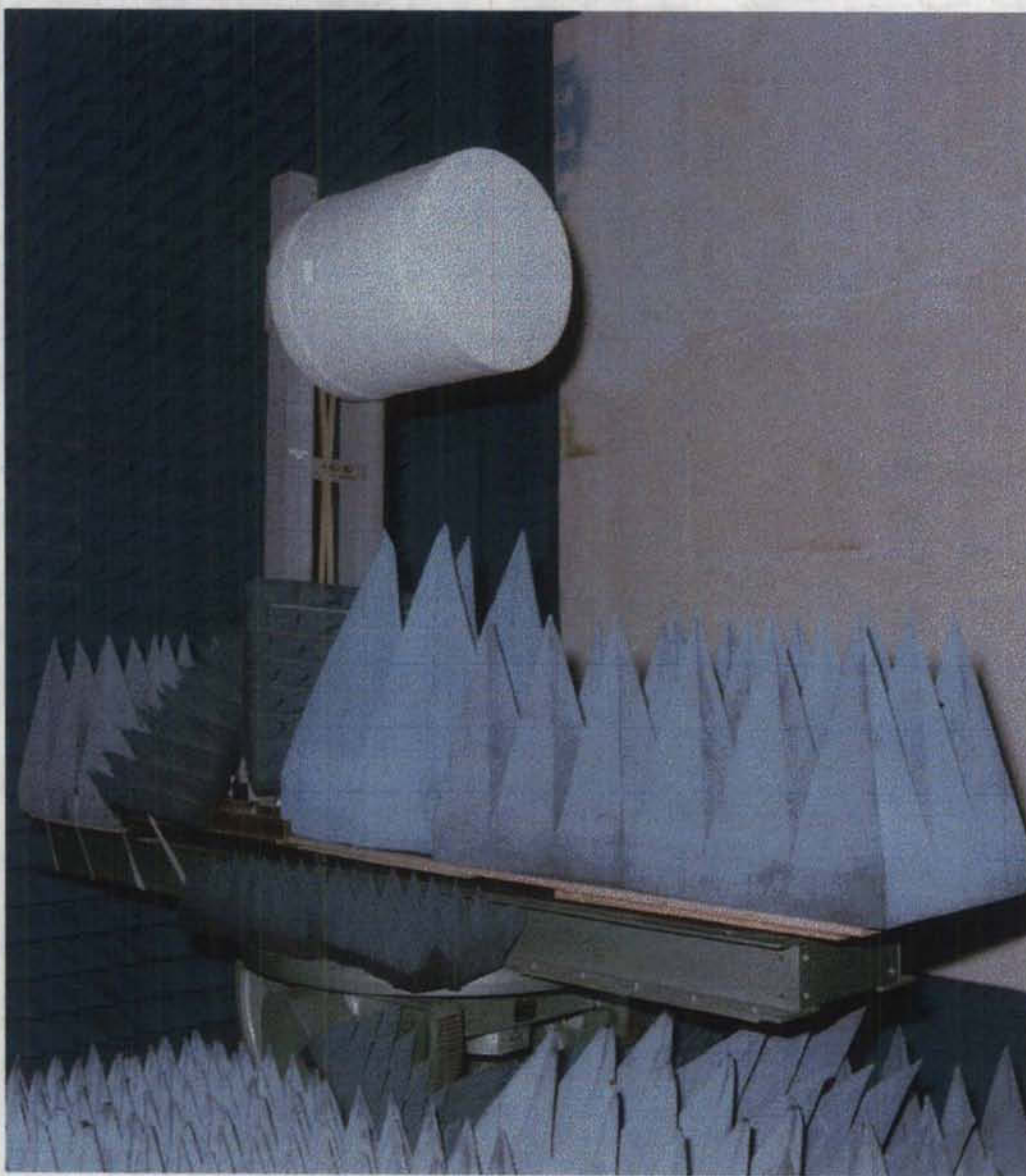
Figure 1.4: View of the fiberglass tower, the mounting plate and the styro-foam jig that encases the transmitter under test.

Chapter 2

Wave phenomena at the planar interface of two isotropic homogeneous and possibly lossy media

This section presents a correction and a generalization of the solution presented in References [6, 21] for the effective propagation constants of non-uniform plane waves at the planar interface of two isotropic homogeneous possibly lossy media of infinite transverse dimensions.

2.1 Introduction

With the classical formulation, media losses are taken into account by analytical continuation of the lossless expressions by allowing the propagation vector to become complex-valued. The application of Snell's law of refraction at a planar interface then produces a complex value for the transmission angle. Since the plane waves propagate in straight lines between parallel planar interfaces, the incidence angle at the next interface in a multilayer structure becomes also complex-valued and hence, in general, Snell's law of refraction becomes written in terms of complex values for both the incidence and the transmission angles. More physically meaningful, however, is the Adler-Chu-Fano formulation where all angles remain real-valued but the plane wave is allowed to become non-uniform, i.e. the amplitude wavefront is given its own propagation constant $\vec{\alpha}$ separate from the phase wavefront propagation constant $\vec{\beta}$. Incidentally, an equivalence between these two formulations is presented herein as part of the validation process for the new results also

presented herein.

The problem of a planar interface between two lossy half-spaces has been treated with the Adler-Chu-Fano formulation by Holmes [8] for the case where the incident plane wave was uniform, and by Radcliff [6] for the more general case where the incident plane wave was non-uniform but the vectors $\vec{\alpha_1}$, $\vec{\beta_1}$ and the unit vector normal to the interface $\hat{z}$ were coplanar. However, Radcliff in generalizing Holmes' expressions used inappropriately the intrinsic propagation constants α_{o1} and β_{o1} instead of the effective propagation constants α_1 and β_1 for the incidence medium when carrying out the phase matching at the interface.

This chapter consists of four sections. The first section presents the Adler-Chu-Fano formulation and the symbolism used herein. The second section presents the correction to Radcliff's treatment. The third section presents the treatment of the general case where the incidence propagation vectors are not necessarily coplanar. The fourth section presents the results for both the coplanar case and the general case, and they include the case of negative values of ρ which case was not treated by Radcliff nor Holmes. The results for the coplanar case are obtained by setting $\psi = 0$ in the expressions for the general case. These coplanar results are then compared with the results for the classical formulation by invoking an equivalence between the two formulations. Results are then presented for cases with $\psi \neq 0$. Since the general case cannot be obtained as the mere extension of Snell's law of refraction from real to complex propagation angles, the results for the general case are presented without any comparison.

2.2 Adler-Chu-Fano formulation

Herein, the $e^{+j\omega t}$ time harmonic dependency is implicitly assumed such that the magnitude of a non-uniform plane wave progagating with the complex propagation vector $+\hat{\gamma}$ is written as $e^{-\vec{\gamma}\cdot\vec{r}}$. For an isotropic homogeneous lossy medium, the following equations apply (see Reference [4, equations (8.5-8.6), p. 403]):

$$\vec{\gamma} = \vec{\alpha} + j\vec{\beta} \tag{2.1}$$

$$\vec{\gamma} \cdot \vec{\gamma} = \gamma_o^2 \tag{2.2}$$

$$\gamma_o = \alpha_o + j\beta_o = j\omega\sqrt{\mu_o \varepsilon_r \varepsilon_o} = jk_o\sqrt{\varepsilon_r} \tag{2.3}$$

where the parameters α_o, β_o and γ_o are, respectively, the intrinsic propagation constants for the attenuation and the phase wavefronts, and the intrinsic complex propagation constant for the wave propagating in the lossy medium. In contrast, α and β are the effective propagation constants corresponding

to α_o and β_o, respectively. We note, however, that μ_o, ε_o and k_o refer to intrinsic variables of free space, not those of the lossy medium. The relative permittivity is generally a complex number given by:

$$\varepsilon_r = \varepsilon_r'(1 - j\tan(\delta)) = \varepsilon_r' - j\left(\frac{\sigma}{\omega\varepsilon_o}\right) \tag{2.4}$$

where $\varepsilon_r' \geq 1$, $\tan(\delta) = \sigma/(\omega\varepsilon_r'\varepsilon_o)$, $\sigma \geq 0$, $\omega = 2\pi f$, $|\vec{\alpha}| = \alpha$, $|\vec{\beta}| = \beta$ and ε_o are all real-valued. The intrinsic propagation constants are obtained from Equations (2.3) and (2.4) as [4, Equation (8.9), p. 404]:

$$\alpha_o = \frac{\omega\sqrt{\mu_o\varepsilon_o\varepsilon_r'}}{\sqrt{2}}\sqrt{\sqrt{1 + \left(\frac{\sigma}{\omega\varepsilon_o\varepsilon_r'}\right)^2} - 1} \tag{2.5}$$

$$\beta_o = \frac{\omega\sqrt{\mu_o\varepsilon_o\varepsilon_r'}}{\sqrt{2}}\sqrt{\sqrt{1 + \left(\frac{\sigma}{\omega\varepsilon_o\varepsilon_r'}\right)^2} + 1} \tag{2.6}$$

We note that α is not necessarily zero in a lossless medium ($\alpha_o = 0$), and that β is not necessarily equal to β_o unless the plane wave is uniform. In fact, the case for $\alpha = \alpha_o$ and $\beta = \beta_o$ occurs only for a uniform plane wave, i.e. $\rho = 0$ (see Reference [4, p. 410]), in either lossless or lossy media. Thus, $\alpha \neq 0$ does not imply that the plane wave is non-uniform nor that the medium is lossy. However, $\alpha = 0$ does imply that the plane wave is uniform and that the medium is lossless. Moreover, in general, it is not possible to relate α and β to some effective permittivity $\varepsilon_r^{\text{eff}}$ the same way that we can relate α_o and β_o to some intrinsic permittivity ε_r. The reason is that although we can write $\gamma_o = \alpha_o + j\beta_o = jk_o\sqrt{\varepsilon_r}$ as in Equation (2.3), we cannot write $\gamma = \alpha + j\beta = jk_o\sqrt{\varepsilon_r^{\text{eff}}}$ unless $\vec{\alpha}$ and $\vec{\beta}$ point in the same direction, i.e. unless the plane wave is uniform.

Performing[1] $\vec{\gamma} \cdot \vec{\gamma}$ and using Equations (2.1-2.3), then separating real and imaginary parts produces the following two expressions:

$$\alpha^2 - \beta^2 = \alpha_o^2 - \beta_o^2 \tag{2.7}$$

---

[1]For a general complex-valued vector $\vec{\gamma} = (\vec{\alpha} + j\vec{\beta})$, two different definitions exist for γ^2. In References [80, 81], γ^2 is defined as $\gamma^2 = \vec{\gamma} \cdot \vec{\gamma}^* = \alpha^2 + \beta^2$ and is a real-valued scalar quantity that represents the square of the magnitude of the vector. However, in Reference [4], γ^2 is defined as $\gamma^2 = \vec{\gamma} \cdot \vec{\gamma} = (\alpha^2 - \beta^2) + j(2\vec{\alpha} \cdot \vec{\beta})$ and is a complex-valued scalar quantity. Since γ_o in Equation (2.3) is a complex-valued scalar quantity, γ_o^2 is clearly a complex-valued scalar quantity and we need to use the latter definition for γ^2 as per Equation (2.2).

$$\alpha\beta\cos(\rho) = \alpha_o\beta_o \qquad (2.8)$$

where ρ is the acute (i.e. interior) angle between $\vec{\alpha}$ and $\vec{\beta}$. All constants α_o, β_o, α and β are taken to be positive real values. From Equations (2.7) and (2.8), one obtains the effective propagation constants as follows:

$$\alpha = \frac{\sqrt{\beta_o^2 - \alpha_o^2}}{\sqrt{2}} \sqrt{\sqrt{1 + \left(\frac{2\alpha_o\beta_o}{(\beta_o^2 - \alpha_o^2)\cos(\rho)}\right)^2} - 1} \qquad (2.9)$$

$$\beta = \frac{\sqrt{\beta_o^2 - \alpha_o^2}}{\sqrt{2}} \sqrt{\sqrt{1 + \left(\frac{2\alpha_o\beta_o}{(\beta_o^2 - \alpha_o^2)\cos(\rho)}\right)^2} + 1} \qquad (2.10)$$

Equations (2.9) and (2.10) are not valid for a non-uniform plane wave in a lossless medium because the indetermination $\alpha_o/\cos(\rho) = 0/0$ arises since both $\alpha_o = 0$ and $\cos(\rho) = 0$ for a non-uniform plane wave in a lossless medium (see Reference [4, p. 426]). The equations are valid for any other case. From Equations (2.5) and (2.6), we obtain:

$$2\alpha_o\beta_o = \omega\mu_o\sigma \qquad (2.11)$$

$$(\beta_o^2 - \alpha_o^2) = \omega^2\mu_o\varepsilon_o\varepsilon_r' \qquad (2.12)$$

and Equations (2.9) and (2.10) become:

$$\alpha = \frac{\omega\sqrt{\mu_o\varepsilon_o\varepsilon_r'}}{\sqrt{2}} \sqrt{\sqrt{1 + \left(\frac{\sigma}{\omega\varepsilon_o\varepsilon_r'\cos(\rho)}\right)^2} - 1} \qquad (2.13)$$

$$\beta = \frac{\omega\sqrt{\mu_o\varepsilon_o\varepsilon_r'}}{\sqrt{2}} \sqrt{\sqrt{1 + \left(\frac{\sigma}{\omega\varepsilon_o\varepsilon_r'\cos(\rho)}\right)^2} + 1} \qquad (2.14)$$

Equations (2.13) and (2.14) are equivalent to those given in Equation (8.14) of Reference [4, p. 409]. From Equations (2.13) and (2.5), and from Equations (2.14) and (2.6), we see that $\alpha = \alpha_o$ and $\beta = \beta_o$ when $\rho = 0°$ as mentioned above. The case $\rho = 0°$ is the case of a uniform plane wave in a lossy medium (see Reference [4, p. 410]).

13

2.3 Case when $\vec{\alpha_1}$, $\vec{\beta_1}$ and $\hat{z}$ are coplanar: Correction to Radcliff's formulation

Figure 2.1 shows the wave phenomena in the incidence plane at the interface of two lossy media. It is assumed here that the interface is planar and of infinite transverse dimensions, and that the propagation vectors $\vec{\alpha}$, $\vec{\beta}$ and the normal of the interface $\hat{z}$ are coplanar. The solution consisting of a single reflected wave and a single transmitted wave is complete and valid everywhere in both half-spaces, i.e. even in the near-field region of the interface. The interface is illuminated by a non-uniform plane wave of arbitrary incidence angle and of polarization either parallel or perpendicular to the indicence plane. The treatment of these two polarizations is sufficent[2] to obtain the treatment of an arbitrary polarization, just as with uniform plane waves (see Reference [4, p. 423]). However, the determination of $\vec{\alpha}$ and $\vec{\beta}$ does not require the knowledge of the polarization of the waves (even in anisotropic media) because it proceeds solely from the phase matching requirement at the interface (see Reference [9, pp. 506-508]). From References [4, 6, 8], Snell's law at the interface of two isotropic homogeneous lossy media, identified herein as media 1 and 2 in Figure 2.1, is given as:

$$\alpha_1 \sin(\xi_1 + \rho_1) = \alpha_2 \sin(\xi_2 + \rho_2) \tag{2.15}$$

$$\beta_1 \sin(\xi_1) = \beta_2 \sin(\xi_2) \tag{2.16}$$

where all parameters take real values. Holmes' expressions for computing β_2 and α_2 are [6, Equations (18-19)]:

$$\beta_2 = \sqrt{\frac{|\gamma_{1t}|^2 - \mathrm{Re}\left(\gamma_{o2}^2\right) + |\gamma_{1t}^2 - \gamma_{o2}^2|}{2}} \tag{2.17}$$

$$\alpha_2 = \sqrt{\frac{|\gamma_{1t}|^2 + \mathrm{Re}\left(\gamma_{o2}^2\right) + |\gamma_{1t}^2 - \gamma_{o2}^2|}{2}} \tag{2.18}$$

---

[2]A wave of arbitrary polarization propagating with propagation constants $\vec{\alpha}$ and $\vec{\beta}$ can be decomposed into a pure TE^u wave and a pure TM^u wave where $\hat{u} = (\hat{\alpha} \times \hat{\beta})$ is the direction for which the fields have no spatial variation, hence $\hat{E} = \hat{u}$ for pure TM^u waves, and $\hat{H} = \hat{u}$ for pure TE^u waves (see References [4, pp. 422-423], [85, p. 31, problem 1.3]). It turns out, however, that when $\vec{\alpha}$, $\vec{\beta}$ and $\hat{z}$ are coplanar, the two incidence planes of the general case reduce to a single incidence plane, and the normal unit vector of this single incidence plane is also parallel to $\hat{u}$ for both the transmitted and the reflected waves. Consequently, a decomposition into a TE^u and a TM^u waves corresponds to a decomposition into the usual TE^v and TM^v waves where $\hat{v}$ is the normal of the incidence plane. For instance, when the incidence plane is the xz plane, then $\hat{v} = \hat{y}$.

Radcliff has used inappropriately α_{o1} instead of α_1 in Equation (2.15) (see [6, Equation (9)]), and β_{o1} instead of β_1 in Equation (2.16) (see [6, Equation (10)]). This led to incorrect values for the propagation constants α_2 and β_2 in his Figure 3. When $\gamma_{1t} = \alpha_1 \sin(\xi_1 + \rho_1) + j\beta_1 \sin(\xi_1)$ is used instead of $\gamma_{1t} = \alpha_{o1} \sin(\xi_1 + \rho_1) + j\beta_{o1} \sin(\xi_1)$ in Holmes' expressions, the correct values are obtained for α_2 and β_2.

Solving for ξ_2 from Equation (2.16) and the knowledge of β_2 leads to two possible solutions:

$$\xi_2 = \begin{cases} \arcsin\left(\frac{W}{\beta_2}\right) \\ 180° - \arcsin\left(\frac{W}{\beta_2}\right) \end{cases} \tag{2.19}$$

where $W = \beta_1 \sin(\xi_1)$. Solving for ρ_2 from Equation (2.15), from the knowledge of α_2 and from the knowledge of the two possible solutions for ξ_2 leads to four possible solutions:

$$\rho_2 = \begin{cases} \arcsin\left(\frac{V}{\alpha_2}\right) - \arcsin\left(\frac{W}{\beta_2}\right) \\ 180° - \arcsin\left(\frac{V}{\alpha_2}\right) - \arcsin\left(\frac{W}{\beta_2}\right) \\ \arcsin\left(\frac{V}{\alpha_2}\right) + \arcsin\left(\frac{W}{\beta_2}\right) - 180° \\ -\arcsin\left(\frac{V}{\alpha_2}\right) + \arcsin\left(\frac{W}{\beta_2}\right) \end{cases} \tag{2.20}$$

where $V = \alpha_1 \sin(\xi_1 + \rho_1)$. The difficulty here lies in selecting the proper solution among these various expressions because the solution does not remain with the same expression for all values of ξ_1 and ρ_1 (see Appendix C). The correct results will be presented in section 2.5.1.

2.4 Case when $\vec{\alpha_1}$, $\vec{\beta_1}$ and $\hat{z}$ are not coplanar

When the vectors $\vec{\alpha_1}$, $\vec{\beta_1}$ and the unit vector normal to the interface $\hat{z}$ are not coplanar, the phase matching at the interface proceeds as follows:

$$(\vec{\gamma}_{1t} = \vec{\gamma}_{2t}) \Longrightarrow \hat{z} \times \left((\vec{\alpha_1} + j\vec{\beta_1}) \times \hat{z}\right) = \hat{z} \times \left((\vec{\alpha_2} + j\vec{\beta_2}) \times \hat{z}\right) \tag{2.21}$$

where the subscript t refers to the component tangential to the interface. Separating real and imaginary parts leads to these two equations:

$$\alpha_1 \sin(\zeta_1) = \alpha_2 \sin(\zeta_2) \tag{2.22}$$

$$\beta_1 \sin(\xi_1) = \beta_2 \sin(\xi_2) \tag{2.23}$$

where the angles ζ_1, ζ_2, ξ_1 and ξ_2 are shown in Figure 2.2. To simplify the figure, the azimuth angle for the vector $\vec{\beta_1}$ was taken as zero. Thus, we have two separate incidence planes[3], one containing the vectors $\hat{z}$, $\vec{\alpha_1}$ and $\vec{\alpha_2}$, and another incidence plane containing the vectors $\hat{z}$, $\vec{\beta_1}$ and $\vec{\beta_2}$, with Snell's law of refraction being valid in each incidence plane as shown by Equations (2.22) and (2.23).

From spherical trigonometry, we have:

$$\cos(\rho_1) = \sin(\xi_1) \sin(\zeta_1) \cos(\psi) + \cos(\xi_1) \cos(\zeta_1) \tag{2.24}$$

$$\cos(\rho_2) = \sin(\xi_2) \sin(\zeta_2) \cos(\psi) + \cos(\xi_2) \cos(\zeta_2) \tag{2.25}$$

When $\psi = 0$, these two equations reduce to $\rho_1 = \zeta_1 - \xi_1$ and $\rho_2 = \zeta_2 - \xi_2$, respectively. Multiplying together Equations (2.22) and (2.23), then using Equations (2.8), (2.10), (2.23), and (2.25), and performing some algebraic manipulations valid for the case $\xi_2 \neq 0°$ and $\zeta_2 \neq \pm 90°$, one obtains the two following expressions where all quantities are known from the knowledge of α_{o1}, β_{o1}, α_{o2}, β_{o2}, ξ_1 and ζ_1:

$$\cos^2(\xi_2) = \frac{2H + R^2 - HF - 2 + \sqrt{M}}{2(2H + R^2 - 1)} \tag{2.26}$$

---

[3]Contrary to the previous case where $\vec{\alpha}$, $\vec{\beta}$ and $\hat{z}$ were coplanar, here the normal of each incidence plane is no longer parallel to $\hat{u} = (\hat{\alpha} \times \hat{\beta})$ for the transmitted or the reflected waves. Consequently, the decomposition of a wave of arbitrary polarization propagating with propagation constants $\vec{\alpha}$ and $\vec{\beta}$ into a TE^u and a TM^u waves no longer corresponds to a decomposition into the usual TE^v and TM^v waves where $\hat{v}$ would be the normal of the incidence plane. However, because the determination of the propagation constants is carried out from the phase matching requirement at the interface, the conclusion that the incident, the reflected and the transmitted (complex) propagation vectors all reside in the same (two) incidence plane(s) is independent of the polarizations of the plane waves. Furthermore, the conclusion is also independent of the nature of the two media on either side of the interface, and independent of the nature of the plane waves (i.e. uniform or non-uniform). Therefore, this conclusion is remarkably general!

$$\cos^2(\zeta_2) = \frac{2H + R^2 + HF - \sqrt{M}}{2H - R^2 + HF + R^2(R^2 + 2H - HF) + (R^2 - 1)\sqrt{M}} \quad (2.27)$$

where:

$$
\begin{aligned}
M &= (HF - R^2)^2 + 4H(H + F - (HF - R^2)) \\
A &= \alpha_{o2}\beta_{o2} \\
W &= \beta_1 \sin(\xi_1) \\
V &= \alpha_1 \sin(\zeta_1) \\
U &= \beta_{o2}^2 - \alpha_{o2}^2 \\
Q &= VW/A \\
R &= Q/(1 - Q\cos(\psi)) \\
F &= 2W^2/U \\
G &= (2A/U)^2 \\
H &= (1 + R\cos(\psi))^2 F/G \\
\alpha_1 &= \sqrt{\frac{\beta_{o1}^2 - \alpha_{o1}^2}{2}} \sqrt{\sqrt{1 + \left(\frac{2\alpha_{o1}\beta_{o1}}{(\beta_{o1}^2 - \alpha_{o1}^2)\cos(\rho_1)}\right)^2} - 1} \\
\beta_1 &= \sqrt{\frac{\beta_{o1}^2 - \alpha_{o1}^2}{2}} \sqrt{\sqrt{1 + \left(\frac{2\alpha_{o1}\beta_{o1}}{(\beta_{o1}^2 - \alpha_{o1}^2)\cos(\rho_1)}\right)^2} + 1}
\end{aligned}
\quad (2.28)
$$

Once ξ_2 and ζ_2 are known, we compute $\cos(\rho_2)$ from expression (2.25). Then, substituting the value of $\cos(\rho_2)$ into Equations (2.9) and (2.10) yields the knowledge of α_2 and β_2, respectively.

For the case $\xi_2 = 0°$, the solution can be obtained even more easily. Substituting $\xi_2 = 0°$ into Equation (2.23) yields $\xi_1 = 0°$ and hence, $\rho_1 = \zeta_1$ and $\rho_2 = \zeta_2$. Substituting these values into Equation (2.15), then using Equation (2.9) for α_2 and performing some algebraic manipulations yields the following expressions:

$$\cos(\rho_2) = \sqrt{\frac{S - \alpha_1 \sin(\rho_1)\sqrt{T}}{2\left(\alpha_1^2 \sin^2(\rho_1)U + A^2\right)}} \quad (2.29)$$

where all variables have been previously defined, except for S and T which are given as:

$$
\begin{aligned}
S &= \alpha_1^4 \sin^4(\rho_1) + \alpha_1^2 \sin^2(\rho_1)U + 2A^2 \\
T &= \alpha_1^6 \sin^6(\rho_1) + 2\alpha_1^4 \sin^4(\rho_1)U + \alpha_1^2 \sin^2(\rho_1)U^2 + 4A^2\left(1 - U + \alpha_1^2 \sin^2(\rho_1)\right)
\end{aligned}
$$
$$(2.30)$$

We note that in spite of the fact that Equation (2.9) was not valid for a non-uniform plane wave in a lossless medium due to the indetermination mentioned previously, Equation (2.29) which was obtained from using Equation (2.9), produces nevertheless the correct value $\cos(\rho_2) = 0$ when $\alpha_{o2} = 0$, except when both $\xi_1 = 0°$ and $\rho_1 = 0°$ in which case Equation (2.29) results in the indetermination $0/0$. When both $\xi_1 = 0°$ and $\rho_1 = 0°$, one obtains $\xi_2 = 0°$ and $\rho_2 = 0°$ from symmetry principle, irrespective of whether either one or both media is either lossy or lossless.

When the incidence medium is lossless, i.e. $\alpha_{o1} = 0$, the incident plane wave is usually assumed to be uniform and thus, $\alpha_1 = \alpha_{o1} = 0$ and thus, $V = \alpha_1 \sin(\zeta_1) = 0$. This situation results in $\zeta_2 = 0$, i.e. $\rho_2 = -\xi_2$, from applying Equation (2.22) with an arbitrary value of α_2. This situation corresponds to $\vec{\alpha}_2$ being normal to the interface. This result, which agrees with References [7, p. 172],[20, p. 369] and [84, p. 502], is remarkably general because it is based solely on the phase matching requirement at the interface, and thus, this result applies to any transmission medium, even the most general anisotropic medium. The case of $V = 0$ is also one of practical importance as it arises at all parallel interfaces of a planar multilayered structure standing in free space, illuminated by a uniform plane wave. At the first interface of the structure, $V = 0$ because $\alpha_1 = \alpha_{o1} = 0$. At any other interface of the structure, $V = 0$ because $\rho_2 = -\xi_2$ at the preceding interface, and the waves travel in straight lines between interfaces, thus making $\rho_1 = -\xi_1$ and $V = 0$ at the current interface.

When the transmission medium is lossless, i.e. $\alpha_{o2} = 0$, the transmitted wave is a uniform plane wave when $\alpha_2 = \alpha_{02} = 0$ which results in $\zeta_1 = 0$, i.e. $\rho_1 = -\xi_1$, from applying Equation (2.22) with an arbitrary value of α_1. This situation corresponds to $\vec{\alpha}_1$ being normal to the interface. Otherwise, the transmitted wave is a non-uniform plane wave which leads to $\cos(\rho_2) = 0$.

When the two media are lossy or, if either one or both media are lossless, when no non-uniform plane wave exists in a lossless medium, the procedure consists of solving Equations (2.26-2.27) when $\xi_1 \neq 0°$ or Equation (2.29) when $\xi_1 = 0°$. Then, substituting the value of $\cos(\rho_2)$ into Equations (2.9) and (2.10) yields the knowledge of α_2 and β_2, respectively. In practice, however, it was more convenient to use Equations (2.26-2.27) with $\alpha_{o2} = \epsilon$ or $\xi_1 = \epsilon$ whenever $\alpha_{o2} = 0$ or $\xi_1 = 0°$, respectively, where the constant ϵ represents a very small arbitrary positive value.

2.4.1 Special case of practical importance

As seen in the previous section, when the incidence medium is lossless, i.e. $\alpha_{o1} = 0$, the incident plane wave is usually assumed to be uniform and

thus, $\alpha_1 = \alpha_{o1} = 0$ and thus, $V = \alpha_1 \sin(\zeta_1) = 0$. This situation results in $\zeta_2 = 0$, i.e. $\rho_2 = -\xi_2$, from applying Equation (2.22) with an arbitrary value of α_2. This situation corresponds to $\vec{\alpha}_2$ being normal to the interface. This case arises whenever the scatterer is a multilayer slab (of infinite size in the transverse directions) whose layers are parallel to the two faces of the slab, and the slab resides in a lossless host medium (e.g. free space) and is illuminated by a uniform plane wave. Since $\rho_2 = -\xi_2$, we can easily obtain α_2 and β_2 as follows. From Snell's law for the phase wavefront as per Equation (2.23), we obtain:

$$\cos^2 \rho_2 = (1 - \sin^2 \xi_2) = 1 - \left(\frac{\beta_1}{\beta_2} \sin \xi_1\right)^2 \qquad (2.31)$$

Substituting this result into Equation (2.14), regrouping the terms in β_2 and solving the resulting quadratic polynomial in β_2^2 produces:

$$\beta_2^2 = \frac{\omega^2 \mu_o \varepsilon_o}{2} \left(\varepsilon'_{r2} + \varepsilon'_{r1} \sin^2 \xi_1 \pm \sqrt{(\varepsilon'_{r2} - \varepsilon'_{r1} \sin^2 \xi_1)^2 + \left(\frac{\sigma_2}{\omega \varepsilon_o}\right)^2}\right) \qquad (2.32)$$

where:

$$\varepsilon_{r1} = \varepsilon'_{r1} \qquad (2.33)$$

$$\varepsilon_{r2} = \varepsilon'_{r2} - j \left(\frac{\sigma_2}{\omega \varepsilon_o}\right) \qquad (2.34)$$

Since $\beta_2 = \beta_{o2} = \omega \sqrt{\mu o \varepsilon_o \varepsilon'_{r2}}$ when $\sigma_2 = 0$, the $+$ sign is the correct choice of sign in Equation (2.32). Therefore, we obtain:

$$\beta_2 = \frac{\omega \sqrt{\mu_o \varepsilon_o}}{\sqrt{2}} \sqrt{\varepsilon'_{r2} + \varepsilon'_{r1} \sin^2 \xi_1 + \sqrt{(\varepsilon'_{r2} - \varepsilon'_{r1} \sin^2 \xi_1)^2 + \left(\frac{\sigma_2}{\omega \varepsilon_o}\right)^2}} \qquad (2.35)$$

From Equations (2.14) and (2.35), we obtain:

$$\varepsilon'_{r2} \sqrt{1 + \left(\frac{\sigma_2}{\omega \varepsilon_o \varepsilon'_{r2} \cos(\rho_2)}\right)^2} = \varepsilon'_{r1} \sin^2 \xi_1 + \sqrt{(\varepsilon'_{r2} - \varepsilon'_{r1} \sin^2 \xi_1)^2 + \left(\frac{\sigma_2}{\omega \varepsilon_o}\right)^2}$$

Substituting this last result into Equation (2.13) produces:

$$\alpha_2 = \frac{\omega\sqrt{\mu_o \varepsilon_o}}{\sqrt{2}}\sqrt{-\varepsilon_{r2}' + \varepsilon_{r1}' \sin^2 \xi_1 + \sqrt{(\varepsilon_{r2}' - \varepsilon_{r1}' \sin^2 \xi_1)^2 + \left(\frac{\sigma_2}{\omega\varepsilon_o}\right)^2}} \quad (2.36)$$

On the other hand, with $\zeta_2 = 0$ we obtain:

$$\gamma_{2z} = \underbrace{\alpha_2 \cos \zeta_2}_{\alpha_{2z}} + j \underbrace{\beta_2 \cos \xi_2}_{\beta_{2z}} = \alpha_2 + j\beta_2 \cos \xi_2 \quad (2.37)$$

From Equations (2.31) and (2.35) and the fact that $\xi_2 = -\rho_2$, we obtain:

$$\begin{aligned}
(\beta_{2z})^2 &= (\beta_2 \cos \xi_2)^2 \\
&= (\beta_2 \cos \rho_2)^2 \\
&= \beta_2^2 - (\beta_1 \sin \xi_1)^2 \\
&= \frac{\omega^2 \mu_o \varepsilon_o}{2}\left(\varepsilon_{r2}' - \varepsilon_{r1}' \sin^2 \xi_1 + \sqrt{(\varepsilon_{r2}' - \varepsilon_{r1}' \sin^2 \xi_1)^2 + \left(\frac{\sigma_2}{\omega\varepsilon_o}\right)^2}\right)
\end{aligned}$$
$$(2.38)$$

From the knowledge of α_{2z} and β_{2z}, we obtain γ_{2z}. From the knowledge that the transverse variation of the scattered field is dictated by the incident field as with $\beta_{2z}^2 = \beta_2^2 - (\beta_1 \sin \xi_1)^2$ shown in Equation (2.38), we also obtain:

$$\gamma_{2z} = \sqrt{\gamma_2^2 - (\gamma_1 \sin \xi_1)^2} \quad (2.39)$$

where:

$$\gamma_1 = j\omega\sqrt{\mu_o \varepsilon_o \varepsilon_{r1}}$$

$$\gamma_2 = j\omega\sqrt{\mu_o \varepsilon_o \varepsilon_{r2}}$$

Pulling the last three equations together with Equations (2.33) and (2.34) produces:

$$\begin{aligned}
\gamma_{2z} &= \omega\sqrt{\mu_o \varepsilon_o}\sqrt{-\left(\varepsilon_{r2}' - \varepsilon_{r1}' \sin^2 \xi_1\right) + j\left(\frac{\sigma_2}{\omega\varepsilon_o}\right)} \\
&= \omega\sqrt{\mu_o \varepsilon_o}\left[\left(\varepsilon_{r2}' - \varepsilon_{r1}' \sin^2 \xi_1\right)^2 + \left(\frac{\sigma_2}{\omega\varepsilon_o}\right)^2\right]^{1/4} e^{j\frac{1}{2}\arctan \Phi}
\end{aligned}$$
$$(2.40)$$

where:

$$\arctan \Phi = \arctan \left(\frac{\frac{\sigma_2}{\omega \varepsilon_o}}{-\left(\varepsilon_{r2}' - \varepsilon_{r1}' \sin^2 \xi_1 \right)} \right) = \pi - \arctan \left(\frac{\frac{\sigma_2}{\omega \varepsilon_o}}{\varepsilon_{r2}' - \varepsilon_{r1}' \sin^2 \xi_1} \right)$$

Hence, we obtain:

$$e^{j \frac{1}{2} \arctan \Phi} = j \left[\begin{array}{c} \cos \left(\frac{1}{2} \arctan \left(\frac{\frac{\sigma_2}{\omega \varepsilon_o}}{\varepsilon_{r2}' - \varepsilon_{r1}' \sin^2 \xi_1} \right) \right) \\ -j \sin \left(\frac{1}{2} \arctan \left(\frac{\frac{\sigma_2}{\omega \varepsilon_o}}{\varepsilon_{r2}' - \varepsilon_{r1}' \sin^2 \xi_1} \right) \right) \end{array} \right]$$

Applying $\cos(x/2) = \sqrt{1 + \cos x}/\sqrt{2}$ and $\sin(x/2) = \sqrt{1 - \cos x}/\sqrt{2}$ and $\cos(\arctan x) = 1/\sqrt{1 + x^2}$ and carrying out some algebraic manipulations produces:

$$e^{j \frac{1}{2} \arctan \Phi} = \frac{\left[\begin{array}{c} \sqrt{\sqrt{\left(\varepsilon_{r2}' - \varepsilon_{r1}' \sin^2 \xi_1 \right)^2 + \left(\frac{\sigma_2}{\omega \varepsilon_o} \right)^2} - \left(\varepsilon_{r2}' - \varepsilon_{r1}' \sin^2 \xi_1 \right)} \\ +j \sqrt{\sqrt{\left(\varepsilon_{r2}' - \varepsilon_{r1}' \sin^2 \xi_1 \right)^2 + \left(\frac{\sigma_2}{\omega \varepsilon_o} \right)^2} + \left(\varepsilon_{r2}' - \varepsilon_{r1}' \sin^2 \xi_1 \right)} \end{array} \right]}{\sqrt{2} \left[\left(\varepsilon_{r2}' - \varepsilon_{r1}' \sin^2 \xi_1 \right)^2 + \left(\frac{\sigma_2}{\omega \varepsilon_o} \right)^2 \right]^{1/4}}$$

Substituting into Equation (2.40) produces:

$$\gamma_{2z} = \frac{\omega \sqrt{\mu_o \varepsilon_o}}{\sqrt{2}} \left[\begin{array}{c} \sqrt{\sqrt{\left(\varepsilon_{r2}' - \varepsilon_{r1}' \sin^2 \xi_1 \right)^2 + \left(\frac{\sigma_2}{\omega \varepsilon_o} \right)^2} - \left(\varepsilon_{r2}' - \varepsilon_{r1}' \sin^2 \xi_1 \right)} \\ +j \sqrt{\sqrt{\left(\varepsilon_{r2}' - \varepsilon_{r1}' \sin^2 \xi_1 \right)^2 + \left(\frac{\sigma_2}{\omega \varepsilon_o} \right)^2} + \left(\varepsilon_{r2}' - \varepsilon_{r1}' \sin^2 \xi_1 \right)} \end{array} \right]$$

(2.41)

Therefore, we see that the real and imaginary parts of the last expression are restatements of Equations (2.36) and (2.38), respectively. This equality proves the validity of the Adler-Fano-Chu formulation for this special case of pratical importance.

2.5 Results

All computations presented here pertain to a case found in Reference [6], i.e. $f = 1$ MHz, $\varepsilon_{r1}' = 4.0$, $\sigma_1 = 0.01$ S/m, $\varepsilon_{r2}' = 10.0$ and $\sigma_2 = 0.001$ S/m.

2.5.1 Case with $\psi = 0$

Figures 2.3, 2.4, 2.5, 2.6 and 2.7 show the results for α_2, β_2, ξ_2, ζ_2, and ρ_2, respectively, when $\rho_1 = -80°$, $-60°$, $-40°$, $-20°$, $-10°$, $-5°$, $0°$, $+5°$, $+10°$, $+20°$, $+40°$, $+60°$, $+80°$, while ξ_1 varied from $0°$ to $90°$ in increments of $1°$. Rigorously speaking, $\xi_1 = 0.01°$ was taken in place of $\xi_1 = 0°$ since Equations (2.26-2.27) are not valid for $\xi_1 = 0$.

We note that the requirement $-90° \leq \rho_2 \leq +90°$ from physical principle (see Reference [4, p. 426]) is borne out by all numerical results. Surprisingly, however, the same numerical results show that the magnitude of the angle $\zeta_2 = (\xi_2 + \rho_2)$ can exceed $90°$, and thus, for self-consistency, the magnitude of the angle $\zeta_1 = (\xi_1 + \rho_1)$ was also allowed to exceed $90°$ in generating these figures. The physical meaning of having $\xi_2 > 90°$ for $\xi_1 \leq 90°$, and having $\zeta_2 = (\xi_2 + \rho_2) > 90°$ for $\zeta_1 = (\xi_1 + \rho_1) \leq 90°$ would seem to indicate the phenomenon of total reflection for the phase and the amplitude wavefronts, respectively.

We note the dramatic change in the behaviour of the curves for $-10° < \rho_1 < -5°$. We note also how the curves of Figure 2.5 tend to the diagonal straight line $\xi_2 = \xi_1$ as ρ_1 varies from $-10°$ to $-80°$ as well as from $+20°$ to $+80°$. Thus, the same straight line $\xi_2 = \xi_1$ would be obtained for both $\rho_1 = +90°$ and $\rho_1 = -90°$, and this makes sense for these two cases of ρ_1 correspond to parallel directions of $\vec{\alpha}_1$. Figure 2.8 shows the results for ζ_2 as a function of $\zeta_1 = (\xi_1 + \rho_1)$. We note that $\zeta_1 = \zeta_2 = 0$ regardless of the value of ρ_1, and that this case corresponds to the case of practical importance $V = 0$ mentioned above.

The trend of the curves is complicated and not always intuitively clear. In order to demonstrate that the above results are correct, the following comparison was carried out. First, the equivalence presented in Appendix B was used to obtain the values of the complex incidence angle from the knowledge of the real incidence angles ξ_1 and ρ_1 for the case $\psi = 0$. Then these values for the complex incidence angle were used in Snell's law of refraction to obtain the values for the complex transmission angle. Of course, if the equivalence could have been used in the reverse direction, we could have obtained directly the values for the real transmission angles corresponding to the values for the complex transmission angle that were just computed from Snell's law. However, such reverse equivalence cannot be established for the reason given in Appendix B. Therefore, we used the same values of the real incidence angles ξ_1 and ρ_1 in the expressions for the general case with $\psi = 0$ to obtain the values for the real transmission angles ξ_2 and ρ_2. Then the equivalence presented in Appendix B was used again to obtain the values for the complex transmission angle corresponding to the values of ξ_2 and ζ_2. Then we compared the two different sets of values for the complex transmission angle

$(\theta_{R2} + j\theta_{I2})$, one set corresponding to the classical formulation and the other set corresponding to the Adler-Chu-Fano formulation. Now, the solution for the general case, the solution for the equivalence between the classical and the Adler-Chu-Fano formulations, and the solution for Snell's law, all offer multiple expressions from which to choose their proper respective solution. The choices that were made here provided a perfect match between the two sets of values for $(\theta_{R2} + j\theta_{I2})$ over the entire ranges of $0° \leq \xi_1 \leq 90°$ and $-90° \leq \rho_1 \leq +90°$ as shown in Figures 2.9 and 2.10. These choices are explained in the following three subsections. We note some similarity between the general trend of Figure 2.7 and that of Figure 2.10, and to some lesser extent, we note also some similarity between some features of Figure 2.5 and some features of Figure 2.9.

Choice of solution for the equivalence between the two formulations

The variables θ_R, θ_I, θ_α and θ_β are defined in Appendix B. Out of the four possible solutions given by MATLAB for $Y = \cos^2(\theta_R)$ shown in Appendix B, the correct solution was obtained as:

$$Y = \begin{cases} \text{fourth solution} & \text{for } (\theta_\alpha > 90°) \text{ OR } (\theta_\beta > 90°) \\ \text{third solution} & \text{otherwise} \end{cases}$$

where OR is a logical operator. From the knowledge of Y, we obtained the knowledge of θ_R as:

$$\theta_R = \begin{cases} \theta_\beta & \text{for } (\theta_\alpha - \theta_\beta) = 0 \\ -\left|\arccos(\sqrt{Y})\right| & \text{for } (\theta_\alpha < 0) \text{ AND } (\theta_\beta \leq \theta_\beta^0) \\ 180° - \left|\arccos(\sqrt{Y})\right| & \text{for } \theta_\beta > \theta_\beta^{90} \\ \left|\arccos(\sqrt{Y})\right| & \text{otherwise} \end{cases}$$

where AND is a logical operator, θ_β^0 and θ_β^{90} are the values of θ_β for which $\left|\arccos(\sqrt{Y})\right|$ reached 0° and 90°, respectively. These values were computed readily as $\theta_\beta^0 = |\theta_R(0)|$ and $\theta_\beta^{90} = 90° - \text{sign}(\theta_\alpha - \theta_\beta)|\theta_R(0)|$ where $\theta_R(0)$ was the value of $\left|\arccos(\sqrt{Y})\right|$ at $\theta_\beta = 0$, and $\text{sign}(x) = \{+1, 0, -1\}$ for $\{x > 0, x = 0, x < 1\}$, respectively. Then substituting the knowledge of θ_R into Equation (B.10), we obtained the knowledge of θ_I as:

$$\theta_I = -\text{sign}(\theta_\alpha - \theta_\beta)\text{arcsinh}(\sqrt{C - Y})$$

The results are presented in Figure 2.17. We see that the curves for θ_R have a slope of 1, and the curves for θ_I have a slope of zero.

Choice of solutions for $\xi 2$, $\zeta 2$ and ρ_2

The solutions for ξ_2 and ζ_2 were obtained from Equations (2.26) and (2.27), respectively, as:

$$\xi_2 = \begin{cases} 180° - \arccos\left(\sqrt{\cos^2(\xi_2)}\right) & \text{for } \xi_1 > \xi_1^\xi \\ \arccos\left(\sqrt{\cos^2(\xi_2)}\right) & \text{otherwise} \end{cases} \tag{2.42}$$

$$\zeta_2 = \begin{cases} 180° - \text{sign}(\zeta_1)\arccos\left(\sqrt{\cos^2(\zeta_2)}\right) & \text{for } \xi_1 > \xi_1^\zeta \\ \text{sign}(\zeta_1)\arccos\left(\sqrt{\cos^2(\zeta_2)}\right) & \text{otherwise} \end{cases} \tag{2.43}$$

The values ξ_1^ξ and ξ_1^ζ correspond to the values of ξ_1 for which $\arccos(\sqrt{\cos^2(\xi_2)})$ and $\text{sign}(\zeta_1)\arccos(\sqrt{\cos^2(\zeta_2)})$ reached 90°, respectively. Once ξ_2 and ζ_2 were known, $\cos(\rho_2)$ was computed from expression (2.25). The solution for ρ_2 was obtained as:

$$\rho_2 = \begin{cases} -\arccos(\cos\rho_2) & \text{for } (\rho_1 \le 0) \text{ AND } (\xi_1 \le \xi_1^\rho) \\ +\arccos(\cos\rho_2) & \text{otherwise} \end{cases} \tag{2.44}$$

The value ξ_1^ρ corresponds to the value of ξ_1 for which $\arccos(\cos\rho_2) = 0$. When the curve did not cross the zero level, ξ_1^ρ was taken as 0 if $\rho_1 > 0$, and as 90° if $\rho_1 < 0$. For the case $\psi = 0$, we see from Figure 2.7 that $\rho_2 = (\zeta_2 - \xi_2)$ as expected. The values ξ_1^ξ, ξ_1^ζ and ξ_1^ρ were found by means of a simple root-searching subroutine using the bisection technique.

Choice of solution for Snell's law with complex angles

The solution for Snell's law with complex angles was obtained as:

$$\theta_{R2} + j\theta_{I2} = \begin{cases} 180° - \arcsin\left(\sqrt{\frac{\varepsilon_1}{\varepsilon_2}}\sin(\theta_{R1} + j\theta_{I1})\right) & \text{for } \xi_1 > \xi_1^{SNELL} \\ \arcsin\left(\sqrt{\frac{\varepsilon_1}{\varepsilon_2}}\sin(\theta_{R1} + j\theta_{I1})\right) & \text{otherwise} \end{cases} \tag{2.45}$$

where ξ_1^{SNELL} corresponds to the value of ξ_1 for which $\text{Real}(\sqrt{\varepsilon_1/\varepsilon_2}\sin(\theta_{R1} + j\theta_{I1}))$ reached 90°. This value was computed as $\xi_1^{SNELL} = \theta_{R1}^{90} - \text{sign}(\rho_1)|\theta_{R1}(0)|$

where $\theta_{R1}{}^{90}$ was the value of θ_{R1} for which $\text{Real}(\sqrt{\varepsilon_1/\varepsilon_2}\sin(\theta_{R1}+j\theta_{I1}))$ reached $90°$, and $\theta_{R1}(0)$ was the value of $|\arccos(\sqrt{Y})|$ at $\xi_1 = 0$, with Y defined in section 2.5.1. The value $\theta_{R1}{}^{90}$ was found by means of a simple root-searching subroutine using the bisection technique.

2.5.2 Case with arbitrary value of ψ

The case with arbitrary values of ψ was generated by introducing the rotation angle δ as shown in Figure 2.11. The spherical coordinate angles corresponding to ξ_1 are shown as θ_β and ϕ_β, whereas the spherical coordinate angles corresponding to ζ_1 are shown as θ_α and ϕ_α. From Figure 2.11, we have:

$$\hat{r}_\alpha = \cos(\rho)\hat{r}_\beta + \sin(\rho)\sin(\delta)\hat{\theta}_\beta + \sin(\rho)\cos(\delta)\hat{\phi}_\beta$$

where:

$$\hat{r}_\beta = \sin(\theta_\beta)\cos(\phi_\beta)\hat{x} + \sin(\theta_\beta)\sin(\phi_\beta)\hat{y} + \cos(\theta_\beta)\hat{z}$$

$$\hat{\theta}_\beta = \cos(\theta_\beta)\cos(\phi_\beta)\hat{x} + \cos(\theta_\beta)\sin(\phi_\beta)\hat{y} - \sin(\theta_\beta)\hat{z}$$

$$\hat{\phi}_\beta = -\sin(\phi_\beta)\hat{x} + \cos(\phi_\beta)\hat{y}$$

Substituting in the above expressions and collecting the terms for each Cartesian component, we obtain the knowledge of θ_α and ϕ_α as:

$$\phi_\alpha = \arctan\left(\frac{Y}{X}\right)$$

$$\theta_\alpha = \arctan\left(\frac{\sqrt{X^2 + Y^2}}{Z}\right)$$

where:

$$X = \cos(\rho)\sin(\theta_\beta)\cos(\phi_\beta) + \sin(\rho)\sin(\delta)\cos(\theta_\beta)\cos(\phi_\beta) - \sin(\rho)\cos(\delta)\sin(\phi_\beta)$$

$$Y = \cos(\rho)\sin(\theta_\beta)\sin(\phi_\beta) + \sin(\rho)\sin(\delta)\cos(\theta_\beta)\sin(\phi_\beta) + \sin(\rho)\cos(\delta)\cos(\phi_\beta)$$

$$Z = \cos(\rho)\cos(\theta_\beta) - \sin(\rho)\sin(\delta)\sin(\theta_\beta)$$

The case $\delta = +90°$ corresponds to the case $\psi = 0$ with $\rho \geq 0$, whereas the case $\delta = -90°$ corresponds to the case $\psi = 0$ with $\rho \leq 0$. Unfortunately,

unlike for $\psi = 0$, we do not know the generalization of Snell's law written with complex angles for $\psi \neq 0$. Thus, our knowledge of Snell's law written in terms of complex angles cannot aid us to confirm that we made the correct choice of expression for the solution when $\psi \neq 0$. The generalization that was used here to generate the results of Figures 2.12, 2.13, 2.14, 2.15 and 2.16 was to add the following condition to the conditions that were used for $\psi = 0$. We changed the sign of the value for $\theta_{\alpha 1}$ whenever $|\psi| > 90°$ and then replace ψ with $(180° - \psi)$. We also defined the ranges for ρ_1 and δ as $-90° \leq \rho_1 \leq +90°$, and $0° \leq \delta \leq 180°$, respectively.

There are too many plots to present here for all the same values of ρ_1 that were used for the case $\psi = 0$. The value of $\rho_1 = -10°$ was chosen because it represents a difficult case for the interface at hand. Figures 2.12, 2.13, 2.14, 2.15 and 2.16 show the results for α_2, β_2, ξ_2, ζ_2, and ρ_2, respectively, when $\rho_1 = -10°$ while ξ_1 varied from $0°$ to $90°$ in increments of $1°$, and δ varied from $0°$ to $180°$ in increments of $5°$. Again, $\xi_1 = 0.01°$ was taken in place of $\xi_1 = 0°$ since Equations (2.26-2.27) are not valid for $\xi_1 = 0$. We note that in these figures, the curves for $\delta = 90°$ correspond to the curves presented earlier for $\psi = 0$ and $\rho_1 = -10°$.

2.6   Chapter summary

This section has presented a correction and a generalization of the solution presented in References [6, 21] for the effective propagation constants of non-uniform plane waves at the planar interface of two isotropic homogeneous possibly lossy media of infinite transverse dimensions. The analysis proceeded from the Adler-Chu-Fano formulation. The validity of the results obtained here for the case $\psi = 0$ was demonstrated by comparing these results with those obtained by Snell's law written in terms of complex angles. No such comparison, however, could be made for the case $\psi \neq 0$ because the generalization of Snell's law written with complex angles is not known for $\psi \neq 0$. The trends of the curves are rather complicated and not always intuitive, even for the case $\psi = 0$. The case of $V = \alpha_1 \sin(\zeta_1) = 0$ is one of practical importance in a planar multilayered structure, and results in $\vec{\alpha}$ being normal to all parallel interfaces of the structure regardless of the values of the intrinsic propagation constants of the layers of the structure. In other words, $\vec{\alpha}$ is normal to all parallel interfaces of the structure, even for the most general anisotropic layers. When $\vec{\alpha}_2$ is normal to the interfaces of the structure, the Adler-Chu-Fano formulation was also proved directly in Section 2.4.1 by showing that the same result was obtained for γ_z when using the Adler-Chu-Fano approach as when using the complex-valued approach embodied by Equation (2.39).
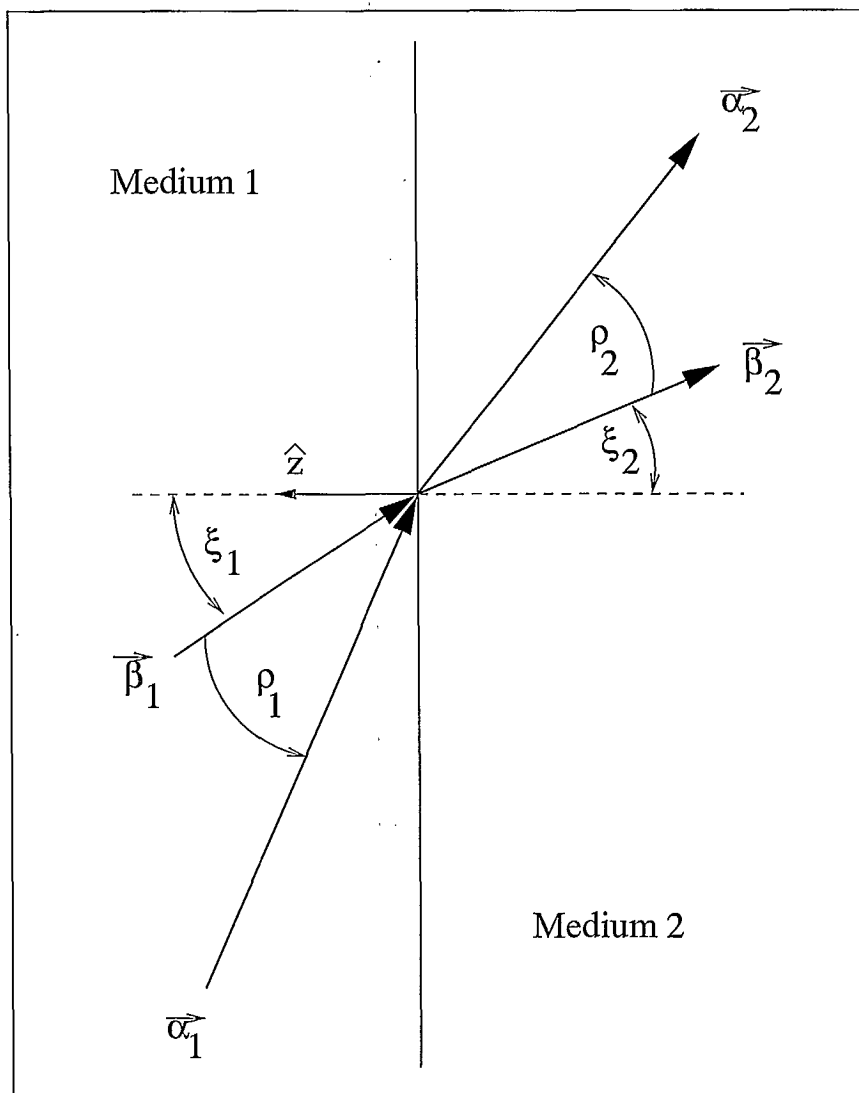
Figure 2.1: Special case of a non-uniform plane wave incident on a planar interface between two isotropic homogeneous possibly lossy media. Here, the vectors $\vec{\alpha}_1$, $\vec{\beta}_1$ and the unit vector normal to the interface $\hat{z}$ are coplanar.
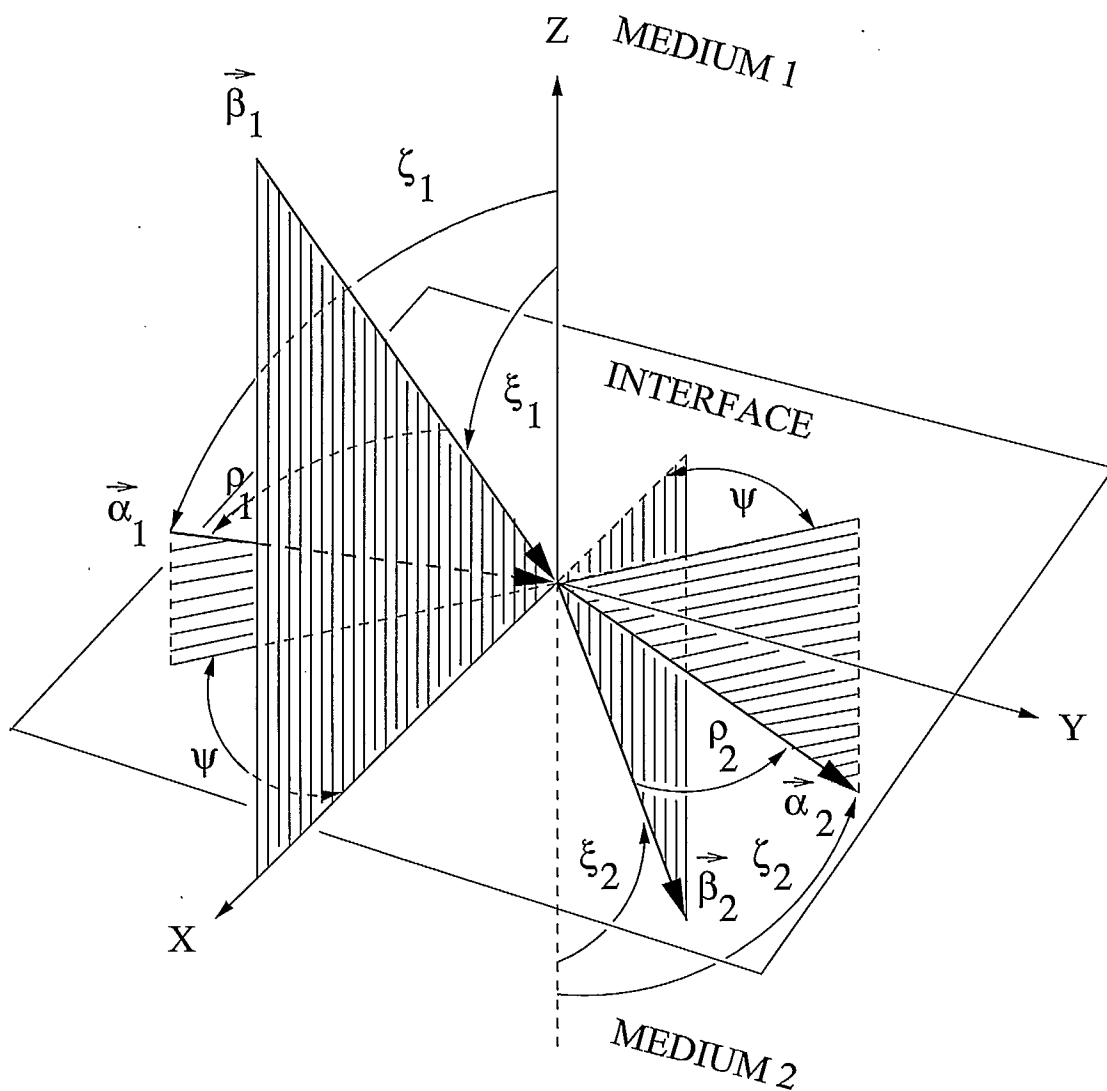
Figure 2.2: General case of a non-uniform plane wave incident on a planar interface between two isotropic homogeneous possibly lossy media. To simplify the figure, the incidence plane for the phase wavefront propagation vectors was taken to lie in the xz plane.

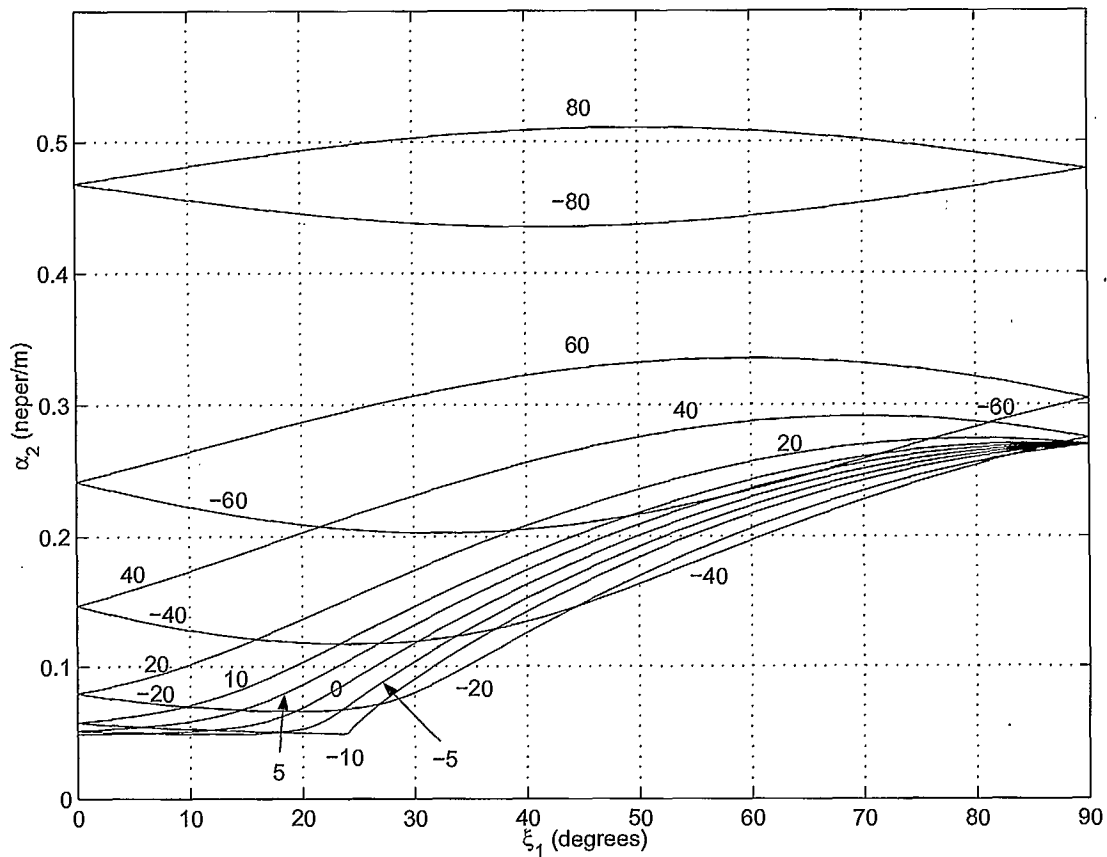Figure 2.3: Effective propagation constant α_2 as ξ_1 varies from 0° to 90° in increments of 1°, $\psi = 0$ and ρ_1 takes successively the values of $-80°$, $-60°$, $-40°$, $-20°$, $-10°$, $-5°$, 0°, $+5°$, $+10°$, $+20°$, $+40°$, $+60°$, $+80°$.
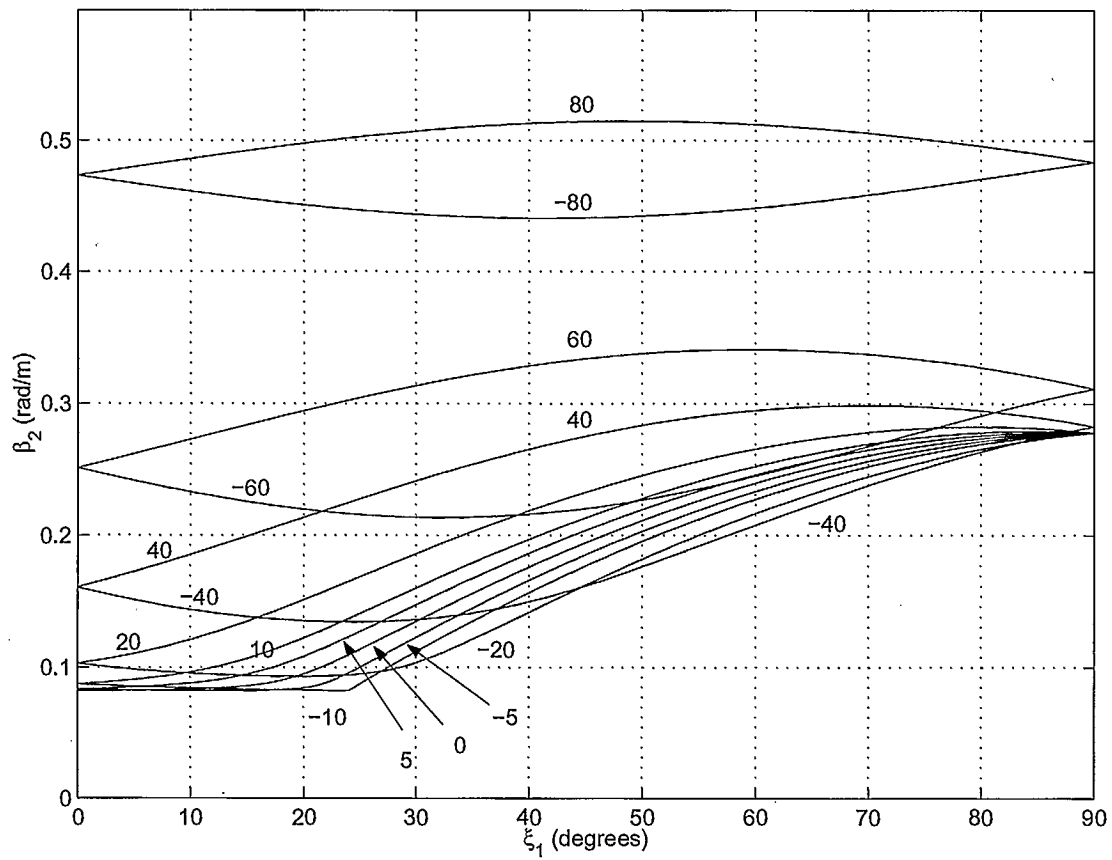
Figure 2.4: Effective propagation constant β_2 as ξ_1 varies from 0° to 90° in increments of 1°, $\psi = 0$ and ρ_1 takes successively the values of $-80°$, $-60°$, $-40°$, $-20°$, $-10°$, $-5°$, $0°$, $+5°$, $+10°$, $+20°$, $+40°$, $+60°$, $+80°$.
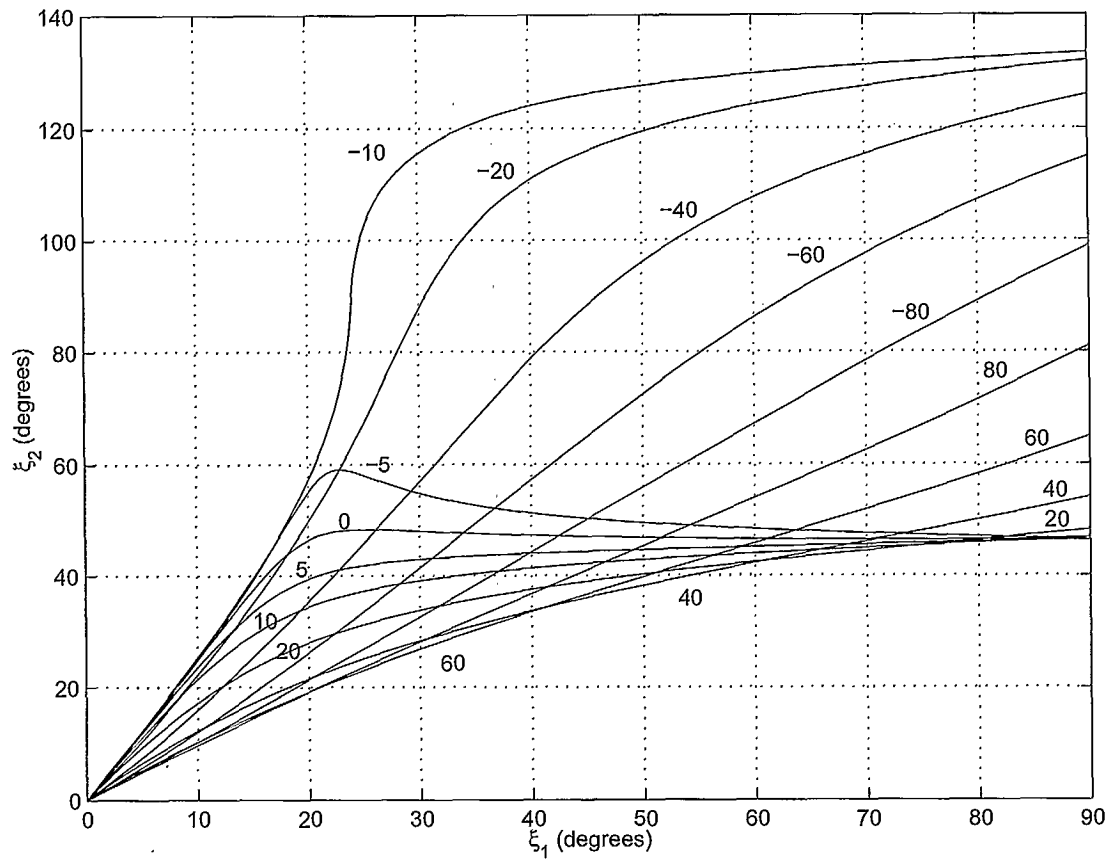
Figure 2.5: Transmission angle ξ_2 as ξ_1 varies from $0°$ to $90°$ in increments of $1°$, $\psi = 0$ and ρ_1 takes successively the values of $-80°$, $-60°$, $-40°$, $-20°$, $-10°$, $-5°$, $0°$, $+5°$, $+10°$, $+20°$, $+40°$, $+60°$, $+80°$.
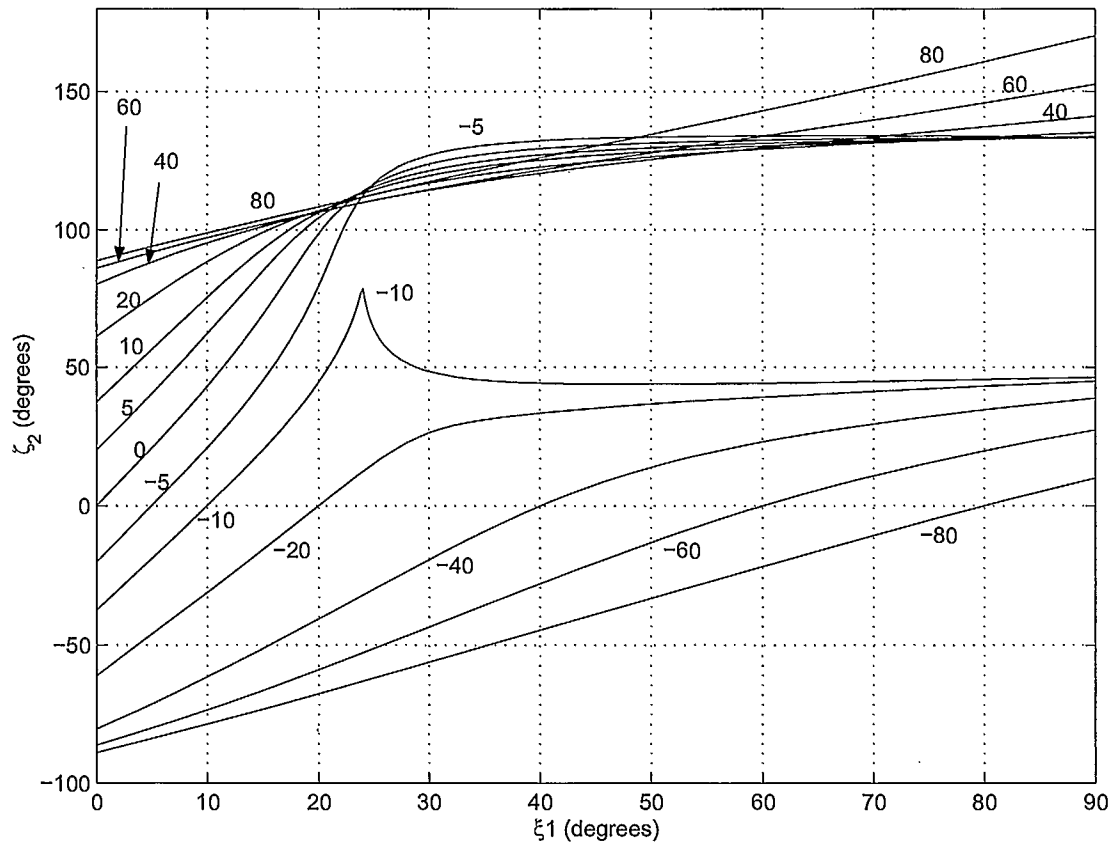
Figure 2.6: Transmission angle ζ_2 as ξ_1 varies from $0°$ to $90°$ in increments of $1°$, $\psi = 0$ and ρ_1 takes successively the values of $-80°$, $-60°$, $-40°$, $-20°$, $-10°$, $-5°$, $0°$, $+5°$, $+10°$, $+20°$, $+40°$, $+60°$, $+80°$.
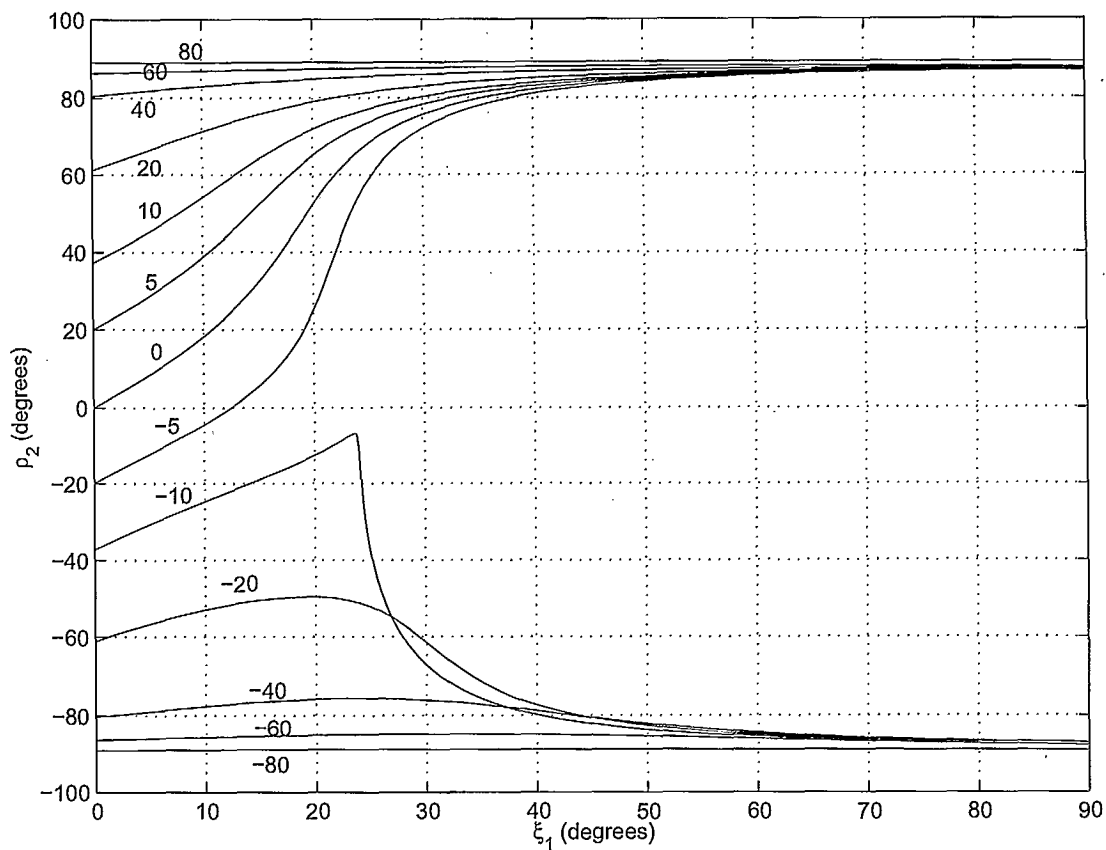
Figure 2.7: Transmission angle ρ_2 as ξ_1 varies from $0°$ to $90°$ in increments of $1°$, $\psi = 0$ and ρ_1 takes successively the values of $-80°$, $-60°$, $-40°$, $-20°$, $-10°$, $-5°$, $0°$, $+5°$, $+10°$, $+20°$, $+40°$, $+60°$, $+80°$. We confirmed that $\rho_2 = (\zeta_2 - \xi_2)$.
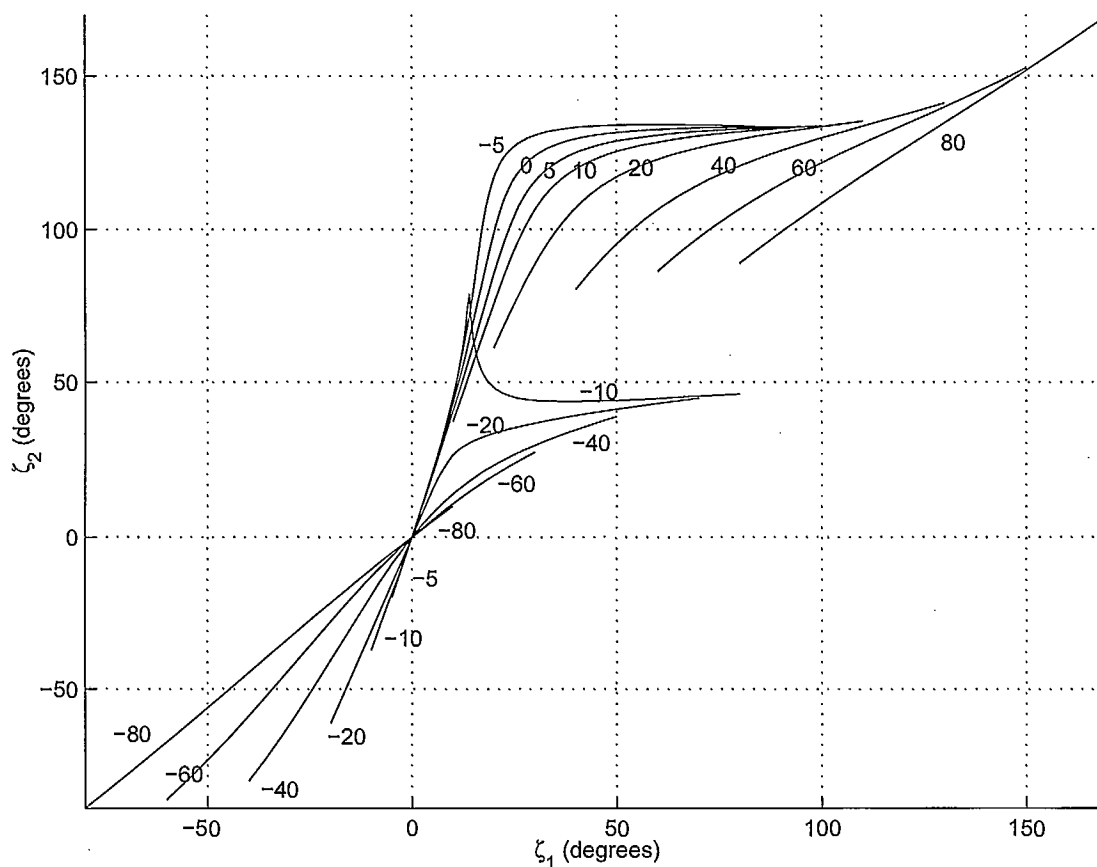
Figure 2.8: Transmission angle ζ_2 as a function of $\zeta_1 = (\xi_1 + \rho_1)$ as ξ_1 varies from $0°$ to $90°$ in increments of $1°$, $\psi = 0$ and ρ_1 takes successively the values of $-80°$, $-60°$, $-40°$, $-20°$, $-10°$, $-5°$, $0°$, $+5°$, $+10°$, $+20°$, $+40°$, $+60°$, $+80°$.

34
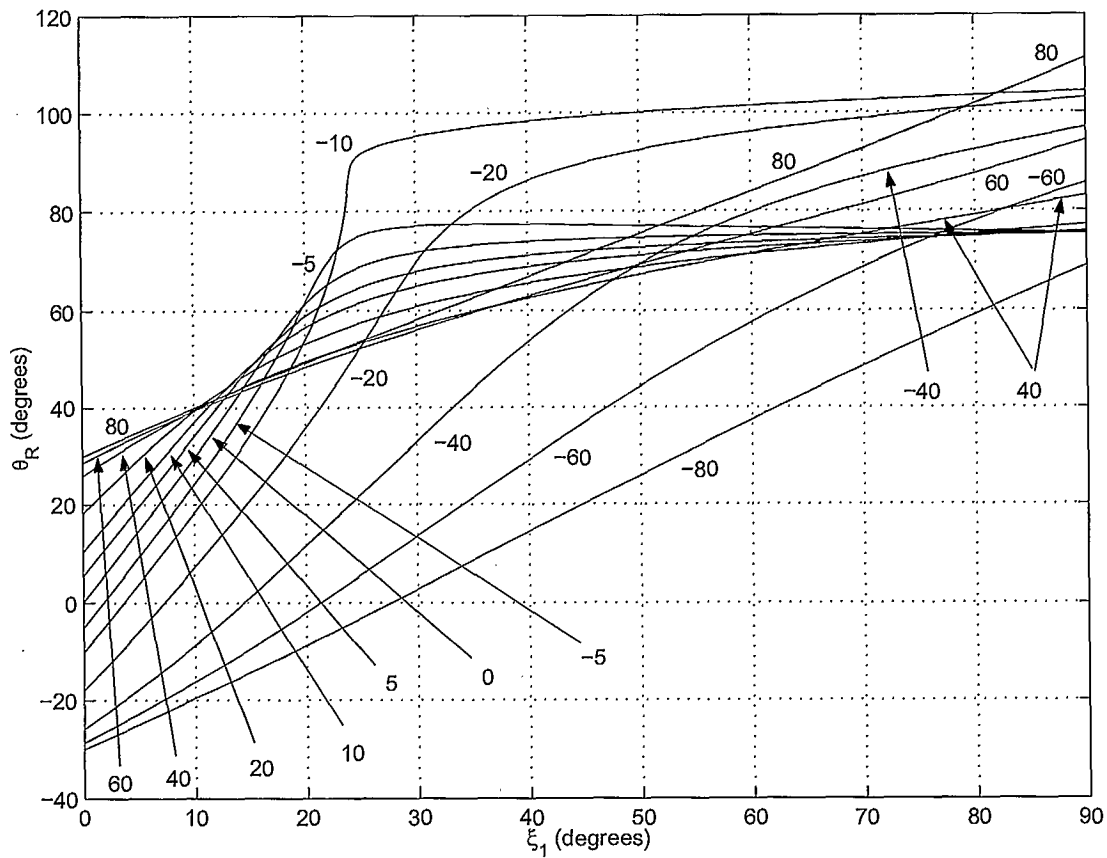
Figure 2.9: Transmission angle θ_{R2} as ξ_1 varies from 0° to 90° in increments of 1°, $\psi = 0$ and ρ_1 takes successively the values of $-80°$, $-60°$, $-40°$, $-20°$, $-10°$, $-5°$, $0°$, $+5°$, $+10°$, $+20°$, $+40°$, $+60°$, $+80°$.

35
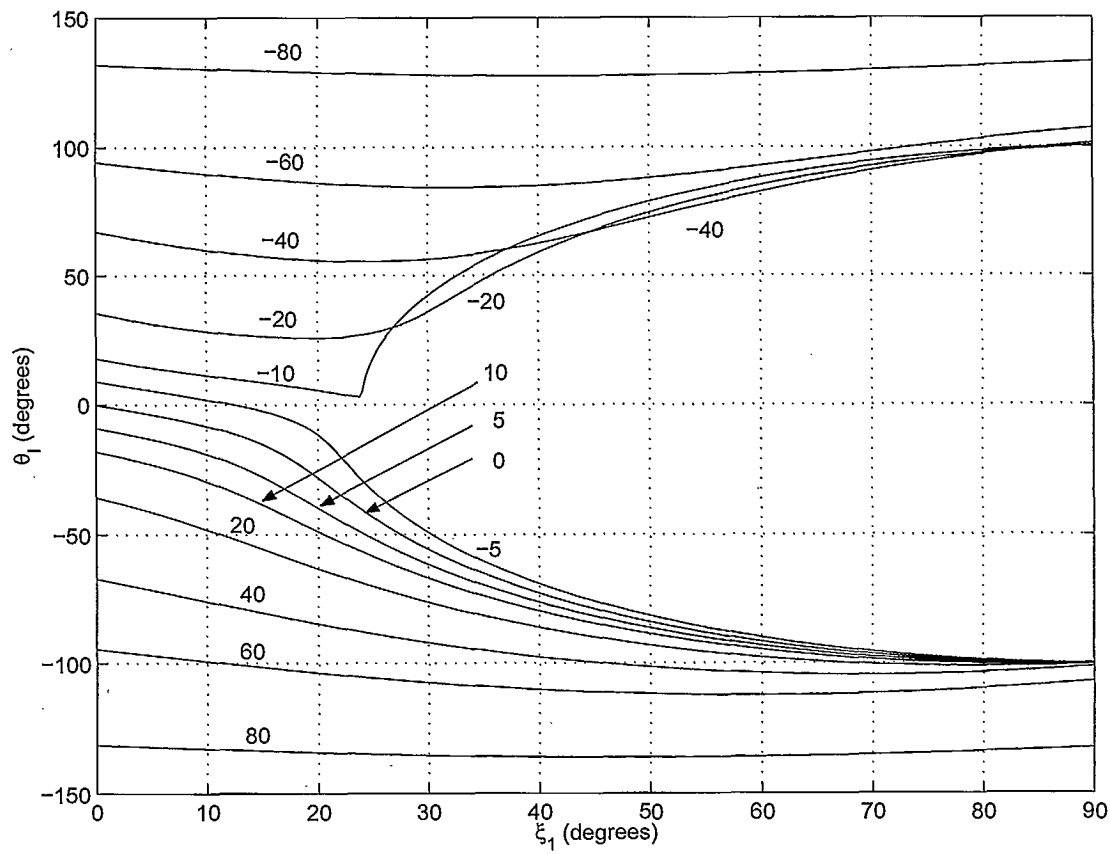
Figure 2.10: Transmission angle θ_{I2} as ξ_1 varies from 0° to 90° in increments of 1°, $\psi = 0$ and ρ_1 takes successively the values of −80°, −60°, −40°, −20°, −10°, −5°, 0°, +5°, +10°, +20°, +40°, +60°, +80°.

36
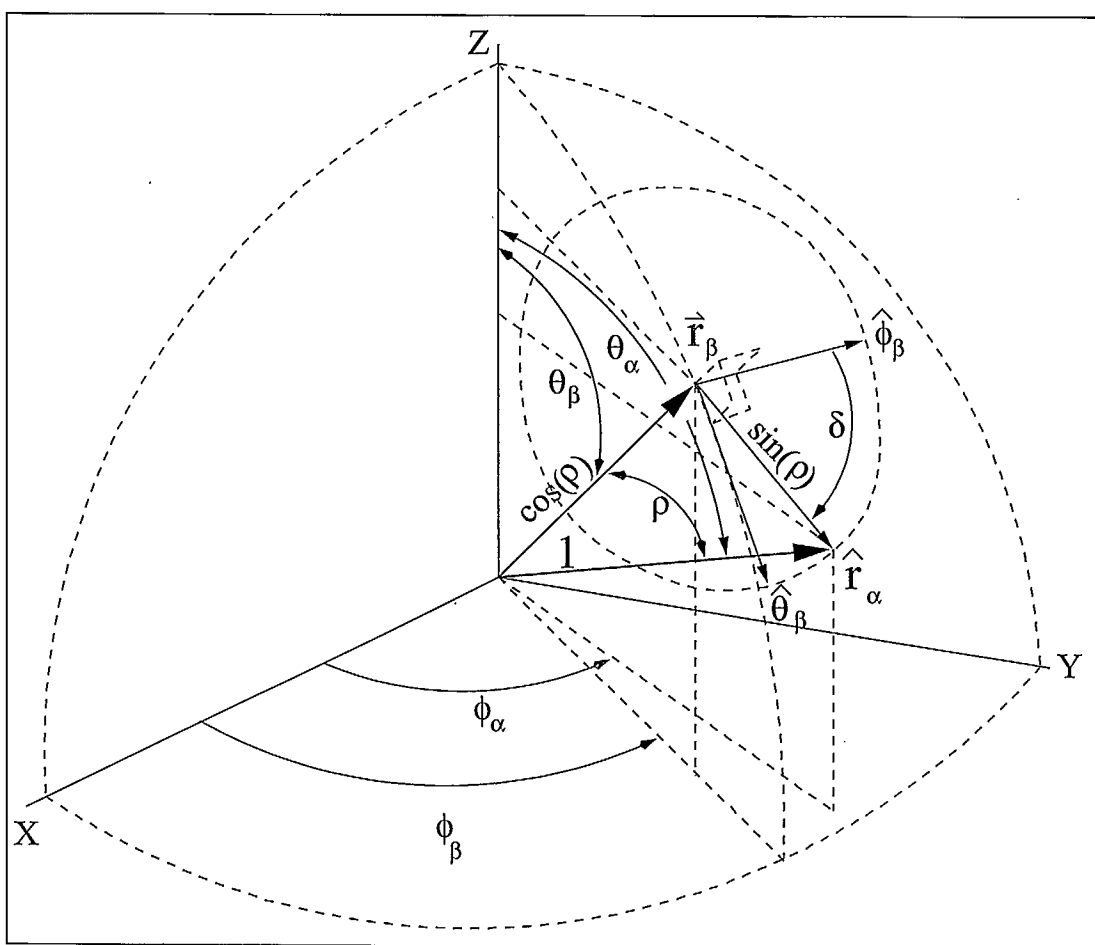
Figure 2.11: Coordinate system for computing θ_α and ϕ_α from the knowledge of θ_β, ϕ_β, ρ and δ.
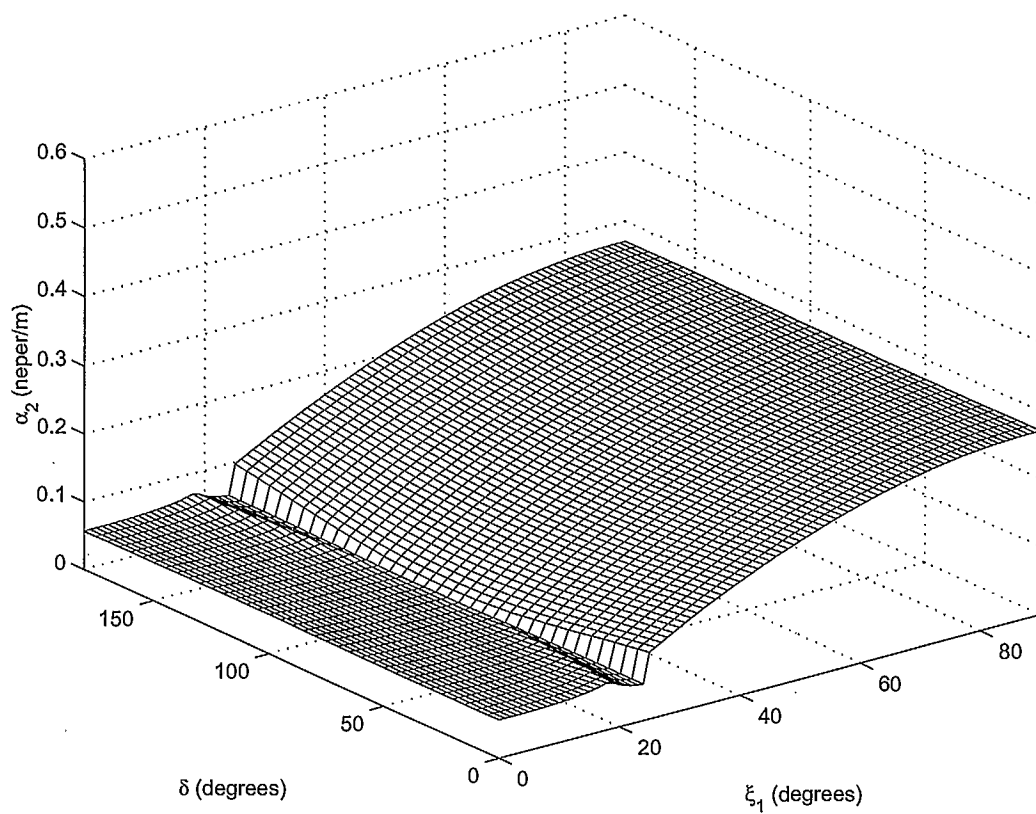
Figure 2.12: Effective propagation constant α_2 as ξ_1 varies from $0°$ to $90°$ in increments of $1°$, δ varies from $0°$ to $180°$ in increments of $5°$, and $\rho_1 = -10°$.
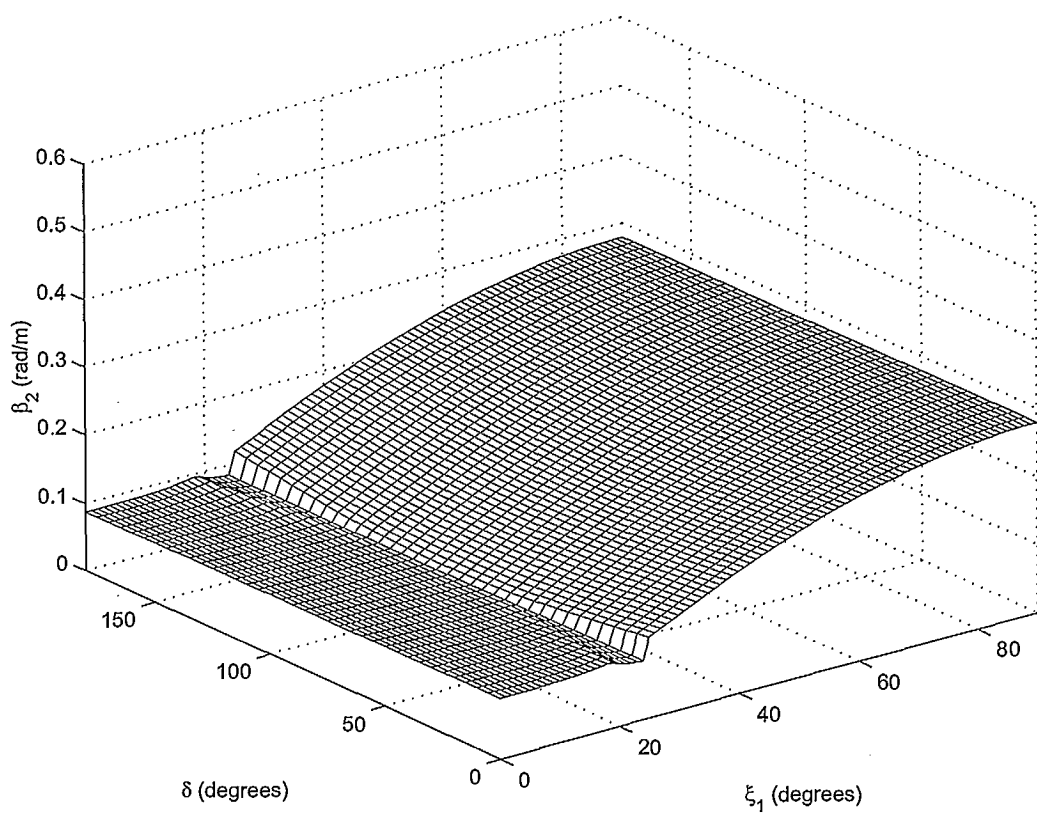
Figure 2.13: Effective propagation constant β_2 as ξ_1 varies from 0° to 90° in increments of 1°, δ varies from 0° to 180° in increments of 5°, and $\rho_1 = -10°$.
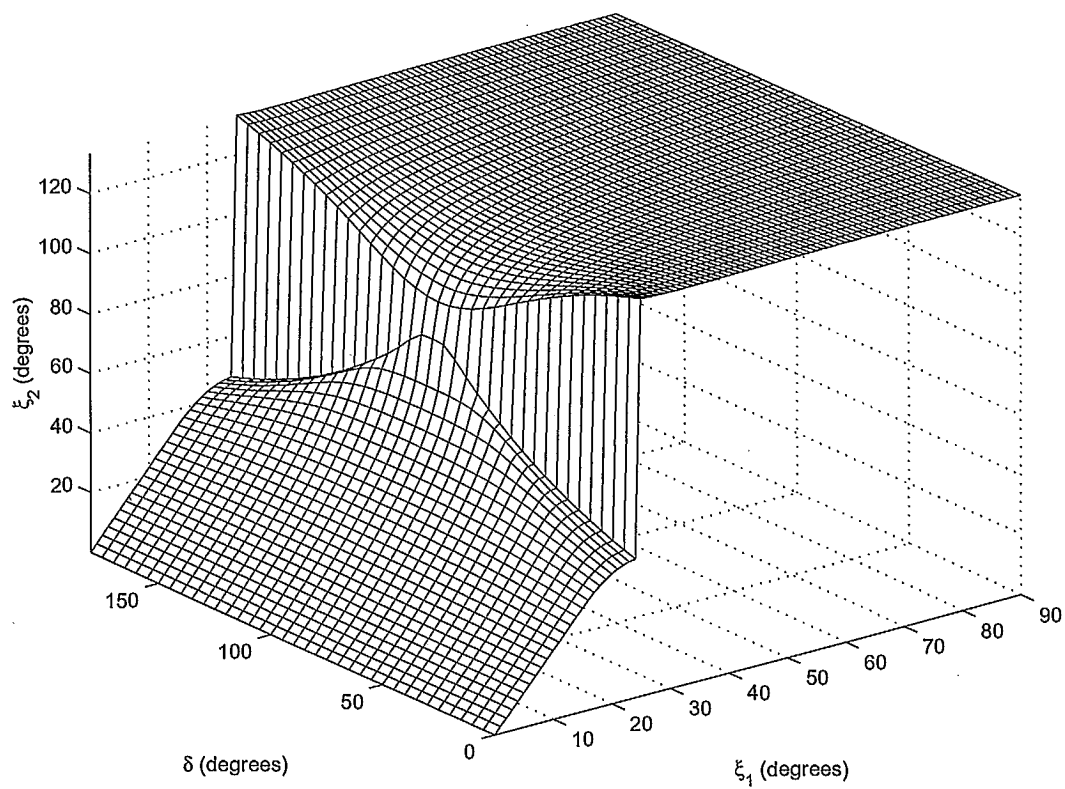
Figure 2.14: Transmission angle ξ_2 as ξ_1 varies from 0° to 90° in increments of 1°, δ varies from 0° to 180° in increments of 5°, and $\rho_1 = -10°$.
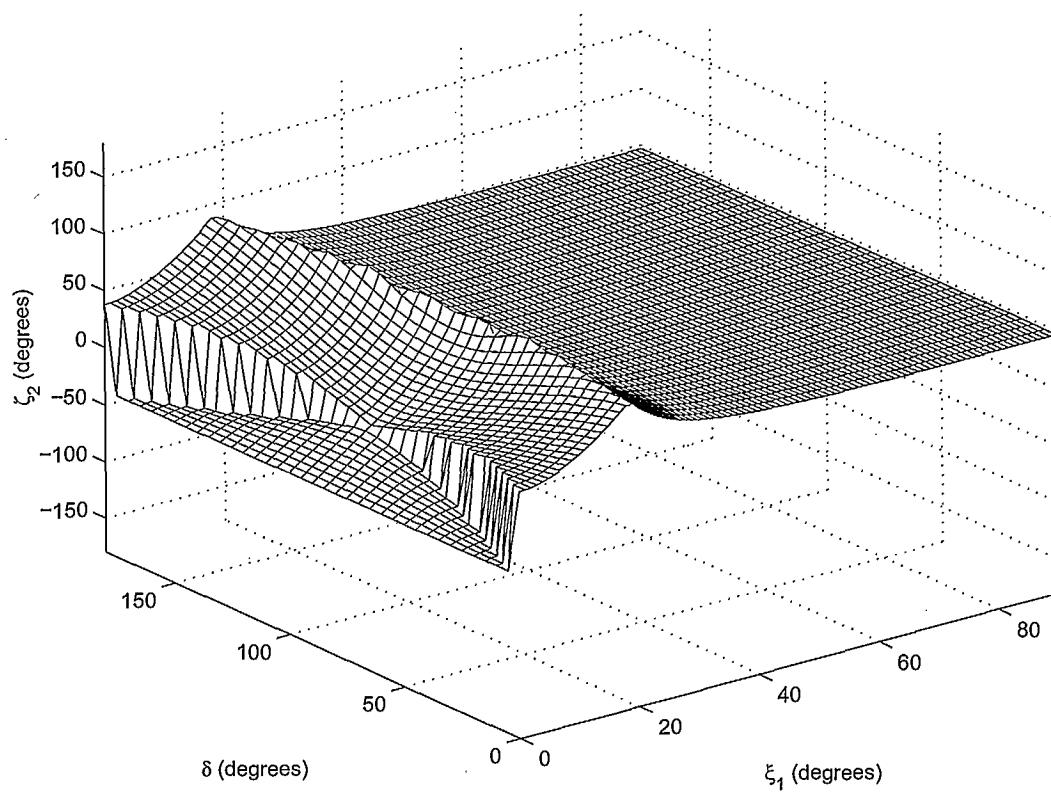
Figure 2.15: Transmission angle ζ_2 as ξ_1 varies from $0°$ to $90°$ in increments of $1°$, δ varies from $0°$ to $180°$ in increments of $5°$, and $\rho_1 = -10°$.
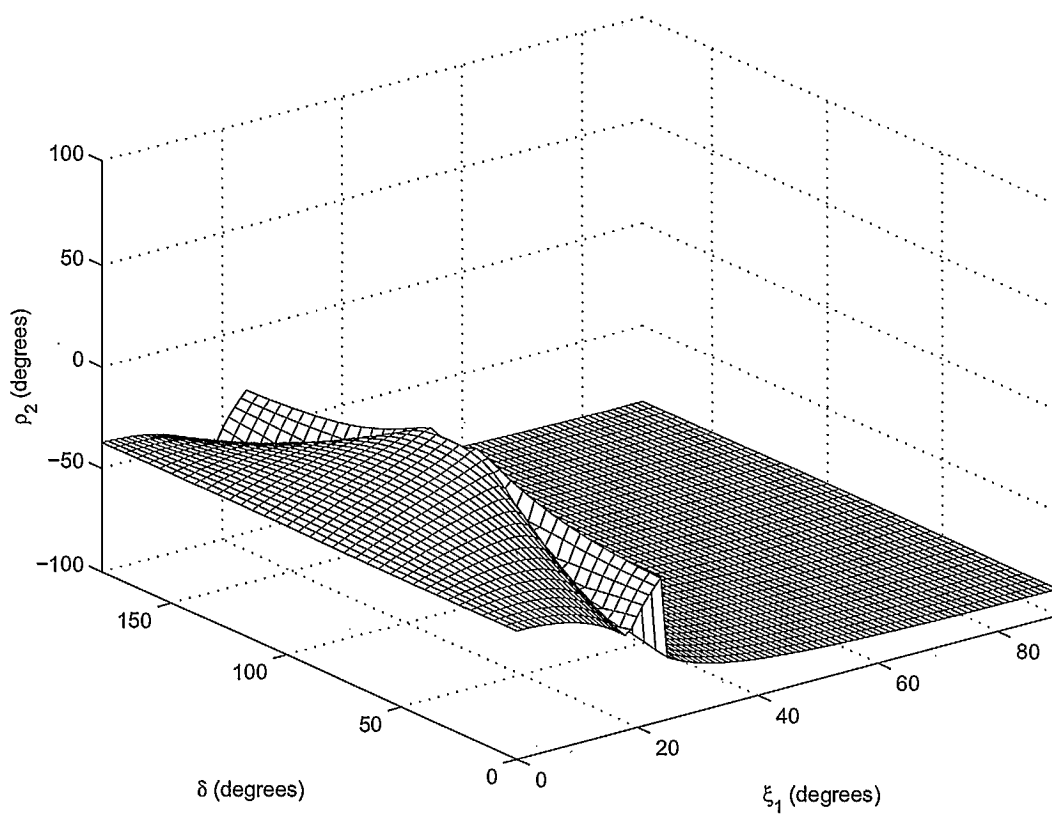
Figure 2.16: Transmission angle ρ_2 as ξ_1 varies from $0°$ to $90°$ in increments of $1°$, δ varies from $0°$ to $180°$ in increments of $5°$, and $\rho_1 = -10°$.
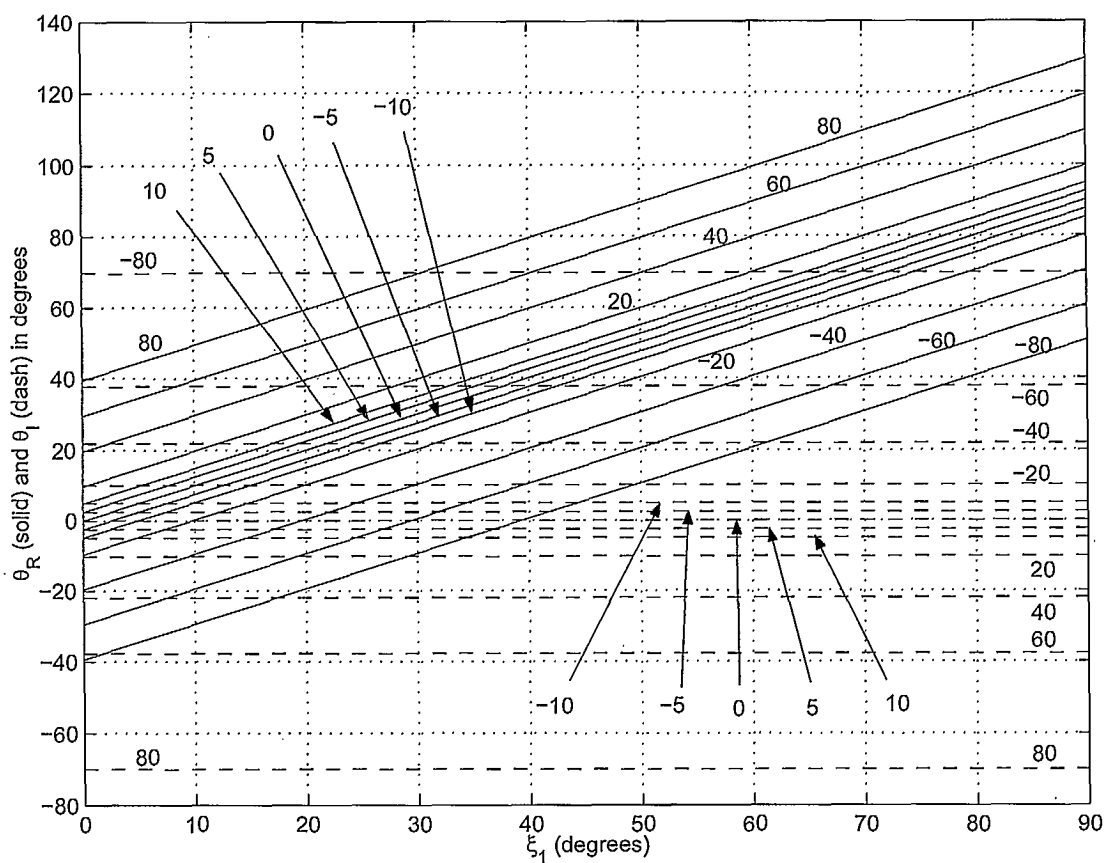
Figure 2.17: Complex incidence angle $\theta_{R1}+j\theta_{I1}$ as a function of the incidence angles ξ_1 and ρ_1 for $\psi = 0$. The solid line is for θ_{R1}, and the dash line for θ_{I1}. The angle ξ_1 varies from 0° to 90° while the angle ρ_1 takes successively the values of $-80°$, $-60°$, $-40°$, $-20°$, $-10°$, $-5°$, $0°$, $+5°$, $+10°$, $+20°$, $+40°$, $+60°$, $+80°$.

Chapter 3

Individual and composite GSM

The GSM for each interface is obtained from the generalized Fresnel equations for a planar interface between two media. The incidence plane is defined as the plane in which lie both the incidence propagation vector $\vec{\gamma}^i = \vec{\alpha}^i + j\vec{\beta}^i$ and the unit vector normal to the interface $\hat{n}$, i.e. the vectors $\vec{\alpha}^i$, $\vec{\beta}^i$ and $\hat{n}$ are assumed to be coplanar[1]. We assume also that $\hat{n} = \hat{z}$ and that the incidence plane is the xz plane. Thus, the TE^z or TM^y, and the TM^z or TE^y polarizations correspond to the polarization with $\vec{E}^i$ being perpendicular and parallel to the incidence plane, respectively.

3.1 Individual GSM

3.1.1 Lossless media

When the two media are lossless, the Fresnel equations for the interface are most conveniently obtained from the interpretation that the transverse electric field of the TE^z (or TM^y) mode corresponds to a voltage travelling wave propagating on an equivalent transmission line modelling the propagation medium, whereas the transverse magnetic field of the TM^z (or TE^y) mode corresponds to a current travelling wave propagating on an equivalent transmission line modelling the propagation medium (see References [33, p. 415], [40, pp. 54-57] and [68, p. 304]). The concept of the equivalent transmission line can also be justified on the basis that the two dimensional Fourier transform of the transverse components of the TE^z or TM^z electromagnetic field obey the telegrapher's equations (see References [34, 35, 36]). The interface between the two media is then modelled as a discontinuity formed by the

---

[1]The more general case where $\psi \neq 0$ in Figure 2.2 is beyond the scope of this section.

junction of the two transmission lines that model the two media [37]. The equivalence is based here on taking the characteristic impedance of the transmission line to be equal to the wave impedance Z_W of the wave propagating in each respective medium. Note that the elements of the scattering matrix can be defined in terms of either the whole electric field or just the tangential (to the interface) component of the electric field or the magnetic field. The latter scattering matrix is identified as S whereas the former is identified as C. The difference in the definition results in different expressions for the reflection or the transmission coefficients of the TM^z mode (see References [13, p. 41], [5, p. 152] and [14, p. 543, Equation (9.100b)] for the transmission[2], and Reference [14, p. 543, Equation (9.100a)] for the reflection).

For the TM^z mode (or TE^y), i.e. parallel polarization, one obtains:

$$\Gamma^I = \frac{H_o^r}{H_o^i} = \frac{E_o^r/(-\eta^i)}{E_o^i/(+\eta^i)} = -\frac{E_o^r}{E_o^i} = \frac{Z_W^i - Z_W^t}{Z_W^i + Z_W^t}$$

$$\implies \frac{E_o^r}{E_o^i} = -\Gamma^I = \frac{Z_W^t - Z_W^i}{Z_W^t + Z_W^i} = \frac{\varepsilon_r^i k_z^t - \varepsilon_r^t k_z^i}{\varepsilon_r^i k_z^t + \varepsilon_r^t k_z^i} \quad (3.1)$$

$$\Upsilon^I = \frac{H_o^t}{H_o^i} = \frac{E_o^t/(+\eta^t)}{E_o^i/(+\eta^i)} = \left(\frac{\eta^i}{\eta^t}\right)\frac{E_o^t}{E_o^i} = \frac{2Z_W^i}{Z_W^i + Z_W^t}$$

$$\implies \frac{E_o^t}{E_o^i} = \left(\frac{\eta^t}{\eta^i}\right)\Upsilon^I = \left(\frac{\eta^t}{\eta^i}\right)\frac{2Z_W^i}{Z_W^t + Z_W^i} = \frac{\left(\sqrt{\varepsilon_r^i\varepsilon_r^t}\right)2k_z^i}{\varepsilon_r^i k_z^t + \varepsilon_r^t k_z^i} \quad (3.2)$$

where Γ and Υ refer to the reflection and the transmission coefficients, respectively, the super-index I refers to current travelling wave parameters, the super-indices i, r and t on the E_o or H_o fields refer to the incident, reflected and transmitted fields, respectively, the super-indices i and t on η, ε_r, k_z and Z_W refer to the incidence and the transmission regions, respectively, $\eta^l = \sqrt{\mu_o/(\varepsilon_r^l\varepsilon_o)}$ is the intrinsic impedance of the region l and $Z_W^l = k_z^l/(\omega\varepsilon_r^l\varepsilon_o)$ is the wave impedance of the region l with $l = \{i, t\}$.

These expressions agree with References [9, p. 514], [15, p. 454] and [16, p. 314]. Note that some authors (see References [7, p. 152, Equation (4.207)] and [48, p. 59, Equation (2.144d)]) show a difference in sign for the expression of the voltage reflection coefficient of the TM^z mode. The reason for this difference in sign owes to the difference[3] in defining the direction for which

---

[2]In Reference [18, p. 415, Equation (70)] the expression given for the transmission coefficient of the TM^z mode is wrong! In fact, it corresponds to the expression given in [14, p. 543, equation (9.100b)] but the latter defines the transmission coefficient in terms of the tangential (to the interface) components whereas the former claims to define it in terms of the whole field.

[3]Yet other authors ignore this distinction and end up missing the minus sign that would be required according to their figures (see References [17, p. 248, equation (7.76)] and [18, p. 415, Equation (69)]).

$\vec{E}_o$ is positive (e.g. compare Figure 12.5 in [9, p. 511] or Figure 10.16 in [15, p. 454] or Figure 8.16 in [16, p. 314] with Figure 4.5 in [7, p. 147] or Figure 2.25 in [48, p. 57]). In the former three figures, the positive direction of $\vec{E}$ is defined as per a transmission line, i.e. the positive direction of $\vec{E}$ is that whose tangential (to the interface) component of $\vec{E}$ points in the same direction for the incident, reflected and transmitted waves. This makes identical the reflection coefficients of the parallel and the perpendicular polarizations at normal incidence. In the latter two figures, however, the positive direction of $\vec{E}$ is defined by the $\hat{\theta}$ or $\hat{\phi}$ unit vectors of the spherical coordinate system whose z axis is normal to the interface. This makes differ by a minus sign the reflection coefficients of the parallel and the perpendicular polarizations at normal incidence with the outward convention (but not with the inward convention). To distinguish between these two definitions, different matrices are used herein. The matrices S and C correspond to the transmission line definition whereas the matrix $\mathcal{C}$ corresponds to the spherical coordinate definition[4] with the outward convention.

For the TE^z (or TM^y) mode, i.e. perpendicular polarization, one obtains:

$$\Gamma^V = \frac{E_o^r}{E_o^i} = \frac{E_t^r}{E_t^i} = \frac{Z_W^t - Z_W^i}{Z_W^t + Z_W^i}$$

$$\implies \frac{E_o^r}{E_o^i} = +\Gamma^V = \frac{Z_W^t - Z_W^i}{Z_W^t + Z_W^i} = \frac{k_z^i - k_z^t}{k_z^i + k_z^t} \tag{3.3}$$

$$\Upsilon^V = \frac{E_o^t}{E_o^i} = \frac{E_t^t}{E_t^i} = \frac{2Z_W^t}{Z_W^t + Z_W^i}$$

$$\implies \frac{E_o^t}{E_o^i} = \Upsilon^V = \frac{2Z_W^t}{Z_W^t + Z_W^i} = \frac{2k_z^i}{k_z^i + k_z^t} \tag{3.4}$$

where the super-index V refers to voltage travelling wave parameters and $Z_W^l = (\omega\mu_o)/k_z^l$ is the wave impedance of the region l with $l = \{i, t\}$.

3.1.2 Lossy media

The case of lossy media is obtained from the case of lossless media by merely generalizing the concept of the wave impedance (see Reference [38, Equations (9a) and (9b)]), and by taking the permittivities to be complex-valued.

---

[4]In Reference [13], the distinction between the two definitions was embodied in Equation (2.3) on p. 38, which shows $S_{ii}^{EE}(X, Y) = -S_{ii}^{EE}(E, H)$ with the superscript E referring, here, to the E-mode, i.e. the TM^z mode. Note, however, that on p. 34, the matrices S and C used the spherical coordinate definition whereas on pp. 40-43, the matrices S and C used the transmission line definition. Fortunately, the conclusions in [13] remain unaffected by this distinction, because comparisons between S and C matrices were made while both matrices used the same definition.

The Fresnel equations are said to be still valid (References [84, p. 501] and [7, p. 171]) but they become complex-valued. Furthermore, the scattered $\vec{E}$ and $\vec{H}$ fields acquire[5] a component parallel to the direction of the phase wavefront propagation vector $\vec{\beta}$ (References [84, p. 502] and [4, p. 422]). The C scattering matrix written in terms of the TM^z and TE^z modes as given by Fresnel equations, however, determines only the transverse $\vec{E}$ components that are in the $\hat{\theta}_\beta$ and $\hat{\phi}_\beta$ directions, respectively. The longitudinal component that lies in the direction of the phase wavefront propagation vector $\vec{\beta}$ is not taken into account by the C scattering matrix. Hence, it might not be sufficient to rely on the analytical continuation of the Fresnel equations in the complex plane to account fully for all the effects that are due to the presence of losses in the slab.

For the TM^z (or TE^y) polarization, one obtains:

$$Z_W = \frac{\gamma_z}{j\omega\varepsilon} = \frac{\alpha\cos(\xi+\rho) + j\beta\cos(\xi)}{j\omega\varepsilon} \tag{3.5}$$

$$R_{PARALLEL} = \frac{E_o^r}{E_o^i} = \frac{Z_W^t - Z_W^i}{Z_W^t + Z_W^i} = \frac{\varepsilon_r^i\gamma_z^t - \varepsilon_r^t\gamma_z^i}{\varepsilon_r^i\gamma_z^t + \varepsilon_r^t\gamma_z^i} \tag{3.6}$$

$$T_{PARALLEL} = \frac{E_o^t}{E_o^i} = \left(\frac{\eta^t}{\eta^i}\right)\frac{2Z_W^i}{Z_W^t + Z_W^i} = \frac{\left(\sqrt{\varepsilon_r^i\varepsilon_r^t}\right)2\gamma_z^i}{\varepsilon_r^i\gamma_z^t + \varepsilon_r^t\gamma_z^i} \tag{3.7}$$

For the TE^z (or TM^y) polarization, one obtains:

$$Z_W = \frac{j\omega\mu}{\gamma_z} = \frac{j\omega\mu}{\alpha\cos(\xi+\rho) + j\beta\cos(\xi)} \tag{3.8}$$

$$R_{PERPENDICULAR} = \frac{E_o^r}{E_o^i} = \frac{Z_W^t - Z_W^i}{Z_W^t + Z_W^i} = \frac{\gamma_z^i - \gamma_z^t}{\gamma_z^i + \gamma_z^t} \tag{3.9}$$

$$T_{PERPENDICULAR} = \frac{E_o^t}{E_o^i} = \frac{2Z_W^t}{Z_W^t + Z_W^i} = \frac{2\gamma_z^i}{\gamma_z^i + \gamma_z^t} \tag{3.10}$$

Clearly, the generalized Fresnel equations for lossy media reduce to the ordinary Fresnel equations when both $\alpha_1 = 0$ and $\alpha_2 = 0$, i.e. for lossless media. Note also that Equations (3.6), (3.7), (3.9) and (3.10) are independent of $k_o = 2\pi/\lambda_o$ where λ_o refers to the wavelength in free space. Therefore,

---

[5]Comparison between simulation results for lossy ($\sigma = 0.15$ S/m) and lossless slabs suggests the presence of an E field component along the direction of the phase wavefront propagation vector $\vec{\beta}$, as shown by a slight shift in the direction of both axes of the polarization ellipses at various points in the incidence aperture within the slab. In the numerical simulations, the scattered field of even the lossless slab was elliptically polarized because the Maxwellian excitation beam was itself elliptically polarized. This situation makes it difficult to assess the phase relationship between the E field components parallel and perpendicular to $\vec{\beta}$.

these equations are frequency independent as long as the various complex permittivities are frequency independent. This observation has practical importance. Rigorously, the Kronig-Kramer dispersion relations force the permittivity or permeability to be frequency dependent if the material has electric or magnetic losses, respectively. However, the permittivity and permeability can be approximated as being constant over a frequency band of interest when the material losses are small enough.

3.1.3 GSM

The GSM for each interface is defined as follows:

$$
\begin{pmatrix} (E_o^s)_1^H \\ (E_o^s)_1^E \\ (E_o^s)_2^H \\ (E_o^s)_2^E \end{pmatrix} = \underbrace{\begin{pmatrix} C_{11}^{HH} & C_{11}^{HE} & C_{12}^{HH} & C_{12}^{HE} \\ C_{11}^{EH} & C_{11}^{EE} & C_{12}^{EH} & C_{12}^{EE} \\ C_{21}^{HH} & C_{21}^{HE} & C_{22}^{HH} & C_{22}^{HE} \\ C_{21}^{EH} & C_{21}^{EE} & C_{22}^{EH} & C_{22}^{EE} \end{pmatrix}}_{C} \begin{pmatrix} (E_o^i)_1^H \\ (E_o^i)_1^E \\ (E_o^i)_2^H \\ (E_o^i)_2^E \end{pmatrix}
\tag{3.11}
$$

where:

- the superscripts E and H refer[6] to the E^y and H^y modes, i.e. the perpendicular and the parallel polarizations, respectively. When material losses are present, the elements of the scattering matrix for an interface become, in general, complex-valued for the TE^z and TM^z modes but the GSM formalism remains valid if the modes have all the essential non-zero field components to represent the whole electromagnetic field. Thus the modes in a lossy transmission medium would not be purely TEM due to the presence of an E field component in the direction of propagation (see Reference [84, p. 502]).

---

[6]The TM^z and TE^z waves are sometimes referred to as the E-type and H-type waves, respectively. However, in this report, the superscripts E and H refer merely to the field that has only a y component. Hence, a pure TM^z wave has only E_x, H_y and E_z and is called herein a TE^y or H^y wave or a wave with a polarization parallel to the incidence plane. Similarly, a pure TE^z wave has only H_x, E_y and H_z and is called herein a TM^y or E^y wave or a wave with a polarization perpendicular to the incidence plane. The superscript for the TE and TM modes varies depending on whether the emphasis is on the normal of the interface or the normal of the incidence plane. Note that when a plane wave is a linearly polarized TEM plane waves, there are truly only two essential non-zero field components. The only reason why the TE and TM modes show up with three instead of just two non-zero field components is that $\hat{x}$, $\hat{y}$ and $\hat{z}$ of the coordinate system do not coincide with $\hat{E}$, $\hat{H}$ and $\hat{k}$. However, when a plane wave is elliptically polarized due, for instance, to the presence of material losses, there are truly three essential non-zero field components because the wave is no longer purely TEM (see References [84, p. 502] and [4, p. 422]).

- the superscripts s and i indicate the scattered (reflected or transmitted) and incident waves, respectively;

- the subscripts 1 and 2 refer to the regions on the left and on the right of the interface under study, respectively, as shown in Figure 2.1;

- the subscript o indicates that the field is the whole field rather than just its component tangential to the interface.

Since an interface between two dielectrics does not produce any cross-polarized field, all cross-polarization terms of the GSM for a dielectric interface are zero. By substituting the region number for the super-indices i and t in Equations (3.6), (3.7), (3.9) and (3.10), the GSM for a dielectric interface becomes:

$$C = \begin{pmatrix} \frac{\varepsilon_r^{\#1}\gamma_z^{\#2} - \varepsilon_r^{\#2}\gamma_z^{\#1}}{\varepsilon_r^{\#1}\gamma_z^{\#2} + \varepsilon_r^{\#2}\gamma_z^{\#1}} & 0 & \frac{2\sqrt{\varepsilon_r^{\#2}\varepsilon_r^{\#1}}\gamma_z^{\#2}}{\varepsilon_r^{\#2}\gamma_z^{\#1} + \varepsilon_r^{\#1}\gamma_z^{\#2}} & 0 \\ 0 & \frac{\gamma_z^{\#1} - \gamma_z^{\#2}}{\gamma_z^{\#1} + \gamma_z^{\#2}} & 0 & \frac{2\gamma_z^{\#2}}{\gamma_z^{\#1} + \gamma_z^{\#2}} \\ \frac{2\sqrt{\varepsilon_r^{\#1}\varepsilon_r^{\#2}}\gamma_z^{\#1}}{\varepsilon_r^{\#1}\gamma_z^{\#2} + \varepsilon_r^{\#2}\gamma_z^{\#1}} & 0 & \frac{\varepsilon_r^{\#2}\gamma_z^{\#1} - \varepsilon_r^{\#1}\gamma_z^{\#2}}{\varepsilon_r^{\#2}\gamma_z^{\#1} + \varepsilon_r^{\#1}\gamma_z^{\#2}} & 0 \\ 0 & \frac{2\gamma_z^{\#1}}{\gamma_z^{\#1} + \gamma_z^{\#2}} & 0 & \frac{\gamma_z^{\#2} - \gamma_z^{\#1}}{\gamma_z^{\#2} + \gamma_z^{\#1}} \end{pmatrix}$$

$$(3.12)$$

The expression for the matrix C can be simplified as follows:

$$C = \begin{pmatrix} C_A & gC_B \\ C_B & -C_A \end{pmatrix} \tag{3.13}$$

where:

$$C_A = \begin{pmatrix} A^H & 0 \\ 0 & A^E \end{pmatrix}$$

$$C_B = \begin{pmatrix} B^H & 0 \\ 0 & B^E \end{pmatrix}$$

$$g = \frac{\gamma_z^{\#2}}{\gamma_z^{\#1}}$$

49

$$A^H = \frac{\varepsilon_r^{\#1}\gamma_z^{\#2} - \varepsilon_r^{\#2}\gamma_z^{\#1}}{\varepsilon_r^{\#1}\gamma_z^{\#2} + \varepsilon_r^{\#2}\gamma_z^{\#1}}$$

$$A^E = \frac{\gamma_z^{\#1} - \gamma_z^{\#2}}{\gamma_z^{\#1} + \gamma_z^{\#2}}$$

$$B^H = \frac{2\sqrt{\varepsilon_r^{\#1}\varepsilon_r^{\#2}}\gamma_z^{\#1}}{\varepsilon_r^{\#1}\gamma_z^{\#2} + \varepsilon_r^{\#2}\gamma_z^{\#1}}$$

$$B^E = \frac{2\gamma_z^{\#1}}{\gamma_z^{\#1} + \gamma_z^{\#2}}$$

The angles ξ_1 and ξ_2 as seen in Figure 2.1 are defined as the acute (i.e. interior) angles between the normal of the interface and the corresponding propagation vectors for the phase wavefronts $\vec{\beta_1}$ and $\vec{\beta_2}$ in regions 1 and 2, respectively. The angles ξ_1 and ξ_2 are general angles in that they are valid for describing the field behaviour at one interface without making reference to any particular coordinate system. When many interfaces are cascaded together, the transmission from one interface represents an incident wave applied onto the input port of the next interface in the cascade, and the reflection off the next interface in the cascade represents an incident wave applied onto the output port of the interface under study. The proper angular relationship between these propagation vectors could be taken into account explicitly by defining all angles with respect to a same reference direction, say the $+\hat{z}$ direction. However, owing to the facts that all angles are defined as acute angles with respect to the same line, i.e. the normal to all parallel interfaces, and that the scattering coefficients in Equation (3.12) do not depend on the sinus of the propagation angles, there is no need to define the angles with respect to a particular axis of a particular coordinate system. Therefore, in the rest of this document, γ_z will actually mean $|\gamma_z|$ in order to avoid using the the absolute value symbol on the various terms of the scattering coefficients (see Reference [13, pp. 40-42]).

Owing to the facts that all plane waves propagate in straight line between all interfaces, that the reflection angle has the same value as the incidence angle at a planar interface, and that all interfaces are planar and parallel, one obtains[7] $\xi_1^{II} = \xi_2^{I}$ in Figure 3.1. Furthermore, from reciprocity one knows that the propagation angles at an interface remain the same upon reversing the propagation direction of the waves. Thus, from the knowledge of the incidence angle ξ_2^{I} for the backward wave incident onto the interface from right to left, one obtains that the transmission angle for the multiply reflected wave that exits from the input side of the interface has the same value as the incidence angle for the forward wave incident onto the same

---

[7]The same comments can be made for the angles ρ_1 and ρ_2, and the angles ζ_1 and ζ_2, respectively.

interface from left to right. Consequently, the multiply reflected wave and the directly reflected wave propagate in the same direction and combine into a single reflection wave that exits from the input port of the interface at the propagation angle ξ_1^I. Consequently also, the scattering matrix is written for directions that are related by reciprocity. However, the matrix C in Equations (3.12) and (3.13) is not symmetrical even though the interface is a reciprocal device (see Reference [13, pp. 36,38]), and similarly for the $\mathcal{C}$ scattering matrix.

If the planar interfaces of a multilayer slab were not parallel, or more generally, if the scatterers confined entirely between the two infinite parallel z reference planes for which the scattering matrix was defined, were of arbitrary geometry, a backward wave would not, in general, trace back the propagation path of its corresponding forward wave as shown in Figure 3.1 for parallel interfaces. Hence, the two ports of the scattering matrix would no longer be in the same geometrical relationship. In the case of an arbitrarily shaped scatterer, a single incident plane wave would even give rise to a multitude of reflected and transmitted plane waves. The size of the scattering matrix would then need to be increased to include twice as many ports as there are different directions involved in the solution, with two orthogonal polarizations (hence two ports) per direction. However, if the scattering matrix were defined in terms of the tangential E field components of the waves at the two reference planes instead of the whole E field, only the $+z$ and the $-z$ directions would be relevant as the scattering matrix would then characterize an equivalent transmission line parallel to the z direction. These two directions would necessarily always be in the same geometrical relationship as with plane waves propagating normally to parallel interfaces. Nevertheless, the size of the scattering matrix would still need to be increased so that two ports corresponded to every different field structure (i.e. field mode)[8] , with two orthogonal polarizations (hence two ports) per field mode. Hence, the number of ports in the scattering matrix is not determined by the number of reference planes, but by the number of different propagating directions or equivalently, by the number of different field modes on a $z = cte$ plane (see

---

[8]Waves propagating at different oblique angles cast on a $z = cte$ plane different mode patterns according to their respective $\gamma_x = j\beta_x$ and $\gamma_y = j\beta_y$ values (with $-\infty < \{\beta_x, \beta_y\} < +\infty$). To each mode pattern corresponds a transverse spectrum but all transverse spectra (and hence, the plane wave spectrum as a whole) merely propagate (see Reference [41, p. 114]) along the z direction according to $e^{-\gamma_z z}$ where $\gamma_z = (\alpha_z + j\beta_z)$ with forward waves having $\{\beta_z, \alpha_z\} > 0$, and backward waves having $\{\beta_z, \alpha_z\} < 0$. For example, for the case that the scatterers consisted of a planar interface made from the juxtaposition of two isotropic media, with medium #1 being lossless and medium #2 being lossy, and the excitation being a uniform plane wave incident from the side of the lossless medium, we would have $\alpha_x^{\#1} = \alpha_y^{\#1} = \alpha_z^{\#1} = 0$, $\left(\beta_x^{\#1}\right)^2 + \left(\beta_y^{\#1}\right)^2 \leq \omega^2 \mu_1 \varepsilon_1$ and $\left(\beta_z^{\#1}\right)^2 = \omega^2 \mu_1 \varepsilon_1 - \left(\beta_x^{\#1}\right)^2 - \left(\beta_y^{\#1}\right)^2$ for both the incident and the reflected plane waves in medium #1, and $\alpha_x^{\#2} = \alpha_y^{\#2} = 0$, $\beta_x^{\#2} = \beta_x^{\#1}$, $\beta_y^{\#2} = \beta_y^{\#1}$, and $\gamma_z^{\#2}$ given by Equation (2.41) for the transmitted plane wave in medium #2.

Reference [40, pp. 20,35,63]).

3.1.4 Composite GSM from the scattering matrix propagator technique

The scattering matrix propagator technique can be applied to either the S, C or $\mathcal{C}$ matrices but not a mixture of them. The cascade connection shown in Figure 3.1 produces the following expressions written here in terms of S matrices but equally valid for C or $\mathcal{C}$ matrices (see Reference [40, pp. 82,121]):

$$
\begin{pmatrix} b_1^{H,I} \\ b_1^{E,I} \\ b_2^{H,I} \\ b_2^{E,I} \end{pmatrix} = \underbrace{\begin{pmatrix} S_{11}^{HH,I} & S_{11}^{HE,I} & S_{12}^{HH,I} & S_{12}^{HE,I} \\ S_{11}^{EH,I} & S_{11}^{EE,I} & S_{12}^{EH,I} & S_{12}^{EE,I} \\ S_{21}^{HH,I} & S_{21}^{HE,I} & S_{22}^{HH,I} & S_{22}^{HE,I} \\ S_{21}^{EH,I} & S_{21}^{EE,I} & S_{22}^{EH,I} & S_{22}^{EE,I} \end{pmatrix}}_{S^I} \begin{pmatrix} a_1^{H,I} \\ a_1^{E,I} \\ a_2^{H,I} \\ a_2^{E,I} \end{pmatrix}
\tag{3.14}
$$

$$
\begin{pmatrix} b_1^{H,II} \\ b_1^{E,II} \\ b_2^{H,II} \\ b_2^{E,II} \end{pmatrix} = \underbrace{\begin{pmatrix} S_{11}^{HH,II} & S_{11}^{HE,II} & S_{12}^{HH,II} & S_{12}^{HE,II} \\ S_{11}^{EH,II} & S_{11}^{EE,II} & S_{12}^{EH,II} & S_{12}^{EE,II} \\ S_{21}^{HH,II} & S_{21}^{HE,II} & S_{22}^{HH,II} & S_{22}^{HE,II} \\ S_{21}^{EH,II} & S_{21}^{EE,II} & S_{22}^{EH,II} & S_{22}^{EE,II} \end{pmatrix}}_{S^{II}} \begin{pmatrix} a_1^{H,II} \\ a_1^{E,II} \\ a_2^{H,II} \\ a_2^{E,II} \end{pmatrix}
\tag{3.15}
$$

$$
\begin{pmatrix} a_2^{H,I} \\ a_2^{E,I} \end{pmatrix} = \underbrace{\begin{pmatrix} e^{-\gamma_{-z}^H d} & 0 \\ 0 & e^{-\gamma_{-z}^E d} \end{pmatrix}}_{P_-} \begin{pmatrix} b_1^{H,II} \\ b_1^{E,II} \end{pmatrix}
\tag{3.16}
$$

$$
\begin{pmatrix} a_1^{H,II} \\ a_1^{E,II} \end{pmatrix} = \underbrace{\begin{pmatrix} e^{-\gamma_{+z}^H d} & 0 \\ 0 & e^{-\gamma_{+z}^E d} \end{pmatrix}}_{P_+} \begin{pmatrix} b_2^{H,I} \\ b_2^{E,I} \end{pmatrix}
\tag{3.17}
$$

$$
\begin{pmatrix} b_1^{H,I} \\ b_1^{E,I} \\ b_2^{H,II} \\ b_2^{E,II} \end{pmatrix} = \underbrace{\begin{pmatrix} S_{11}^{HH,\Sigma} & S_{11}^{HE,\Sigma} & S_{12}^{HH,\Sigma} & S_{12}^{HE,\Sigma} \\ S_{11}^{EH,\Sigma} & S_{11}^{EE,\Sigma} & S_{12}^{EH,\Sigma} & S_{12}^{EE,\Sigma} \\ S_{21}^{HH,\Sigma} & S_{21}^{HE,\Sigma} & S_{22}^{HH,\Sigma} & S_{22}^{HE,\Sigma} \\ S_{21}^{EH,\Sigma} & S_{21}^{EE,\Sigma} & S_{22}^{EH,\Sigma} & S_{22}^{EE,\Sigma} \end{pmatrix}}_{S^{\Sigma}} \begin{pmatrix} a_1^{H,I} \\ a_1^{E,I} \\ a_2^{H,II} \\ a_2^{E,II} \end{pmatrix}
\tag{3.18}
$$

where d is the separation distance between two consecutive parallel planar interfaces. For convenience, the matrix S^Σ is written in terms of its four submatrices S_{ij}^Σ with $\{i,j\} = \{1,2\}$, and similarly for matrices S^I and S^{II}. From simple matrix manipulations, the submatrices S_{ij}^Σ of the composite scattering matrix S^Σ are obtained (see [33, p. 419]) as:

$$
\begin{aligned}
S_{11}^\Sigma &= S_{11}^I + S_{12}^I G_2 S_{11}^{II} P_+ S_{21}^I \\
S_{12}^\Sigma &= S_{12}^I G_2 S_{12}^{II} \\
S_{21}^\Sigma &= S_{21}^{II} G_1 S_{21}^I \\
S_{22}^\Sigma &= S_{22}^{II} + S_{21}^{II} G_1 S_{22}^I P_- S_{12}^{II}
\end{aligned}
\tag{3.19}
$$

where:

$$
\begin{aligned}
G_1 &= (P_+^{-1} - S_{22}^I P_- S_{11}^{II})^{-1} \\
G_2 &= (P_-^{-1} - S_{11}^{II} P_+ S_{22}^I)^{-1}
\end{aligned}
\tag{3.20}
$$

with $\gamma_z = \alpha \cos(\xi + \rho) + j\beta \cos(\xi)$ in each respective medium. When $\gamma_{+z} = \gamma_{-z}$, the above expressions become equivalent to those given by Redheffer in Reference [39, Equation 20, p. 10] for the specific case of $d = 0$, and by Kerns in Reference [40, Equations (2.11)-(2.14), p. 84] for the general case. However, the expression for S_{21}^Σ reported by Cwik and Mittra in References [10, 12] as $S_{\gamma\alpha}^\Sigma$ contains the same two typographical errors. $S_{\gamma\alpha}^\Sigma$ should read as being equal to $S_{\gamma\beta_2} G_1 S_{\beta_1\alpha}$ instead of $S_{\alpha\beta_2} G_1 S_{\beta_2\alpha}$. Redheffer refers to the above matrix operation as the star product of scattering matrices in contrast to the regular matrix product of the corresponding transmission (or ABCD) matrices [39, p. 13].

When there is no coupling between the TE$_z$ and TM$_z$ modes, $S_{ij}^{pq,\Sigma} = 0$ for $p \neq q$ and the cascade system reduces to two separate but simpler cascade systems, one for each mode.

For a cascade system consisting of N-1 interfaces separating N regions, the above procedure can be repeated N-2 times to reduce the N-1 scattering matrices to a single matrix that corresponds to the GSM for the overall structure. The reflection coefficient for the scatterer is obtained as the S_{11} element of the composite GSM for the cascade. According to Equation (3.19) for S_{11}^Σ, the S_{11} element of the composite GSM for a cascade of interfaces depends not only on the S_{11} element of every individual interface of the cascade but also on the other elements S_{12}, S_{21} and S_{22} of every individual interface of the cascade. This mutual coupling between the interfaces is needed in order to account properly for the presence of the multiple reflections existing between the interfaces. These multiple reflections could not be taken into account by the scattering matrix of any individual interface because the scattering matrix for each interface was obtained with the interface being alone between two half-spaces, hence being isolated from any other interface.

The phases of both the reflection and the transmission coefficients for the overall cascade system are defined with respect to the reference planes of the first and last interfaces of the cascade, i.e. one reference plane is at the position of the interface separating regions 1 and 2, and the other reference plane is at the position of the interface separating regions N-1 and N. Note that when the media are lossless, the Fresnel coefficients are real-valued but nevertheless, the values of the composite scattering matrix for the entire slab are, in general, complex-valued due to matrices P_- and P_+ which account for the propagation delay through the slab.

The fact that the values of the scattering coefficients for a device in situ remain the same as the values when the device was being characterized in a reference environment whereby all the ports of the device were impedance matched, owes to the fact that the scattering coefficients are geometical parameters that are independent of external excitations. The fact that the scattering parameters can be of any use when the device is in situ in spite of the fact that the incoming and outgoing waves at the various ports of the devices are generally different when the device is in situ than when the device was characterized in a reference environment, owes to the fact that the system is linear.

One consequence of these two observations is that the cascading of two devices that have been characterized in a same reference environment, (e.g. 50 ohm transmission lines) is equivalent to embedding each device in its reference environment and letting shrink to zero the thickness of the reference environment (i.e. the length of the 50 ohm transmission line) that lies between the two devices (see [39, p. 28] and [19, pp. 21-22]). This property was used herein in a MATLAB program that computes the composite scattering matrix when two interfaces happen to coincide as a result of the discretization scheme of the structure.

If the devices were characterized in different reference environments, then an additional scattering matrix[9] like S in equation (3.12) would be introduced in the cascade to model the discontinuity created by butting the two different reference environments (see [44, pp. 178-179] with the series element $jX = 0$ or with the shunt element $jB = \infty$). This approach can be used to model a two-layer slab standing in free space as a 3-layer slab whose middle layer is a zero-thickness layer of free space (see Reference [19, pp. 22-23]). This approach has the advantage of replacing the more difficult treatment of the interface between media #1 and #2 by the simpler treatment consisting of the cascade of two simpler interfaces A and B, separated by a zero-length free-space transmission line, whereby interface A lies between medium #1 and free space, and interface B lies between free space and medium #2.

---

[9]For a different treatment, see Reference [45].

If the structure is reciprocal, the scattering coefficients are purely geometrical parameters, i.e. their values do not[10] depend on the method of excitation or the number of waves present at the interface, and furthermore, the values of the transmission coefficients for an incidence from one side can be obtained from the values of transmission coefficients for the corresponding incidence from the other side. From Reference [13, p. 51], electromagnetic reciprocity can be stated as:

$$C_{vu}^{qp}(\theta^s = a, \phi^s = b, \theta^i = c, \phi^i = d) =$$
$$\epsilon C_{uv}^{pq}(\theta^s = 180° - c, \phi^s = 180° + d, \theta^i = 180° - a, \phi^i = 180° + b) \quad (3.21)$$

where C_{uv}^{pq} is the voltage scattering coefficients defined in terms of the whole fields, from medium v to medium u, with the polarization p of the scattered wave and the polarization q of the incident wave given by the $\hat{\theta}$ or $\hat{\phi}$ unit vectors of the spherical coordinate system[11] whose $\hat{z}$ axis is parallel to the normal of the interface, with θ and ϕ values specifying a propagation direction of the phase wavefront in the outwards[12] convention, $\epsilon = +1$ for $p = q$ and $\epsilon = -1$ for $p \neq q$, the angles $0° \leq \{a, c, \theta^i, \theta^s\} \leq 180°$ with $u = v$ if both a and c are larger or smaller than $90°$, and $0° \leq \{b, d, \phi^i, \phi^s\} \leq 360°$. The factor ϵ arises from the behaviour of the $\hat{\theta}$ and $\hat{\phi}$ unit vectors of the spherical coordinate system. The statement of reciprocity given in Equation (3.21) was developed for a scatterer embedded in a same host medium on both sides of the interface, i.e. for the medium being the same at both ports u and v. If the host medium is different in each half-space, refraction and impedance mismatch must also be taken into account. References [40, Equation (1-16) on p. 122], [42, p. 140], and [43, Equation (20)] indicate that γ_z^u and γ_z^v are then needed. The statement of reciprocity becomes[13] :

$$C_{vu}^{qp}(\theta^s = a, \phi^s = b, \theta^i = c, \phi^i = d) =$$
$$\epsilon \left| \frac{\gamma_z^v}{\gamma_z^u} \right| C_{uv}^{pq}(\theta^s = 180° - c, \phi^s = 180° + d, \theta^i = 180° - a, \phi^i = 180° + b)$$
$$(3.22)$$

---

[10]If at least one of the two media composing the interface is not reciprocal (e.g. a gyrotropic medium), then the method of excitation (e.g. the orientation and strength of an external static magnetic field) can modify the values of the constitutive parameters of the medium.

[11]The matrix C on p. 51 of Reference [13] corresponds to the matrix $\mathcal{C}$ herein. Recall that $C_{vv}^{EE} = R_{PERPENDICULAR}$ but $C_{vv}^{HH} = -R_{PARALLEL}$. At normal incidence, $R_{PARALLEL} = R_{PERPENDICULAR}$ and thus $C_{vv}^{HH} = -C_{vv}^{EE}$.

[12]In the outwards convention, the spherical coordinate angles θ^i and ϕ^i that specify the direction of $\vec{\beta}^i$ are those for $\vec{\beta}^i$ pointing outwards from the origin of the coordinate system.

[13]This agrees with Equation (3.13) and Reference [42, p. 140] but it seems to disagree with References [40, Equation (1-16) on p. 122] and [43, Equation (20)]. In these last two references, γ_z^u and γ_z^v seem to be interchanged.

The absolute value symbol on $\frac{\gamma_z^v}{\gamma_z^u}$ is needed only if γ_z is computed from the θ angle of the spherical coordinate system instead of the accute ξ angles of Figure 3.1. The absolute value symbol becomes the magnitude symbol if the ratio becomes complex-valued. Interestingly, Reference [43, Equations (20,35,36)] shows that reciprocity holds true for any two waves, i.e. for two propagating waves, or for two evanescent waves, or for one propagating wave and one evanescent wave. This is in agreement with the understanding that reciprocity is a property of the medium rather than a property of the waves.

The values of the reflection coefficients for an incidence from one side can also be obtained from the values of reflection coefficients for the corresponding incidence from the other side. From interchanging input and output media, and input and output propagation vectors in Equations (3.6) and (3.9), one obtains readily:

$$
\begin{gathered}
\mathcal{C}_{vv}^{qp}(\theta^s = a, \phi^s = b, \theta^i = c, \phi^i = d) = \\
-\mathcal{C}_{uu}^{pq}(\theta^s = 180° - c, \phi^s = 180° + d, \theta^i = 180° - a, \phi^i = 180° + b)
\end{gathered}
\tag{3.23}
$$

with $u \neq v$. Equation (3.23) agrees[14] also with Equation (3.13) as well as with Reference [19, p. 19]. Note that Equation (3.21) with $u = v$ and $p \neq q$ gives $\mathcal{C}_{vv}^{qp} = -\mathcal{C}_{vv}^{pq}$ which is not the same as $\mathcal{C}_{vv}^{qp} = -\mathcal{C}_{uu}^{pq}$ of Equation (3.23). Hence, Equation (3.23) is due not to reciprocity, but to reflection symmetry about the interface. Equation (3.23) also agrees with the behaviour of the reflection coefficient in transmission line theory, i.e. if $\Gamma_{2,1} \equiv (Z_2 - Z_1)/(Z_2 + Z_1)$, then $\Gamma_{1,2} = (Z_1 - Z_2)/(Z_1 + Z_2) = -\Gamma_{2,1}$.

Therefore, by introducing a zero-thickness layer between every medium layer of a slab with flat parallel faces, thus making free-standing every medium layer, and by using reciprocity (i.e. Equation (3.22)), reflection symmetry (i.e. Equation (3.23)) and longitudinal symmetry, the scattering matrices for the mth medium layer of thickness d standing in free space can be obtained from the knowledge of only $\mathcal{C}_{11}^I$ and $\mathcal{C}_{21}^I$ as follows:

---

[14]Note that Reference [28] gives the following two relations:

$$
\mathcal{C}_{11}^{HH}\mathcal{C}_{11}^{EE} - \mathcal{C}_{11}^{HE}\mathcal{C}_{11}^{EH} = \mathcal{C}_{22}^{HE}\mathcal{C}_{22}^{EH} - \mathcal{C}_{22}^{HH}\mathcal{C}_{22}^{EE}
\tag{3.24}
$$

$$
\mathcal{C}_{11}^{HH} + \mathcal{C}_{11}^{EE} = \mathcal{C}_{22}^{HH} - \mathcal{C}_{22}^{EE}
\tag{3.25}
$$

However, Equations (3.24) and (3.25) are not believed to be true, even for the simple case of an interface between two lossless isotropic media. For such an interface, $\mathcal{C}_{uu}^{pq} = 0$ for $p \neq q$ and from Equation (3.23), $\mathcal{C}_{vv}^{pp} = -\mathcal{C}_{uu}^{pp}$, hence we have $\mathcal{C}_{11}^{HH}\mathcal{C}_{11}^{EE} = \mathcal{C}_{22}^{HH}\mathcal{C}_{22}^{EE}$ instead of $\mathcal{C}_{11}^{HH}\mathcal{C}_{11}^{EE} = -\mathcal{C}_{22}^{HH}\mathcal{C}_{22}^{EE}$, and we have $(\mathcal{C}_{11}^{HH} + \mathcal{C}_{11}^{EE}) = -(\mathcal{C}_{22}^{HH} + \mathcal{C}_{22}^{EE})$ instead of $(\mathcal{C}_{11}^{HH} + \mathcal{C}_{11}^{EE}) = (\mathcal{C}_{22}^{HH} - \mathcal{C}_{22}^{EE})$.

$$
\mathcal{C}^I = \begin{pmatrix} R^{HH} & R^{HE} & +g\,T^{HH} & -g\,T^{HE} \\ R^{EH} & R^{EE} & -g\,T^{EH} & +g\,T^{EE} \\ T^{HH} & T^{HE} & -R^{HH} & -R^{HE} \\ T^{EH} & T^{EE} & -R^{EH} & -R^{EE} \end{pmatrix} \tag{3.26}
$$

$$
\mathcal{C}^{II} = \begin{pmatrix} -R^{HH} & -R^{HE} & T^{HH} & T^{HE} \\ -R^{EH} & -R^{EE} & T^{EH} & T^{EE} \\ +g\,T^{HH} & -g\,T^{HE} & R^{HH} & R^{HE} \\ -g\,T^{EH} & +g\,T^{EE} & R^{EH} & R^{EE} \end{pmatrix} \tag{3.27}
$$

where:

$$
g = \left| \frac{\gamma_z^{\#m}}{\gamma_z^{\#0}} \right|
$$

$$
\gamma_z^{\#0} = \sqrt{(\gamma^{\#0})^2 - (\gamma^{\#0} \sin \xi^i)^2} = j\omega\sqrt{\mu_o \varepsilon_o}\,\cos \xi^i
$$

$$
\gamma_z^{\#m} = \sqrt{(\gamma^{\#m})^2 - (\gamma^{\#0} \sin \xi^i)^2} = \sqrt{(\gamma^{\#m})^2 + \omega^2 \mu_o \varepsilon_o \sin^2 \xi^i}
$$

$$
(\gamma^{\#m})^2 = \vec{\gamma}^{\#m} \cdot \vec{\gamma}^{\#m} = -\omega^2 \mu^{\#m} \varepsilon^{\#m}
$$

The composite scattering matrix for the free-standing layer becomes:

$$
\mathcal{C}^\Sigma = \begin{pmatrix} R^{HH,\Sigma} & R^{HE,\Sigma} & T^{HH,\Sigma} & T^{HE,\Sigma} \\ R^{EH,\Sigma} & R^{EE,\Sigma} & T^{EH,\Sigma} & T^{EE,\Sigma} \\ T^{HH,\Sigma} & T^{HE,\Sigma} & R^{HH,\Sigma} & R^{HE,\Sigma} \\ T^{EH,\Sigma} & T^{EE,\Sigma} & R^{EH,\Sigma} & R^{EE,\Sigma} \end{pmatrix} \tag{3.28}
$$

which clearly satisfies reciprocity and longitudinal symmetry. The elements of the matrix can be obtained with the Matlab symbolic math toolbox. They are given in Appendix F. The scattering matrix of the multilayer slab is then obtained by cascading the scattering matrices of its layers in free-standing configuration.

This author confirmed numerically that the use of the scattering matrix propagator technique is fully equivalent to the use of the invariant imbedding method presented by Adams and Denman in Reference [19, pp. 22,29] or Weng Cho Chu in Reference [42, p. 140], and by Wait in Reference [5, p. 151], although the recursive schemes of the first two references appear to be different from the one of the third reference. That their recursive schemes are, in fact, equivalent to one another can be shown as follows. Consider the simplest problem of a slab of thickness d separating two half-spaces, thus forming three equivalent transmission lines with characteristic impedances

Z_n where n ranges from 1 to 3 from left to right. The slab is illuminated from the left side. The reflection coefficient at the interface that separates media 1 and 2 is written here as the instantaneous (or local) reflection coefficient

$$\Gamma_1 = \frac{Z_2 - Z_1}{Z_2 + Z_1}$$

rather than the steady-state (or global) reflection coefficient

$$\Gamma_{in} = \frac{Z_{in} - Z_1}{Z_{in} + Z_1}$$

where:

$$Z_{in} = Z_2 \frac{Z_3 + Z_2 \tanh(\gamma_z d)}{Z_2 + Z_3 \tanh(\gamma_z d)}$$

When using the instantaneous reflection coefficient, all multiply reflected waves are accounted for individually whereas when using the steady-state reflection coefficient, only two waves are deemed to exist in every medium, namely the forward propagating wave and the backward propagating wave. Both approaches are equivalent upon lumping together in every medium all the instantaneous waves travelling in a same direction. This results in the following mathematical identity (see Appendix A):

$$\frac{Z_{in} - Z_1}{Z_{in} + Z_1} = \frac{\Gamma_1 + \Gamma_3 e^{-2\gamma_z d}}{1 + \Gamma_1 \Gamma_3 e^{-2\gamma_z d}} \tag{3.29}$$

where:

$$\Gamma_3 = \frac{Z_3 - Z_2}{Z_3 + Z_2}$$

For a problem with N interfaces, the recursive scheme results from writing Z_{in_n} in terms of $Z_{in_{n+1}}$ as was done by Wait in Reference [5, Equation 4.171], or equivalently by Equation (3.29), from writing Γ_n in terms of Γ_{n+1}, as was done[15] by Adams and Denman in Reference [19, Equations (7.14), (7.18)]. Note that although the steady-state reflection coefficient is obtained as $(Z_{in} - Z_1)/(Z_{in} + Z_1)$, the steady-state transmission coefficient is not obtained as $2Z_{in}/(Z_{in} + Z_1)$; see Appendix A and References [5, Equations 4.172, 4.175] and [19, Equations 7.15, 7.19]. The reason for this difference lies in the fact that with the steady-state approach, the rest of the circuit lying beyond the interface where Z_{in} is computed, is effectively enclosed in a black box that does not give access to the output port where the knowledge of the transmitted wave is desired.

---

[15]Note that Adams and Denman's equations are written for the wave being incident from the right. Moreover, this author believes that their expressions given in Equations (7.7-7.10) remain valid in spite of errors in Equation (7.1) on page 11. Furthermore, it must be pointed out that Equations (7.9) and (7.10) are given for the parallel polarization in terms of the tangential (to the interface) electric field rather than the whole electric field.
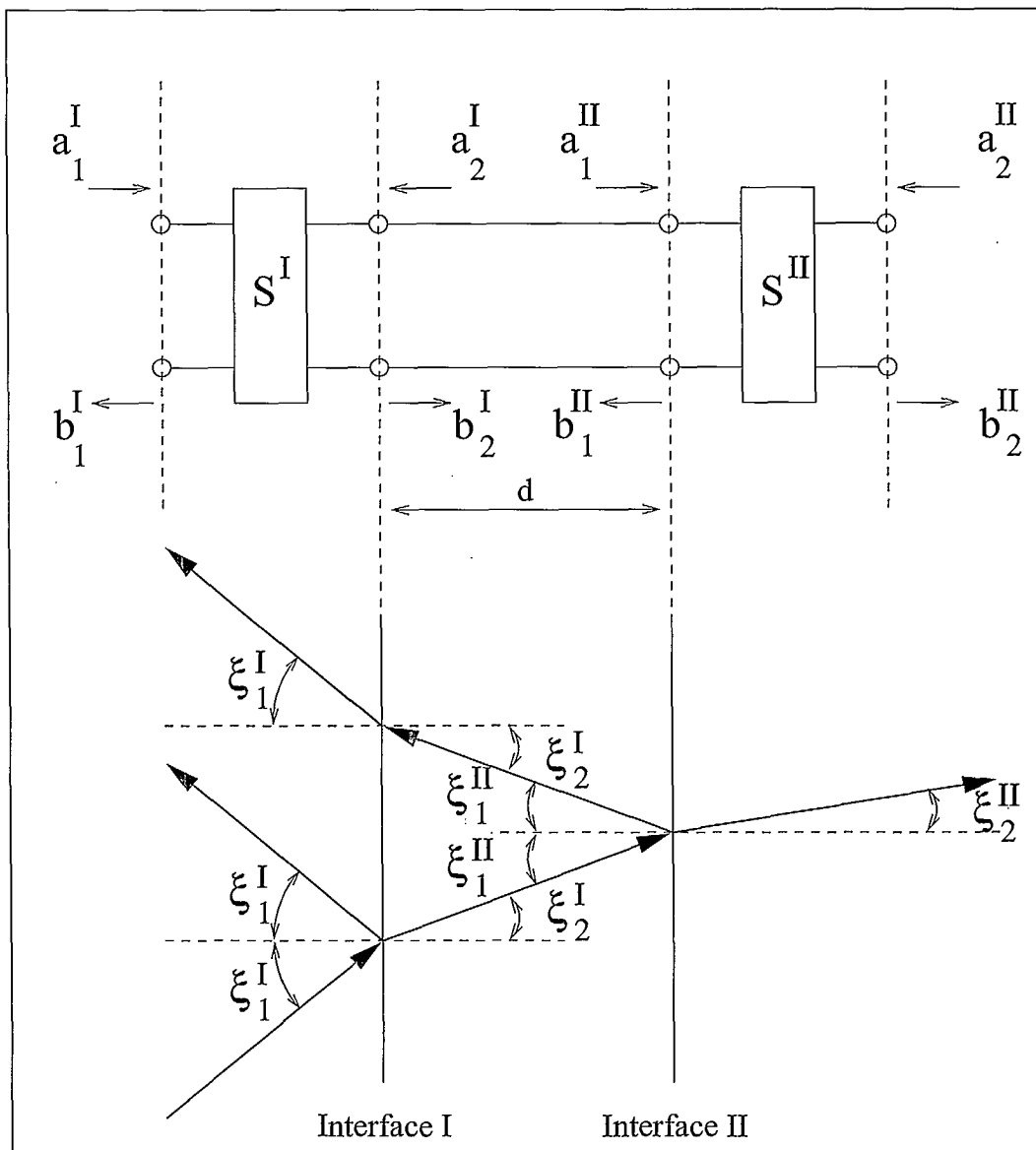
Figure 3.1: The cascade connection of two consecutive parallel planar interfaces separated by a distance d. Each scattering matrix models the scattering phenomenon at one interface while the transmission line models the wave propagation between the two interfaces. Note that the single term b_1^I represents the time-harmonic phasor summation of the two waves travelling leftwards from the interface I.

3.2 Modifications to the GSM for anisotropic media

In a lossless medium that is anisotropic in permittivity, $\vec{E}$ and $\vec{D}$ are no longer[16] parallel but $\vec{E}$, $\vec{D}$ and $\vec{k} \equiv \vec{\beta}$ are still coplanar[17] (see Reference [7, p. 189]), and $E_\perp = \vec{E} \cdot \hat{D} = (\omega^2 \mu_o / k_o^2) D = D / \varepsilon^{\text{eff}}$ (see Reference [75, p. 665]). The two $\vec{D}$ field vectors for the two eigenwaves of the medium are perpendicular[18] to one another and perpendicular to the propagation vector $\vec{k}$ (see Reference [7, pp. 189-190]). Hence, the polarization is now defined in terms of $\vec{D}$ instead of $\vec{E}$, and each eigenwave can be decomposed into a TE^z wave with $\hat{D} = \hat{\phi}_k$ and a TM^z wave with $\hat{D} = \hat{\theta}_k$. When the incidence plane is the xz plane, then $\hat{\phi}_k = \pm \hat{y}$ and the modes become E^y and H^y. Note, however, that even when the polarization is defined with respect to $\vec{D}$ instead of $\vec{E}$, the application of the boundary conditions at the interface between two media still invokes the tangential components of $\vec{E}$, not $\vec{D}$.

When the anisotropic medium is also lossy, the propagation vector becomes $\vec{\gamma} = (\vec{\alpha} + j\vec{\beta})$ and the vector $\vec{D}$ is, in general, no longer perpendicular to $\vec{\beta}$ (see Reference [75, p. 706]). However, the process of taking into account the conductivity σ by means of taking the permittivity ε to become complex-valued effectively replaces the term $\vec{J}_{\text{free}} = \sigma \vec{E}$ by 0 in the curl equation for $\vec{H}$, and replaces, via the continuity equation, the charge density ρ_{free} by 0 in the divergence equation for $\vec{D}$. This latter replacement leads to $(\vec{\gamma} \cdot \vec{D}) = 0$ **without** implying that $\vec{\gamma}$ is orthogonal to $\vec{D}$ because $\vec{\gamma}$ and $\vec{D}$ are now complex-valued vectors whose real and imaginary vectors point, in general, in different directions (see Reference [4, p. 403]). Hence, $\vec{D} = (\vec{D}_R + j\vec{D}_I)$ and $\hat{D}$ is, in general, elliptically polarized[19] . The two eigenwaves with polarizations $\vec{D}'$ and $\vec{D}''$ are no longer necessarily such that $(\hat{D}' \cdot \hat{D}'') = 0$ (see Appendix E). However, the presence of losses does not prohibit the decomposition of a wave into pure TE^u and TM^u waves where $\hat{u} = (\hat{\alpha} \times \hat{\beta})$ is the direction for which the fields have no spatial variation[20] , provided that the polarization[21] in the anisotropic medium is defined in terms

---

[16]For the ordinary wave in a uniaxial medium, $\vec{E}$ and $\vec{D}$ are still parallel as in any isotropic medium.

[17]It is interesting to note that although ε_x, ε_y and ε_z can take any values, E_x, E_y and E_z cannot take any values because $\vec{E} = (E_x \hat{x} + E_y \hat{y} + E_z \hat{z})$ must remain confined to the plane containing $\vec{k}$ and $\vec{D}$.

[18]Section E.1.4 shows that this is certainly the case for uniaxial media but not for biaxial media.

[19]Similarly, $(\vec{\gamma} \cdot \vec{H}) = 0$ and due to the presence of losses, $\vec{H}$ could also be a complex-valued vector $\vec{H} = (\vec{H}_R + j\vec{H}_I)$ that is elliptically polarized (see References [75, p. 706], [4, p. 422] and [77]).

[20]See References [4, pp. 422-423], [85, p. 31, problem 1.3] and [77, p. 584].

[21]When the medium is lossless and anisotropic, $\vec{E}$ acquires a component parallel to $\vec{\beta}$

of $\vec{D}$ instead of $\vec{E}$. According to the case of practical importance presented in Section 2.4.1, we know that the amplitude wavefront propagation vector $\vec{\alpha}$ in the lossy anisotropic medium would be normal to the interfaces if the incidence medium were lossless and the incident plane wave were uniform. Furthermore, from phase matching at the interface, we know that the phase wavefront propagation vector $\vec{\beta}$ in the anisotropic medium always lies in the incidence plane. Therefore, under these conditions, $\hat{u} = (\hat{\alpha} \times \hat{\beta})$ is normal to the incidence plane and the eigenwaves can still be decomposed into pure TE^u and TM^u waves, provided that the polarization in the lossy anisotropic medium refers to $\vec{D}$ instead of $\vec{E}$. If the incidence plane is the xz plane, then $\hat{u} = \hat{y}$.

If the anisotropic medium is uniaxial, there is only one optic axis and the medium is characterized by a transverse[23] permittivity value that is different from the longitudinal permittivity value. The two eigenwaves of the uniaxial medium have $\vec{D}$ or $\vec{H}$ perpendicular to the single optic axis. The propagation vectors $\vec{\alpha}$ and $\vec{\beta}$ take different complex values for each eigenwave (see Reference [46, Appendix]) since each eigenwave (i.e. the ordinary and the extraordinary waves) sees a different effective permittivity. The ordinary wave sees the transverse permittivity while the extraordinary wave sees a mixture of the transverse and the longitudinal permittivities (this inter-

---

due to the anisotropy of the medium. When the medium is lossy and isotropic, $\vec{E}$ also acquires a component parallel to $\vec{\beta}$ due to the losses of the medium (see Reference [84, p. 502]). However, the difference between these two cases is significant: in the lossless anisotropic case, the polarization of $\vec{E}$ remains linear, i.e. the component of $\vec{E}$ parallel to $\vec{\beta}$ remains in phase with the component of $\vec{E}$ perpendicular to $\vec{\beta}$; in the lossy isotropic case, the polarization of $\vec{E}$ is elliptical[22] because the component of $\vec{E}$ parallel to $\vec{\beta}$ is not perfectly in-phase with the component of $\vec{E}$ perpendicular to $\vec{\beta}$. When the medium is both lossy and anisotropic, $\vec{D}$ is also elliptically polarized.

If the C scattering matrix based on using $\hat{\theta}_\beta$ and $\hat{\phi}_\beta$ to define the polarization of waves does not take into account the component of $\vec{E}$ (or $\vec{D}$) that is parallel to $\vec{\beta}$, then why should the TE and TM polarizations be defined in terms of $\vec{D}$ instead of $\vec{E}$ for a lossless anisotropic scatterer, but remain defined in terms of $\vec{E}$ for a lossy isotropic scatterer? Or put another way, why should the use of the C scattering matrix provide the correct solution when the phase difference between the component of $\vec{E}$ (or $\vec{D}$) that is parallel to $\vec{\beta}$ and the component of $\vec{E}$ (or $\vec{D}$) that is perpendicular to $\vec{\beta}$ was $\pm 90°$ but not so when the phase difference was $0°$ or $\pm 180°$?

In the case of the lossless anisotropic medium, it is clear that there is no loss of information (see Reference [7, pp. 190-195]) in characterizing the propagation phenomenon at the interface by using $\vec{D}$ instead of $\vec{E}$ in the anisotropic medium. Since $\hat{D}$ is perpendicular to $\vec{\beta}$, $\vec{D}$ can be decomposed into components along $\hat{\theta}_\beta$ and $\hat{\phi}_\beta$. Thus, it is a natural to use $\vec{D}$ instead of $\vec{E}$ for the elements of the C scattering matrix that pertain to the anisotropic medium. In the case of the lossy medium, however, there would be some loss of information if the C scattering matrix did not take into account the component of either $\vec{E}$ or $\vec{D}$ that was parallel to $\vec{\beta}$. Thus, perhaps we should not expect to obtain the exact solution from using the C scattering matrix with lossy media.

[23]The label "transverse" refers here to any direction perpendicular to the optic axis, and the label "longitudinal" refers here to a direction parallel to the optic axis.

pretation stems from the behaviour of the phase velocity in Reference [49, pp. 359-360]). Either the incidence polarization (defined with reference to the incidence plane) could be decomposed in a mixture of the two eigenpolarizations of the anisotropic medium (see References [46], [47, p. 106] and [48, p. 158]), or conversely, the two eigenwaves of the anisotropic medium could be decomposed into TE^z and TM^z modes defined in terms of $\vec{D}$ instead of $\vec{E}$. However, for lossless[24] uniaxial media with the optic axis parallel to the normal of the interfaces, the following comments apply:

1. the superscript E refers to both the eigenpolarization with $\vec{E}$ and $\vec{D}$ perpendicular to the optic axis, and to the incidence polarization with $\vec{E}$ and $\vec{D}$ perpendicular to the incidence plane, i.e. $\hat{E} = \hat{D} = \hat{\phi}_k$. Similarly, the superscript H refers to both the eigenpolarization with $\vec{H}$ perpendicular to the optic axis, and to the incidence polarization with $\vec{E}$ and $\vec{D}$ parallel to the incidence plane, i.e. $\hat{D} = \hat{\theta}_k$ but $\hat{E} \neq \hat{D}$. Thus, the modal decomposition of the electromagnetic field in TE^z and TM^z modes remains valid (see References [50, p. 170], [51] and [38]).

2. no coupling arises between the ordinary wave of one layer and the extraordinary wave of an adjacent layer, and thus, each wave (i.e. ordinary or extraordinary) can be seen to propagate independently of the other wave (i.e. extraordinary or ordinary) throughout the entire cascade of layers (see References [53] and [27]).

When the medium is uniaxial with its optic axis parallel or perpendicular to the incidence plane, no coupling arises between TE^z and TM^z modes (i.e. $\Gamma_{12} = \Gamma_{21} = 0$ in Reference [7, pp. 239-245]) in the isotropic medium from which the plane wave is incident. Hence, the reflected plane wave has then the same mode as the incident plane wave. However, this is not necessarily the case for the transmitted plane wave because $T_{12} = T_{21} = 0$ in Reference [7, pp. 239-245] means that there is no coupling between the TE^z or TM^z wave incident from the free-space side, and one of the two eigenwaves in the transmission medium. Since each eigenwave in the anisotropic medium is, in general, a mixture of TE^z and TM^z waves defined in terms of $\vec{D}$, the expressions $T_{12} = T_{21} = 0$ does not imply that there is no coupling between TE^z and TM^z waves in the anisotropic medium. Consequently, when the reflected plane wave has the same mode as the incident plane wave, the amplitude matching of the tangential E and H field components at the interface forces the cross-polarization[25] mode of one eigenwave to be cancelled

---

[24]When the uniaxial medium becomes lossy, the vector $\vec{D}$ becomes a complex-valued vector and elliptically polarized. These comments would no longer apply rigorously.

[25]The cross-polarization mode of an eigenwave is defined here with respect to the polarization mode of the incident plane wave, i.e. the cross-polarization mode is TE^z if the incident plane wave is TM^z, and TM^z if the incident plane wave is TE^z.

by the cross-polarization mode of the other eigenwave at the interface in the anisotropic medium. Since Fresnel equations are valid only for zero cross-polarization, Fresnel equations do not necessarily remain valid even when the medium is uniaxial with its optic axis parallel or perpendicular to the incidence plane. In fact, it turns out that Fresnel equations remain valid only when the optic axis is normal to the interface, provided that the permittivity value used in Fresnel equations is that seen by the $\vec{D}$ vector "in the interface" (see next sections).

The use of the scattering matrix propagator technique requires the knowledge of the scattering coefficients for incidence from each side of the interface. When the optic axis of a uniaxial medium is normal to the interface, the ordinary wave is equivalent to a TE^z wave with $\hat{D} = \hat{\phi}_k = \pm\hat{y}$ and $\hat{H} = \hat{\theta}_k$, and the extraordinary wave is equivalent to a TM^z wave with $\hat{D} = \hat{\theta}_k$ and $\hat{H} = -\hat{\phi}_k = \mp\hat{y}$. Hence, a TE^z wave incident from the side of the isotropic medium gives rise only to the ordinary wave in the uniaxial medium, and a TM^z wave incident from the side of the isotropic medium gives rise only to the extraordinary wave in the uniaxial medium. From reciprocity, the ordinary wave incident from the side of the uniaxial medium gives rise only to the TE^z wave in the isotropic medium, and the extraordinary wave incident from the side of the uniaxial medium gives rise only to the TM^z wave in the isotropic medium. Therefore, it is easy to see that in this case as in the case of a planar interface between two isotropic media (see Equation (3.12)), the expressions for the scattering coefficients when the incidence is from the uniaxial medium can be obtained simply by interchanging input and output media, and input and output propagation vectors, in the expressions for the scattering coefficients when the incidence is from the isotropic medium.

When the optic axis is not normal to the interface, both the ordinary and the extraordinary waves exist simultaneously in the uniaxial medium even if the wave incident from the isotropic medium is a pure TEM wave. In this case, the situation is much more complicated and it is no longer evident that the above simple interchange in the expressions for the scattering coefficients when the incidence was from the isotropic side, would produce the expressions for the scattering coefficients when the incidence was from the anisotropic side. However, if the structure is reciprocal, Equations (3.26-3.27) can still be used provided that the polarization of the eigenwaves are defined in terms of $\vec{D}$ instead of $\vec{E}$. This last provision is necessary because Equations (3.26-3.27) were cast in terms of the unit vectors $\hat{\theta}_k$ and $\hat{\phi}_k$ of the spherical coordinate system used to describe the polarization in the $\mathcal{C}$ matrices. When the anisotropic media become lossy, however, $\vec{D}$ becomes elliptically polarized with a component in the direction of the phase wavefront propagation vector $\hat{\beta}$ which is a radial vector in the spherical coordinate system. The behaviour of the radial unit vector $\hat{r}$, however, does not cause a problem with the statement of reciprocity in Equation (3.22), or symmetry in

Equation (3.23). Thus, Equations (3.26-3.27) and the use of the $\mathcal{C}$ matrices and the scattering matrix propagator technique remain valid in the presence of a field component in the direction of $\hat{\beta}$. Furthermore, if this radial component of $\vec{D}$ is in phase quadrature with the transverse components of $\vec{D}$, the scattering matrix for the radial component can be treated separately from the scattering matrix for the transverse components.

Chapter 4

Complex permittivity profile

In this report, a plate with a low reflection level is made from a dielectric structure so that the plate presents to an incident uniform plane wave propagating in free space, a very gradual variation of the effective complex permittivity as the wave propagates through the plate (see References [3, 54, 55, 56]).

4.1 Effective permittivity

The plate consisted, here, of three sections. The front and the back sections consisted of arrays of small circular dielectric cones arranged according to equilateral triangular lattices. The middle section consisted of a dielectric slab in which an array of circular air cones was bored from both the front and the back surfaces according to two interlaced equilateral triangular lattices so as to achieve almost optimum packing of the air cones. Figure 4.7 shows a cut-away section of the plate in its final design. Figure 4.8 shows a conceptual view of the plate. The combination of the front and the back lattices formed a composite array whose unit cell has the hexagonal cross-section shown in Figure 4.9. The resulting structure is honeycomb-like, light (less than about 60% of the original weight of the dielectric slab) and strong.

The assumption that formed the basis on which to compute the permittivity profile was that the effective complex permittivity in each thin layer of the cascade forming the plate could be computed solely from consideration of the fractional volume occupied by the dielectric material with respect to the total volume of a unit volume within the layer. The rationale for this assumption lies in the fact that the dielectric material can be replaced by an equivalent electric polarization current acting in free space and distributed

65

throughout the volume of the dielectric material (see References [57, 58]). If the polarization current were unidirectional throughout the volume of dielectric material, the effective permittivity would be that corresponding to a uniform polarization current density throughout all space, equal to the average polarization current density. The value for the average polarization current density would be obtained by scaling the value of the original polarization current density according to the fraction of volume occupied by the dielectric material with respect to the total volume of the unit volume. Therefore, the relative complex permittivity which accounts for the effect of the equivalent electric polarization current, could be computed by scaling the original complex permittivity value according to the same ratio. However, this approach is not accurate enough for most cases because it ignores the spatial anisotropy of the effective permittivity.

In practice, the complex permittivity of each layer is realized by introducing small bits of a foreign material in an otherwise homogeneous dielectric host material. Morita and Cohn in Reference [59] have used small circular holes as inclusions of air pockets. The holes play the role of macroscopic molecules that become polarized by the total electric field. This effect is the result of the differential charge density appearing on the walls of the cavities excited by the local internal electric field whose distribution is affected by the absence of the dielectric material in the holes. Different shapes of cavities present different polarizability values. The resulting composite material presents an effective permittivity with a value obtained from the weighted average of the permittivity for each material (i.e. dielectric and air) making up the composite material. The weighted average depends on the polarizability of the inclusions (which itself depends on the shape of the inclusions and their orientation with respect to the total electric field), and the distribution of the inclusions throughout the host material. For a uniform distribution of spherical inclusions, the weighted average corresponds simply to the fractional volume occupied by the inclusions within a total unit volume of host material. This approach is well known in the context of artificial dielectrics.

In the context of gratings, however, grooves are normally used as inclusions. For grooves running in one-direction, the presence of the grooves concentrates the electric field differently for different polarizations, thus making the composite material anisotropic, i.e. the effective permittivity value becomes polarization dependent. For instance, such anisotropy is taken explicitly into account in Reference [46] for triangular grooves, and in Reference [60, 62] for rectangular grooves. Other groove profiles have been investigated (see References [63, 64, 65]). Reference [66] mentions that a better prediction is obtained with using a second-order model of effective permittivity. The computation of the effective permittivity becomes even more complex for 2-D periodical arrays. The case for the square pyramidal element has been treated in References [67, 68, 69, 70, 71, 72, 73] in the

context of absorbers for anechoic chambers. The case for a rectangular array of cylindrical rods has been treated in References [74] and [75, p. 704] based on results from Lord Rayleigh, and in References [78, 79] in the context of anisotropic laminated composites.

Here, the spatial anisotropy introduced by the presence of the holes in each thin layer was neglected in the transverse (to the interfaces) directions because this anisotropy was expected to be small for the following two reasons:

1. the element factor had rotational invariance because the holes were circular within each layer;

2. the array factor for a lattice of equilateral triangles was almost rotationnally invariant over the many cells making up the array.

The effective permittivity value that was used herein for the transverse (to the interfaces) directions was an approximate value obtained from Reference [74, p. 192, Equation (7.6)]. Lord Rayleigh's formula was used even though his array was a rectangular array of cylinders of a same diameter whereas our array was triangular and used two different diameters equally distributed among all the cylinders of a same layer. Furthermore, the GSM used here does not include the effect of the evanescent[1] waves created by the sub-wavelength features of the geometry. When the layers are very thin, adjacent interfaces become so close to one another that evanescent waves of one interface can reach adjacent interfaces and couple with the propagating or evanescent waves of adjacent interfaces. Usually, evanescent waves by themselves do not carry real (i.e. active) power and are needed only to make the field distribution satisfy the boundary conditions at the sub-wavelength scale. However, the transfer of active power is possible when evanescent waves couple to other waves (see Reference [40, p. 65]), the prism coupler being an example of applications where such coupling is put to a good use [48, p. 65]. Reference [p. 1321]Sarabandi mentions that the effects of discontinuities (hence, the effect of the evanescent waves) can be neglected. A comparison between numerically simulated (based on a numerical technique

---

[1]Usually, evanescent waves are present in the vicinity of a discontinuity, e.g. an interface between different media or an inclusion in an otherwise homogeneous material. Note, however, that the solution to the problem of a multilayer slab of infinite transverse dimensions, made of homogeneous layers with parallel planar interfaces, standing in free space and illuminated by a uniform propagating plane wave, does not require the presence of any evanescent (i.e. non-uniform) plane waves. Hence, our numerical technique based on modelling the corrugated slab as a multilayer slab where each layer is homogeneous, does not involve the presence of evanescent waves whereas our numerical technique based on modelling the slab with its actual inclusions as part of a FDTD simulation would include the evanescent waves.

presented later) or experimentally measured results could determine if the effects of evanescent waves can be neglected. However, no attempt was made to model the complicated geometry of the profiled slab.

The effective permittivity value that was used herein for the longitudinal (to the interfaces) direction is said to be exact according to References [67, 68], and corresponds to the fractional volume mentioned above. The resulting composite material is uniaxial with the optic axis parallel to the longitudinal direction, i.e. normal to the interface. Thus, the polarization perpendicular to the incidence plane has the $\vec{D}$ field always perpendicular to the optic axis and gives rise to an ordinary wave, i.e. the electromagnetic wave propagates within the composite material as in an isotropic material with an effective permittivity corresponding to that for the transverse (to the optic axis) direction, $\varepsilon_r^{\text{trans}}$. The polarization parallel to the incidence plane has the $\vec{H}$ field always perpendicular to the optic axis, and thus the $\vec{D}$ field inside the uniaxial medium has a component perpendicular and a component parallel to the optic axis. The parallel polarization gives rise to an extraordinary wave, i.e. the electromagnetic wave propagates within the composite material as in an isotropic material with an effective permittivity value $\varepsilon_r^{\parallel}$ that depends on some average of the transverse permittivity $\varepsilon_r^{\text{trans}}$ and the longitudinal permittivity $\varepsilon_r^{\text{long}}$ where the super-indices "trans" and "long" refer to directions perpendicular and parallel to the optic axis, respectively. From the interpretation that the phase velocity of the extraordinary wave is equal to $1/\sqrt{\mu_o \varepsilon_r^{\parallel}}$ and from Equation (10.80) of Reference [49, p. 360], one obtains (See [75, p. 677]):

$$\frac{1}{\varepsilon_r^{\parallel}} = \frac{\cos^2(\theta)}{\varepsilon_r^{\text{trans}}} + \frac{\sin^2(\theta)}{\varepsilon_r^{\text{long}}} \tag{4.1}$$

where the angle $0 \leq \theta \leq 90°$ corresponds to the acute angle between the optic axis and the propagation vector $\vec{\beta}$. We confirm that for $\theta = 0°$, thus for $\vec{D}$ being perpendicular to the optic axis, Equation (4.1) produces the result $\varepsilon_r^{\parallel} = \varepsilon_r^{\text{trans}}$. We confirm also that for $\theta = 90°$, thus for $\vec{D}$ being parallel to the optic axis, Equation (4.1) produces the result $\varepsilon_r^{\parallel} = \varepsilon_r^{\text{long}}$. For any intermediary θ value, the value for $1/\varepsilon_r^{\parallel}$ lies between the values for $1/\varepsilon_r^{\text{trans}}$ and $1/\varepsilon_r^{\text{long}}$.

Since both the ordinary and the extraordinary waves see different effective permittivity values, the transmission angle at an interface between two layers is different for each eigenwave, but it is still given by Snell's law of refraction (generalized here to take into account the non-uniform wave propagation caused by the presence of material losses). Bodnar and Bassett in reference [46] treated the case of an interface of two uniaxial lossless media.

When the media are both lossy and uniaxial (or, more generally, anisotropic), the question arises as to how to obtain for the non-uniform extraordinary wave, the intrinsic effective propagation constants α_o and β_o from which to obtain the effective propagation constants α and β and the real-valued propagation angles ξ_2 and $\zeta_2 = (\xi_2 + \rho_2)$ by the procedure presented in Chapter 2. The answer is provided in the next two sections.

4.2 Computation of the intrinsic propagation constants α_o and β_o for the extraordinary wave

By analogy with the expression $\gamma_o = jk_o\sqrt{\varepsilon_r}$ of Equation (2.3) we give the interpretation that $\gamma^2 = -k_o^2\varepsilon_r^\parallel$ where $\varepsilon_r^\parallel$ represents the overall effective permittivity that the wave sees, and k_o is the usual wave number in free space. We apply this interpretation to the specific case of the extraordinary wave in the uniaxial medium. From Equation (2.2), we know:

$$\gamma^2 = \vec{\gamma} \cdot \vec{\gamma} = \gamma_o^2 = \left(\alpha_o^2 - \beta_o^2\right) + j\left(2\alpha_o\beta_o\right)$$

Equating the real and the imaginary parts of the last equation with those of equation $\gamma^2 = -k_o^2\varepsilon_r^\parallel$ results in a system of two equations in the two unknowns α_o and β_o with the following solution:

$$\alpha_o = k_o\sqrt{\frac{\left|\varepsilon_r^\parallel\right| - \mathrm{Re}\left[\varepsilon_r^\parallel\right]}{2}} \tag{4.2}$$

$$\beta_o = k_o\sqrt{\frac{\left|\varepsilon_r^\parallel\right| + \mathrm{Re}\left[\varepsilon_r^\parallel\right]}{2}} \tag{4.3}$$

where $\varepsilon_r^\parallel = \left(\mathrm{Re}\left[\varepsilon_r^\parallel\right] - j\mathrm{Im}\left[\varepsilon_r^\parallel\right]\right)$. For $\left|\varepsilon_r^\parallel\right| = \mathrm{Re}\left[\varepsilon_r^\parallel\right]$, i.e. for $\mathrm{Im}\left[\varepsilon_r^\parallel\right] = 0$, Equations (4.2) and (4.3) produce the expected results $\alpha_o = 0$ and $\beta_o = k_o\sqrt{\varepsilon_r^\parallel}$, respectively. Substituting α_o of Equation (4.2), and substituting β_o of Equation (4.3) into Equations (2.11) and (2.12) produces:

$$\frac{\sigma}{\omega\varepsilon_o} = \sqrt{\left|\varepsilon_r^\parallel\right|^2 - \mathrm{Re}^2\left[\varepsilon_r^\parallel\right]} = \mathrm{Im}\left[\varepsilon_r^\parallel\right] \tag{4.4}$$

$$\varepsilon_r^{'} = \mathrm{Re}\left[\varepsilon_r^{\parallel}\right] \qquad (4.5)$$

which is consistent with the expression $\varepsilon_r^{\parallel} = \left(\mathrm{Re}\left[\varepsilon_r^{\parallel}\right] - j\mathrm{Im}\left[\varepsilon_r^{\parallel}\right]\right)$ and the expression $\varepsilon_r = \varepsilon_r^{'} - j\left(\frac{\sigma}{\omega\varepsilon_o}\right)$ of Equation (2.4).

In general, the effective propagation constants α and β cannot be computed without invoking α_o and β_o because the equation $\gamma^2 = \alpha^2 - \beta^2 + 2j\alpha\beta\cos(\rho)$ has three unknowns, whereas the equation $\gamma^2 = \alpha_o^2 - \beta_o^2 + 2j\alpha_o\beta_o$ has only two unknowns[2]. Moreover, it is not possible to relate α and β to some permittivity $\varepsilon_r^{\mathrm{eff}}$ the same way that we can relate α_o and β_o to $\varepsilon_r^{\parallel}$. The reason is that although we can write $\gamma_o = \alpha_o + j\beta_o = jk_o\sqrt{\varepsilon_r^{\parallel}}$, we cannot write $\gamma = \alpha + j\beta = jk_o\sqrt{\varepsilon_r^{\mathrm{eff}}}$ unless $\vec{\alpha}$ and $\vec{\beta}$ point in the same direction. However, the above procedure works because we can always write $\vec{\gamma}\cdot\vec{\gamma} = \gamma^2 = \gamma_o^2$.

4.3 Computation of the effective permittivity $\varepsilon_r^{\parallel}$ for the extraordinary wave

For the case that the incidence medium is free space, and the transmission medium is a lossless uniaxial medium, and the optic axis lies in the incidence plane at an angle θ_o with respect to the normal of the interface, the application of Johnson's equation (10.80) (see Reference [49, p. 360]) for the velocity c_t of the extraordinary wave, and Johnson's equation (10.83) (see Reference [49, p. 361]) for Snell's law, allows to find $\varepsilon_r^{\parallel} = (c_o/c_t)^2$ for any value of θ_o, where $c_o = 1/\sqrt{\mu_o\varepsilon_o}$. As explained in Appendix D.1, the effective relative permittivity[3] for the extraordinary wave propagating in the uniaxial half-space for both cases of $\theta_o = 0°$ and $\theta_o = \pm90°$ can be written as Equation (D.23), which translates into:

$$\varepsilon_r^{\parallel} = \varepsilon_r^{\mathrm{trans}} + \varepsilon_r^{\mathrm{inc}}\sin^2(\xi^{\mathrm{inc}})\left(1 - \frac{\varepsilon_r^{\mathrm{trans}}}{\varepsilon_r^{\mathrm{long}}}\right) \qquad (4.6)$$

---

[2]For the special case of practical importance presented in Section (2.4.1) whereby ρ is known a priori from the fact that $\vec{\alpha}$ is normal to the interface, β and α could be computed directly from the knowledge of $\varepsilon_r^{'}$ and $\sigma/(\omega\varepsilon_o)$ as per Equations (2.35) and (2.36), respectively. However, there would still remain the necessity to find the values of $\varepsilon_r^{'}$ and σ that correspond to the extraordinary wave.

[3]The effective permittivity in Equation (4.6) corresponds to that in $\gamma_o = \alpha_o + j\beta_o = jk_o\sqrt{\varepsilon_r^{\parallel}}$, not that in $\gamma = \alpha + j\beta = jk_o\sqrt{\varepsilon_r^{\mathrm{eff}}}$.

where here[4] "trans" and "long" refer to the directions parallel and perpendicular to the interface, respectively. This last equation corresponds to Collin's equation (118c) in Reference [47, p. 103] for a case where the optic axis is parallel to the interface, i.e. $\theta_o = \pm 90°$. One surprising consequence of this last equation is that although $\varepsilon_r^{\parallel} = \varepsilon_r{}^{\text{trans}}$ at normal incidence (i.e. $\xi^{\text{inc}} = 0$), the value for $\varepsilon_r^{\parallel}$ is not bounded by the value for $\varepsilon_r{}^{\text{long}}$ at grazing incidence ($\xi^{\text{inc}} \approx 90°$). In fact, depending on the value for $(\varepsilon_r{}^{\text{trans}} / \varepsilon_r{}^{\text{long}})$, it might be possible to have $\varepsilon_r^{\parallel} < 1$ or even $\varepsilon_r^{\parallel} < 0$.

In our case, we assume that a triangular array of circular cones presents an almost perfect rotational symmetry in the transverse (to the interfaces) plane such that the medium can be approximated by a uniaxial medium with its optic axis parallel to the normal of the interface, i.e. $\theta_o = 0°$.

Equation (4.6) can be generalized to include intrinsic losses in both the incidence and the transmission media by replacing in each respective medium the propagation vector $\vec{k} = \vec{\beta}$ by $\vec{\gamma} = \vec{\alpha} + j\vec{\beta}$ and taking $\gamma^2 = \vec{\gamma} \cdot \vec{\gamma} = \alpha^2 - \beta^2 + 2j\alpha \cdot \beta \cos(r)$ as in Equation (2.2). From Collin's development in reference [47, pp. 97-103], we obtain $\vec{\gamma} \cdot \vec{D} = 0$ as in reference [47, p. 97] and Collin's Equation (118c) becomes:

$$\gamma^2 = -k_o^2 \underbrace{\left(\varepsilon_r{}^{\text{trans}} - \left(\frac{\alpha^{\text{inc}} \sin(\xi^{\text{inc}} + \rho^{\text{inc}}) + j\beta^{\text{inc}} \sin(\xi^{\text{inc}})}{k_o} \right)^2 \left(1 - \frac{\varepsilon_r{}^{\text{trans}}}{\varepsilon_r{}^{\text{long}}} \right) \right)}_{\varepsilon_r^{\parallel}}.$$

(4.7)

For the incidence medium being free space, i.e. $\alpha^{\text{inc}} = 0$ and $\beta^{\text{inc}} = k_o$, Equation (4.7) is consistent with Equation (4.6), as expected, since our γ^2 corresponds to $-\beta^2$ of Collin.

In summary, the new procedure for computing the equivalent intrinsic propagation constants α_o and β_o that a transmitted wave sees in the lossy uniaxial medium beyond an interface, is based on the following sequence of reasoning steps:

1. using the interpretation $\gamma^2 = -k_o^2 \varepsilon_r^{\parallel}$ where $\varepsilon_r^{\parallel}$ is the overall effective

---

[4]In Appendix D.1, "trans" and "long" refered to the directions parallel and perpendicular to the optic axis, respectively. Equation (4.6) with "trans" and "long" referring to the directions parallel and perpendicular to the interface, respectively, is thus valid for $\theta_o = 0°, \pm 90°$ as per Equation (D.23), but not for intermediates values between 0° and 90°.

complex permittivity that the transmitted wave sees in the lossy uni-axial transmission medium;

2. generalizing Equation (4.6) to include the presence of intrinsic losses in both the incidence and the transmission media, and computing γ^2 as $-k_o^2 \varepsilon_r^{\parallel}$; when the incidence medium is uniaxial, Equation (4.6) remains valid because it is based on the use of Snell's law of refraction which remains valid because Snell's law is based only on phase matching at the interface.

3. using Equation (2.2) which leads to Equations (4.2) and (4.3) from which to compute the effective propagation constants α and β by the technique presented in Chapter 2; note that the values of the intrinsic propagation constants α_o and β_o are generally different between the two eigenwaves inside each uniaxial layer.

This procedure relies on a bootstrap approach because it is circular[5] in thinking and thus, in order to work, it requires the knowledge of an independent method to determine α_2 and β_2. The motivation for using this bootstrap approach, however, is to be able to reuse the method of Chapter 2 that was developed for the case where α_{o2} and β_{o2} were known a priori. Furthermore, the independent method needed for the procedure can be generalized to the case of biaxial media (see Appendix D.2). Finally, this procedure has a clear physical interpretation. Note, however, that since Fresnel equations require the knowledge of only $\gamma_z = \sqrt{\gamma^2 - (\gamma^{\text{inc}} \sin \xi^{\text{inc}})^2}$ with γ^2 for the extraordinary wave given by Equation (4.7), Fresnel equations could be computed without having to find the values of intrinsic α_o, β_o, the values of effective α and β and the values of the propagation angles ρ and ξ. This is precisely how Wait proceeded, as shown in the next section.

4.4 Wait's method

In comparison, Wait [31, pp. 98, 110-113] gives, for the case $\theta_o = 0°$, the reflection coefficients as:

$$R_{PERPENDICULAR} = \frac{u^i - u^t}{u^i + u^t} \tag{4.8}$$

---

[5]The computation of the effective propagation constants α_2 and β_2 of the transmission uniaxial medium by the procedure presented in Chapter 2 is made from the knowledge of the intrinsic propagation constants α_{o2} and β_{o2} of the transmission uniaxial medium. These, in turn, are themselves computed from the knowledge of effective propagation constants α_2 and β_2 obtained by an independent method (Collin's equation generalized to include losses and the uniaxial property in both the incidence and the transmission media).

$$R_{PARALLEL} = \frac{\dfrac{v^i}{\gamma^{i2}} - \dfrac{v^t}{\gamma^{t2}}}{\dfrac{v^i}{\gamma^{i2}} + \dfrac{v^t}{\gamma^{t2}}} \qquad (4.9)$$

where:

$$\gamma^2 = (j\omega\mu_o)\left(\sigma^{\text{trans}} + j\omega\varepsilon'^{\text{trans}}\right) = -k_o^2\varepsilon_r^{\text{trans}} \qquad (4.10)$$

$$u = \sqrt{\lambda^2 + \gamma^2} \qquad (4.11)$$

$$v = \sqrt{\lambda^2\kappa + \gamma^2} \qquad (4.12)$$

$$\lambda = -j\gamma^i\sin(\theta^i) \qquad (4.13)$$

$$\kappa = \frac{\sigma^{\text{trans}} + j\omega\varepsilon'^{\text{trans}}}{\sigma^{\text{long}} + j\omega\varepsilon'^{\text{long}}} = \frac{\varepsilon'^{\text{trans}} - \frac{j}{\omega}\sigma^{\text{trans}}}{\varepsilon'^{\text{long}} - \frac{j}{\omega}\sigma^{\text{long}}} = \frac{\varepsilon_r^{\text{trans}}}{\varepsilon_r^{\text{long}}} \qquad (4.14)$$

Note that in Wait's development:

- the variable called g is called σ here;

- $R_{PARALLEL}$ is the negative of our own as per Reference [5, p. 152];

- the real parts of u and v are chosen to be positive;

- the propagation angles are complex-valued and thus, θ^i can be complex-valued;

- the incidence medium is free space, i.e. isotropic, which situation results in $v^i = u^i$ in Equation (4.9), and results in the expressions given by Wait in Reference [31, p. 113].

Note that γ corresponds to the complex propagation constant for the ordinary wave as shown in Equation (4.10). Note also that the term $j\lambda = \gamma^i\sin(\theta^i)$ corresponds to the transverse component of γ^i. The phase matching requirement of all waves at the planar interface forces the transverse variation of the fields for the transmitted eigenwaves to be precisely that of the fields for the incident plane wave, and results in the law of reflection and Snell's law of refraction. Consequently, we have:

$$u^i = \sqrt{\lambda^2 + \gamma^{i2}} = \sqrt{-\gamma^{i2}\sin^2(\theta^i) + \gamma^{i2}} = \gamma^i\cos(\theta^i) = \gamma_z^i \qquad (4.15)$$

73

and

$$u^t = \sqrt{\lambda^2 + \gamma^{t2}} = \sqrt{-\gamma^{i2}\sin^2(\theta^i) + \gamma^{t2}} = jk_o\sqrt{-\varepsilon_r^i\sin^2(\theta^i) + \varepsilon_r^t}$$
$$= jk_o\sqrt{\varepsilon_r^t}\sqrt{1 - \frac{\varepsilon_r^i}{\varepsilon_r^t}\sin^2(\theta^i)} = jk_o\sqrt{\varepsilon_r^t}\sqrt{1 - \sin^2(\theta^t)} = \gamma^t\cos(\theta^t) = \gamma_z^t$$

(4.16)

where the super-index "trans" for ε_r was suppressed to minimize cluttering the expressions. Thus, the variable u corresponds to the longitudinal component of the complex propagation constant for the ordinary wave in the transmission medium as well as in the incidence medium. Therefore, the reflection coefficient $R_{PERPENDICULAR}$ given by Equation (4.8) corresponds exactly to the expression given in Equation (3.9) since the eigenwave corresponding to this polarization is the ordinary wave.

The expression (4.9) can be modified easily to obtain:

$$R_{PARALLEL} = \frac{v^i\gamma^{t2} - v^t\gamma^{i2}}{v^i\gamma^{t2} + v^t\gamma^{i2}} = \frac{\varepsilon_r^t v^i - \varepsilon_r^i v^t}{\varepsilon_r^t v^i + \varepsilon_r^i v^t}$$

(4.17)

where all permittivity values refer to the transverse permittivity values. Recalling that $R_{PARALLEL}$ is the negative of our own as per Reference [5, p. 152], we see that Equation (4.17) is the same as Equation (3.6) provided that all permittivity values in Equation (4.17) are the transverse (not the effective) permittivity values, and that $v \equiv \gamma_z$. This expression also agrees with Equation (6.107) of Reference [7, p. 245]. For the isotropic case, it is clear that $\kappa = 1$ and thus, $v \equiv \gamma_z$, and Equation (4.17) reduces (notwithstanding the aforementioned difference in sign) to Equation (3.6). Now, Equation (4.7) can be re-written as:

$$\underbrace{-k_o^2\varepsilon_r{}^\parallel}_{\gamma_{\text{Collin}}^2} = \underbrace{\left(-\left(\alpha^{\text{inc}}\sin(\xi^{\text{inc}} + \rho^{\text{inc}}) + j\beta^{\text{inc}}\sin(\xi^{\text{inc}})\right)^2\right)}_{\lambda^2}\underbrace{\left(\frac{\varepsilon_r{}^{\text{trans}}}{\varepsilon_r{}^{\text{long}}}\right)}_{\kappa}$$
$$+ \underbrace{\left(-k_o^2\varepsilon_r{}^{\text{trans}}\right)}_{\gamma_{\text{Wait}}^2} + \underbrace{\left(\left(\alpha^{\text{inc}}\sin(\xi^{\text{inc}} + \rho^{\text{inc}}) + j\beta^{\text{inc}}\sin(\xi^{\text{inc}})\right)^2\right)}_{-\lambda^2}$$
$$= \underbrace{v^2}_{\gamma_z^2} + \underbrace{\left(-\lambda^2\right)}_{\gamma_\rho^2}$$

(4.18)

where γ_z and γ_ρ are the longitudinal and the transverse components of $\vec{\gamma}_{\text{Collin}}$, respectively. Recall that $\gamma_\rho = j\lambda$ because the phase matching of the fields at every interface forces the transverse variation of the scattered fields to be that of the incident field (see Reference [5, p. 150]). Hence, we see that Wait's formulation corresponds, in fact, to Collin's formulation when

the optic axis is parallel to the normal of the interface, i.e. $\theta_o = 0°$. In other words, Wait's Equation (4.12) can be obtained from Equation (4.7) and $v^2 \equiv \gamma_z^2 = (\gamma_{\text{Collin}}^2 - \gamma_\rho^2)$. When $\rho^{\text{inc}} = -\xi^{\text{inc}}$ as a result of $\vec{\alpha}^{\text{inc}}$ being normal to the interface, or when $\alpha^{\text{inc}} = 0$ as a result of the incidence region being lossless, and since $\beta^{\text{inc}} = k_o\sqrt{\varepsilon_r^{\text{inc}}}$, there results for the extraordinary wave:

$$\gamma_z = jk_o\sqrt{\varepsilon_r^{\text{trans}} - \varepsilon_r^{\text{inc}}\sin^2(\xi^{\text{inc}})\left(\frac{\varepsilon_r^{\text{trans}}}{\varepsilon_r^{\text{long}}}\right)} \qquad (4.19)$$

which agrees[6] with Equation (4.12). For an isotropic slab, one obtains $\varepsilon^{\text{trans}} = \varepsilon_{r2} = \varepsilon_r^{\text{long}}$ and thus, Equation (4.19) reduces to Equation (4.16) upon using Snell's law $\sqrt{\varepsilon_{r2}}\sin(\xi_2) = \sqrt{\varepsilon_{r1}}\sin(\xi_1)$ where $\xi^{\text{inc}} \equiv \xi_1$ and $\varepsilon_r^{\text{inc}} \equiv \varepsilon_{r1}$.

From the above observations, the transmission coefficients for Wait's method could be obtained as follows:

$$T_{PERPENDICULAR} = \frac{2u^i}{u^i + u^t} \qquad (4.20)$$

$$T_{PARALLEL} = \frac{\left(\sqrt{\varepsilon_r^i\varepsilon_r^t}\right)2v^i}{\varepsilon_r^i v^t + \varepsilon_r^t v^i} \qquad (4.21)$$

where all permittivity values are again transverse permittivity values. This expression agrees[7] with Equation (6.106) of Reference [7, p. 245].

4.5 Validation

For a structure consisting of two adjacent layers in otherwise free space, illuminated by a uniform plane wave, both predicted and numerical results

---

[6]Note the difference between the expression for γ_z given by Equation (4.19) and the expression for $\gamma_o = jk_o\sqrt{\varepsilon_r^{\parallel}}$ with $\varepsilon_r^{\parallel}$ given by Equation (4.6).

[7]The agreement is seen when Equation (6.106) is divided by $-k_t$ to account for the fact that $C_{\parallel} = -k_t C_-$ as mentioned on page 234 of Reference [7]. Note that in Equation (6.106), $\varepsilon_{\perp}$ and $\varepsilon_{\parallel}$ refer to the principal dielectric values in the directions perpendicular and parallel to the optic axis, respectively, whereas here $\varepsilon^{\text{trans}}$ and $\varepsilon^{\text{long}}$ refer to the permittivity values in the directions perpendicular and parallel to the normal of the interface, respectively. In the present case, however, $\varepsilon_{\perp} = \varepsilon^{\text{trans}}$ and $\varepsilon_{\parallel} = \varepsilon^{\text{long}}$ because the optic axis and the normal of the interface are parallel to one another.

were obtained for various types of interfaces (i.e. lossless vs lossy, isotropic vs uniaxial, input vs output media) and for $\theta_o = 0°$ or $\pm 90°$. The predicted results were generated by the analytical method based on the Adler-Chu-Fano formulation, with the generalized Fresnel equations modified to use the permittivity values "in the interface", i.e. ε_y for the TE^z polarization and ε_x for the TM^z polarization.

Two FORTRAN programs were written to compute the composite scattering matrix of the free-standing multilayer slab. One program cascaded the scattering matrix given by Equation (3.28) for each free-standing layer, i.e. using a fictitious zero-thickness layer at every internal interface to make each layer free-standing, and then using reciprocity and longitudinal symmetry. The other FORTRAN program cascaded the scattering matrices of all interfaces and intervening media in situ with the scattering matrix of each interface given by Equation (3.12) modified to use the permittivity values "in the interface". Both programs gave identical results. This confirms the validity of using fictitious zero-thickness layers and Equations (3.26)-(3.28).

The numerical results were generated by a numerical technique[8] based on FDTD simulations as explained here. The scattered field of an infinite-size slab was computed by a FDTD method that uses the separate field formalism so that the infinite-size slab could be modeled simply by extending the slab all the way to the outer boundaries that were terminated by eight PML layers. The excitation was a time-harmonic Maxwellian tapered beam synthesized and positioned such as not to illuminate the edges of the slab and such as to have negligible excitation over the innermost PML layer. The prescribed dominant polarization of the excitation beam was either TM^z or TE^z. The prescribed incidence of the excitation beam was $45°$ in the inward convention. After having computed the scattered field by the FDTD method, some post-processing was carried out to compute the spectrum of the incident, reflected and transmitted beams, and the values of the scattering coefficients were obtained by forming the ratio of the E-field phasor of the spectrum for the scattered beams, over the E-field phasor of the spectrum for the incident beam, for all incidence angles of interest.

4.5.1 Case of $\theta_o = 0°$, i.e. $\varepsilon_x = \varepsilon_y \neq \varepsilon_z$

Figures 4.1, 4.2 and 4.3 show the results for the case that the optic axis was oriented in a direction parallel to the normal of the interface, i.e. $\theta_o = 0°$. Wait's method was also used as a second analytical method, with:

---

[8]For more information on the numerical technique that computes the values of plane wave scattering coefficients, see CRC Technical report #CRC-RP-2008-002.

$$\begin{cases} \varepsilon^{\text{trans}} = \varepsilon_x = \varepsilon_y \\ \varepsilon^{\text{long}} = \varepsilon_z \end{cases}$$

where "trans" and "long" refer to both the optic axis and the normal of the interfaces.

The results predicted by the two analytical methods are identical. The very good correspondence[9] confirm that the permittivities to be used in the generalized Fresnel equations are, indeed, the permittivity values "in the interface". The slight remaining discrepancy between the numerical curves and the analytical curves owe to numerical issues with the FDTD method mostly (e.g. numerical anisotropy from spatial and temporal discretizations, second-order accuracy from the finite-difference algorithm, modeling of the interface by using the average of the two permittivity values on the two sides of the interface, modeling an infinite-size slab by terminating the slab model into PML layers, spurious residual reflections from the PML layers, carrying out the floating-point computation in single precision, etc.). The oscillations of the numerical curves about the analytical curves due to aperture truncation from computing the far fields from apertures of a necessarily finite size were mitigated by the technique of "window averaging".

We note that the propagation angle values are different between the perpendicular and the parallel polarizations. We note also that, by finding the mathematical equivalence (see Appendix B) between a uniform plane wave with complex-valued propagation angle δ and a non-uniform plane wave with real-valued propagation angles (ξ for $\vec{\beta}$ and $\xi + \rho$ for $\vec{\alpha}$), the complex-valued propagation angle corresponding to the real-valued propagation angles does not, in general, correspond to $\delta = \xi + i(\xi + \rho)$. Recall that according to the case of practical importance presented in Section 2.4.1, we know that the amplitude wavefront propagation vector $\vec{\alpha}_2$ would be normal to the interface if the incidence medium were lossless and the incident plane wave were uniform. Thus $(\xi + \rho) = 0$ and $\xi + i(\xi + \rho)$ would become real-valued. However,

---

[9]Since Wait's equations reduce to Fresnel equations when the uniaxial media become isotropic, and if the predicted curves of plane wave scattering coefficient values for lossy media computed by the generalized Fresnel equations became less accurate as the conductivity values of the media increased, why should the correspondence between predicted values and numerically computed values be better for the lossy uniaxial slab than for the lossy isotropic slab? A possible reason is that both the losses and the anisotropy of a medium make the E and/or H field acquire a component parallel to the propagation direction of the phase wavefront. However, the component due to losses might point in one direction along the propagation direction while the component due to the anisotropy might point in the opposite direction. If so, the combined effect due to the presence of both these components parallel to the direction of propagation would be less for the lossy anisotropic media than for the lossy isotropic slab.

we know from Snell's law of refraction that δ is not real-valued when the transmission medium is lossy, hence $\delta \neq \xi + i(\xi + \rho)$.

Since all results of the two analytical methods are identical, we could also confirm that the complex values of the propagation angle corresponding to the real values of the propagation angle would be the same as the complex values computed by Snell's law with complex propagation angles. More importantly however, the fact that the results of the two analytical methods are identical indicate that the procedure presented in Appendix D for arriving at Equation (4.6), remains valid even if the uniaxial medium becomes lossy, which situation causes the plane waves to become non-uniform in the lossy uniaxial medium (with $\vec{\alpha}_2$ being normal to the interface). This observation is important because the procedure in Appendix D can be generalized to compute the effective relative permittivity that a plane wave would see as it propagated through a more general anisotropic medium (i.e. a biaxial medium; see Appendix D.2), and from this knowledge, the problem could be solved by the Adler-Chu-Fano formulation.

When at least one medium of the structure is uniaxial, Wait's formulation in Reference [31] does not indicate how Snell's law must be modified to compute the transmission angle for the extraordinary wave in the uniaxial medium. In fact, Wait's solution does not even require the explicit knowledge of the transmission angle since v given by Equation (4.12) is not written explicitly as a function of the transmission angle. Hence, our method is more comprehensive than Wait's method because it provides the explicit knowledge of all real-valued propagation angles in every layer. However, Wait's computation of γ_z from expressions (4.11) and (4.12) is much simpler than our method which requires solving for α, β, ξ and ρ, and then computing $\gamma_z = (\alpha \cos(\xi + \rho) + j\beta \cos(\xi))$. Our method, however, can be generalized to treat the case of more general anisotropic media (see Appendix D.2).
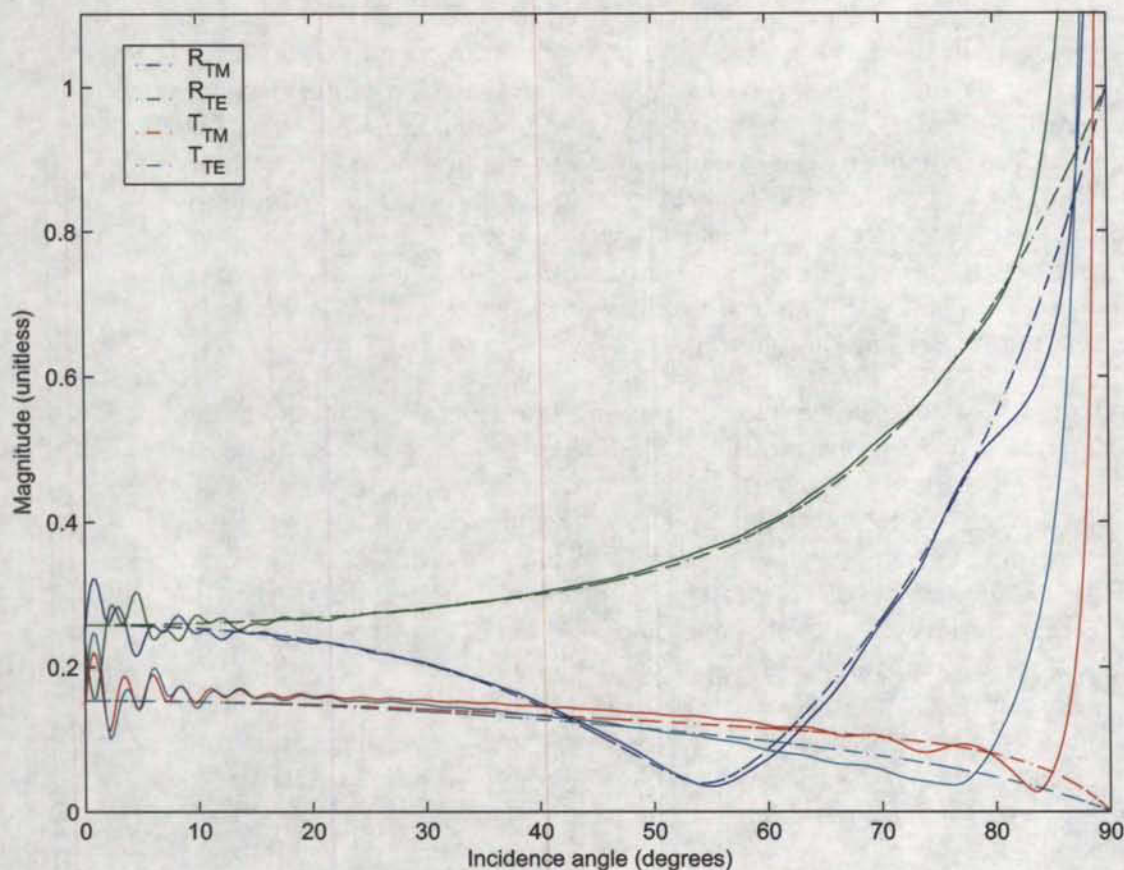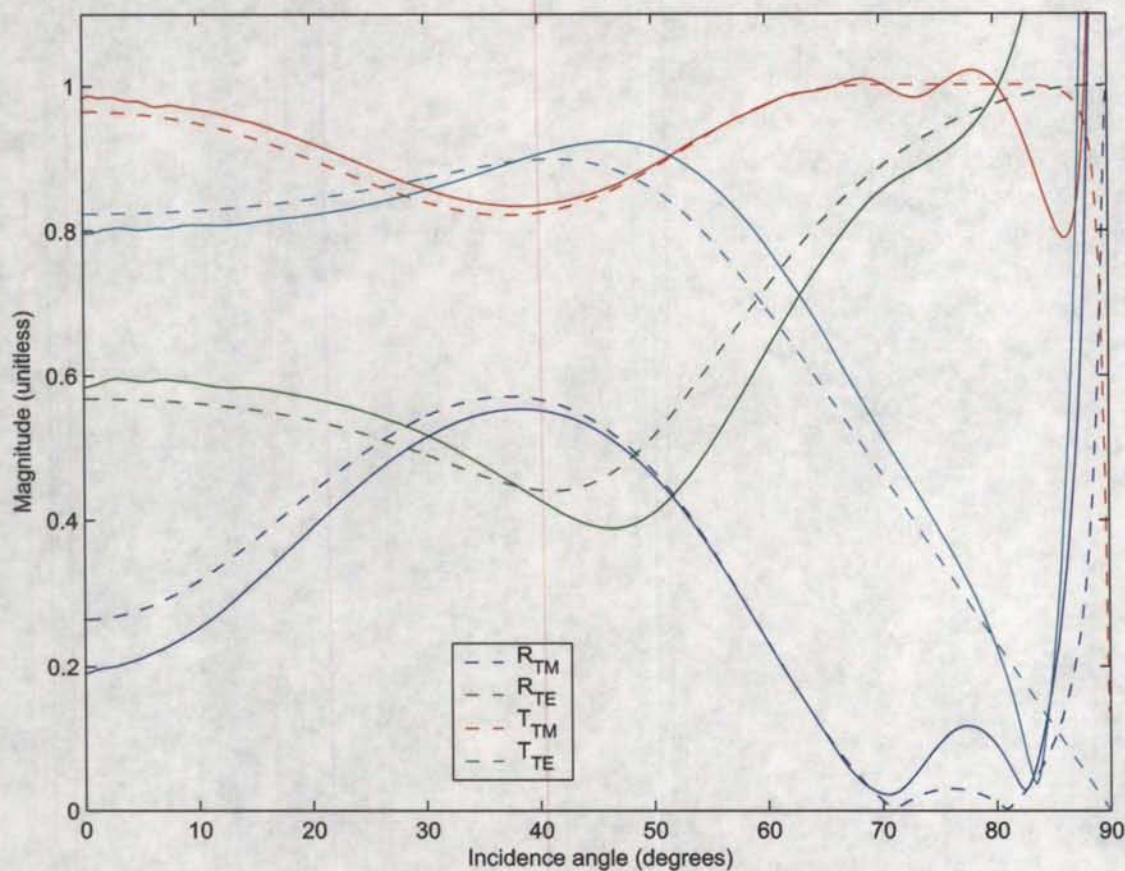
Figure 4.1: The magnitude results plotted on a linear scale, for the reflection coefficient of a two-layer slab standing in free space, obtained by three different methods: 1) Wait's analytical method (dot-dash); 2) analytical method by this author (dash); 3) numerical method by this author (solid). The parameters for the two-layer slab were $d_1 = 0.05$ m, $d_2 = 0.10$ m, $\varepsilon_x^{\#1} = \varepsilon_y^{\#1} = 2(1 - j0.3)\varepsilon_o$, $\varepsilon_x^{\#2} = \varepsilon_y^{\#2} = 5(1 - j0.3)\varepsilon_o$, $\varepsilon_z^{\#1} = 5(1 - j0.3)\varepsilon_o$, $\varepsilon_z^{\#2} = 2(1 - j0.3)\varepsilon_o$, and the frequency was $f = 1900$ MHz. All results are identical between the two analytical methods.
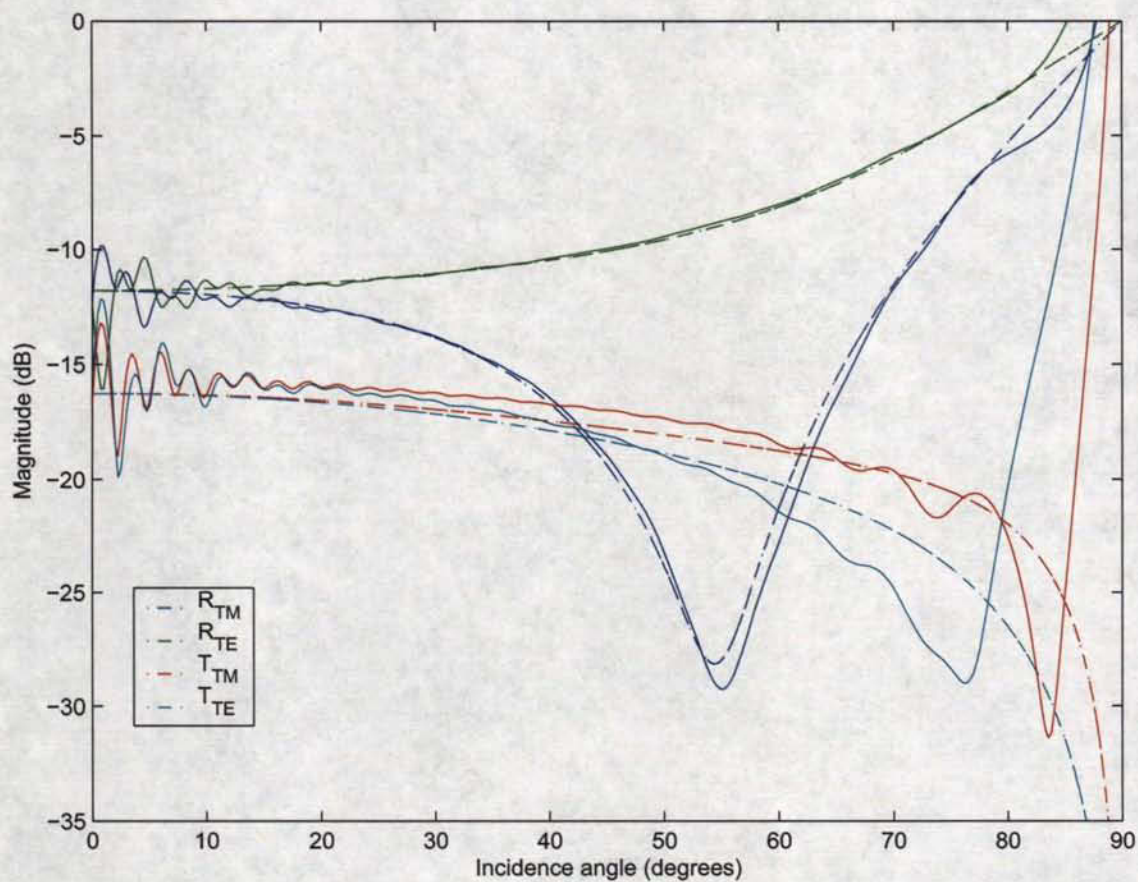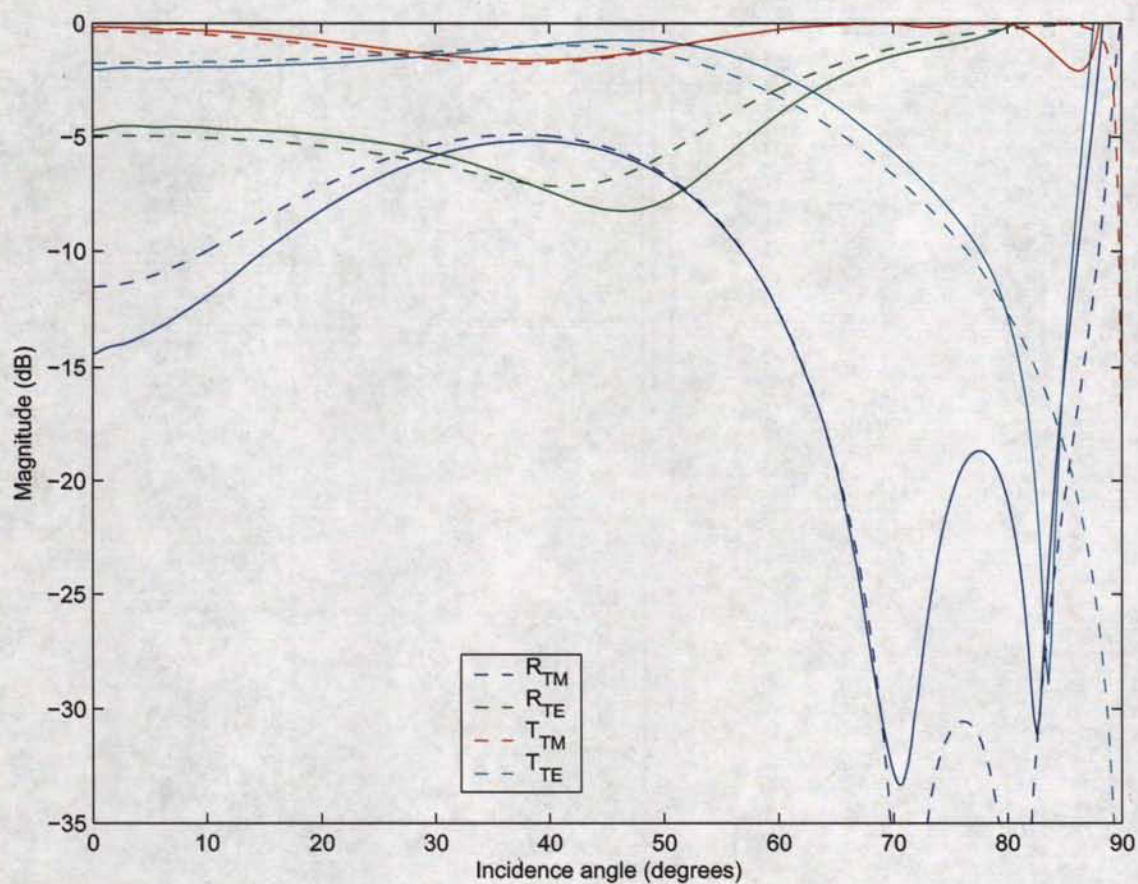
Figure 4.2: Same as Figure 4.1 except that the results are plotted on a dB scale. All results are identical between the two analytical methods.
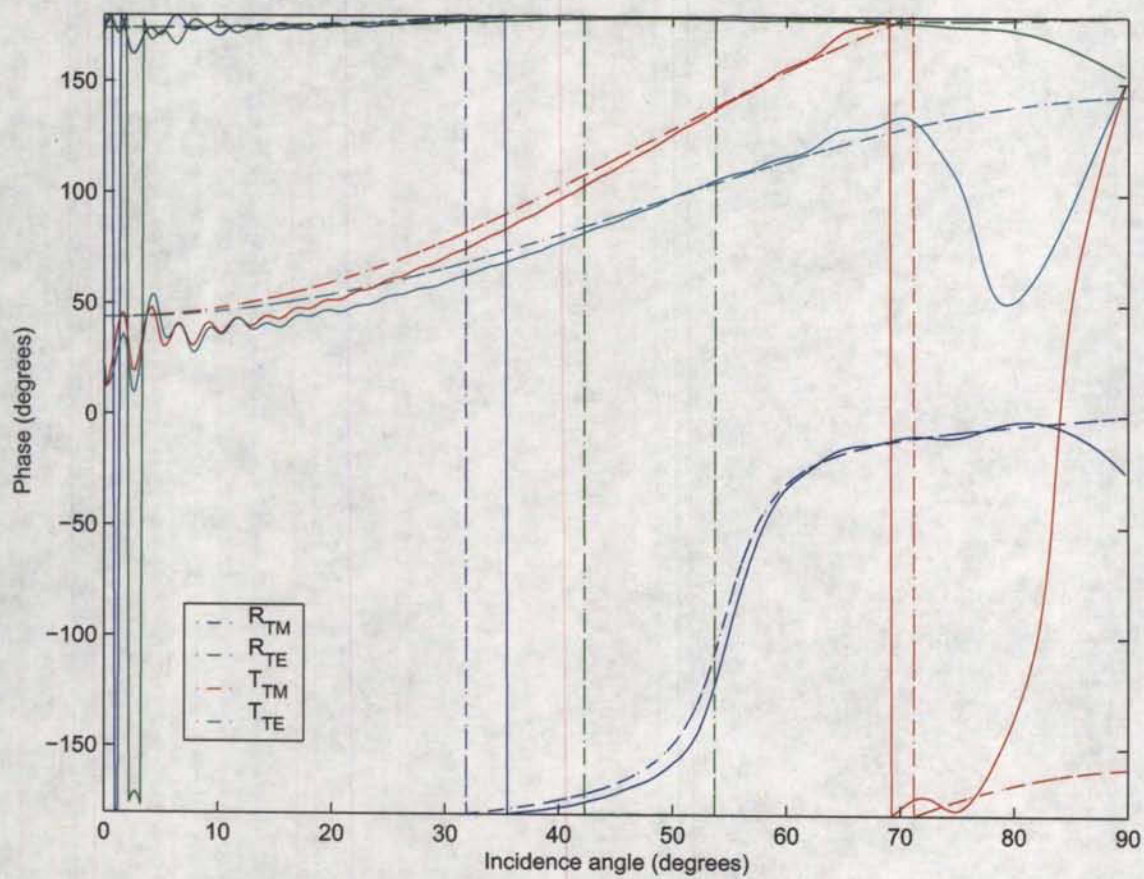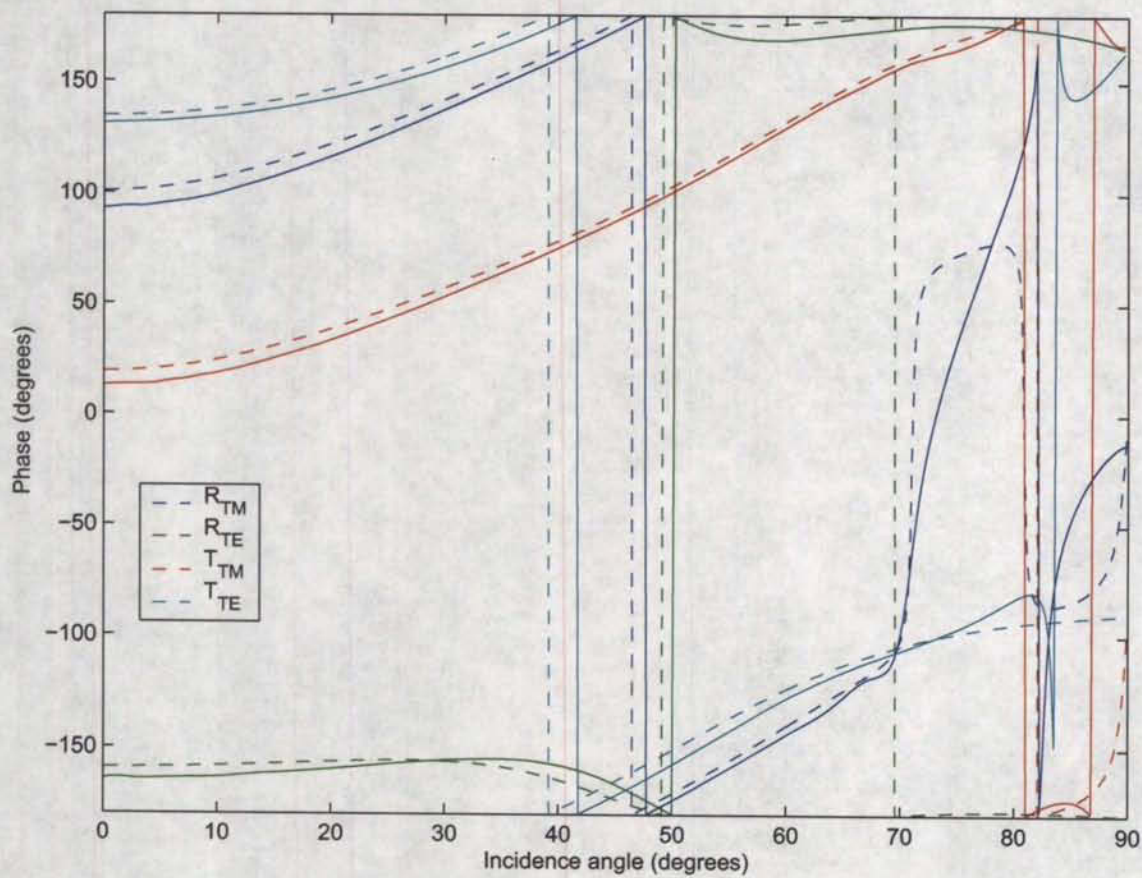
Figure 4.3: The phase results corresponding to Figures 4.1 and 4.2. All results are identical between the two analytical methods.

4.5.2 Case of $\theta_o = 90°$, i.e. $\varepsilon_x \neq \varepsilon_y = \varepsilon_x$

Figures 4.4, 4.5 and 4.6 show the results for the case that the optic axis was oriented in a direction parallel to the interface, i.e. $\theta_o = 90°$, in the incidence plane. Wait's method was also used as a second analytical method, with:

$$\begin{cases} \varepsilon^{\mathrm{trans}} = \varepsilon_z = \varepsilon_y \\ \varepsilon^{\mathrm{long}} = \varepsilon_x \end{cases}$$

where "trans" and "long" refer to the optic axis. The two analytical methods provided again identical results. The correspondence between the predicted and the numerical results is poor even for lossless media. This means that the generalized Fresnel equations cannot be used even when the permittivity values are those "in the interface", i.e. ε_y for the TE^z polarization and ε_x for the TM^z polarization.

Figure 4.4: The magnitude results plotted on a linear scale, for the reflection coefficient of a two-layer slab standing in free space, obtained by three different methods: 1) Wait's analytical method (dot-dash); 2) analytical method by this author (dash); 3) numerical method by this author (solid). The parameters for the two-layer slab were $d_1 = 0.05$ m, $d_2 = 0.10$ m, $\varepsilon_z^{\#1} = \varepsilon_y^{\#1} = 5(1 - j0.0)\varepsilon_o$, $\varepsilon_z^{\#2} = \varepsilon_y^{\#2} = 2(1 - j0.0)\varepsilon_o$, $\varepsilon_x^{\#1} = 3(1 - j0.0)\varepsilon_o$, $\varepsilon_x^{\#2} = 5(1 - j0.0)\varepsilon_o$, and the frequency was $f = 1900$ MHz. All results are identical between the two analytical methods.

Figure 4.5: Same as Figure 4.4 except that the results are plotted on a dB scale. All results are identical between the two analytical methods.

Figure 4.6: The phase results corresponding to Figures 4.4 and 4.5. All results are identical between the two analytical methods.

4.6 Computation of $\varepsilon_r{}^{\text{trans}}$ and $\varepsilon_r{}^{\text{long}}$

Since each layer consists of a two-dimensional periodic structure, the analysis is restricted to the unit cell of that periodic structure. Stacking the unit cell of every layer in the order that the layers appear in the plate produces an hexagonal unit cell of height corresponding to the thickness of the plate. In the stacking process, however, the present analysis does not take into account how the dielectric material within each layer aligns from one layer to the next because each layer is modelled as a homogeneous layer (see Reference [66]).

The cross-section of the hexagonal unit cell is composed of six equilateral triangles of length equal to $2s/\sqrt{3}$ per side, where $2s$, labelled herein the cell size, is the diameter of the circle inscribed by the hexagonal unit cell in Figure 4.9. The cell size $2s$ must be much smaller than the wavelength in a homogeneous dielectric with permittivity value equal to the effective permittivity value of the thin layer of interest, so that the material appears to be macroscopically homogeneous to an electromagnetic plane wave propagating through that layer (otherwise, higher order modes could begin to propagate and form grating lobes). Richmond in Reference [57] suggested for his volume integral equation technique that each cell not exceed a dimension of $0.2/\sqrt{\varepsilon_r}$ wavelengths. Bodnar and Bassett in Reference [46, Equation (19)] showed that the critical cell size for the onset of grating lobes becomes even smaller as the incidence angle increases in value.

The volume of the hexagonal cell shown in Figure 4.9 contains:

- one complete circular cone corresponding to the air cone bored into the front face of the dielectric slab;

- the equivalent of one complete circular cone corresponding to the sum of three one-third sections of air cones bored into the back face of the dielectric slab;

- the equivalent of two complete small cones corresponding to the sum of six one-third sections of dielectric cones protruding out from the front face of the dielectric slab;

- the equivalent of two complete small cones corresponding to the sum of one complete and three one-third sections of dielectric cones protruding out from the back face of the dielectric slab.

The permittivity profile was symmetrical with respect to the mid-thickness point of the plate in order to allow the electromagnetic wave to leave the plate as smoothly as it entered the plate. Consequently, only the front half-thickness region is shown in Figure 4.10 which depicts the geometry of a

dielectric cone protruding from the front face of the dielectric slab and the geometry of one inverted and one non-inverted air cone bored into the dielectric slab. A small separation distance between adjacent cone walls w given by:

$$w = 2(s - a_2) \qquad (4.22)$$

was purposefully introduced and taken into account as part of the analysis in order to guarantee that the integrity of the walls of the air cones would not get compromised by fabrication tolerances. It turns out that the parameter w has also a significant effect on the response. The thickness of the dielectric slab HH and the minimum cone wall separation w were chosen according to the parametric analysis carried out in the next chapter. The drill bits used herein set the slope of the air cones to $\frac{A}{H_2} = \frac{1}{8}$, and the length of the missing tip of the air cones to $\Delta H_2 = 1\ cm$. The height h_1 and the base radius a_1 of the dielectric cones were chosen such that the permittivity profile would form a continuous function, i.e. without discontinuity in the permittivity function nor its first derivative. The base radius of the air cones a_2, the cell size $2s$ and the vertical separation between the inverted and non-inverted air cones D were computed according to the development below.

Since two adjacent dielectric cones would touch at their base when their base radius was equal to $s/\sqrt{3}$ (when $w = 0$), the requirement that the volume of the two dielectric cones be mutually exclusive was insured by limiting the base radius value to $s/\sqrt{3}$. The height of the dielectric cone was H_1 and its apex was located at $z = h_1$. Hence, the radius of the circular cross-section for a dielectric cone varied linearly from $A_1 = 0$ at $z = h_1$ to $A_1 = s/\sqrt{3}$ at $z = (h_1 - H_1)$, hence:

$$A_1(z) = \frac{s}{\sqrt{3}} \left(\frac{h_1 - z}{H_1} \right) \qquad (4.23)$$

Since the hexagonal unit cell contained the equivalent of two complete dielectric cones protruding from the front face of the dielectric slab, the volume of dielectric material per hexagonal unit cell in a layer of thickness dz in the front section was obtained as:

$$V_f(z) = 2\pi A_1^2(z)dz = \frac{2}{3} \left(\frac{h_1 - z}{H_1} \right)^2 \pi s^2 dz$$

Similarly, the height of an inverted air cone was H_2 and its apex was located at $z = (h_2 - H_2)$. Since two inverted air cones would touch at their

base when their base radius was equal to s (when $w = 0$), the radius of the circular cross-section for an inverted air cone varied linearly from $A_2 = s$ at $z = h_2$ to $A_2 = 0$ at $z = (h_2 - H_2)$, hence:

$$A_2(z) = s \left(\frac{z - h_2 + H_2}{H_2} \right) \tag{4.24}$$

Similarly, the height of a non-inverted air cone was H_2, its apex was located at $z = 0$ and the radius of the circular cross-section varied linearly from $A_2' = 0$ at $z = 0$ to $A_2' = s$ at $z = -H_2$, hence:

$$A_2'(z) = s \left(\frac{-z}{H_2} \right) \tag{4.25}$$

Since the hexagonal unit cell contained one complete inverted air cone bored from the front face of the dielectric slab, and the equivalent of one complete non-inverted air cone bored from the back face of the dielectric slab, the air volume per hexagonal unit cell in a layer of thickness dz in the middle section was obtained as:

$$V_m(z) = \left(\frac{z - h_2 + H_2}{H_2} \right)^2 \pi s^2 dz + \left(\frac{-z}{H_2} \right)^2 \pi s^2 dz$$

The total volume of the hexagonal unit cell in a layer of thickness dz is obtained as $V_c(z) = 2\sqrt{3}s^2 dz$. Assuming that the host material has intrinsic permittivity ε_{r1}, and the inclusion material has intrinsic permittivity ε_{r2}, and denoting the fill fraction by $v = \frac{V_2(z)}{V_c(z)} = 1 - \left(\frac{V_1}{V_c} \right)$, the longitudinal effective permittivity is given exactly by [67, 68, 30]:

$$
\begin{aligned}
\varepsilon_r^{\text{long}}(z) &= v\varepsilon_{r2} + (1 - v)\varepsilon_{r1} \\
&= \varepsilon_{r1} + v(\varepsilon_{r2} - \varepsilon_{r1})
\end{aligned}
\tag{4.26}
$$

while the transverse effective permittivity is given approximately by [74, p. 192, Equation (7.6)]:

$$\varepsilon_r^{\text{trans}}(z) = \frac{\sqrt{(1-2v)^2\left(\varepsilon_{r2}^2 + \varepsilon_{r1}^2\right) + (1 + 4v - 4v^2)2\varepsilon_{r2}\varepsilon_{r1}} - (1-2v)(\varepsilon_{r2} - \varepsilon_{r1})}{2} \tag{4.27}$$

The last expression was obtained by Lord Rayleigh for a rectangular array of cylinders embedded in an otherwise homogeneous medium. The

dependence of the last equation onto the radius of the cylinders appears only through the volume fraction v. Thus, the expression was used in this work even though two different radius values could be present within a same layer.

Figures 4.11 and 4.12 show $\varepsilon_r^{\text{trans}}$ and $\varepsilon_r^{\text{long}}$ as a function of the fill fraction v. Note is made that even if the real and the imaginary parts of $\varepsilon_r = \varepsilon_r' - j\varepsilon_r'' = \varepsilon_r'(1 - j\tan(\delta))$ varied linearly, as in the case for the longitudinal effective permittivity, the loss tangent, which is the ratio of the imaginary part over the real part of the relative permittivity, would not vary linearly. This situation is clearly shown in Figure 4.12.

Another point needs to be made and this point will be more easily brought out by invoking the following mathematical results:

$$\left. \begin{array}{rcl} \text{Real}(A + B) & = & \text{Real}(A) + \text{Real}(B) \\ \text{Imag}(A + B) & = & \text{Imag}(A) + \text{Imag}(B) \end{array} \right\} \qquad (4.28)$$

$$\left. \begin{array}{rcl} \text{Real}(\sqrt{A + B}) & \neq & \sqrt{\text{Real}(A)} + \sqrt{\text{Real}(B)} \\ \text{Imag}(\sqrt{A + B}) & \neq & \sqrt{\text{Imag}(A)} + \sqrt{\text{Imag}(B)} \end{array} \right\} \qquad (4.29)$$

Thus, although the same result is obtained from applying Equation (4.26) separately to each component of the variables as with applying the same equation to the complex-valued variables followed by resolving the result into each component, however this is not the case for Equation (4.27). The reason owes to the nature of the complex-valued operations involved in the expressions. In Equation (4.28), the operation of summation leaves separate the real and imaginary parts of the variables. In Equation (4.29), the operation of taking the square root causes the real and imaginary parts of the variables to mix. Hence, the question arose as to which approach should be taken since the expression (4.27) was given for the lossless case without indication as to how it should be generalized to the lossy case. So, both approaches were tried out and it was found that for the case here, the result of computing the imaginary part of $\varepsilon_r^{\text{trans}}$ by applying Equation (4.27) to the imaginary components of ε_{r1} and ε_{r2} produced a non-physical result (some values were positive instead of negative, and some values were larger than the greatest of the imaginary parts of ε_{r1} and ε_{r2}). For this reason, the computation proceeded here by applying the equation to the complex-valued variables followed by resolving the result into its real and imaginary components. This approach corresponds, in fact, to the analytical continuation of a real-valued result to a complex one in the complex plane. However, this approach produced non-physical results of its own for the expression corresponding to the square array of square pyramidal absorbing cones (the value for $\varepsilon_r^{\text{trans}}$ exceeded the value for $\varepsilon_r^{\text{long}}$ as the fill fraction approached 1; perhaps the fact that a non-physical result was obtained with the technique of analytical continuation is in itself

an indication that the expression given in Reference [68, Equation (25)] for evaluating $\varepsilon_r^{\text{trans}}$ is just an approximation).

For the front $((h_1 - \Delta H_1) \geq z \geq 0)$ and back sections $((h_2 - H_2) \geq z \geq (h_2 - H_2 - h_1 + H_1))$, the host material is air and the inclusion material is dielectric whereas for the middle section $(0 \geq z \geq (h_2 - H_2))$, the host material is dielectric and the inclusion material is air. Therefore, the longitudinal effective permittivity becomes:

- For $(h_1 - \Delta H_1) \geq z \geq 0$:

$$\varepsilon_r^{\text{long}} = \varepsilon_{r1} + \frac{\pi}{3\sqrt{3}} \left(\frac{h_1 - z}{H_1} \right)^2 (\varepsilon_{r2} - \varepsilon_{r1})$$

- For $0 \geq z \geq -\Delta H_2$:

$$\varepsilon_r^{\text{long}} = \varepsilon_{r2} + \frac{\pi}{2\sqrt{3}} \left(\frac{z - h_2 + H_2}{H_2} \right)^2 (\varepsilon_{r1} - \varepsilon_{r2})$$

- For $-\Delta H_2 \geq z \geq (h_2 - H_2 + \Delta H_2)$:

$$\varepsilon_r^{\text{long}} = \varepsilon_{r2} + \frac{\pi}{2\sqrt{3}} \frac{(z - h_2 + H_2)^2 + z^2}{H_2^2} (\varepsilon_{r1} - \varepsilon_{r2})$$

- For $(h_2 - H_2 + \Delta H_2) \geq z \geq (h_2 - H_2)$:

$$\varepsilon_r^{\text{long}} = \varepsilon_{r2} + \frac{\pi}{2\sqrt{3}} \left(\frac{z}{H_2} \right)^2 (\varepsilon_{r1} - \varepsilon_{r2})$$

- For $(h_2 - H_2) \geq z \geq (h_2 - H_2 - h_1 + \Delta H_1)$:

$$\varepsilon_r^{\text{long}} = \varepsilon_{r1} + \frac{\pi}{3\sqrt{3}} \left(\frac{h_2 - H_2 - h_1 - z}{H_1} \right)^2 (\varepsilon_{r2} - \varepsilon_{r1})$$

It is interesting to note that these equations are independent of the cell size $2s$.

For the complex permittivity profile to form a continuous function at $z = 0$, the permittivities $\varepsilon_r^{\text{trans}}$ and $\varepsilon_r^{\text{long}}$ must themselves be continuous functions at $z = 0$. For a function to be continuous at $z = 0$, the function must have the same ordinate and the same first derivative at $z = 0^-$ and $z = 0^+$. Hence, from the above expressions for $\varepsilon_r^{\text{long}}$, the continuity of $\varepsilon_r^{\text{trans}}$ is insured with:

$$h_1 = \left(\frac{2H_2}{1 - \frac{h_2}{H_2}} \right) \left(\frac{\sqrt{3}}{\pi} - \frac{1}{2} \left(1 - \frac{h_2}{H_2} \right)^2 \right) \qquad (4.30)$$

$$H_1 = \frac{1}{\sqrt{3}} \left(\frac{2H_2}{1 - \frac{h_2}{H_2}} \right) \sqrt{\frac{\sqrt{3}}{\pi} - \frac{1}{2} \left(1 - \frac{h_2}{H_2} \right)^2} \qquad (4.31)$$

which expressions are independent of ε_{r1}, ε_{r2} and s. Since both functions $\varepsilon_r^{\text{trans}}$ and $\varepsilon_r^{\text{long}}$ vary smoothly with the fill fraction $v(z)$, insuring the continuity of $\varepsilon_r^{\text{long}}$ also insures the continuity of $\varepsilon_r^{\text{trans}}$.

In order to insure a non-zero wall separation w between adjacent air cones at $z = 0$ and $z = -HH$, the optimum packing of the air cones must be avoided. Instead, one must use:

$$h_2 = D = \left(\frac{w}{2} \right) \left(\frac{H_2}{s} \right) \Longrightarrow \frac{h_2}{H_2} = \frac{1}{2} \frac{w}{s} \qquad (4.32)$$

where s is yet to be determined (but note that $\frac{s}{H_2} = \frac{1}{8}$ is set by the slope of the drill bits). The optimum packing of the air cones at $z = 0$ would have required $w = h_2 = D = 0$. With $h_2 = D$ and $(h_2 - H_2) = -HH$, and using Equation (4.32), one obtains:

$$h_1 = \frac{2(D + HH)}{1 - \frac{1}{2} \frac{w}{s}} \left(\frac{\sqrt{3}}{\pi} - \frac{1}{2} \left(1 - \frac{1}{2} \frac{w}{s} \right)^2 \right) \qquad (4.33)$$

$$H_1 = \frac{1}{\sqrt{3}} \frac{2(D + HH)}{1 - \frac{1}{2} \frac{w}{s}} \sqrt{\frac{\sqrt{3}}{\pi} - \frac{1}{2} \left(1 - \frac{1}{2} \frac{w}{s} \right)^2} \qquad (4.34)$$

Therefore the dielectric cones have a physical height equal to h_1 and a base radius a_1 obtained from Equations (4.23), (4.33) and (4.34) as:

$$a_1 = A_1(z = 0) = \frac{s}{\sqrt{3}} \frac{h_1}{H_1} = s\sqrt{\frac{\sqrt{3}}{\pi} - \frac{1}{2}\left(1 - \frac{1}{2}\frac{w}{s}\right)^2} \qquad (4.35)$$

Since the value a_1 must be smaller than $(s/\sqrt{3}) \approx 0.5774s$ for which two adjacent dielectric cones would be touching at their base, one obtains:

$$\frac{s}{\sqrt{3}}\left(\frac{h_1}{H_1}\right) < \frac{s}{\sqrt{3}} \implies \frac{h_1}{H_1} < 1$$

which result makes physical sense for, otherwise, the dielectric cone could not possibly exist. Thus one obtains:

$$w < \underbrace{\left(1 - \sqrt{2\left(\frac{\sqrt{3}}{\pi} - \frac{1}{3}\right)}\right)}_{\approx 0.34} 2s$$

The corresponding half-angle at the apex of the dielectric cone is obtained as:

$$\xi = \arctan\left(\frac{a_1}{h_1}\right) \qquad (4.36)$$

Similarly, the inverted and the non-inverted air cones have a physical height of H_2 and a base radius a_2 obtained from Equations (4.24) and (4.32) as:

$$a_2 = A_2(z = 0) = s\underbrace{\left(1 - \frac{h_2}{H_2}\right)}_{\frac{HH}{H_2}} = s\left(1 - \frac{1}{2}\frac{w}{s}\right) \qquad (4.37)$$

Equations (4.22) and (4.37) are consistent with one another. The half-angle for the air cones is set to:

$$\xi = \arctan\left(\frac{1}{8}\right) \qquad (4.38)$$

It is interesting to note that none of the geometrical parameters of the cones depends on the complex permittivities ε_{r1} and ε_{r2}. Hence, the same values for h_1, a_1, a_2, D and s would result for a same choice of values for

$\frac{s}{H_2} = \frac{1}{8}$, HH and w, regardless of whether the dielectric material was Teflon, Plexiglas, Delrin, Nylon or else. Also, the same electromagnetic response is obtained from a frequency-scaled version of the geometry if the values for ε_{r1} and ε_{r2} remain the same at the new design frequency, and if $2s$ remains much smaller than the new wavelength.

No effort was made to minimize the discontinuity incurred by the missing tips for the dielectric cones or those for the air cones. The drill bits used herein corresponded to the case of having $\Delta H_2 = 1.0$ cm.

The combined use of the scattering matrix propagator technique and the approximation of the permittivity profile as being a cascade of homogeneous layers:

- permits to deal with the simpler 2-D geometry of a circular cylinder in each thin layer rather than the 3-D geometry of a circular cone;

- permits to account readily for the presence of a longitudinal discontinuity of the permittivity profile (e.g. the presence of a layer of glue at the mid-thickness point of a plate if the plate needs to be fabricated from two separate thinner dielectric plates, or the absence of the tips for the air cones or the dielectric cones as a result of fabrication limitations);

- does not permit to account readily for the presence of a transverse discontinuity of the permittivity (e.g. the absence of air cones or dielectric cones at the centre of the plate in order to accomodate a hole for an axle, or the presence of the edge in truncating the infinite array to dimensions of a few wavelengths across).

The effect of the staircase approximation of the complex permittivity profile is neglected here because, in principle, the staircase approximation can be made very small by taking each layer to be very thin. Although not mentioned in the literature, it might be possible that the process of computing the effective permittivity by the above method becomes more approximative or even invalid as the thickness of the homogeneous layer becomes much smaller than the transverse dimensions of the unit cell. Thus again, we will have to rely on experimental results to determine if such is the case.
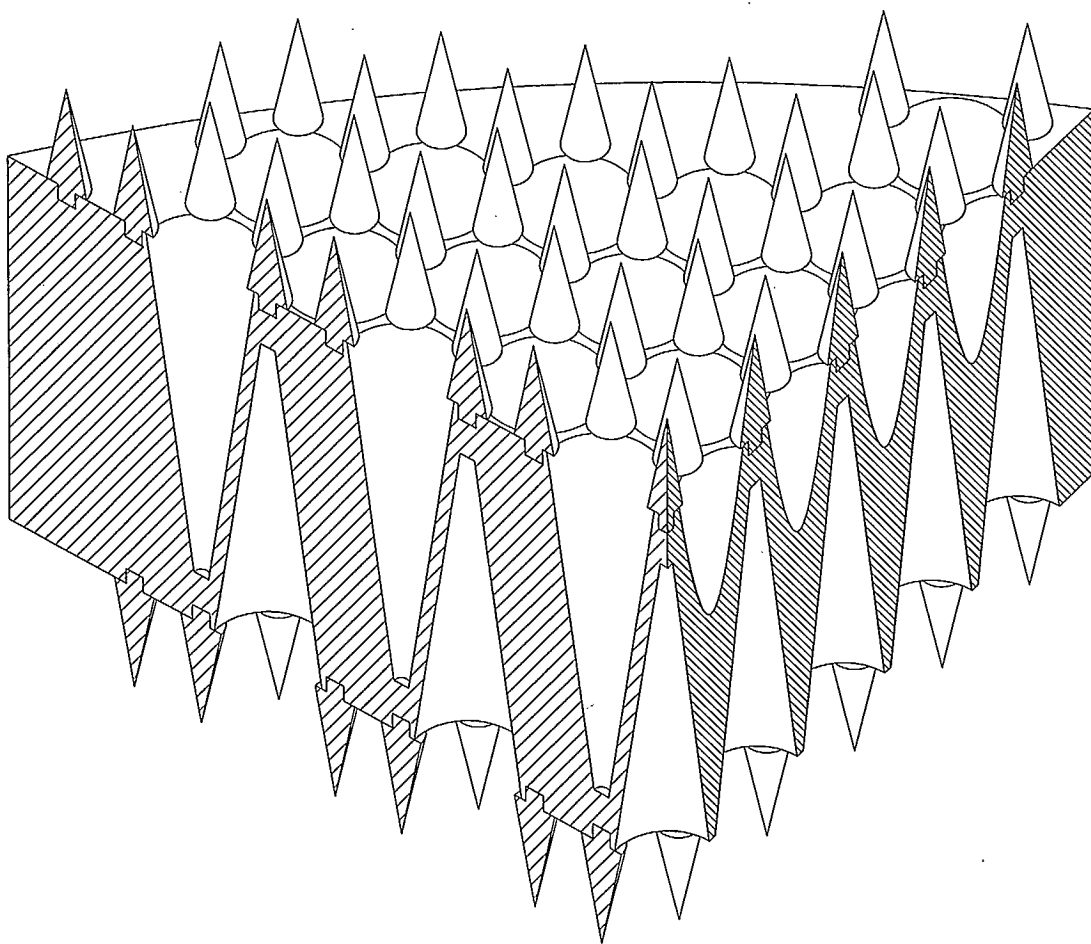
Figure 4.7: 3-D representation of a small section cut away at the periphery
of the round plate in its final design.
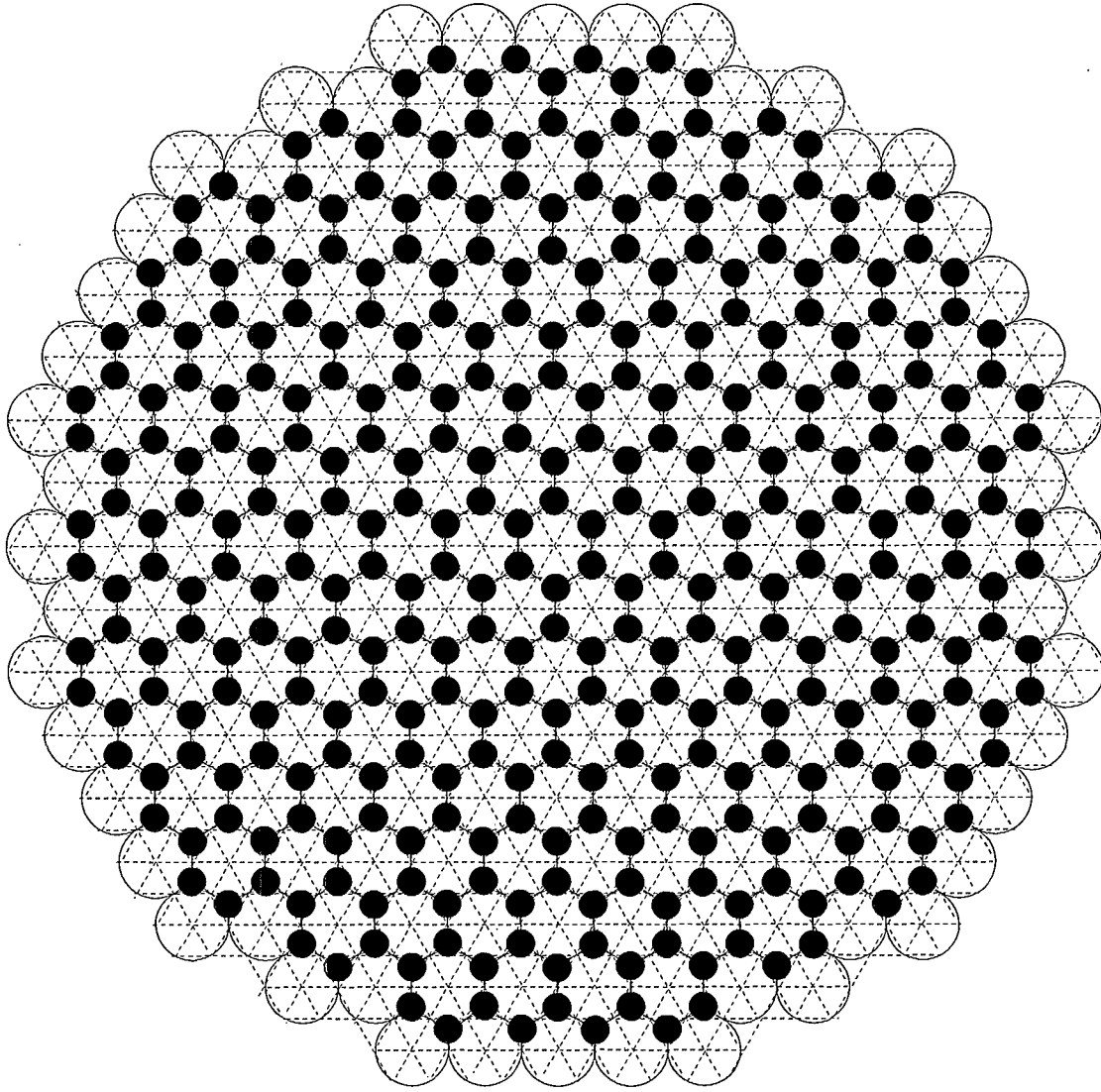
Figure 4.8: Conceptual rear view of the plate showing in dash line the equilateral triangular lattice, in solid line the footprints of the air cones bored into the back face of the dielectric slab forming the middle section, and in solid dark color the footprint of the dielectric cones protruding out from the back face of the middle section. The front face looks identical except that the equilateral triangular lattice is vertically offset as shown in Figure 4.9 in order that the air cones bored from the front face be interlaced with the air cones bored from the back face. The hole for the axle at the centre of the plate is not shown here. For convenience of representation, this figure shows a zero cone wall separation between adjacent cones, i.e. $w = 0$ and $s = a_2$, resulting in adjacent cones touching one another.
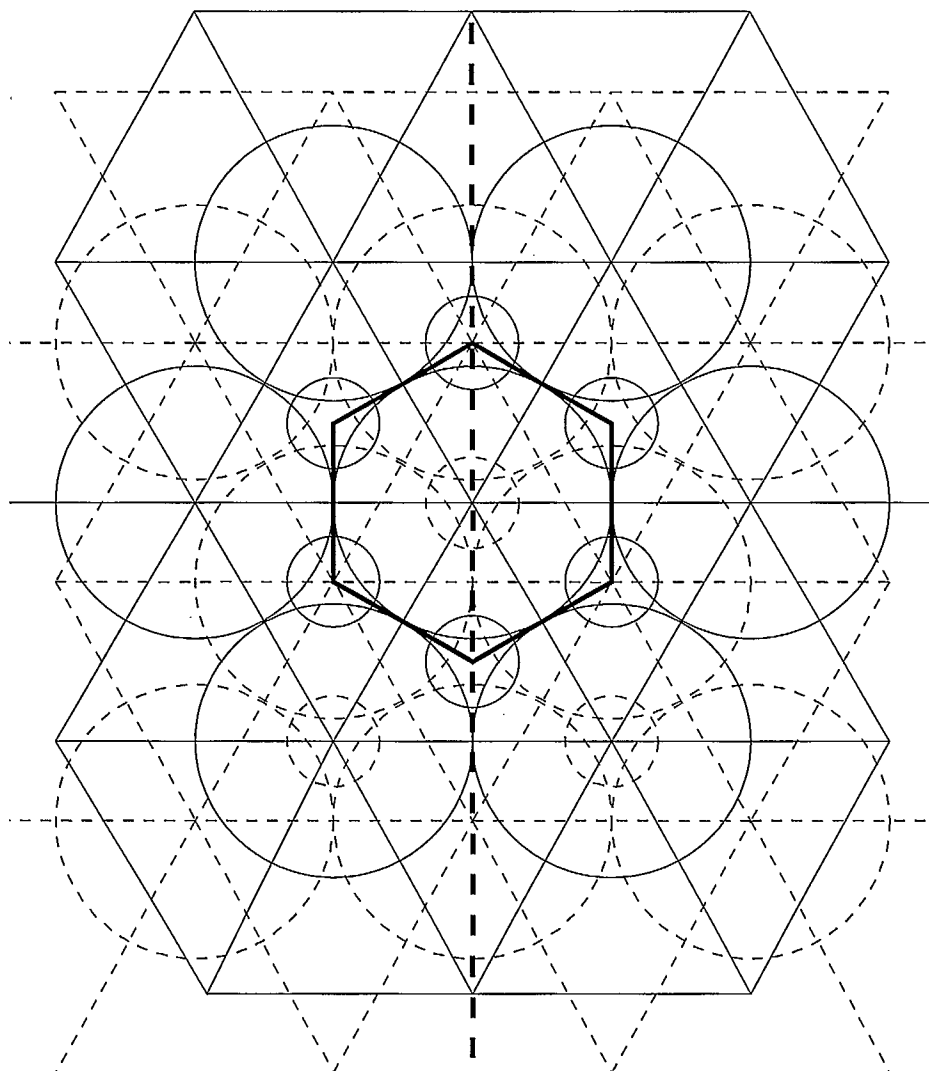
Figure 4.9: A close-up view of the composite array consisting of the overlay of the front (solid) and back (dash) interlaced triangular lattices. The two lattices are identical except for a vertical offset equal to $2s/\sqrt{3}$ where s is the radius of the large circle inscribed by the hexagonal unit cell at the centre of the figure. The footprints for the circular air cones (large circles) and for the circular dielectric cones (small circles) are also shown in solid or dash (unless overlaid) line according to the lattice to which they correspond. The end result is that each lattice has every large circle surrounded by six small circles located at the periphery of the large circle. The composite array is symmetrical about the fat vertical dashed line. For convenience of representation, this figure shows a zero cone wall separation between adjacent cones, i.e. $w = 0$ and $s = a_2$, resulting in adjacent cones touching one another.

Figure 4.10: This variable arrangement of the cones contained in the hexagonal unit cell of Figure 4.9 for the front and the middle sections of the plate was used to compute the values of h_1 and H_1 that produce a continuous complex permittivity function. The blank regions at the tips of both air cones are the missing tips of length ΔH_2, modelling the drill bits being truncated for practical purposes. The blank region at the tip of the dielectric cone is the missing tip of length ΔH_1, modelling possible fabrication imperfections.

Figure 4.11: Variation of the real part of $\varepsilon_r^{\text{trans}}$ and $\varepsilon_r^{\text{long}}$ as a function of the fill fraction v.
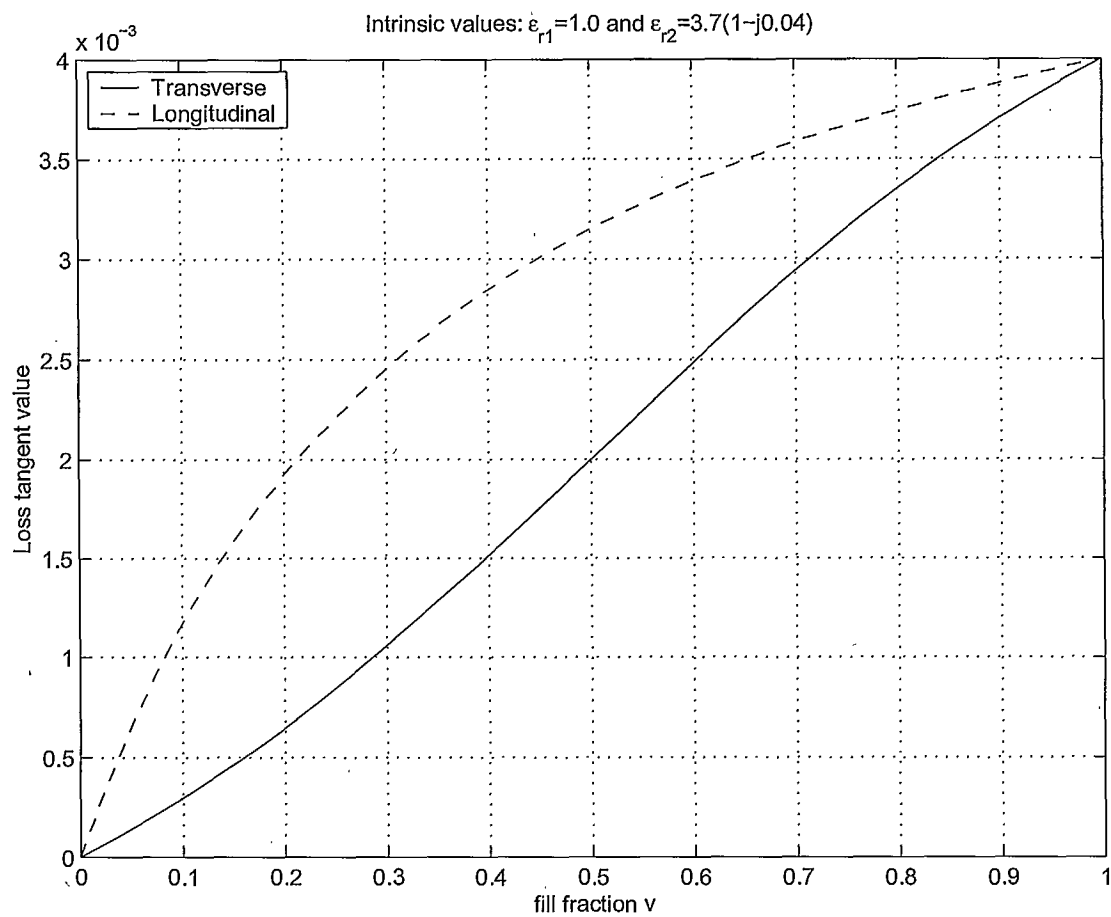
Figure 4.12: Variation of the loss tangent for $\varepsilon_r^{\text{trans}}$ and $\varepsilon_r^{\text{long}}$ as a function of the fill fraction v.

Figure 4.13: This figure shows the staircase approximation of the structural profile of the hexagonal unit cell which is schematically represented here by a lens shape object for convenience. There are N regions with region n=1 and n=N being half-spaces. The permittivity is taken to be constant in every region, with a value corresponding to the permittivity at the mid-point of the region except for regions n=1 and n=N where the value ε_r is assigned. No region is thicker than the nominal value dz.

Chapter 5

Design of the mounting plate

5.1 Computed results

This section presents the results of a parametric analysis for the reflection and the transmission level for both the perpendicular and the parallel polarizations. All computations were carried out with double precision in Matlab 5.3.0 which corresponds to about a precision of 32 digits (see Reference [82, p. 1.65]) on a SUN Ultra Sparc workstation running OpenWindows 3.5.1. The values for the reflection and the transmission level in dB were computed as $\mathcal{R}(\text{dB}) = 20 \log_{10} |R|$ and $\mathcal{T}(\text{dB}) = 20 \log_{10} |T|$, respectively, where R and T correspond to the co-polarization elements of the S_{11} and S_{21} sub-matrices for the composite GSM of the whole cascade system, with respect to either the parallel or the perpendicular polarization.

The parameters investigated here are:

- complex permittivity profile, i.e. shaped versus uniform profile;

- incidence angle ξ_1, assuming that the incident waveform from the air medium was always a uniform plane wave, i.e. $\rho_1 = 0$;

- slab thickness HH (m);

- minimum cone wall separation w (m) at $z = 0$ and $z = -HH$.

- layer thickness dz (m) for discretizing the geometry;

Since there are too many parameters to explore every combination of all parameters, the parameters for all computations carried out below were as per the following baseline design unless mentioned otherwise:

- $\varepsilon_r = 3.7(1 - j0.004)$;

- $HH = 0.074$ m;

- $\Delta H_2 = 0.010$ m;

- $w = 0.0014$ m;

- $\Delta H_1 = 0$ m;

- $H_3 = 0$ m where H_3 is the thickness (m) of the layer of glue at the mid-thickness point of the dielectric slab;

- incidence angle $0° \leq \xi_1 \leq 90°$ which range requires to use both Equations (2.25) and (2.29);

- $f = 1900$ MHz;

- layer thickness $dz \leq 0.0025$ m throughout the plate (in practice, the cone walls are smooth which correspond to having dz tending toward the limit 0).

Because the optimum shaped profile that produces the least amount of reflection (see References [54] and [31, chapter 15]) may not be easily realizable by means of boring holes of some particular geometrical shape into the dielectric, the strategy here was to start with the shaped profile corresponding to circular cones and to find a particular value of HH and w that yielded a low reflection level of about -20 dB over as wide as possible a range of the incidence angle ξ_1. Hence, some performance at normal incidence was sacrificed for the sake of maintaining a better performance at off-normal incidence. The resulting design is also less susceptible to parameter variations than a design relying on the resonance phenomenon (e.g. a quarter-wave plate transformer, and designs mentioned on the next page with $HH = 0.041$ m and $HH = 0.082$ m).

From Figure 5.1, we see that the choice of $HH = 0.074$ m and $w = 0.0010$ m makes the two polarizations track each other almost perfectly over the range $0° \leq \xi_1 \leq 35°$. For $HH > 0.074$ m, the notch for the perpendicular polarization would follow that for the parallel polarization whereas for $HH < 0.074$ m, the notch for the perpendicular polarization would precede that for the parallel polarization. At the same time, the reflection level at normal incidence $\xi_1 = 0$ increases with increasing the HH value. Since the perpendicular polarization is the one that limits the angular range for the incidence angle ξ_1, the range of operation over which all reflection curves lie below -20 dB would increase if HH was chosen greater than 0.074 m but the reflection level at normal incidence would also increase. Note that the

maximum thickness that can be readily supplied by the manufacturer of Delrin material is about 0.076 m (i.e. 3 inches), and a minimum of 0.075 m is required for achieving a reasonably flat plate by machining both the front and the back surfaces of the Delrin slab. Therefore, no value of HH greater than 0.075 m was investigated systematically.

The effect of varying the parameter w turns out to be larger on the perpendicular polarization than on the parallel polarization. This situation affords us an additional degree of freedom to shape the response. The choice of $HH = 0.074$ m and $w = 0.0014$ m was retained for the final design at 1900 MHz. The drill bit imposed the limitations corresponding to $\Delta H_2 = 0.010$ m and $\frac{s}{H_2} = \frac{1}{8}$. Consequently, $h_2 = D = 0.0056$ m, $H_2 = 0.0796$ m, $2s = 0.0199$ m, $h_1 = 0.0204$ m and $H_1 = 0.0341$ m.

Numerical experiments show that a low level of reflection is not necessarily achieved just because the complex permittivity profile is a continuous function of z, and vice-versa, a large amount of reflection is not necessarily incurred just because the complex permittivity profile presents large discontinuities. It is possible to obtain a low level of reflection from the uniform profile by choosing the thickness to correspond to some resonant length within the dielectric. The values of $HH = 0.041$ m and 0.082 m for the case of the uniform profile with $\xi_1 = 0$ corresponds to very nearly 0.5 and 1.0 wavelength in the dielectric, respectively. As the resonance phenomenon is achieved only over a narrow range of thickness values, frequencies and incidence angles, a low reflection level due to the resonance phenomenon is correspondingly achieved over only the corresponding narrow range of parameter values. In contrast to the use of the uniform profile at resonance, the use of the optimum shaped profile permits to maintain a reasonably low reflection level over a broader range of incidence angles for both polarizations.

Figure 5.3 shows that the shape profile provides a reflection level below about -22 dB for both polarizations over the range $0° \leq \xi_1 \leq 52°$. In comparison, Figure 5.5 shows that the uniform profile produces significantly larger values of reflection level over the same angular range, specially for the perpendicular polarization. The Brewster angle[1] for a lossless slab with $\varepsilon_r = 3.7$ would be $\xi_1^B = \arctan\left(\sqrt{3.7}\right) \approx 62.5°$. The reflection level corresponding to an incidence angle value equal to $\arctan\left(\sqrt{3.7}\right)$ for $\varepsilon_r' = 3.7$ was computed as -304.49 dB and -47.20 dB for $\tan(\delta) = 0$ and 0.004, respectively. The difference between $-\infty$ dB and -304.49 dB is due to roundoff errors during

---

[1]For a dielectric slab with its two interfaces being parallel to one another, the Brewster angle for the second interface is the 90° complement of the Brewster angle for the first interface, i.e. $\xi_1^B + \xi_2^B = 90°$ since $\arctan\left(\sqrt{\varepsilon_2/\varepsilon_1}\right) + \arctan\left(\sqrt{\varepsilon_1/\varepsilon_2}\right) = 90°$; since the Brewster's law gives $\xi_1^B + \xi_2 = 90°$, one obtains $\xi_2 = \xi_2^B$; therefore, both interfaces are operated at their respective Brewster angle and thus, the reflection level from the slab should theoretically be $-\infty$ dB, for any thickness of a lossless homogeneous uniform isotropic slab.

the computation whereas the difference between -304.49 dB^2 and -47.20 dB is clearly due to the presence of the dielectric loss corresponding to $\tan(\delta) = 0.004$.

Figures 5.7 and 5.8 show that the dielectric loss corresponding to $\tan(\delta) = 0.004$ does not affect the response of the plate significantly. Figure 5.9 shows that the response for the lossless plate is very consistent with the principle of conservation of energy. The discrepancy is only very slight and is likely due to roundoff errors during the computation. Figure 5.10 shows the variation of the energy lost inside the lossy dielectric plate with respect to the incidence angle ξ_1. That the energy loss increases with increasing incidence angle ξ_1 is consistent with the fact that the energy loss increases with increasing path length for the ray propagating inside the lossy material, and that this path length increases with increasing ξ_1. That the energy loss reaches a maximum then decreases thereafter owes to the fact that reflection becomes so important that little energy is transmitted into the lossy material, thus counteracting the loss increase due to the increased path length inside the lossy material.

Note that a bug in MATLAB 5.3 causes a discrepancy to appear in the position of the label for the curves, between the position as seen on the screen and the position as seen on the printed page. As a result, the labelling process required many iterations to produce the desired effect on the printed page. Owing to this very tedious task, many plots have been left unlabelled but one can easily identify each curve, either naturally by intuition or by referring to a similar plot that was labelled. Furthermore, many figures are provided for thoroughness, without formal comments in the text.

A convergence analysis was carried out by comparing the results obtained with varying the discretization increment dz from 0.0002 m to 0.0064 m by successively doubling dz. Figures 5.21 and 5.22 demonstrate that the method and its numerical implementation produce stable and convergent results for both polarizations. The difference of magnitude was computed by taking the case of $dz = 0.0002$ m as the reference.

The case of $dz = 0.0002$ m incurred a run time of about 20 h whereas the case for $dz = 0.0064$ m incurred a run time of less than 1 h. In contrast, the use of Holmes' expressions whenever $V = 0$ can sometimes cut down the computation time to less than a minute! A value of $dz = 0.0025$ m was chosen as a compromise between accuracy and computation time. The corresponding run time was about 1.5 h and the corresponding convergence results are shown in Figure 5.23. From this figure, one can observe that the

---

^{2}Although values less than about -100 dB might not be practically meaningful, they are nevertheless presented here to show the numerical values as computed from the program written in MATLAB.

error is less than 10^{-3} over the range $0° \leq \xi_1 \leq 52°$ for both polarizations. Thus, the error due to discretization for the reflection curves of Figure 5.3 would make the true value X lie in the range:

$$20 \log \left(10^{\frac{X'}{20}} - \text{Error} \right) \leq X \leq 20 \log \left(10^{\frac{X'}{20}} + \text{Error} \right)$$

For example, for the case of Error$= 10^{-3}$, a computed value of $X' = -60$ would correspond to a true value X ranging between $-\infty$ dB and -57 dB. A computed value of $X' = -22$ would correspond to a true value X ranging between -22.11 dB and -21.89 dB. Such an error is deemed quite acceptable for the purposes of assessing that the reflection level of the mountingplate does not exceed a given threshold value of, say, -22 dB over the range of, say, $0° \leq \xi_1 \leq 50°$.

The results for varying dz can also be interpreted in terms of the effect of the surface roughness of the walls of the cones whereby the average height of the peaks of the rough surface corresponds to $\sqrt{2}dz$. Hence, the reflection level does not appear to be sensitive (within an error of about 10^{-3} over the range $0° \leq \xi_1 \leq 52°$) to a surface roughness corresponding to about 0.0035 m or less. Such a value of surface smoothness is not difficult to achieve at all with a conical drill bit of the appropriate vertex angle.

Figures 5.13 to 5.16 show that the intrinsic propagation constants α_o and β_o are independent of the incidence angle ξ_1 for the perpendicular polarization, but that they increase smoothly with increasing ξ_1 for the parallel polarization. Figures 5.17 to 5.20 show that the transmission angles ξ_2 and ρ_2 are symmetrical about the mid-thickness point of the plate. The stripes appearing in Figures 5.17 and 5.18 show the locations where the process of discretizing the various sections of the plate produced layers of thickness less than the nominal dz value as a result of the overall thickness of a section not being necessarily an exact multiple integer of dz. The excess layer in each section was arbitrarily located at the interface next to $z = (h_1 - \Delta H_1)$ for the front section, at the interfaces next to $z = 0$, $z = -\Delta H_2$, $z = -HH/2$, $z = (-HH + \Delta H_2)$ and $z = -HH$ for the middle section, and finally at the interface next to $z = (-HH - h_1 + \Delta H_1)$ for the back section.

Since the parallel and the perpendicular polarizations are indistinguable at normal incidence, the curves for α_o, β_o, ξ_2 and ρ_2 are the same for both the parallel and the perpendicular polarization whenever $\xi_1 = 0$. Not surprisingly, the shape of the curves for β_o and α_o when $\xi_1 = 0$ is very similar to the shape of the permittivity profile.

Figures 5.24 and 5.25 show clearly the effect of having dielectric cones in the front and back regions of the plate. If we define the range of operation

as that for a reflection level no larger than -22 dB, we observe that the presence of the cones increases the range of operation by about $10°$.
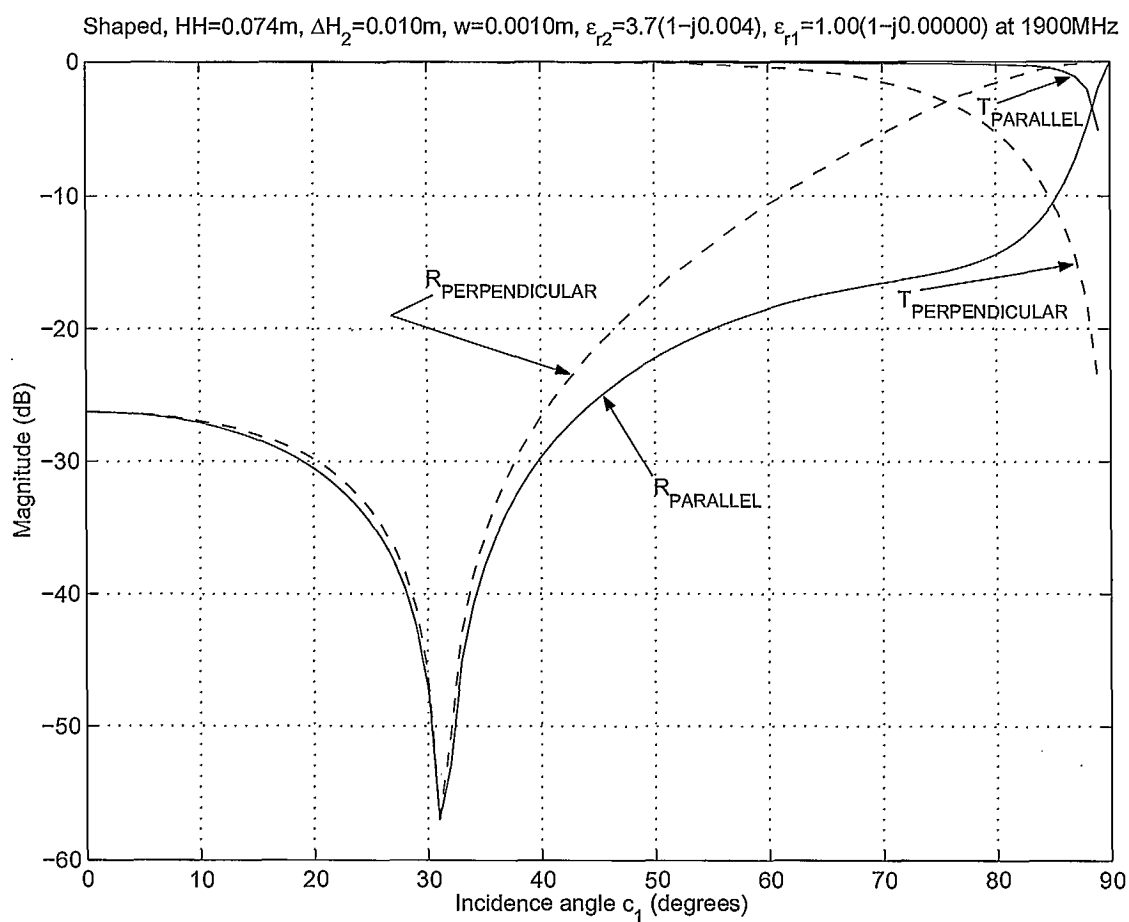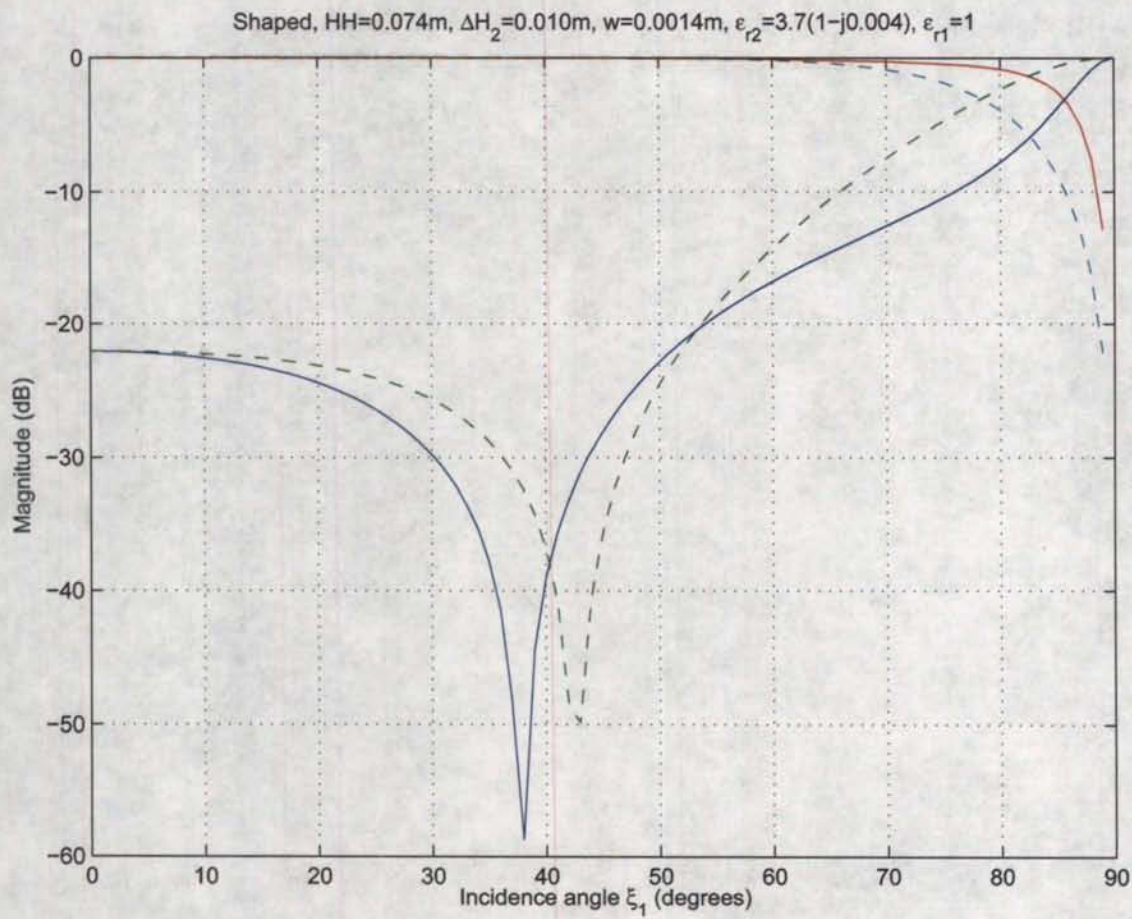
Figure 5.1: This figure shows the computed reflection and the computed transmission levels in dB for the shaped profile with $HH = 0.074$ m and $w = 0.0010$ m.
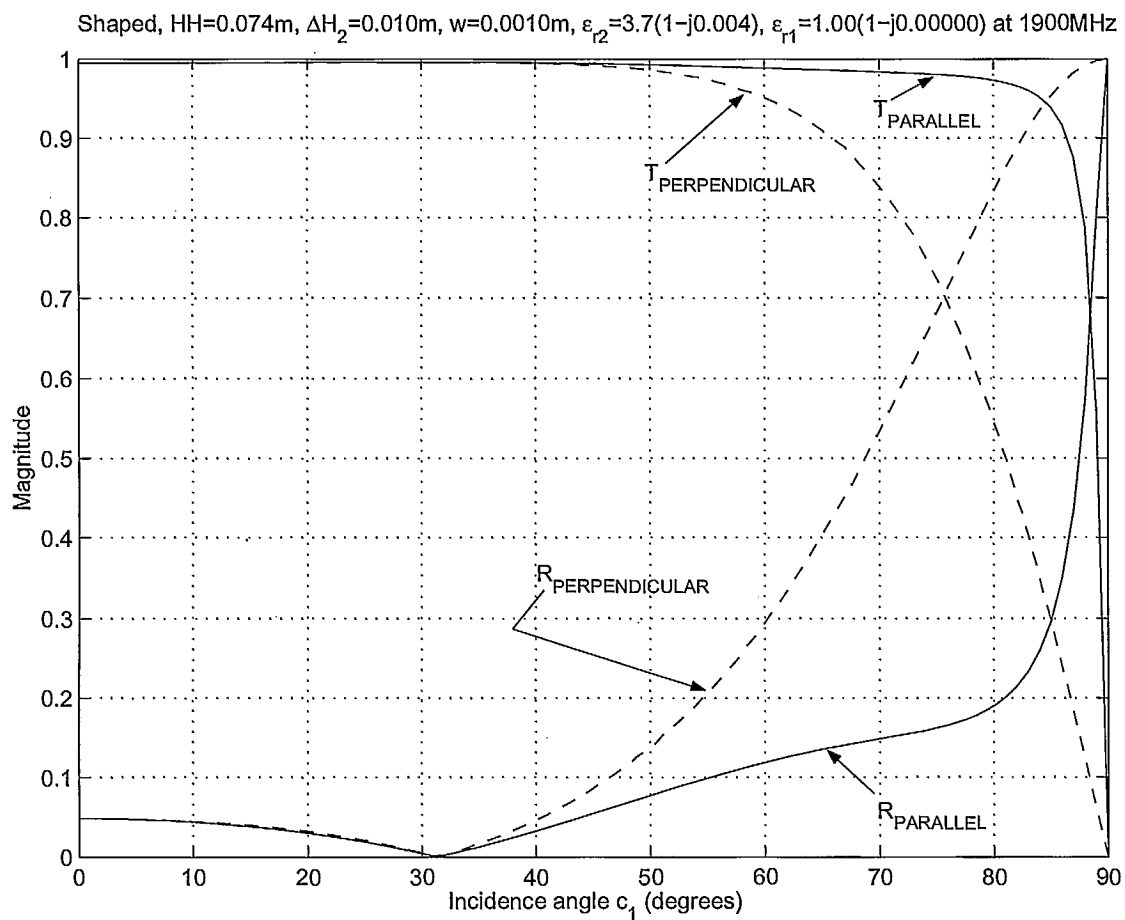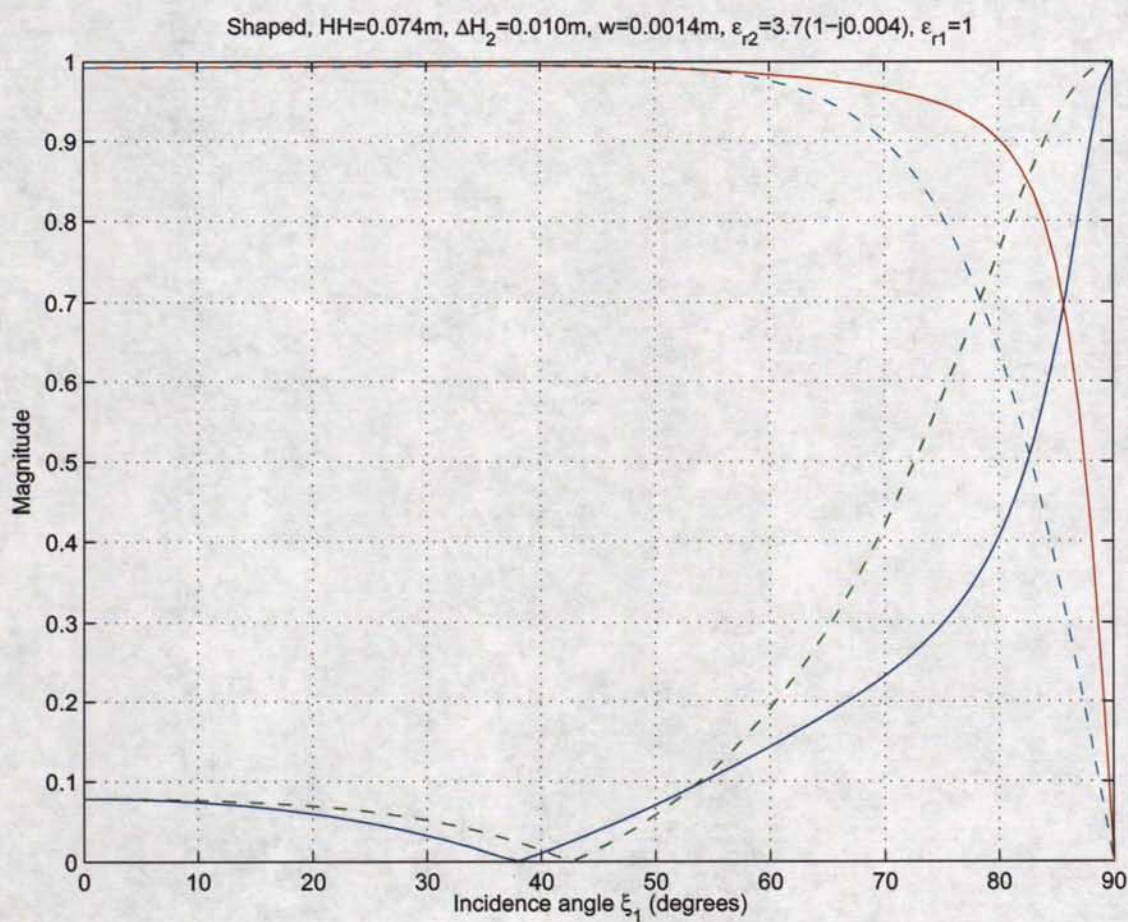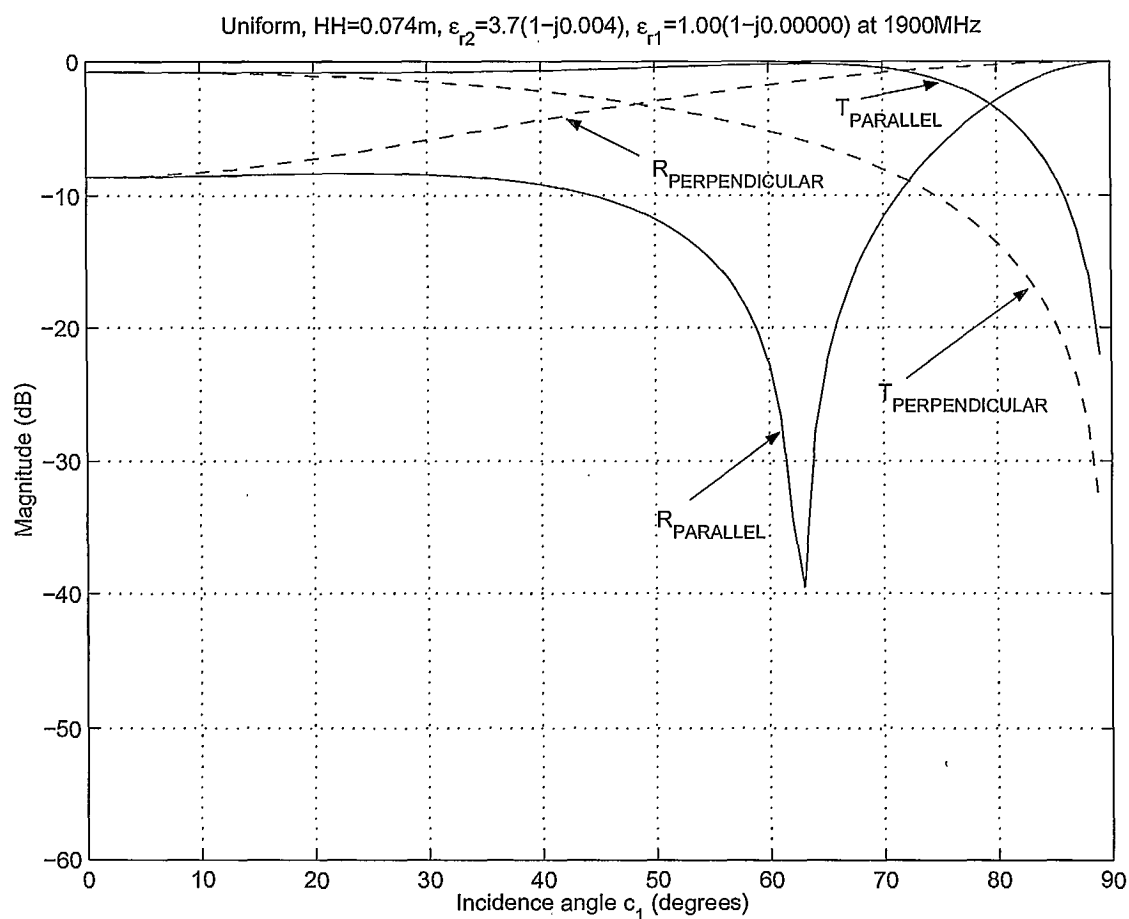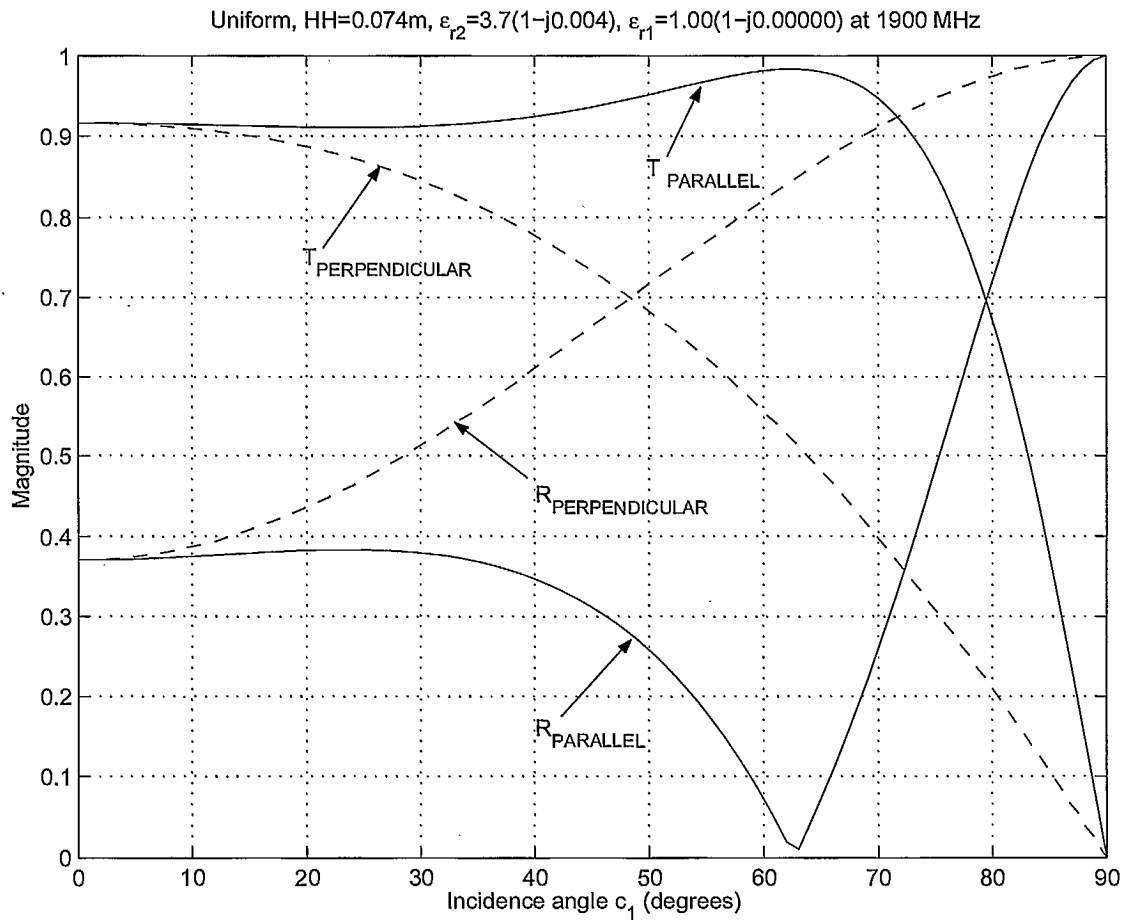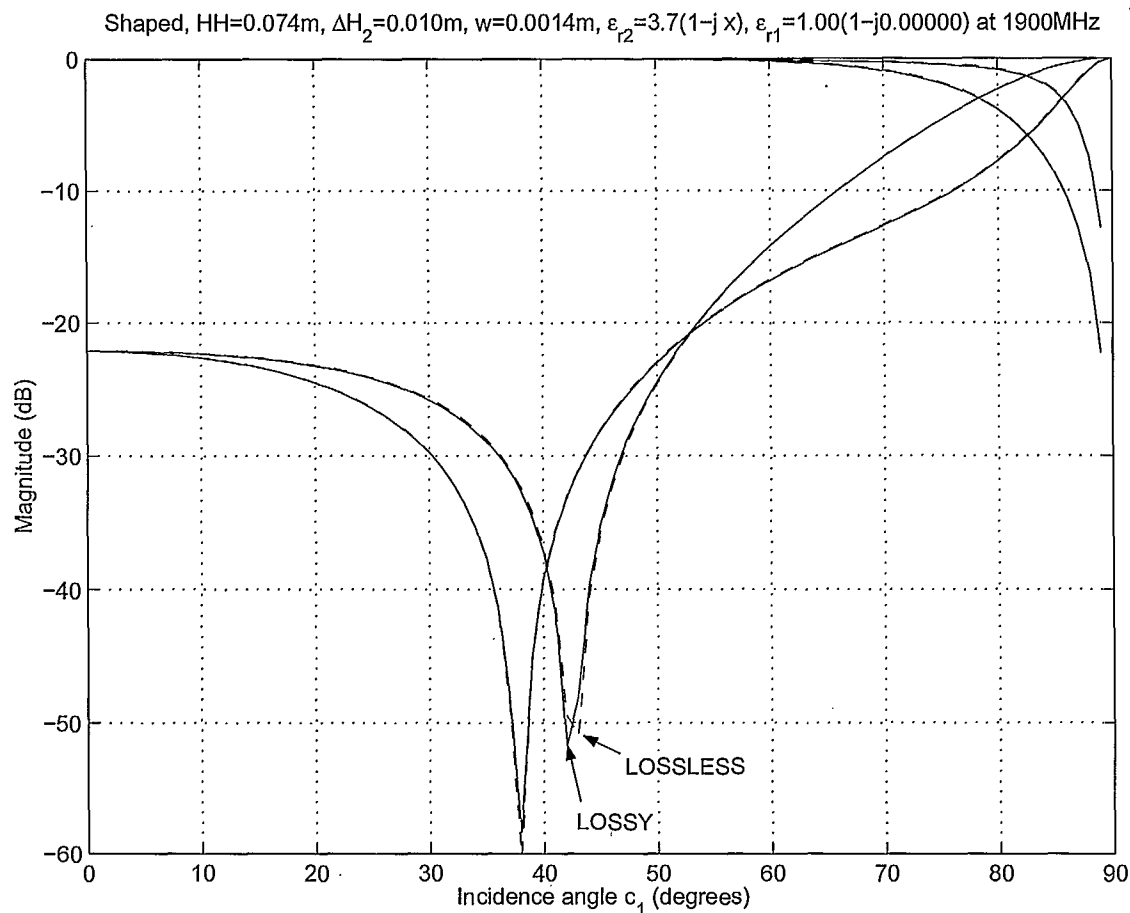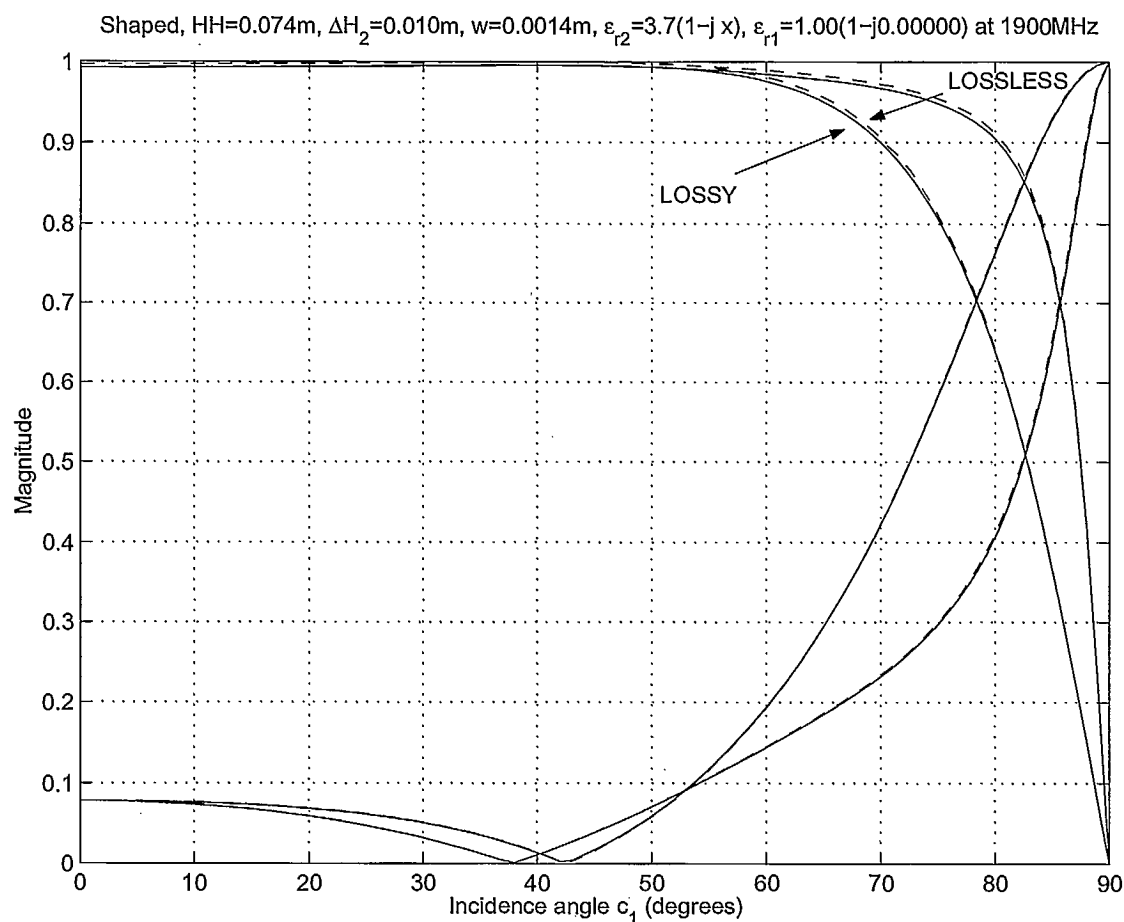
Figure 5.2: This figure shows the computed reflection and the computed transmission levels on the linear scale for the shaped profile with $HH = 0.074$ m and $w = 0.0010$ m.

Figure 5.3: This figure shows the computed reflection and the computed transmission levels in dB for the shaped profile with $HH = 0.074$ m and $w = 0.0014$ m. The discretization was $dz \leq 0.0004$ m throughout the plate.

Figure 5.4: This figure shows the computed reflection and the computed transmission levels on the linear scale for the shaped profile with $HH = 0.074$ m and $w = 0.0014$ m. The discretization was $dz \leq 0.0004$ m throughout the plate.

Figure 5.5: This figure shows the computed reflection and the computed transmission levels in dB for the uniform profile with $HH = 0.074$ m. The Brewster angle value is $\xi_1^B = 62.531°$ and the corresponding reflection level was computed as -47.20 dB which is not part of the plot because the null is much narrower than the 1° increment used in computing the curve.

Figure 5.6: This figure shows the computed reflection and the computed transmission levels on the linear scale for the uniform profile with $HH = 0.074$ m. The Brewster angle value is $\xi_1^B = 62.531°$ and the corresponding reflection level was computed as 0.0044 which is not part of the plot because the null is much narrower than the 1° increment used in computing the curve.

112

Figure 5.7: This figure shows the computed reflection and the computed transmission levels in dB for the shaped profile with $HH = 0.074$ m and $w = 0.0014$ m. The lossless and lossy cases correspond to $\tan(\delta) = 0$ and 0.004, respectively. The discretization was $dz \le 0.0004$ m throughout the plate.

Shaped, HH=0.074m, ΔH_2=0.010m, w=0.0014m, ε_{r2}=3.7(1−j x), ε_{r1}=1.00(1−j0.00000) at 1900MHz

Figure 5.8: This figure shows the computed reflection and the computed transmission levels on the linear scale for the shaped profile with $HH = 0.074$ m and $w = 0.0014$ m. The lossless and lossy cases correspond to $\tan(\delta) = 0$ and 0.004, respectively. The discretization was $dz \leq 0.0004$ m throughout the plate.
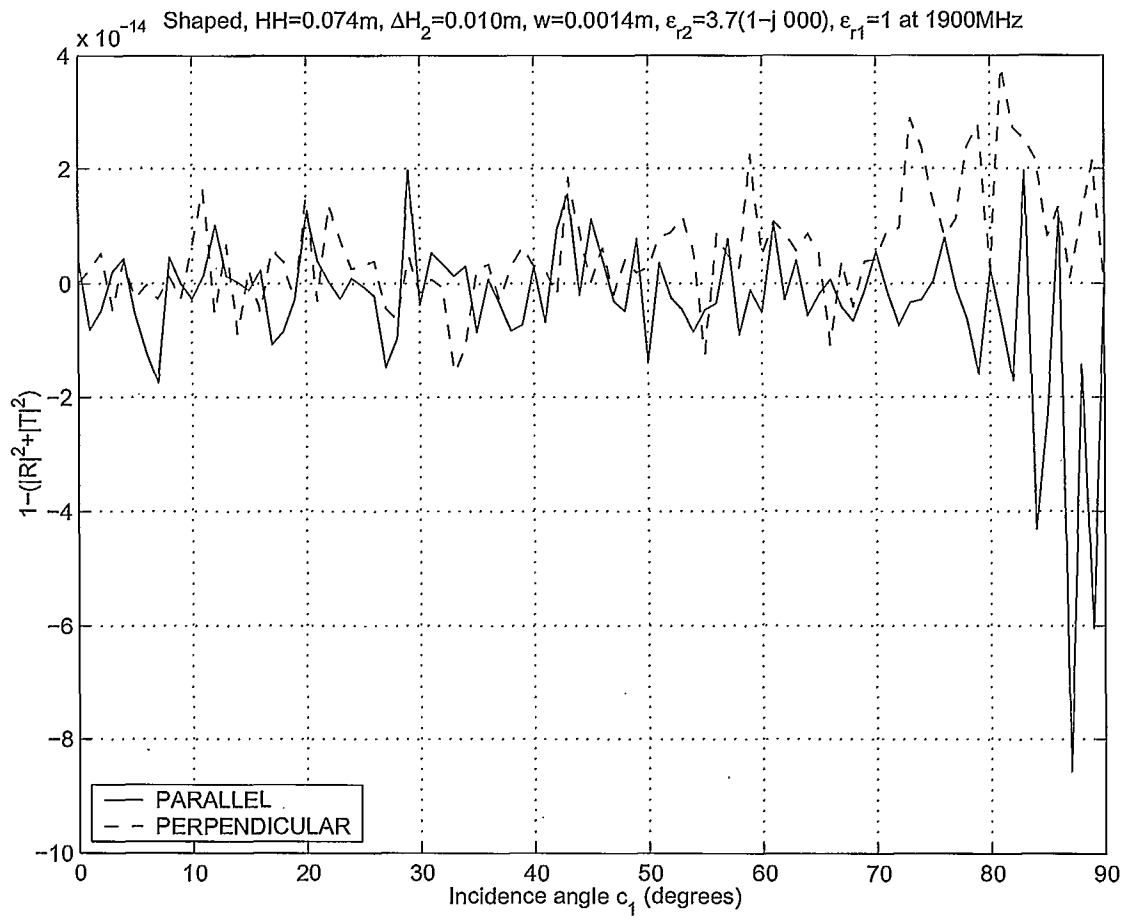
Figure 5.9: This figure shows the energy balance for the shaped profile with $HH = 0.074$ m and $w = 0.0014$ m, for the lossless plate. The discretization was $dz \leq 0.0004$ m throughout the plate.

115

Shaped, HH=0.074m, ΔH_2=0.010m, w=0.0014m, ε_{r2}=3.7(1–j0.004), ε_{r1}=1
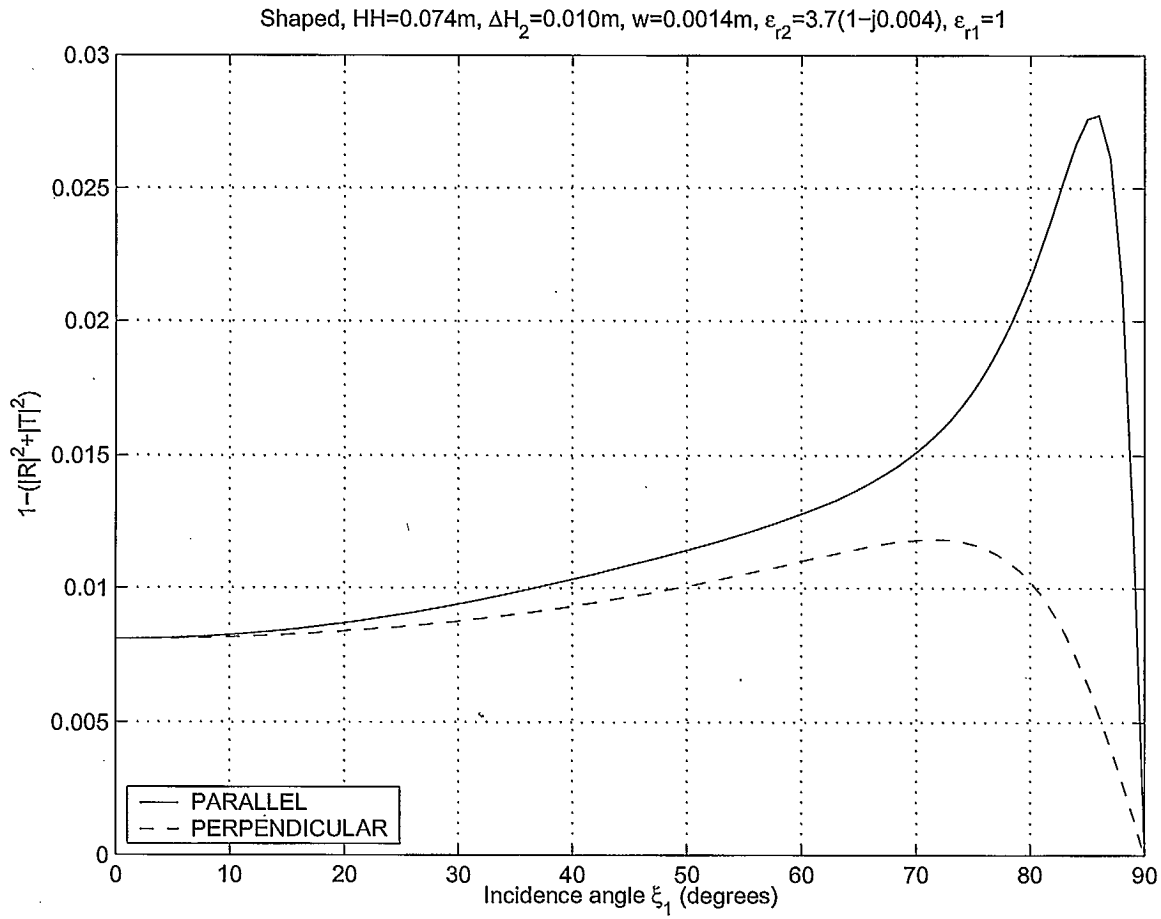
Figure 5.10: This figure shows the energy balance for the shaped profile with $HH = 0.074$ m and $w = 0.0014$ m, for the lossy plate with $\tan(\delta) = 0.004$. The discretization was $dz \leq 0.0004$ m throughout the plate.

116

Shaped, HH=0.074m, ΔH_2=0.010m, w=0.0014m, H_3=0.0000m, ε_{r2}=3.7(1−j0.004), ε_{r1}=1
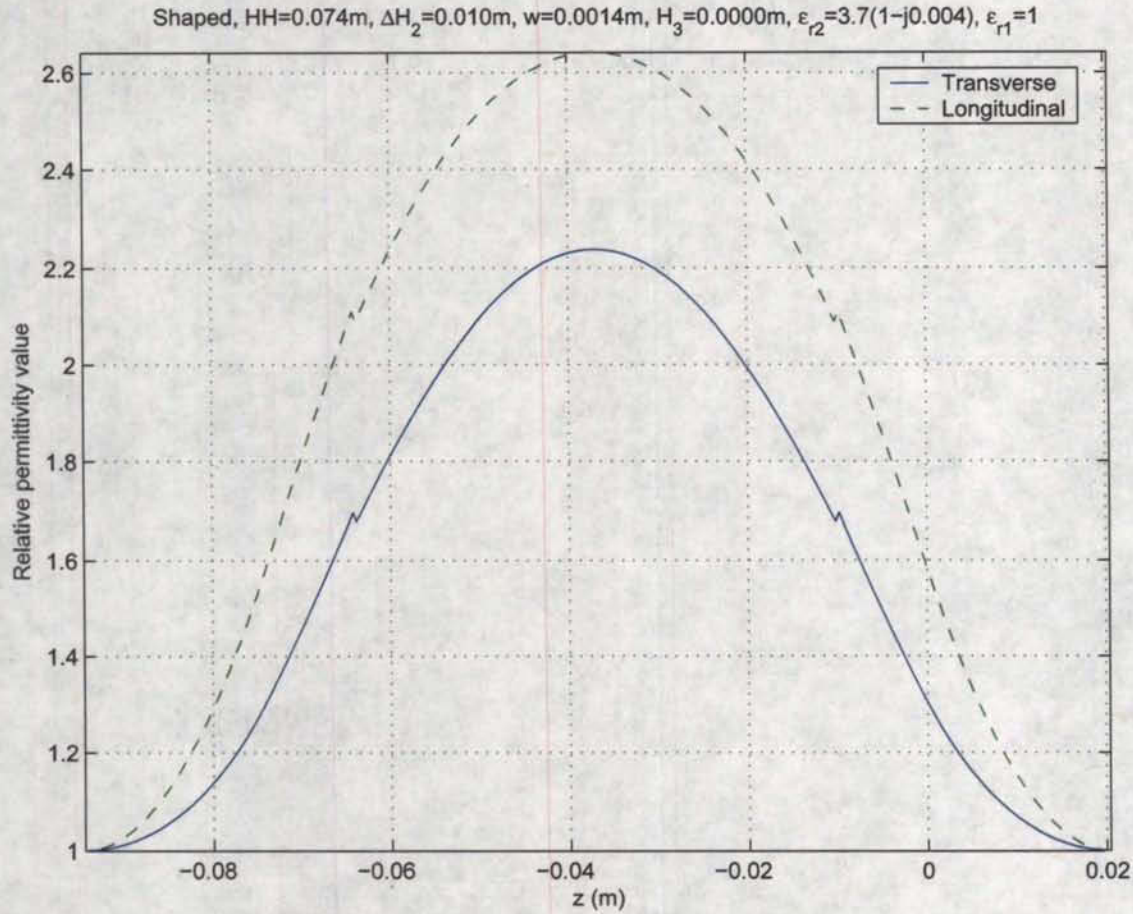
Figure 5.11: This figure shows the profile for the real part of $\varepsilon_r^{\text{trans}}$ and $\varepsilon_r^{\text{long}}$ for the shaped profile with $HH = 0.074$ m. The discretization was $dz \leq 0.0004$ m throughout the plate. Note that the maximum effective permittivity value which occurs at $z = \frac{-HH}{2}$ is significantly less than the intrinsic value of $\varepsilon_r' = 3.7$.
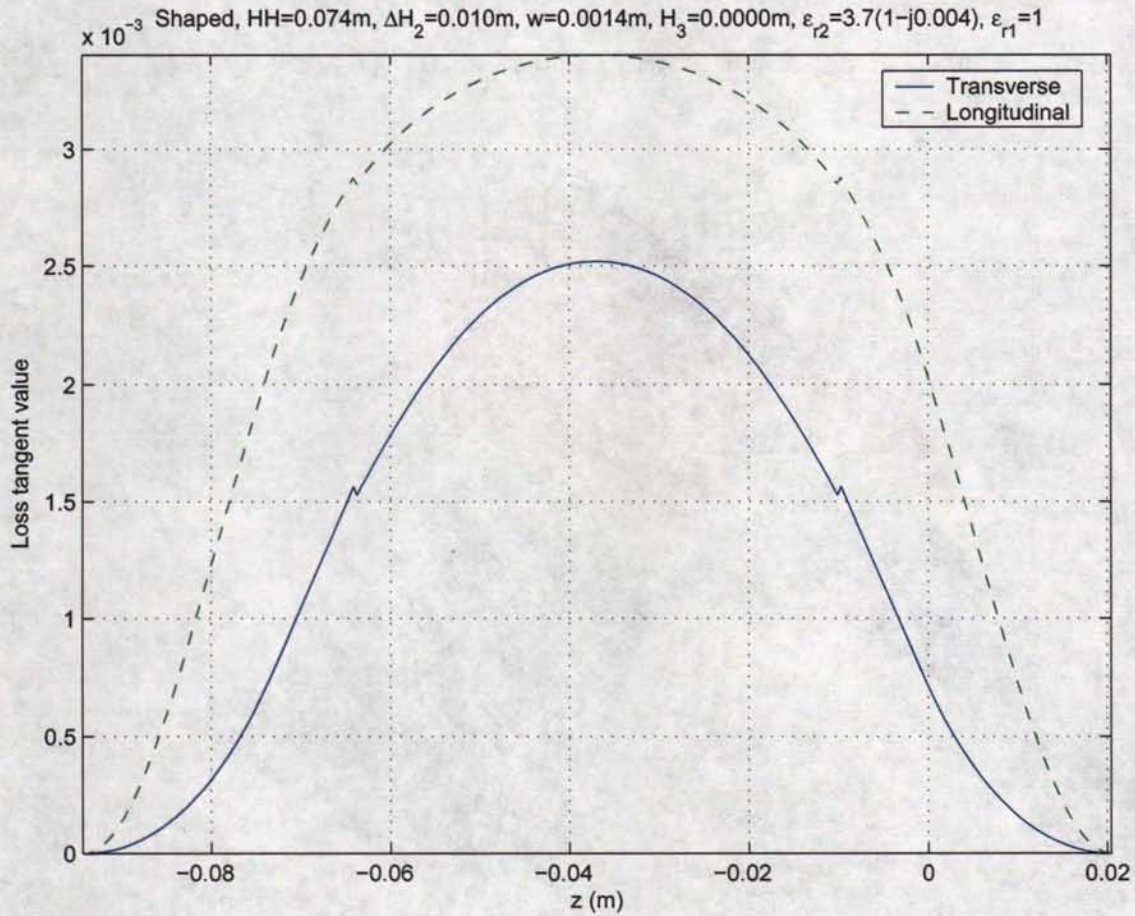
Figure 5.12: This figure shows the profile for loss tangent of $\varepsilon_r^{\text{trans}}$ and $\varepsilon_r^{\text{long}}$ for the shaped profile with $HH = 0.074$ m. The discretization was $dz \leq 0.0004$ m throughout the plate. Note that the maximum effective loss tangent value which occurs at $z = \frac{-HH}{2}$ is significantly less than the intrinsic value of $\tan(\delta) = 0.004$.

Shaped, HH=0.074m, ΔH_2=0.010m, w=0.0014m, H_3=0.0000m, ε_{r2}=3.7(1–j0.004), ε_{r1}=1
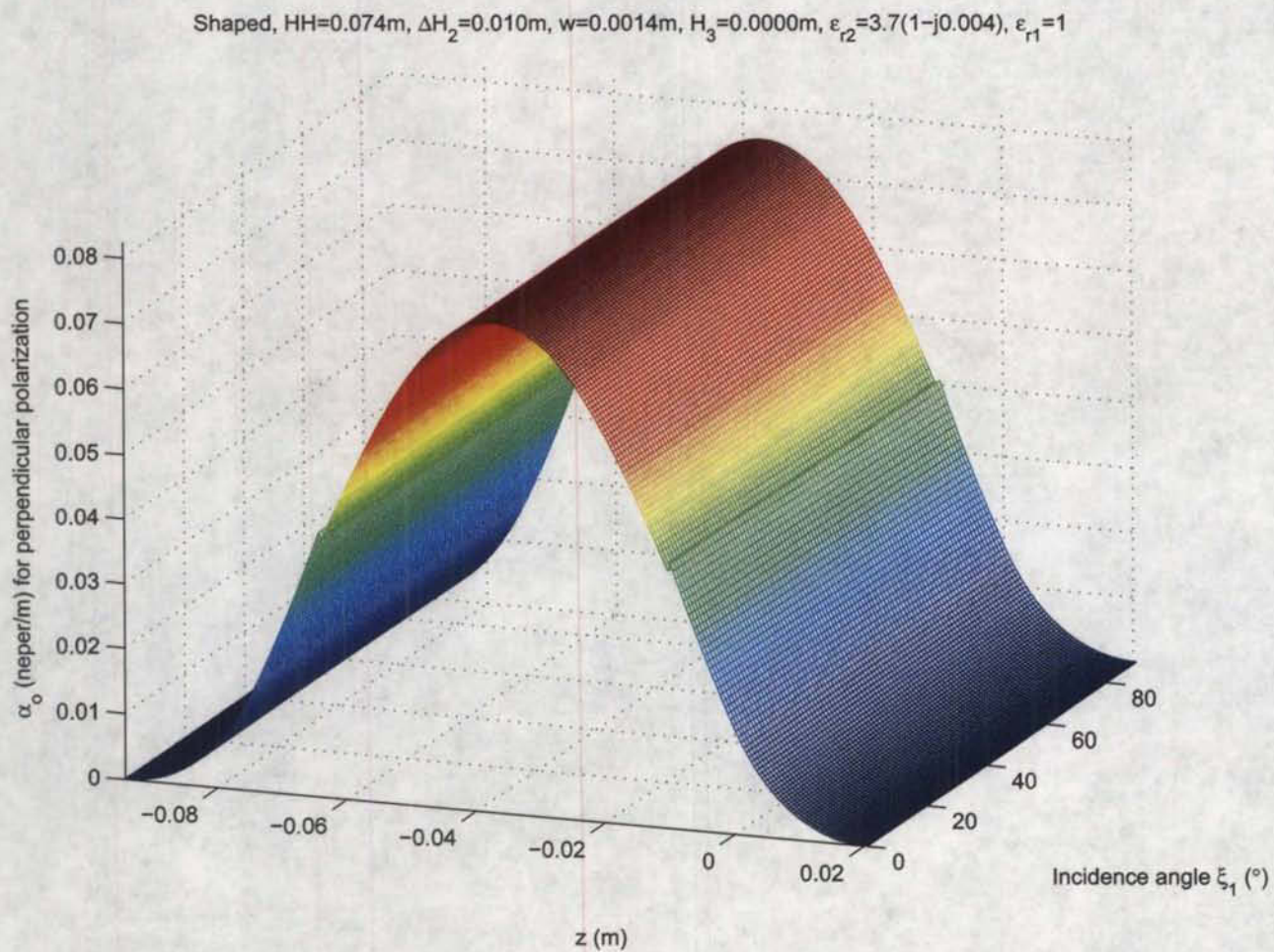
Figure 5.13: This figure shows the intrinsic amplitude propagation constant α_o for the shaped profile with $HH = 0.074$ m for the perpendicular polarization. The discretization was $dz \leq 0.0004$ m throughout the plate.
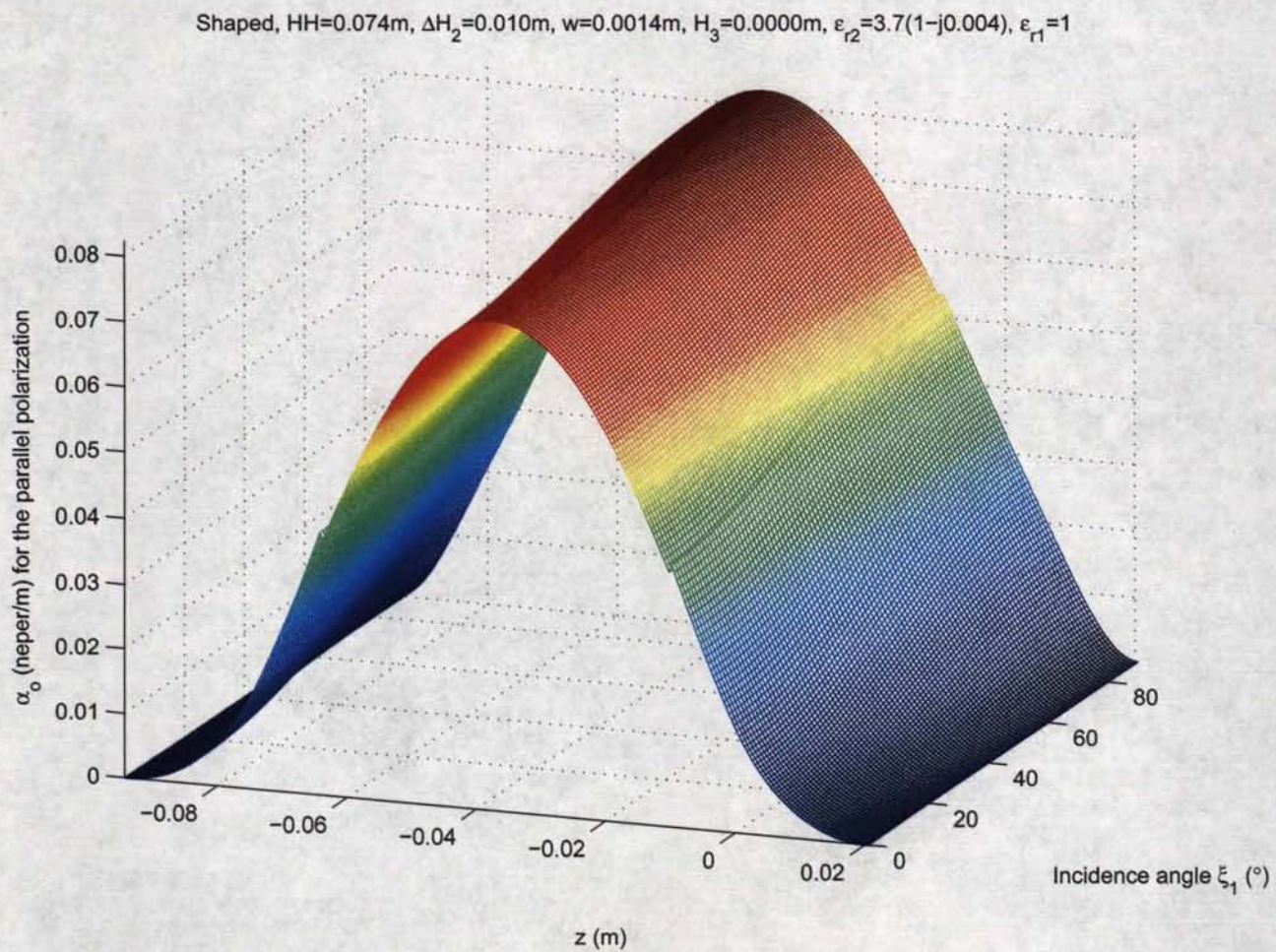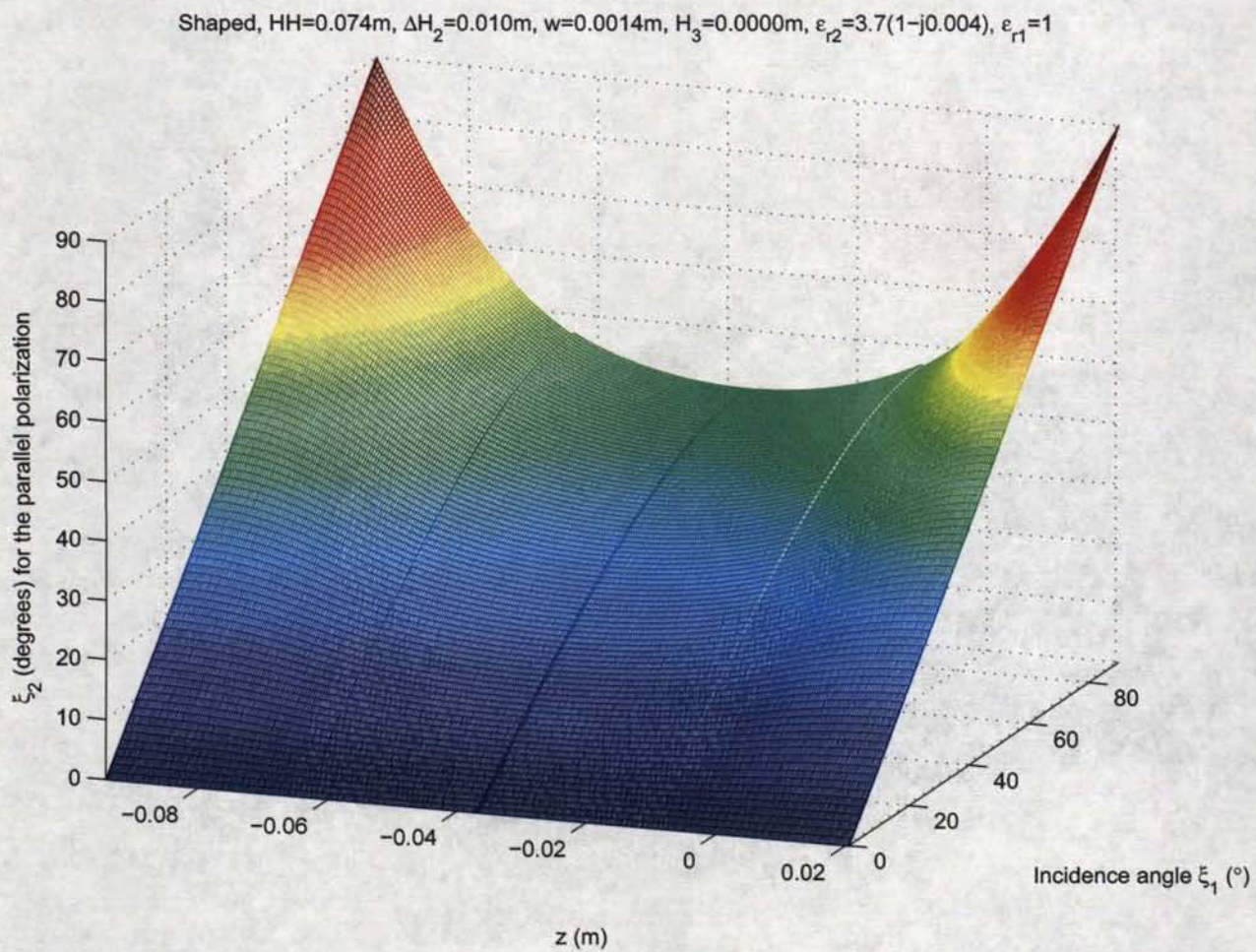
Figure 5.14: This figure shows the intrinsic amplitude propagation constant α_o for the shaped profile with $HH = 0.074$ m for the parallel polarization. The discretization was $dz \leq 0.0004$ m throughout the plate.

Shaped, HH=0.074m, ΔH_2=0.010m, w=0.0014m, H_3=0.0000m, ε_{r2}=3.7(1−j0.004), ε_{r1}=1
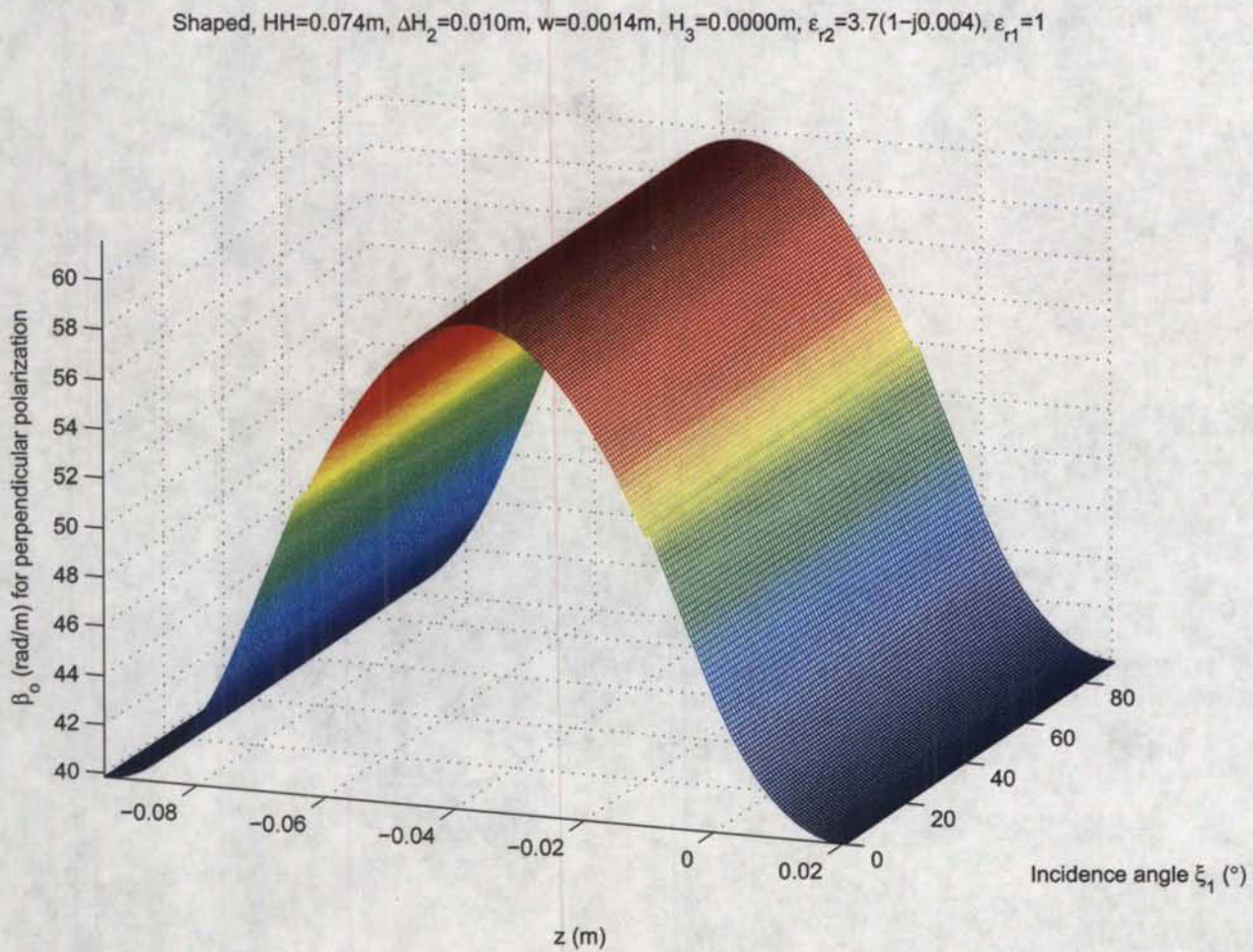
Figure 5.15: This figure shows the intrinsic phase propagation constant β_o for the shaped profile with $HH = 0.074$ m for the perpendicular polarization. The discretization was $dz \leq 0.0004$ m throughout the plate.
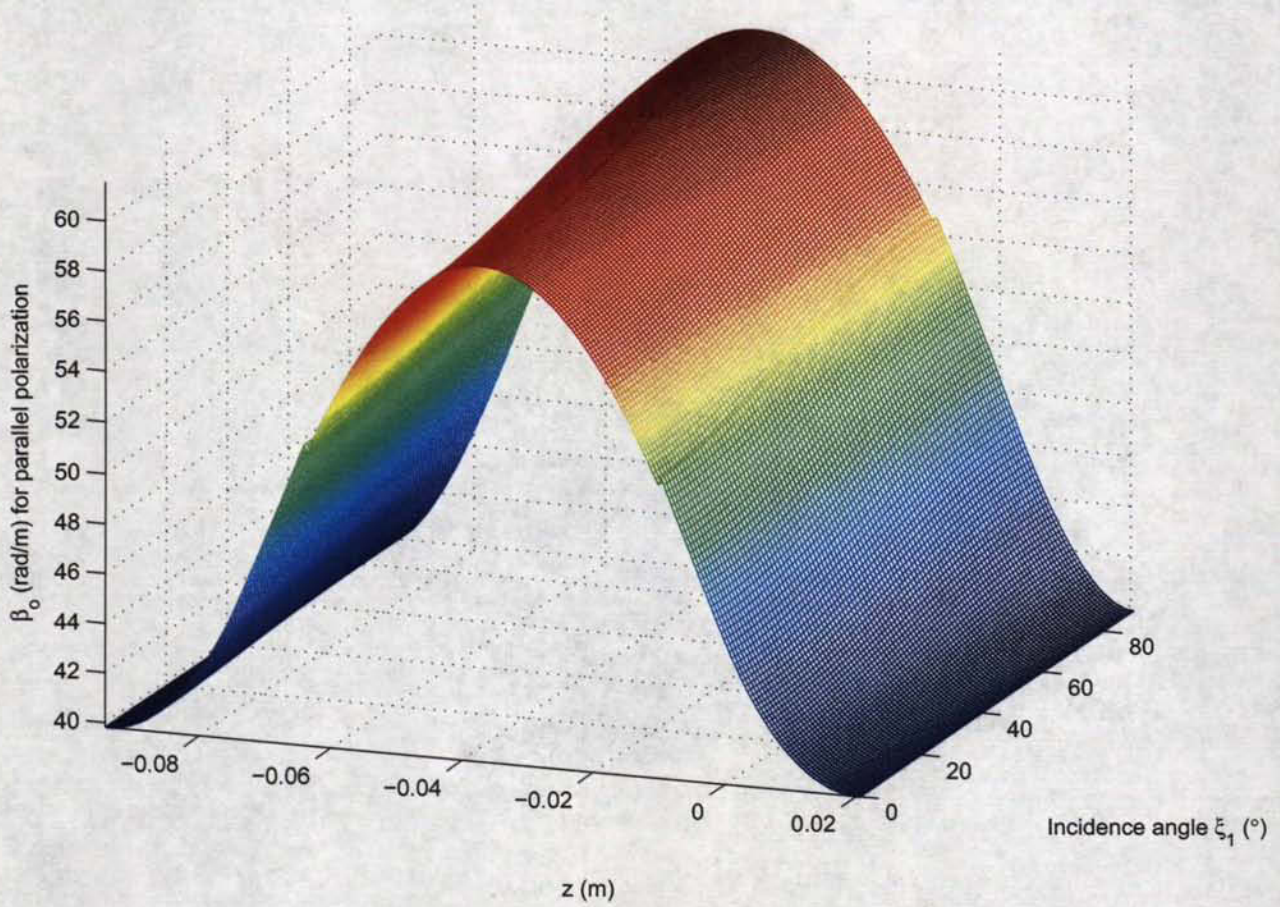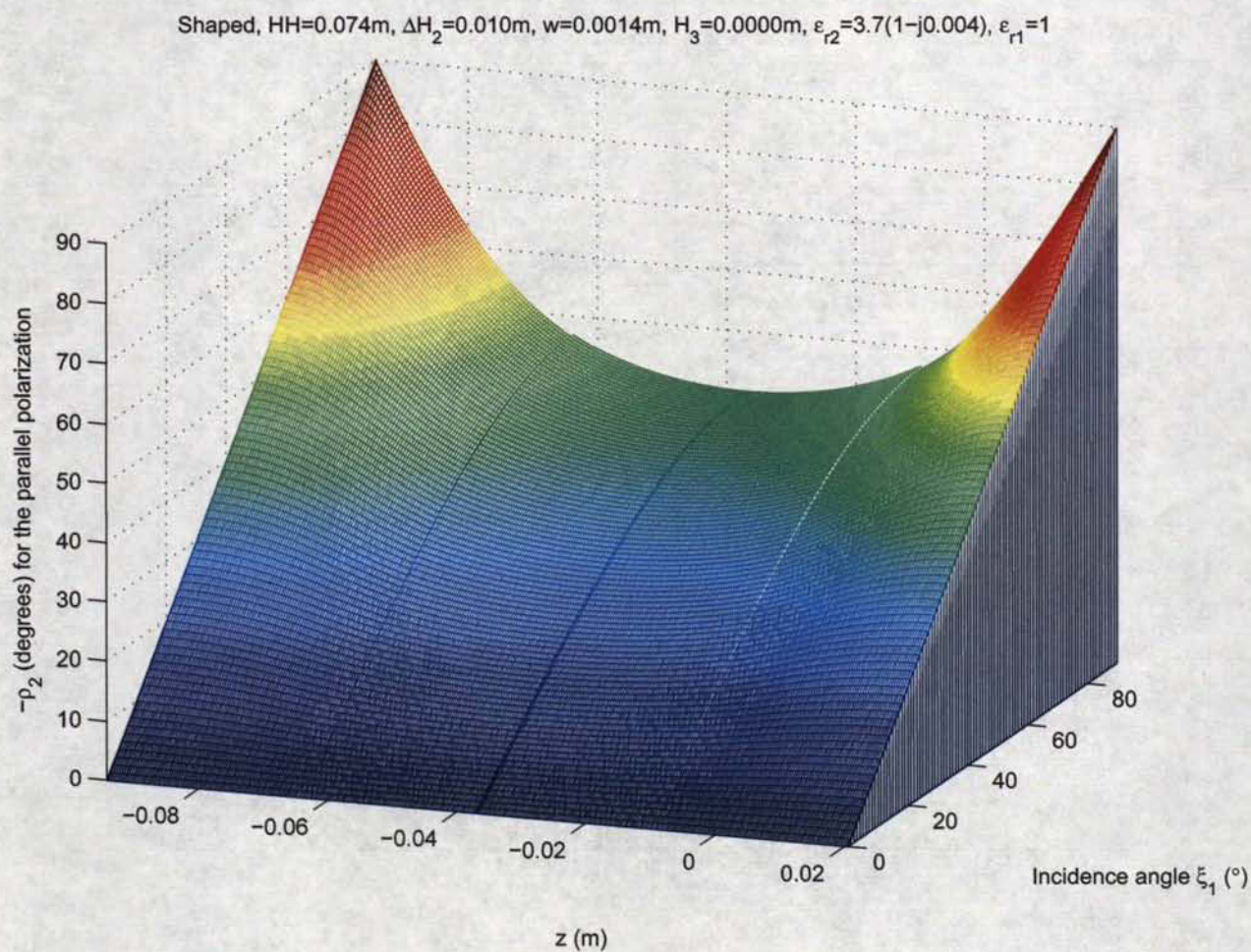
Figure 5.16: This figure shows the intrinsic phase propagation constant β_o for the shaped profile with $HH = 0.074$ m for the parallel polarization. The discretization was $dz \leq 0.0004$ m throughout the plate.
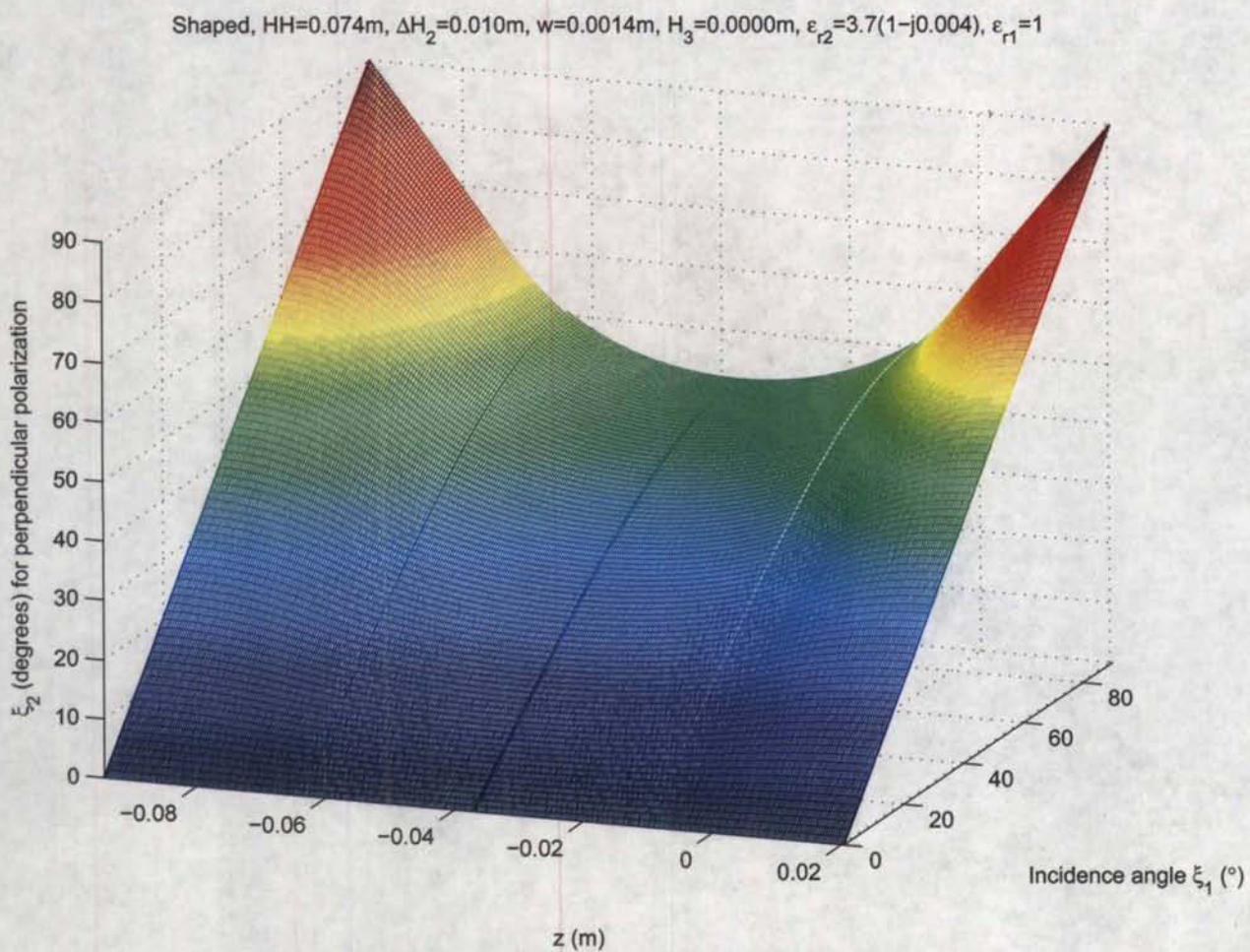
Figure 5.17: This figure shows the value of the angle ξ_2 at all the interfaces through the plate for the shaped profile with $HH = 0.074$ m for the perpendicular polarization. The discretization was $dz \leq 0.0004$ m throughout the plate.

Figure 5.18: This figure shows the value of the angle ξ_2 at all the interfaces through the plate for the shaped profile with $HH = 0.074$ m for the parallel polarization. The discretization was $dz \leq 0.0004$ m throughout the plate.

124
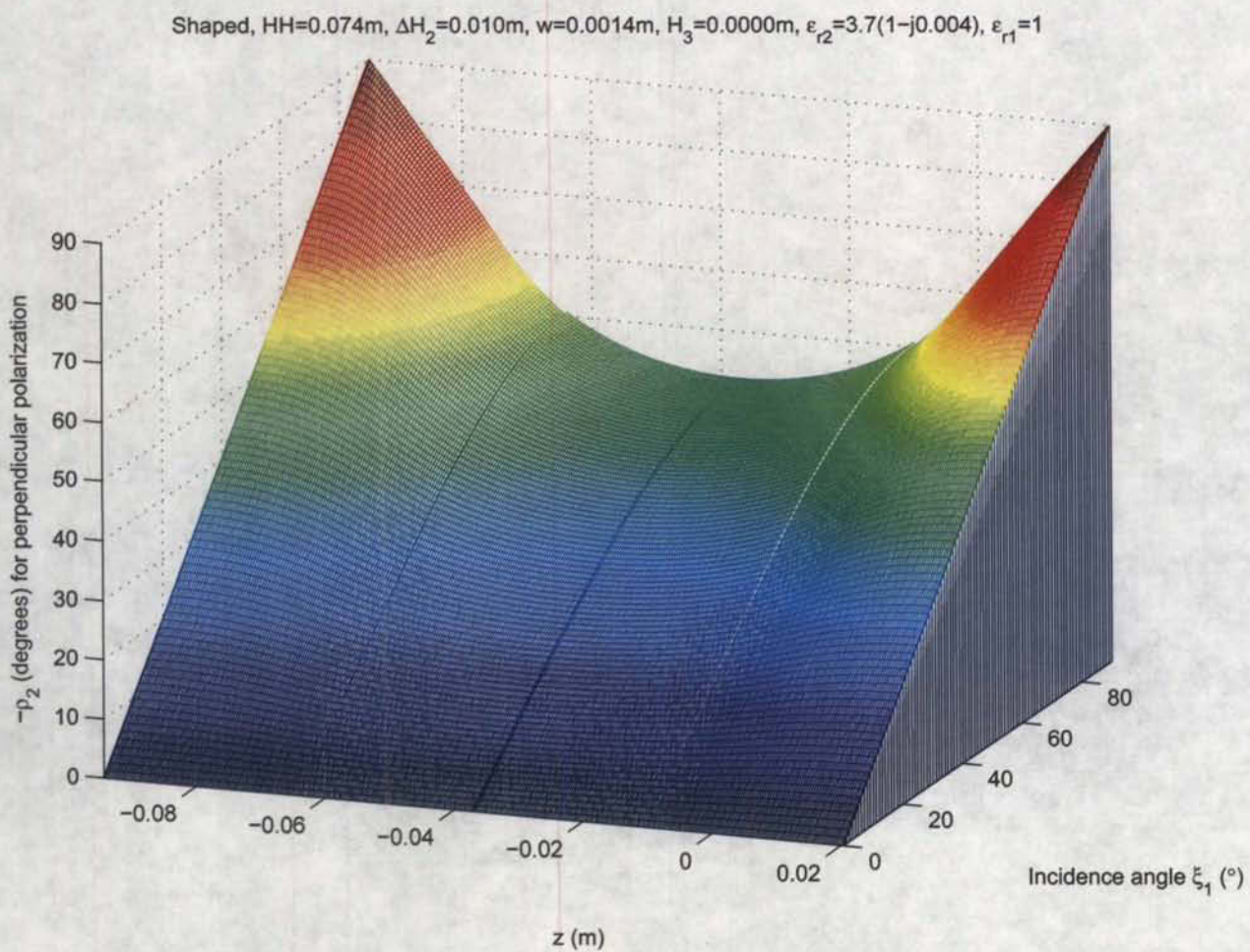
Figure 5.19: This figure shows the value of the angle $-\rho_2$ at all the interfaces through the plate for the shaped profile with $HH = 0.074$ m for the perpendicular polarization. The discretization was $dz \leq 0.0004$ m throughout the plate.

Figure 5.20: This figure shows the value of the angle $-\rho_2$ at all the interfaces through the plate for the shaped profile with $HH = 0.074$ m for the parallel polarization. The discretization was $dz \leq 0.0004$ m throughout the plate.
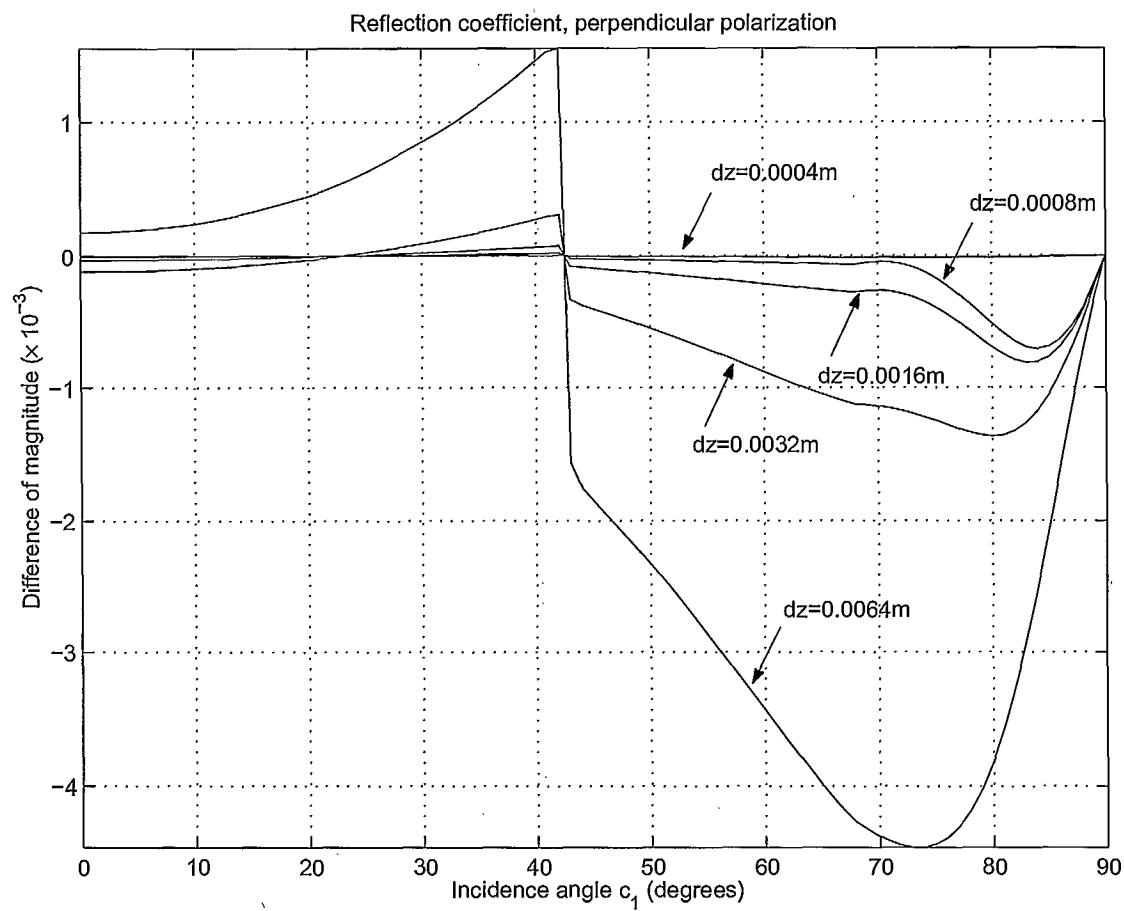
Figure 5.21: This figure shows the convergence in computing the reflection level for the perpendicular polarization. The reference curve was that for the case of $dz = 0.0002$ m.
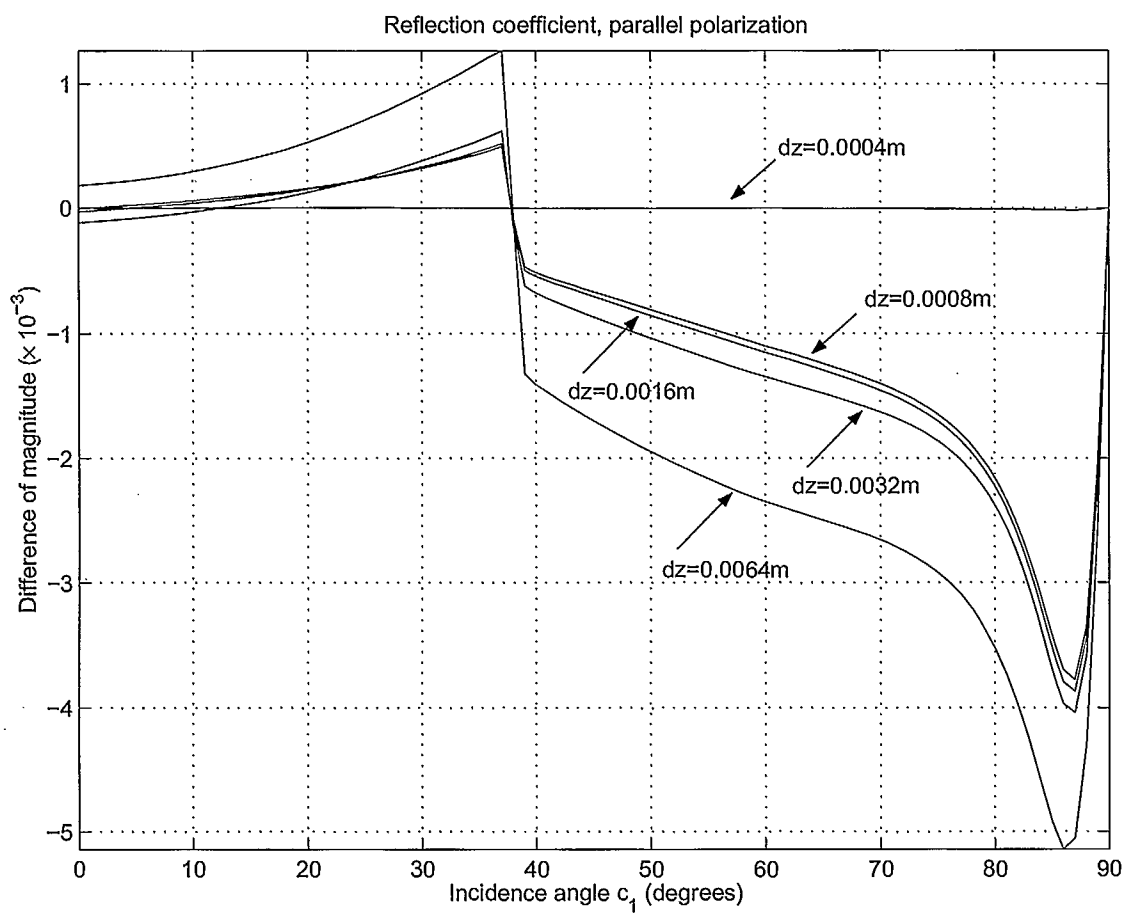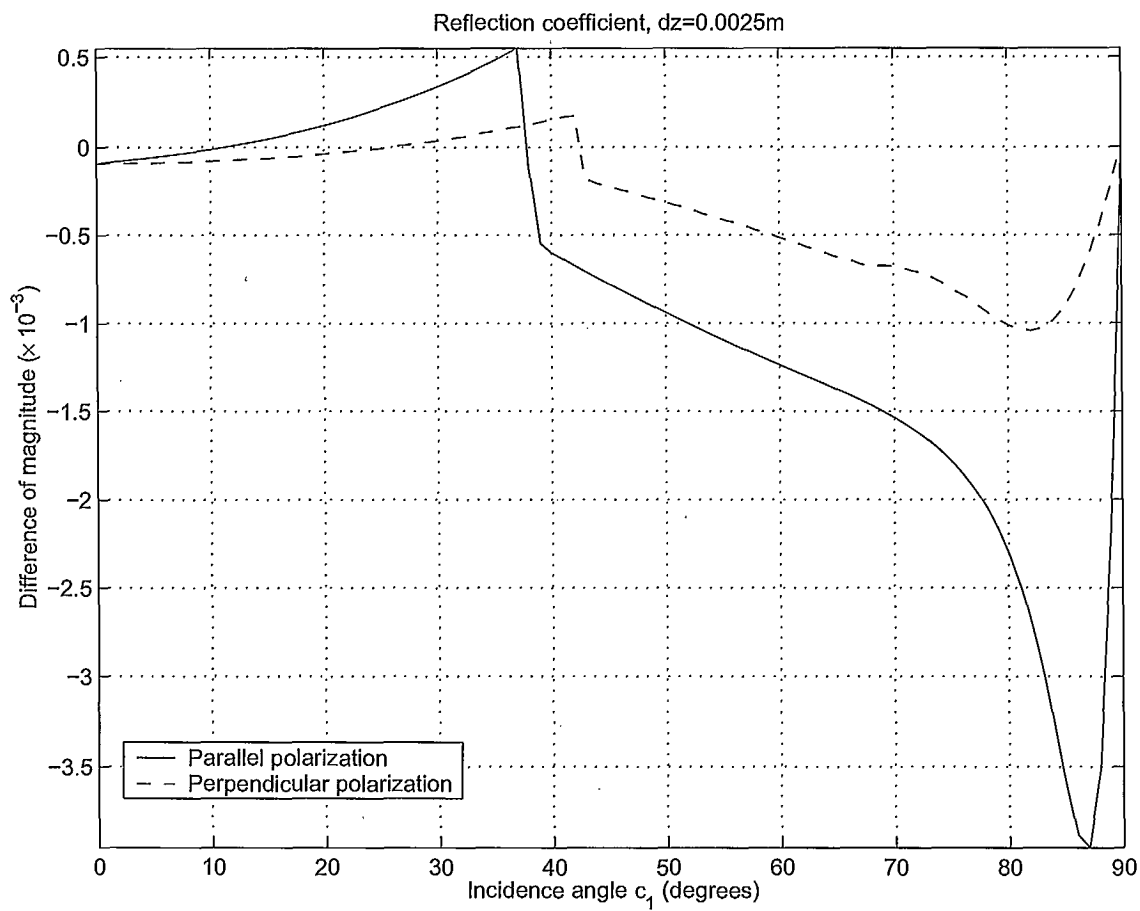
Figure 5.22: This figure shows the convergence in computing the reflection level for the parallel polarization. The reference curve was that for the case of $dz = 0.0002$ m.

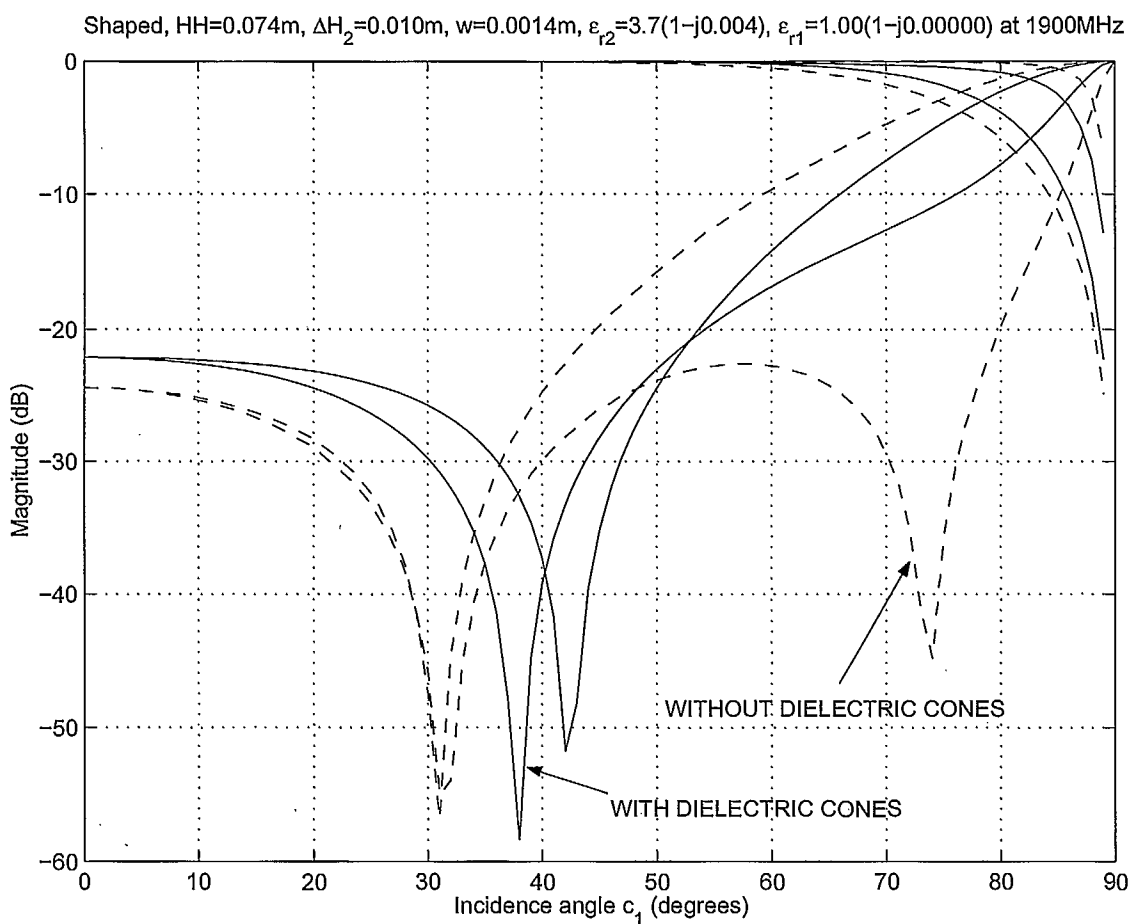Figure 5.23: This figure shows the convergence in computing the reflection level for both polarizations with $dz = 0.0025$ m. The reference curve was again that for the case of $dz = 0.0002$ m.

Shaped, HH=0.074m, ΔH_2=0.010m, w=0.0014m, ε_{r2}=3.7(1-j0.004), ε_{r1}=1.00(1-j0.00000) at 1900MHz

WITHOUT DIELECTRIC CONES

WITH DIELECTRIC CONES

Magnitude (dB)

Incidence angle c_1 (degrees)

Figure 5.24: This figure shows the computed reflection and the computed transmission levels in dB for the shaped profile with $HH = 0.074$ m and $w = 0.0014$ m, with and without dielectric cones. The discretization was $dz \leq 0.0004$ m throughout the plate.
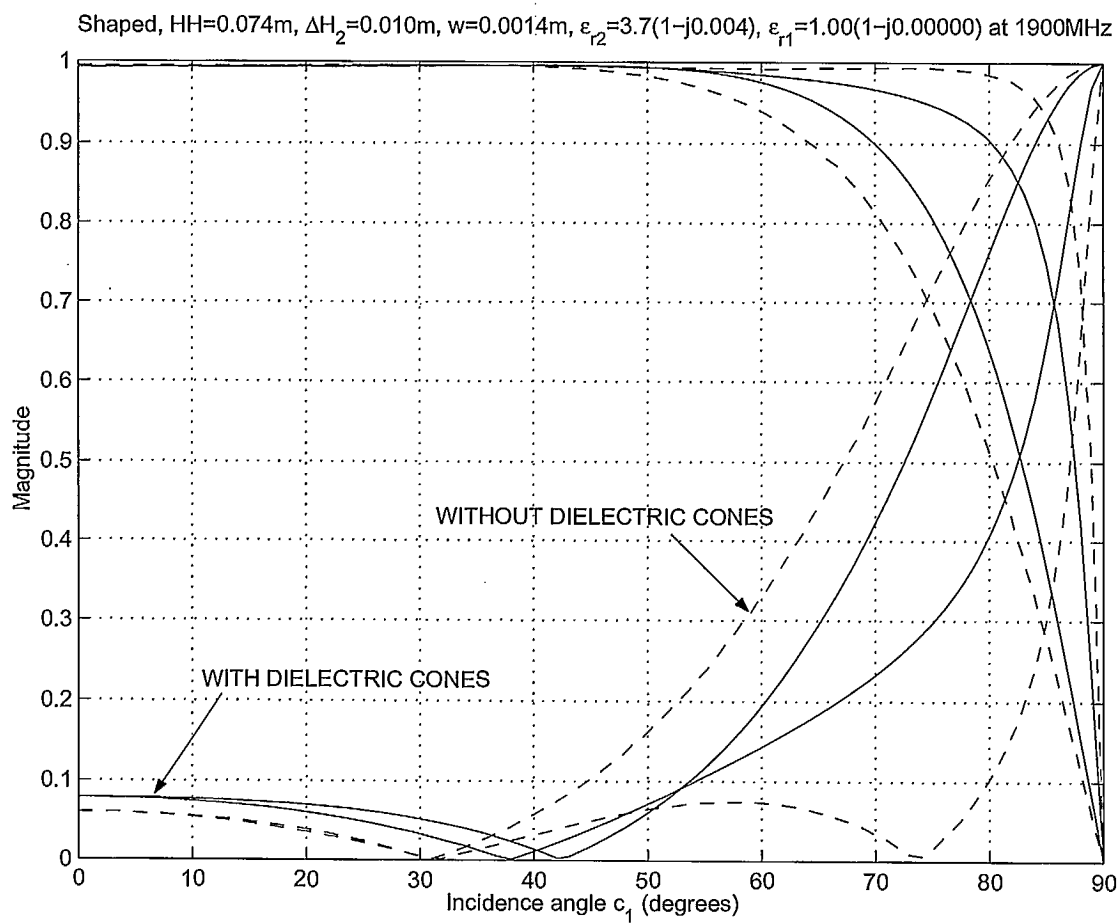
Shaped, HH=0.074m, ΔH_2=0.010m, w=0.0014m, ε_{r2}=3.7(1−j0.004), ε_{r1}=1.00(1−j0.00000) at 1900MHz

WITHOUT DIELECTRIC CONES

WITH DIELECTRIC CONES

Magnitude

Incidence angle c_1 (degrees)

Figure 5.25: This figure shows the computed reflection and the computed transmission levels on the linear scale for the shaped profile with $HH = 0.074$ m and $w = 0.0014$ m, with and without the dielectric cones. The discretization was $dz \leq 0.0004$ m throughout the plate.

5.2 Parameter sensitivity analysis

This section presents the results of a parametric analysis whereby only one parameter is varied at a time while all other parameters remain fixed at the value of the baseline design mentioned in the preceding section. In the previous section, the values of h_1 and H_1 were adjusted for any choice of HH and w so as to insure that the permittivity profile would form a continuous function at $z = 0$ and $z = -HH$. In this section, no such an adjustment is made other that which was part of the baseline design. This analysis thus permits to reveal the sensitivity of the parameters to manufacturing tolerances. The parameters investigated here are:

- the slab thickness HH;

- frequency f (MHz);

- complex relative permittivity of the dielectric slab ε_{r2};

- complex relative permittivity of the styrofoam holder ε_{r1};

- the dielectric cone length h_1;

- missing tip length for the dielectric cones in the front and the back sections ΔH_1 (m);

- missing tip length for the air cones in the dielectric slab ΔH_2 (m);

- thickness of the layer of glue at the mid-thickness point of the dielectric slab H_3 (m);

Numerical experiments show that a ± 0.001 m variation of HH is not critical to the response of the plate. More numerical experiments show that the shaped profile produces a low reflection level only over a narrow frequency bandwidth. For instance, if we define the bandwidth on the basis of a -1 dB variation from the reflection values at the nominal frequency, then the plate can be operated from about 1890 MHz where the perpendicular polarization at $\xi_1 = 50°$ is the limiting factor, to about 1930 MHz where the reflection at normal incidence is the limiting factor. If we define the bandwidth on the basis of a -20 dB threshold value, then the plate can be operated from about 1850 MHz where again the perpendicular polarization at $\xi_1 = 50°$ is the limiting factor, to about 1970 MHz where again the reflection at normal incidence is the limiting factor. In any case, the bandwidth is seen to be rather small. This situation stands in sharp contrast with the very wide bandwidth reported for the anisotropic dielectric structure in Reference [46]. This anisotropic structure consists of a dielectric plate, the front and the back

surfaces of which have been machined to present deep triangular grooves, the grooves on the front surface running perpendicular to the grooves on the back surface. Could it be that the dramatic difference in frequency bandwidth owes to the difference in isotropic property? This author does not think so and is at loss to explain the cause for the dramatic difference in frequency bandwidth between the two differently profiled dielectric plates. In any case, the frequency is a parameter that is very well controlled during the measurement so that any variation of the response with respect to the frequency is not deemed to be a problem if the plate is used at the design frequency.

Numerical experiments show that the reflection and the transmission levels for the shaped profile are not degraded adversely by a variation of ± 0.001 in the loss tangent value. Although the reflection level may increase or decrease depending on whether or not some resonance is occurring within the dielectric, the transmission level always decreases even when the reflection level decreases (e.g. the case for $\tan(\delta) = 100$ with $\xi_1 = 0$), because the wave is partly absorbed within the dielectric as the wave propagates through the dielectric. At the limit, i.e. for a perfect conductor which corresponds to the case $\tan(\delta)$ approaching ∞, the transmission level becomes $-\infty$ dB, i.e. perfect blocking, regardless of the profile type; the reflection level, however, becomes 0 dB, i.e. perfect reflection, only for the uniform profile, not for the shaped profile. This situation is consistent with the fact that a PEC mounting plate with the shaped profile presents, in effect, a very rough surface unlike a uniform PEC slab.

Numerical experiments show that the reflection and the transmissions levels for the shaped profile are not degraded adversely by a variation of ± 0.2 in the relative permittivity value. In contrast, the reflection level for the perpendicular polarization is degraded rapidly (by about 2 dB) for the first -0.001 m variation in the dielectric cone length h_1. However, such a variation of h_1 represents a large variation of the fill fraction at $z = 0$ and is not likely to occur. A much more likely source of error is the missing tip length of the dielectric cones due to fabrication tolerances. Numerical experiments show that the effect due to a variation as large as 0.005 m in the missing tip length ΔH_1 is insignificant, and the effect due to a ± 0.001 m variation in the missing tip length ΔH_2 is not severe either.

Figures 5.26 to 5.36 show the effect of replacing free space with a high density styrofoam ($\varepsilon_r = 1.04(1 - j0.0005)$) in the region $z > 0$. We observe that the loss tangent curve has a clear discontinuity at $z = 0$ in spite of the fact that Equations (4.30) and (4.31) were observed to be independent of the permittivities. The reason for this situation is that these equations are valid only for the case of a two-material composite, i.e. if styrofoam is used as one medium, then it should fill the inclusions of the dielectric slab as well. In our

case, the styrofoam does not fill the inclusions in the regions $z < 0$.

Since the styrofoam is a lossy material, albeit only slightly lossy, the behaviour of the angle ρ_2 in the region $z > 0$ is quite different from that when the inclusion material in the front section was just air (compare Figures 5.19 and 5.20 with Figures 5.39 and 5.40, respectively). Because the foreground medium is now lossy, the amplitude wavefront is no longer normal to the interface at $z = (h_1 - \Delta H_1)$, i.e. ρ_2 is no longer varying linearly from $0°$ to $-90°$ as ξ_1 varies from $0°$ to $90°$. Since $\rho_2 = 0°$ at the interface $z = (h_1 - \Delta H_1)$, the incident and transmitted plane waves are uniform at that interface. Moreover, the reflection and the transmission curves are significantly affected, specially for incidence angle values $\xi_1 \geq 79°$ (compare Figures 5.27 and 5.4). The upper limit for which the reflection level for both polarizations is less than about -22 dB has passed from about $\xi_1 = 52°$ to about $\xi_1 = 48°$ as a result of the curves having a large gradient in that part of the plot.

When styrofoam is present in the region $z > 0$, the transmission level for the parallel polarization T_{parallel} can become greater than 1.0. However, this situation does not violate the principle of energy conservation because the ratio $(P^{\text{out}}/P^{\text{in}}) = \left(1 - |R_{\text{parallel}}|^2\right)$ remains less than or equal to 1. For $\xi_1 \geq 79°$, Figures 5.37 and 5.38 show that the wave is totally reflected, i.e. $\xi_2 = 90°$, for both polarizations. Consequently, Figures 5.27 show $|R| = 1$ and $|T| \neq 0$. The transmission level is different from zero because there is the electromagnetic field of an evanescent wave in the transmission medium (see Reference [4, p. 363]). To be precise, $|R|$ is slightly smaller than 1 because the total reflection occurs at some interface inside the back section near the the output face of the plate and thus, the wave is partly being absorbed all the while that it is travelling within the lossy dielectric material before exiting as the reflected wave. If no losses are present, then $|R| = 1$ exactly (see Figures 5.29 and 5.30).

Note that the transmission angle from the mth interface to the nth interface in a system of parallel planar interfaces depends on the ratio of the permittivity for the medium that acts as the input medium to the mth interface, and the permittivity for the medium that acts as the output medium to the nth interface, and is given by:

$$\theta^{\text{out}} = \arcsin\left(\frac{\sqrt{\varepsilon_r^{\text{in}}}}{\sqrt{\varepsilon_r^{\text{out}}}} \sin\left(\theta^{\text{in}}\right)\right) \tag{5.1}$$

regardless of the presence of any intermediary layer. This equation can be verified easily by successive application of Snell's law at all interfaces from the mth to the nth interface, or by the fact that the phase matching of the

fields at every interface forces the transverse variation of the scattered fields to be dictated by the incident field (see Reference [5, p. 150]). The critical angle is that for which $\theta^{\text{out}} = 90°$, hence one obtains:

$$\theta^{\text{in}} = \arcsin\left(\frac{\sqrt{\varepsilon_r^{\text{out}}}}{\sqrt{\varepsilon_r^{\text{in}}}}\right) = \arcsin\left(\frac{\sqrt{1.0}}{\sqrt{1.04}}\right) = 78.7°$$

Note that intrinsic losses were neglected in the above numerical evaluation of the equation[3] . For instance, if intrinsic losses were so high as to make the output immersing media behave like a very good conductor, then total reflection would occur for any value of the incidence angle, thus making the critical angle value to be effectively zero.

That complete reflection occurs can be understood from the fact that when the input and the output immersing media are the same, Equation (5.1) gives $\theta^{\text{out}} = \theta^{\text{in}}$, and thus, the full visible range of 0° to 90° is spanned by both the transmission and the incidence angles in the same manner, i.e. the transmitted phase wavefront exits the system of parallel interfaces at the same angle as that at which it entered it (see Reference [48, p. 156]). Consequently, no total internal reflection is possible within a parallel face slab that is illuminated by propagating plane waves on one of its two faces because for this geometry, the refracted wave inside the slab is incident on the output face at an angle θ^t given by $\sin\theta^t = \sqrt{\frac{1}{\jmath}\varepsilon_r}\sin\theta^i = \sin\theta^c\sin\theta^i$ and thus $\theta^t < \theta^c$ for $\theta^i < 90°$.

However, when the permittivity for the input immersing medium is higher than that for the output immersing medium, the transmission angle for the output phase wavefront spans its full visible range faster than does the incidence angle for the input phase wavefront because the transmitted phase wavefront bends away from the normal of the interfaces as the incident phase wavefront departs from normal incidence, i.e. $\theta^{\text{out}} \geq \theta^{\text{in}}$. For all incidence angle values greater than the critical value, the transmitted phase wavefront is already travelling parallel to the interface and can bend no further. The transmitted angle thus becomes complex thereby giving rise to an evanescent wave travelling parallel to the interface.

Note that the critical angle value is the same for both polarizations and for both the uniform and the shaped profiles (compare 5.27 and 5.28). That the critical angle is the same for both polarizations owes to Snell's law which is the result of phase matching (i.e. matching of the time harmonic exponential term of the electric and the magnetic fields) at the interface. That the critical

---

[3]In fact, the presence of intrinsic losses affect the value of both the Brewster angle (as seen from Figure 5.5) and the critical angle.

angle is the same for both profiles owes to the fact that Equation (5.1) does not depend on the permittivity of the intermediary layers.

Figures 5.41 to 5.48 show the effect due to the presence of a thin ($H_3 = 0.0003$ m) layer of glue (Loctite #401 with $\varepsilon_r = 2.75(1 - j0.02)$) located at the mid-thickness point of the mounting plate, i.e. $z = -HH/2$, as if the plate were be too thick to be fabricated from a single bulk piece. Note that the thickness of the layer of glue is not discretized according to dz because the program treats that thickness explicitly by means of the parameter H_3. Note also that the results for the layer of glue on Figures 5.43 to 5.48 show a triangular rather than a uniform profile because the curves are plotted by assigning the results for the entire layer to a single point at the centre of the layer. Figures 5.41 and 5.42 show that the effect of a layer of glue generally tends to increase with increasing incidence angle because the waves propagate over a longer distance in the layer of glue as the incidence approaches grazing incidence. It is important to understand that even a very thin layer can have a very significant effect because the mechanism of reflection occurs at the interface, regardless of how thin the layer behind the interface happens to be.
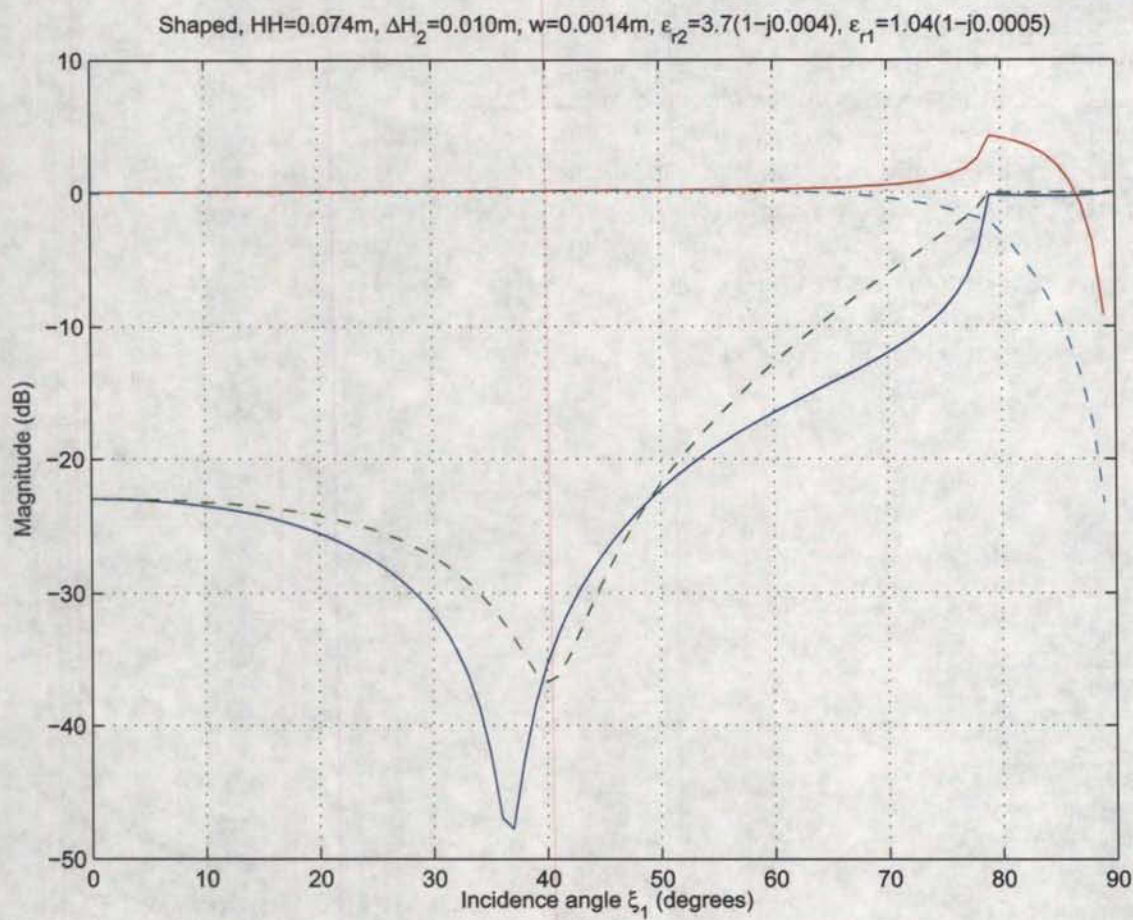
Figure 5.26: This figure shows the computed reflection and the computed transmission levels in dB for the shaped profile with lossy styrofoam present in the region $z > 0$. The discretization was $dz \leq 0.0004$ m throughout the plate.
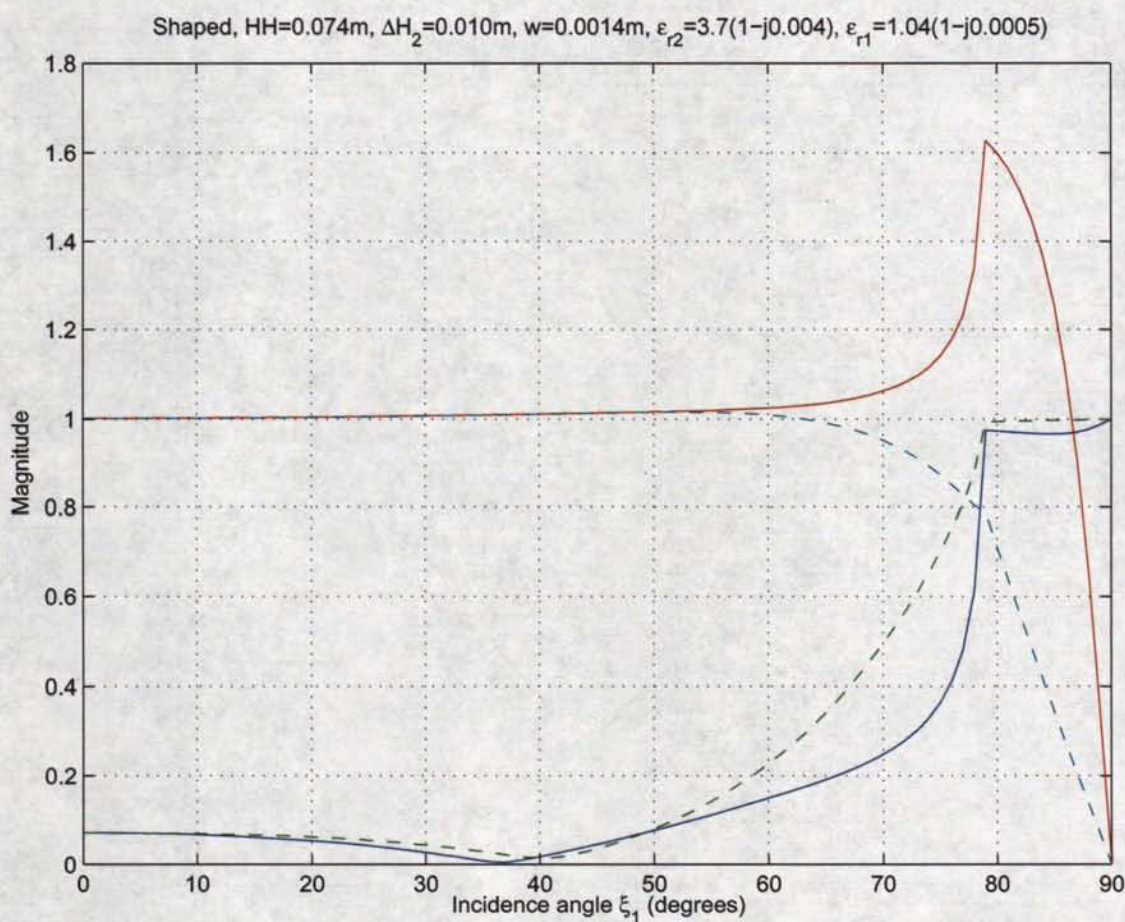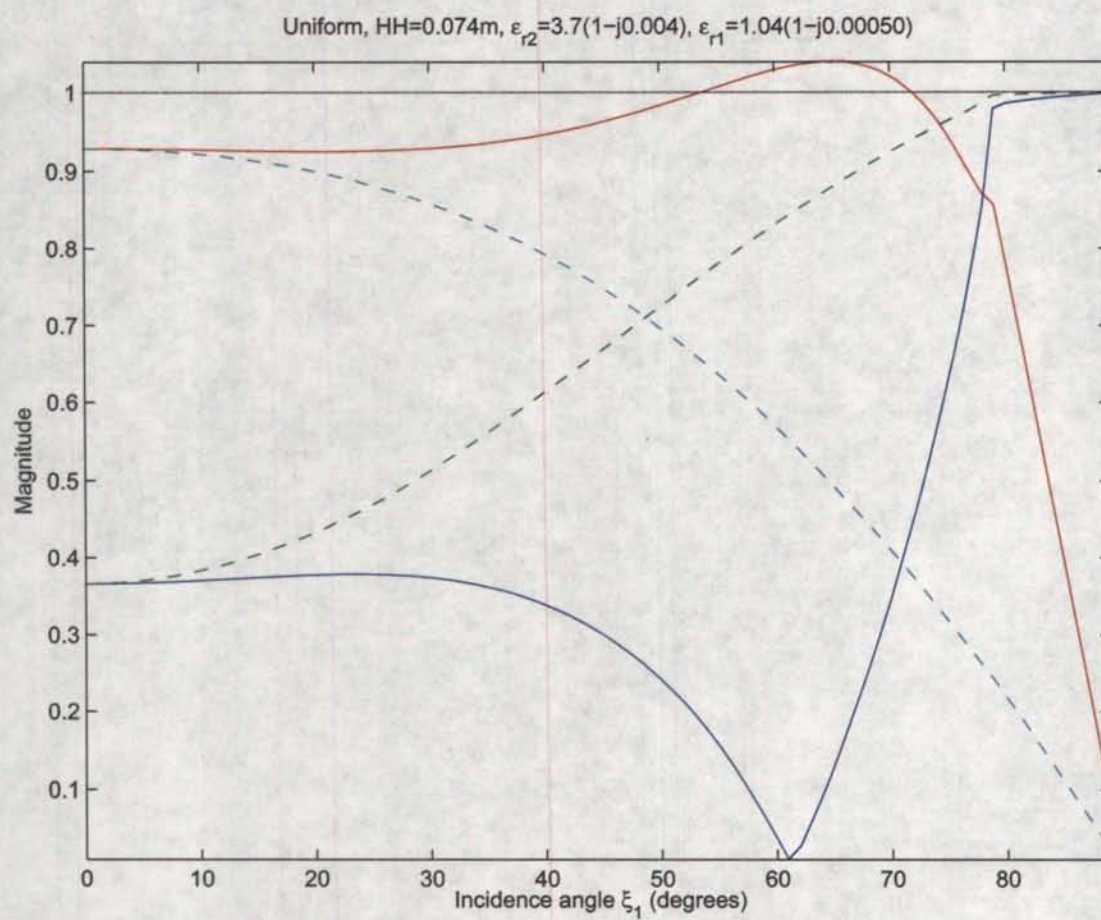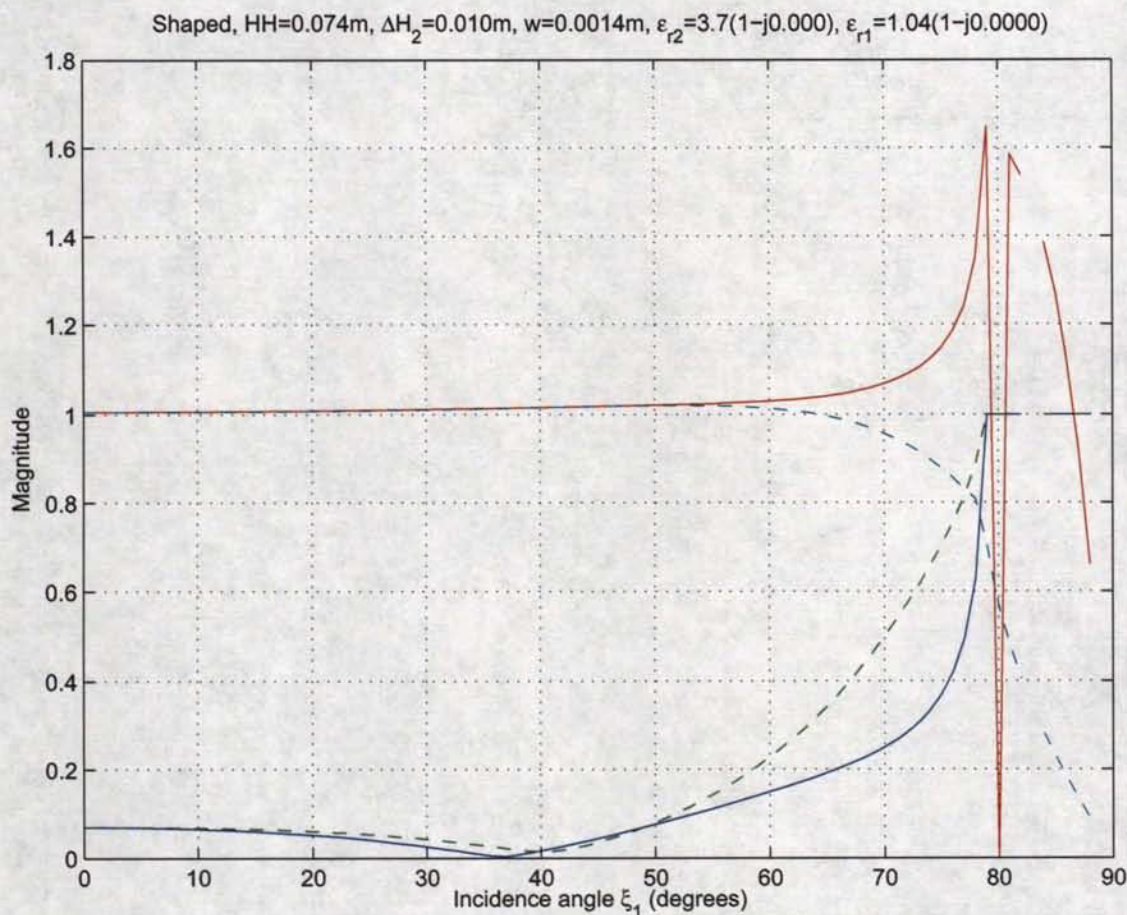
Figure 5.27: This figure shows the computed reflection and the computed transmission levels on the linear scale for the shaped profile with lossy styrofoam present in the region $z > 0$. The discretization was $dz \leq 0.0004$ m throughout the plate.
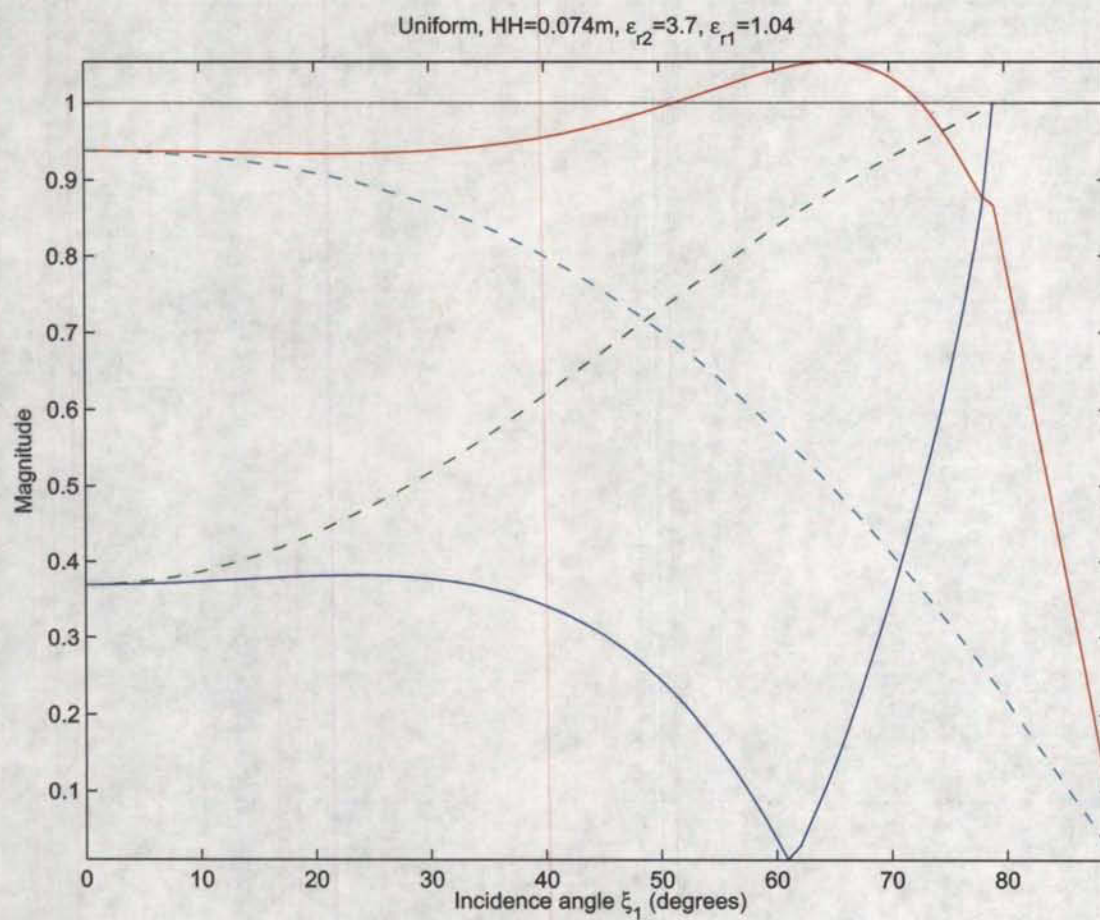
Figure 5.28: This figure shows the computed reflection and the computed transmission levels on the linear scale for the uniform profile with lossy styrofoam present in the region $z > 0$.

Shaped, HH=0.074m, ΔH_2=0.010m, w=0.0014m, ε_{r2}=3.7(1−j0.000), ε_{r1}=1.04(1−j0.0000)

Figure 5.29: This figure shows the computed reflection and the computed transmission levels on the linear scale for the lossless shaped profile with lossless styrofoam present in the region $z > 0$. The discretization was $dz \leq$ 0.0004 m throughout the plate. Note that a small segment of each curve is missing about $\xi_1 = 82°$ because MATLAB produced NAN (i.e. Not A Number) results. The notch in the curve for T^{TM} at $\xi_1 = 80°$ is also suspect.

140

Figure 5.30: This figure shows the computed reflection and the computed transmission levels on the linear scale for the lossless uniform profile with lossless styrofoam present in the region $z > 0$.
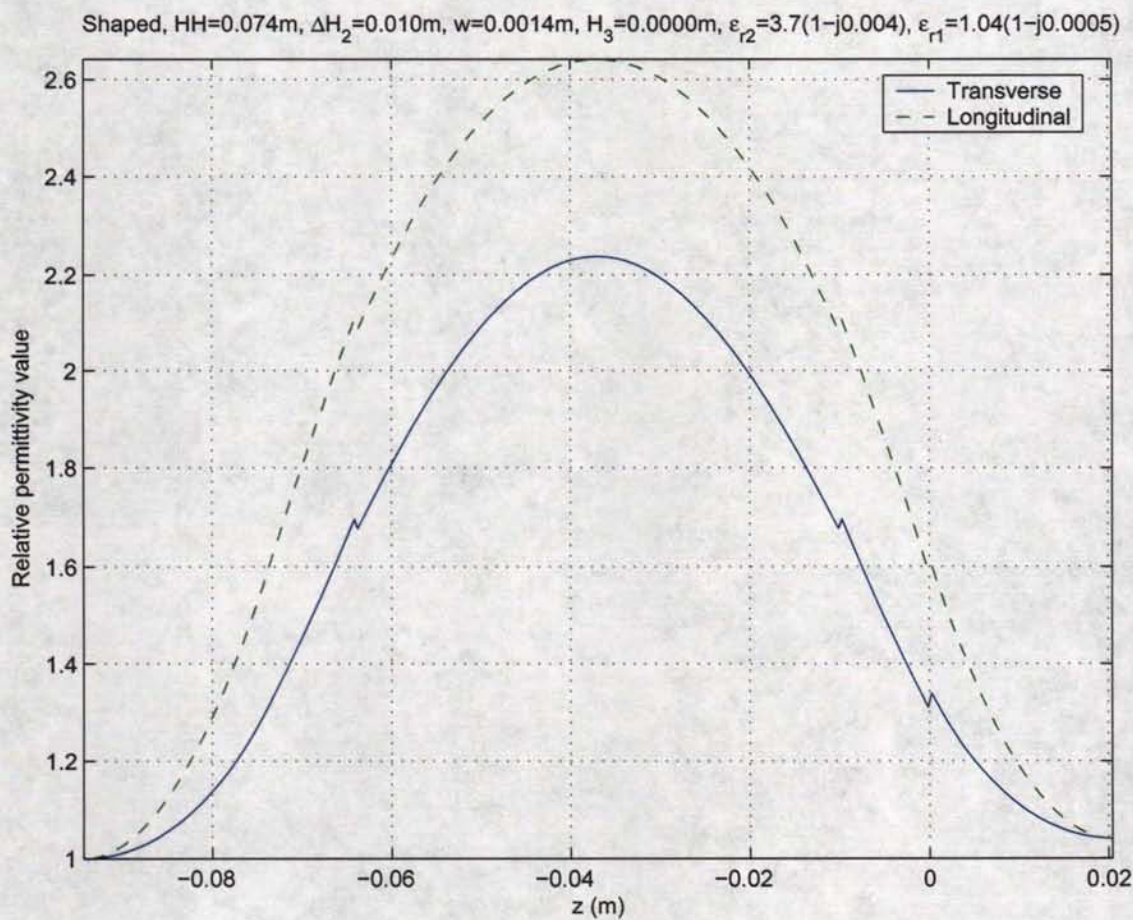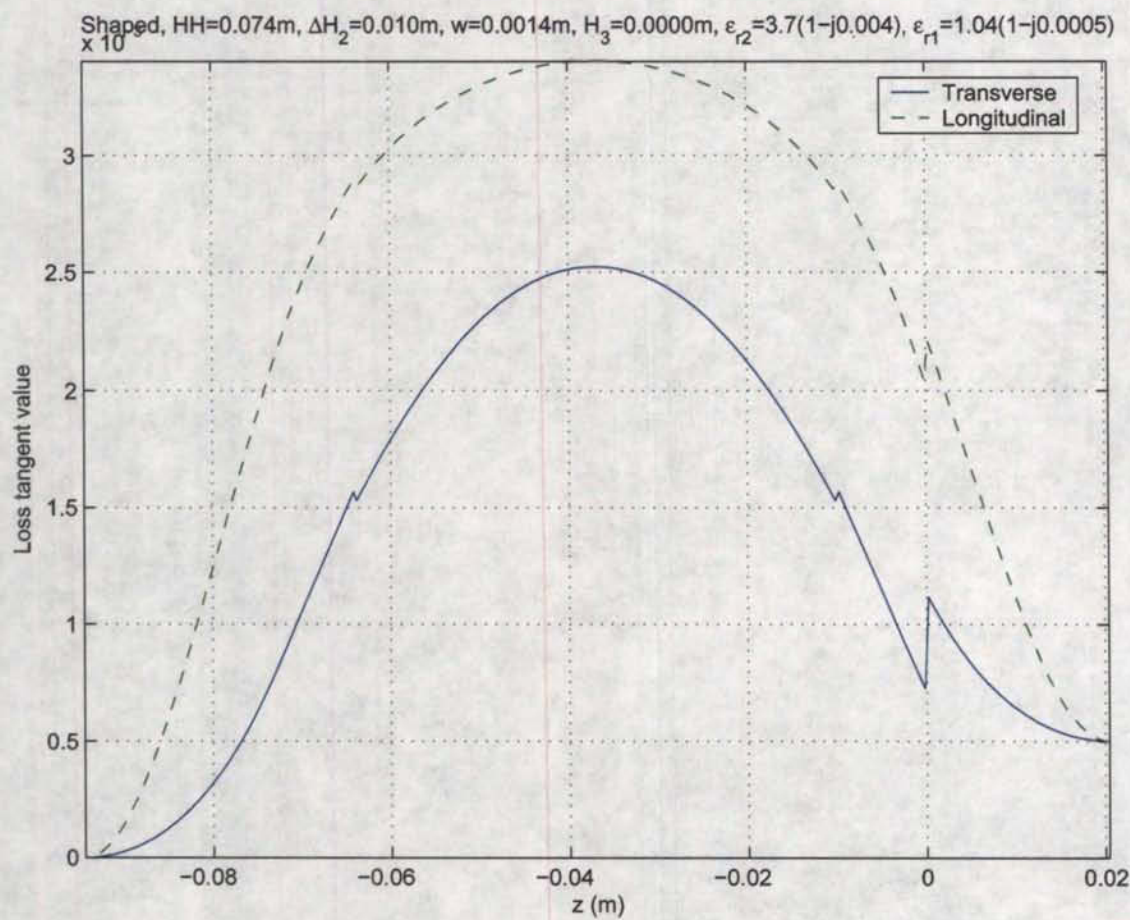
Figure 5.31: This figure shows the profile for the real part of $\varepsilon_r^{\text{trans}}$ and $\varepsilon_r^{\text{long}}$ for the shaped profile with lossy styrofoam present in the region $z > 0$. The discretization was $dz \le 0.0004$ m throughout the plate.

Figure 5.32: This figure shows the profile for loss tangent of $\varepsilon_r^{\text{trans}}$ and $\varepsilon_r^{\text{long}}$ for the shaped profile with lossy styrofoam present in the region $z > 0$. The discretization was $dz \leq 0.0004$ m throughout the plate.

Shaped, HH=0.074m, ΔH_2=0.010m, w=0.0014m, H_3=0.0000m, ε_{r2}=3.7(1−j0.004), ε_{r1}=1.04(1−j0.0005)
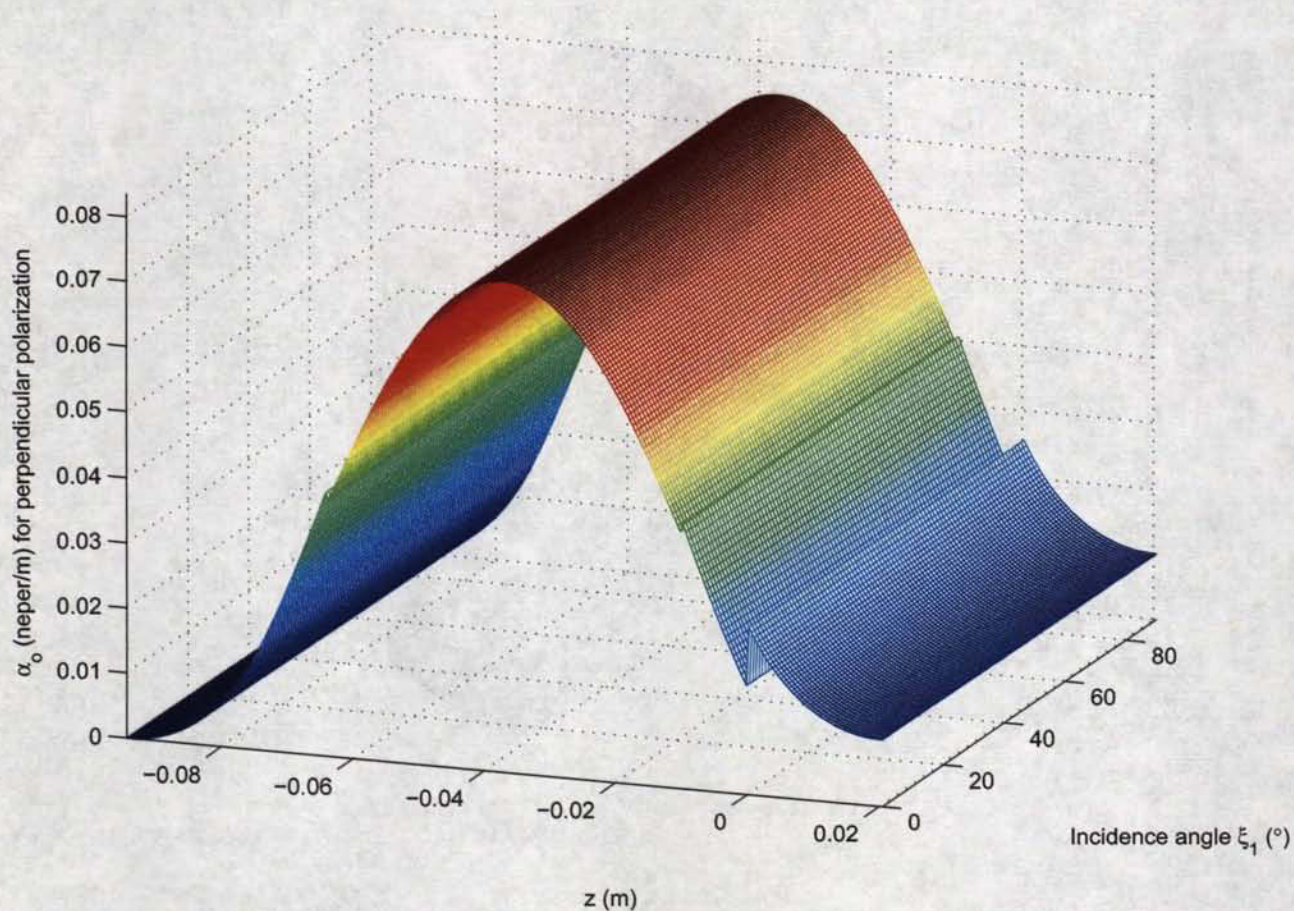
Figure 5.33: This figure shows the intrinsic amplitude propagation constant α_o for the shaped profile with lossy styrofoam present in the region $z > 0$ for the perpendicular polarization. The discretization was $dz \leq 0.0004$ m throughout the plate.
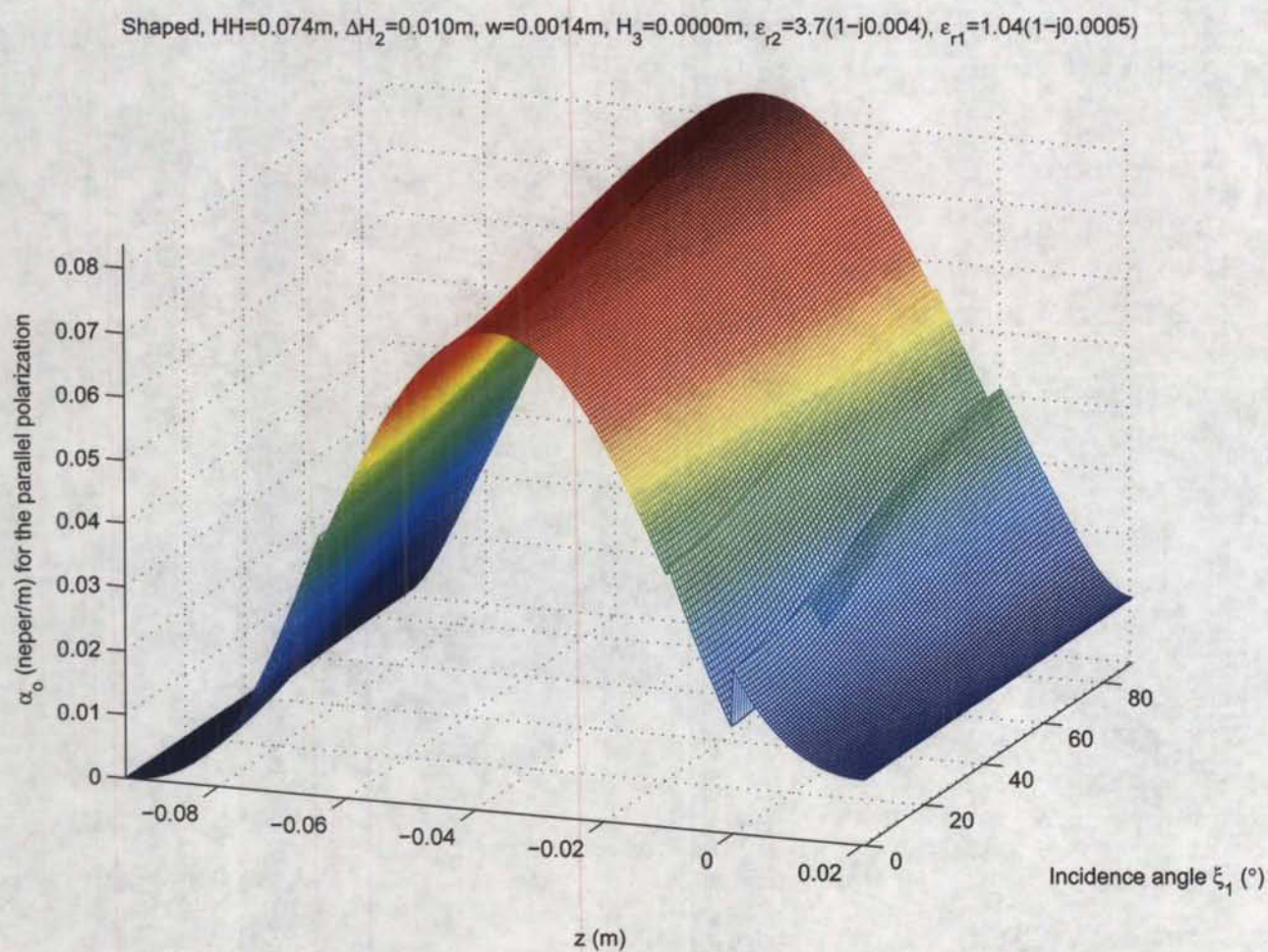
144

Shaped, HH=0.074m, ΔH_2=0.010m, w=0.0014m, H_3=0.0000m, ε_{r2}=3.7(1−j0.004), ε_{r1}=1.04(1−j0.0005)

Figure 5.34: This figure shows the intrinsic amplitude propagation constant α_o for the shaped profile with lossy styrofoam present in the region $z > 0$ for the parallel polarization. The discretization was $dz \leq 0.0004$ m throughout the plate.
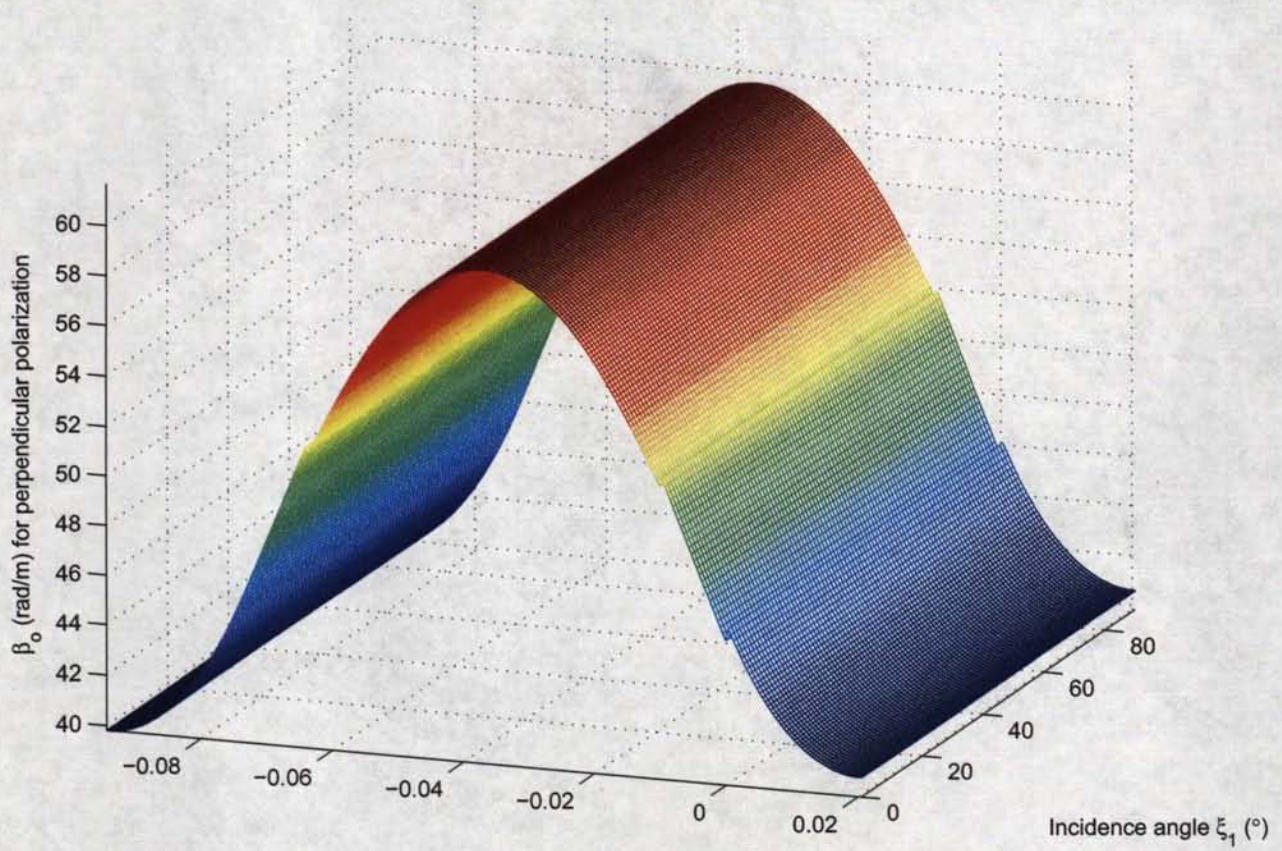
145

Figure 5.35: This figure shows the intrinsic phase propagation constant β_o for the shaped profile with lossy styrofoam present in the region $z > 0$ for the perpendicular polarization. The discretization was $dz \leq 0.0004$ m throughout the plate.
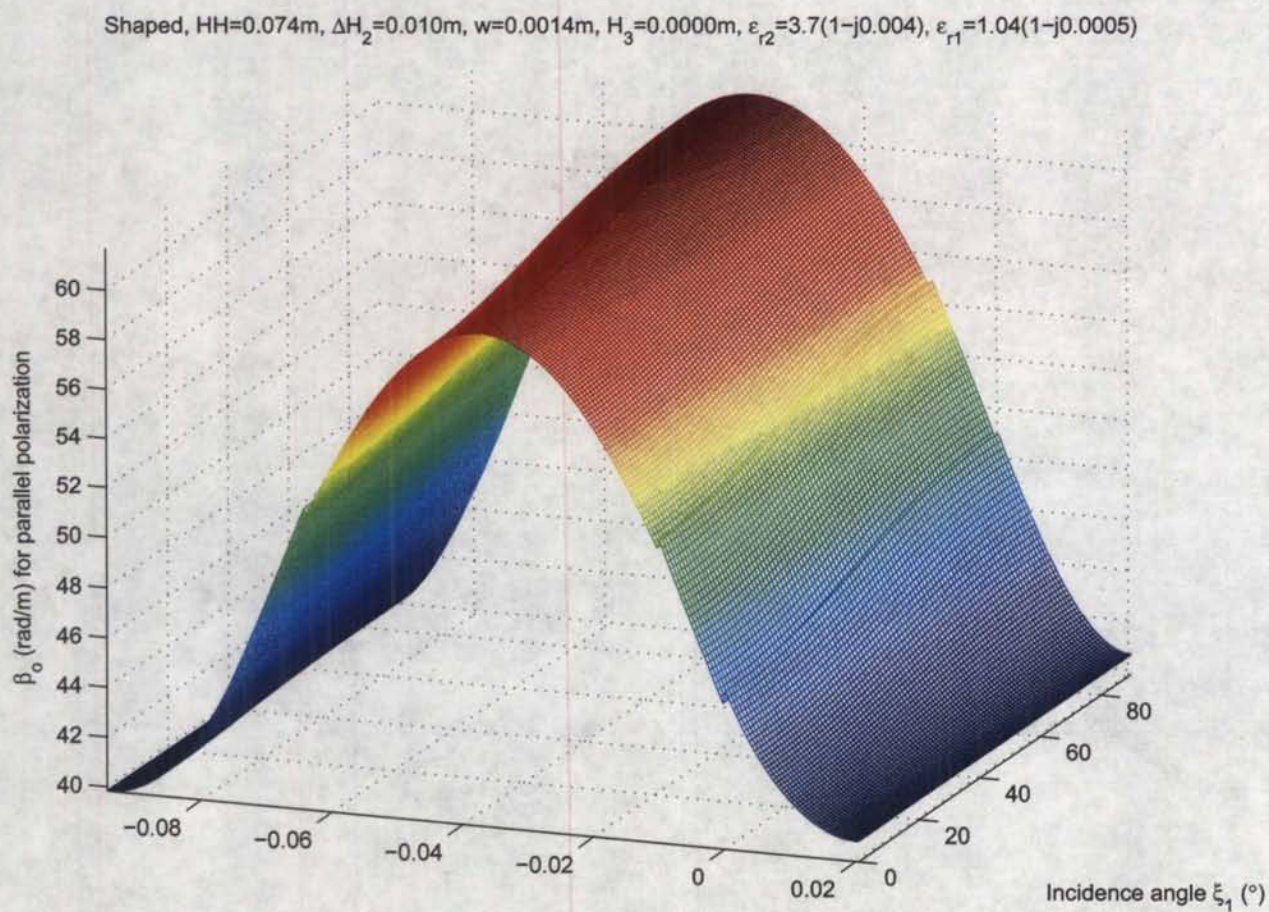
Figure 5.36: This figure shows the intrinsic phase propagation constant β_o for the shaped profile with lossy styrofoam present in the region $z > 0$ for the parallel polarization. The discretization was $dz \leq 0.0004$ m throughout the plate.

Figure 5.37: This figure shows the value of the angle ξ_2 at all the interfaces through the plate for the shaped profile with lossy styrofoam present in the region $z > 0$ for the perpendicular polarization. The discretization was $dz \leq 0.0004$ m throughout the plate.

148

Shaped, HH=0.074m, ΔH_2=0.010m, w=0.0014m, H_3=0.0000m, ε_{r2}=3.7(1−j0.004), ε_{r1}=1.04(1−j0.0005)

Figure 5.38: This figure shows the value of the angle ξ_2 at all the interfaces through the plate for the shaped profile with lossy styrofoam present in the region $z > 0$ for the parallel polarization. The discretization was $dz \leq 0.0004$ m throughout the plate.
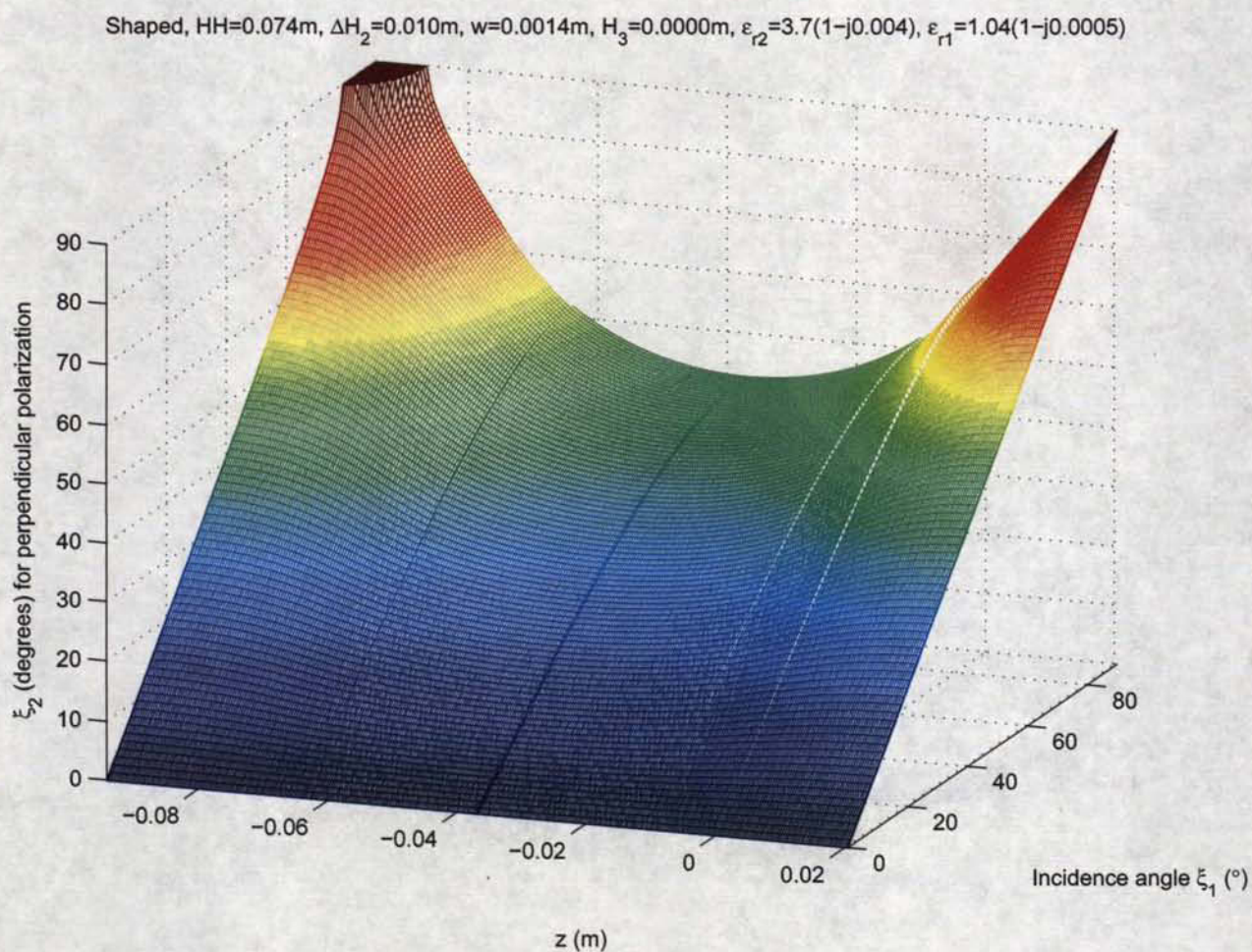
Figure 5.39: This figure shows the value of the angle $-\rho_2$ at all the interfaces through the plate for the shaped profile with lossy styrofoam present in the region $z > 0$ for the perpendicular polarization. The discretization was $dz \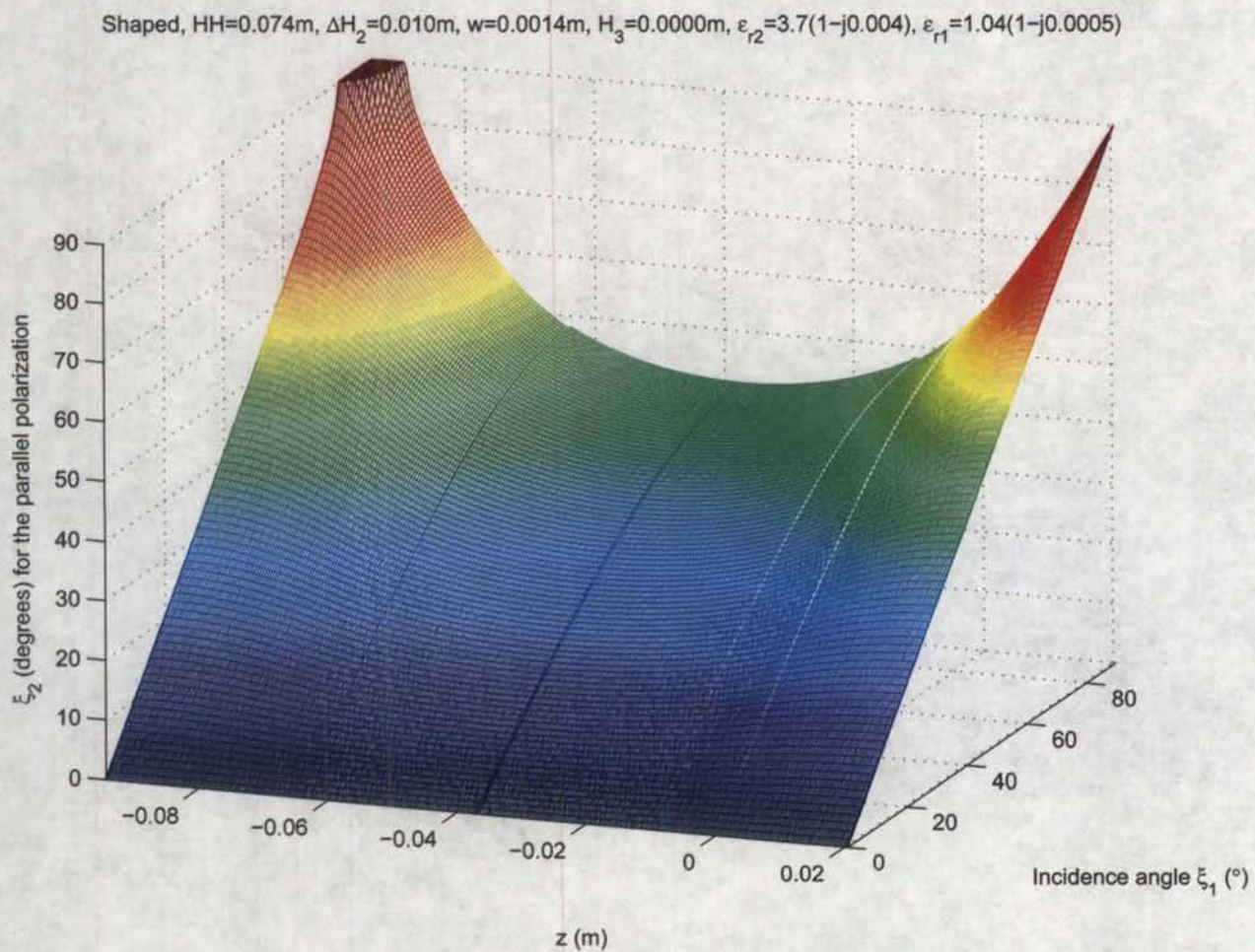leq 0.0004$ m throughout the plate. Note that MATLAB could not produce properly the 3D rendition of the plot below the plane $\rho_2 = 0$ at the back section of the plate.

Figure 5.40: This figure shows the value of the angle $-\rho_2$ at all the interfaces through the plate for the shaped profile with lossy styrofoam present in the region $z > 0$ for the parallel polarization. The discretization was $dz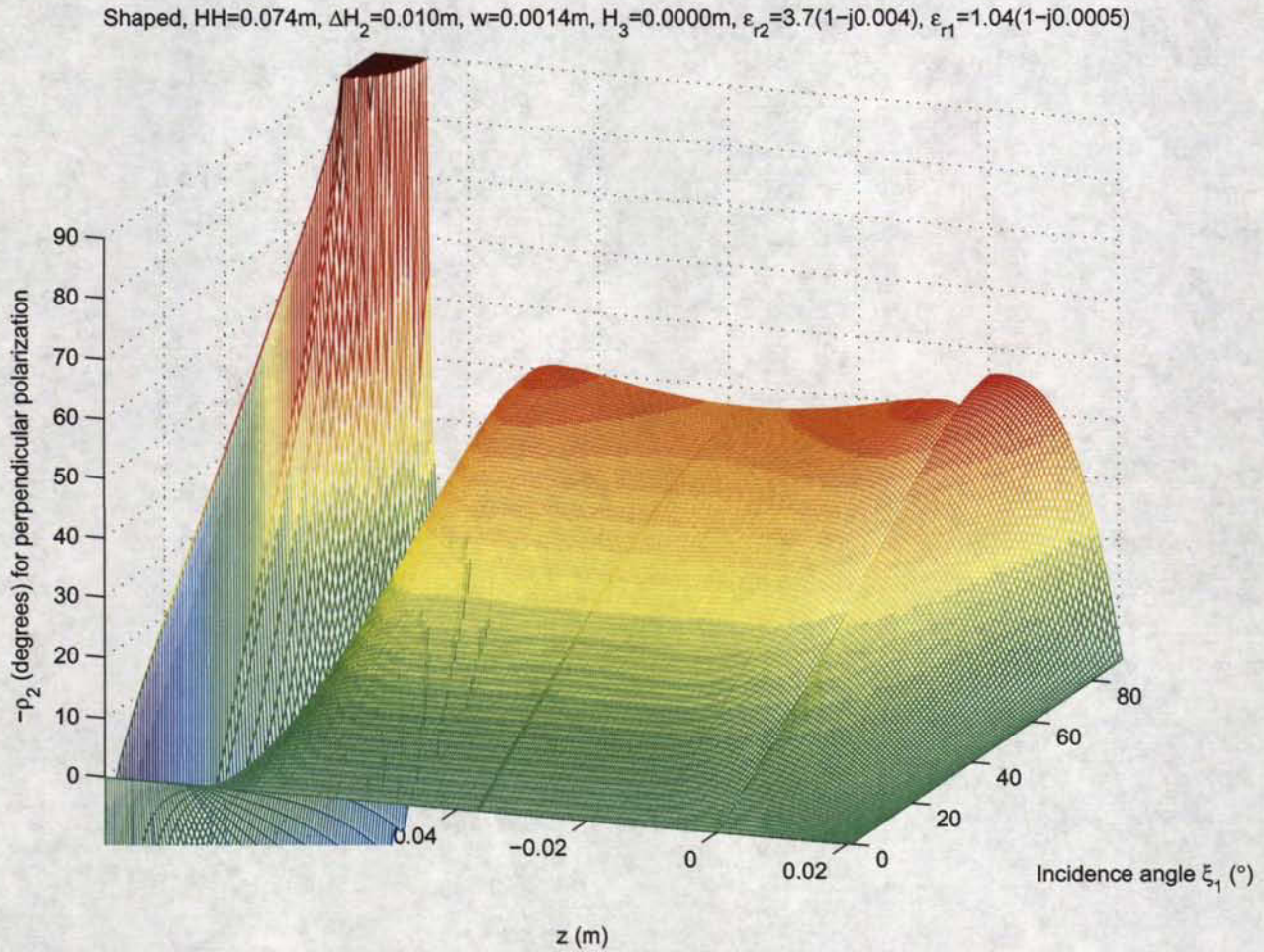 \leq 0.0004$ m throughout the plate. Note that MATLAB could not produce properly the 3D rendition of the plot below the plane $\rho_2 = 0$ at the back section of the plate.
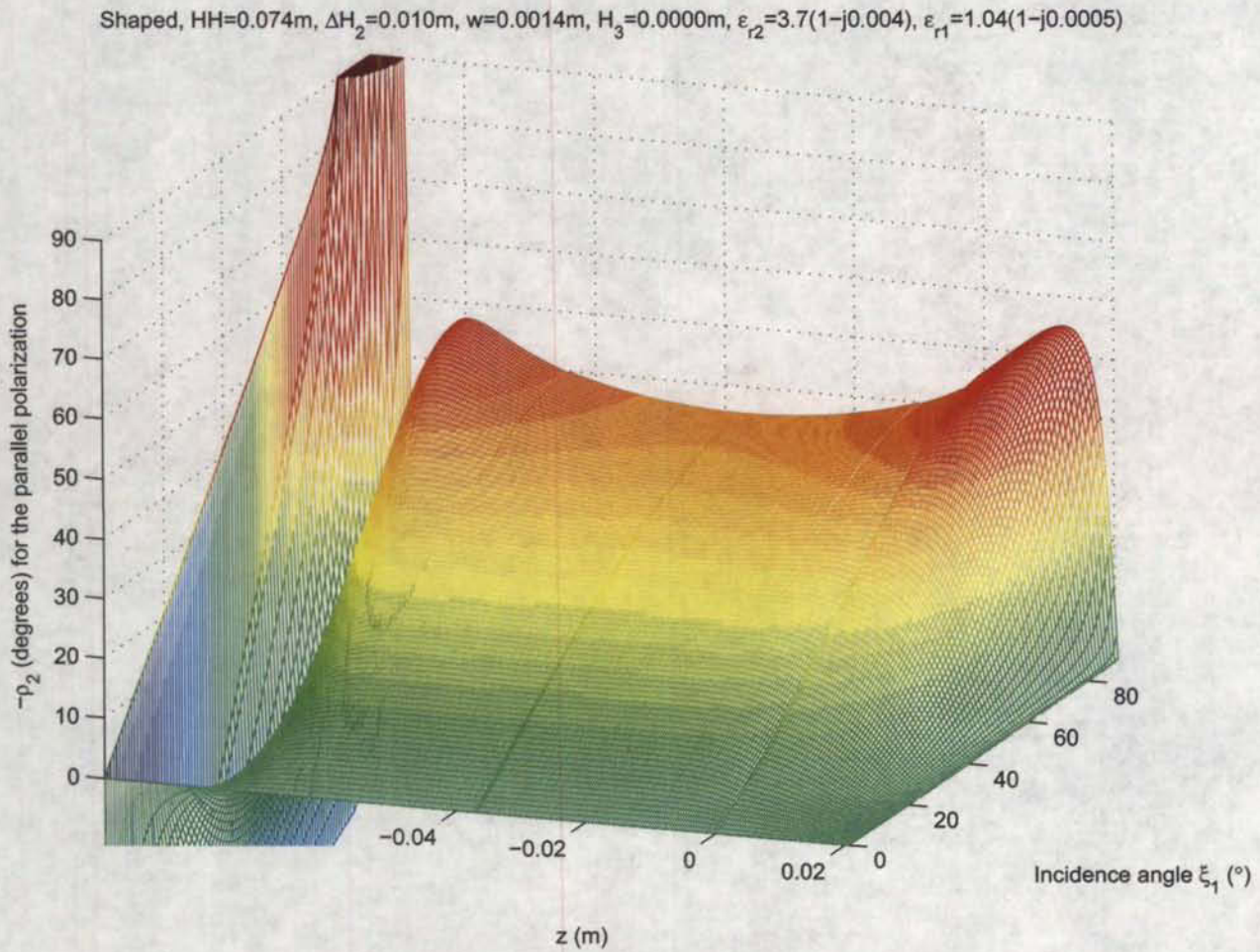
Figure 5.41: This figure shows the computed reflection and the computed transmission levels in dB for the shaped profile with lossy styrofoam present in the region $z > 0$ and $H_3 = 0.0003$ m. The discretization was $dz \leq 0.0004$ m throughout the plate.
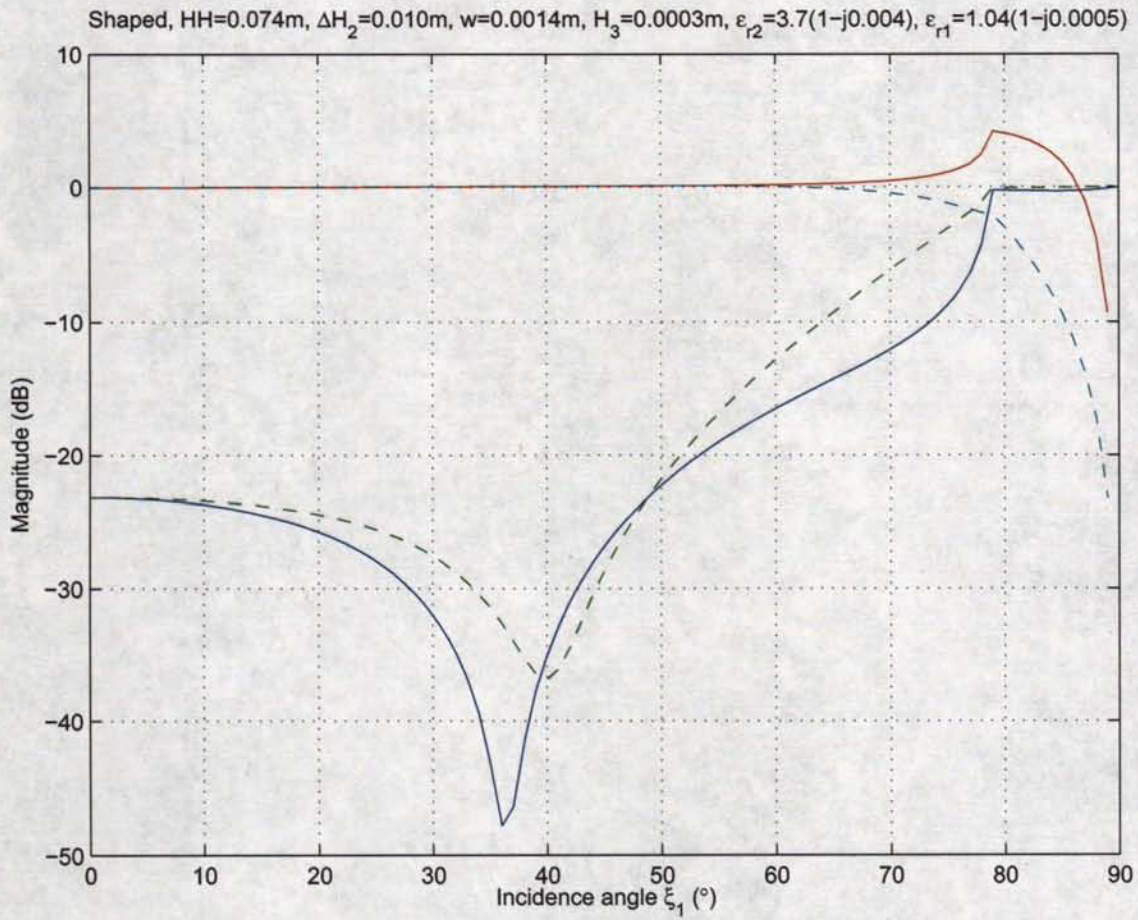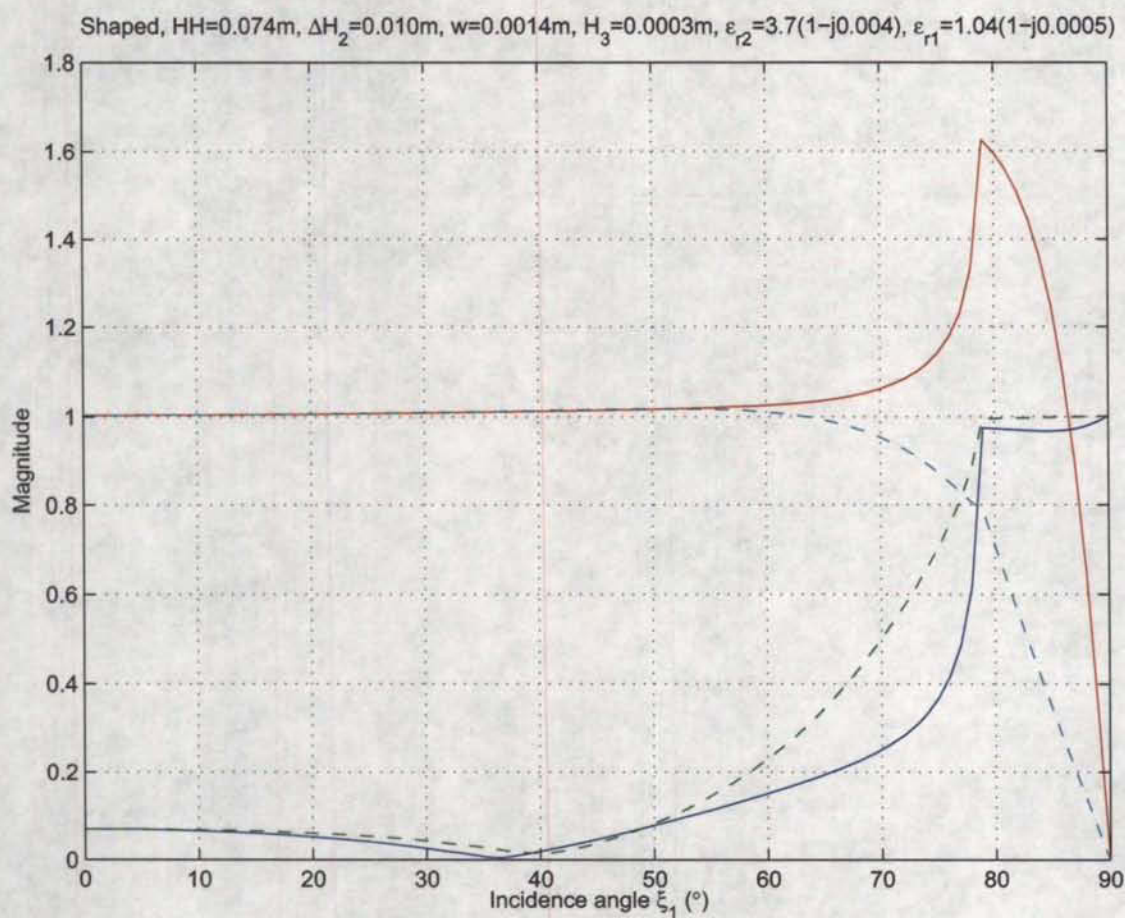
Figure 5.42: This figure shows the computed reflection and the computed transmission levels on the linear scale for the shaped profile with lossy styrofoam present in the region $z > 0$ and $H_3 = 0.0003$ m. The discretization was $dz \leq 0.0004$ m throughout the plate.

Shaped, HH=0.074m, ΔH_2=0.010m, w=0.0014m, H_3=0.0003m, ε_{r2}=3.7(1−j0.004), ε_{r1}=1.04(1−j0.0005)

Figure 5.43: This figure shows the profile for the real part of $\varepsilon_r^{\text{trans}}$ and $\varepsilon_r^{\text{long}}$ for the shaped profile with lossy styrofoam present in the region $z > 0$ and $H_3 = 0.0003$ m. The discretization was $dz \leq 0.0004$ m throughout the plate.

154
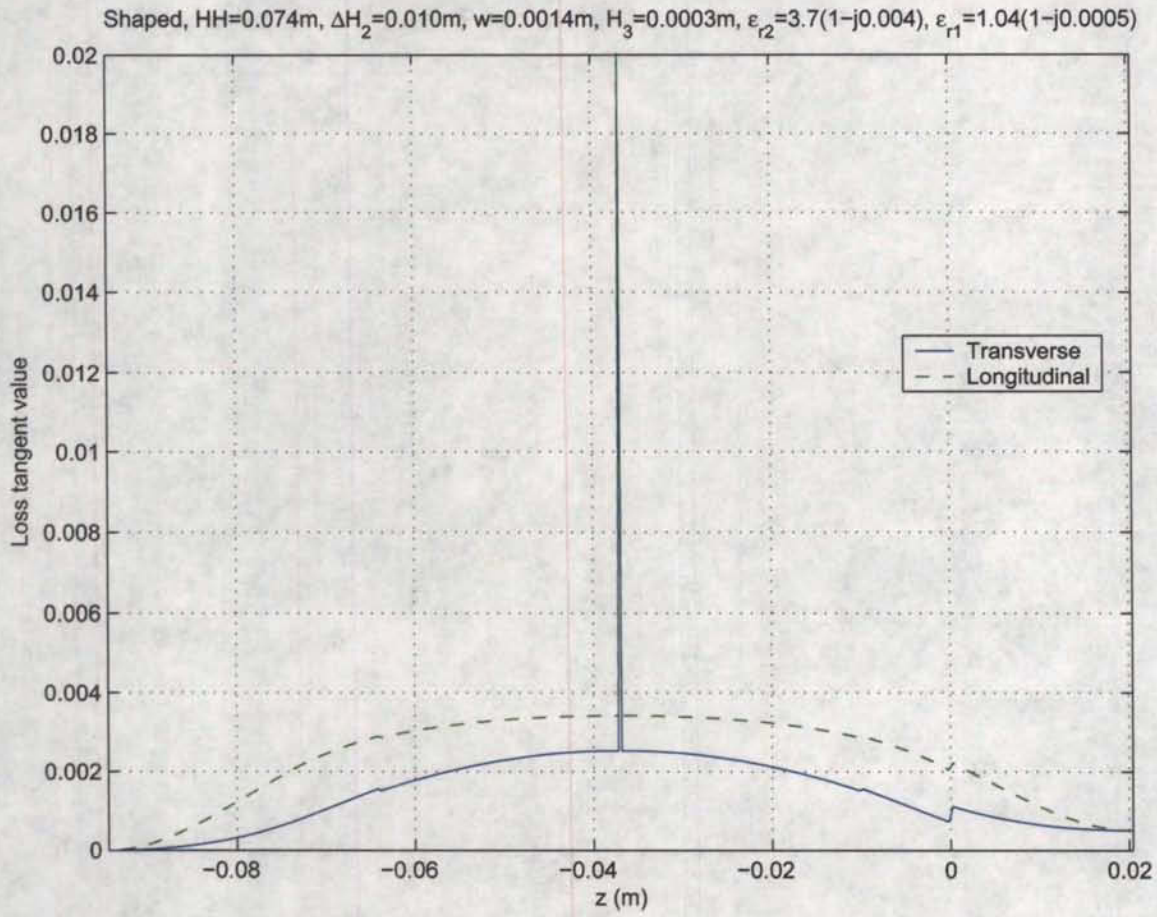
Figure 5.44: This figure shows the profile for loss tangent of $\varepsilon_r^{\text{trans}}$ and $\varepsilon_r^{\text{long}}$ for the shaped profile with lossy styrofoam present in the region $z > 0$ and $H_3 = 0.0003$ m. The discretization was $dz \leq 0.0004$ m throughout the plate.
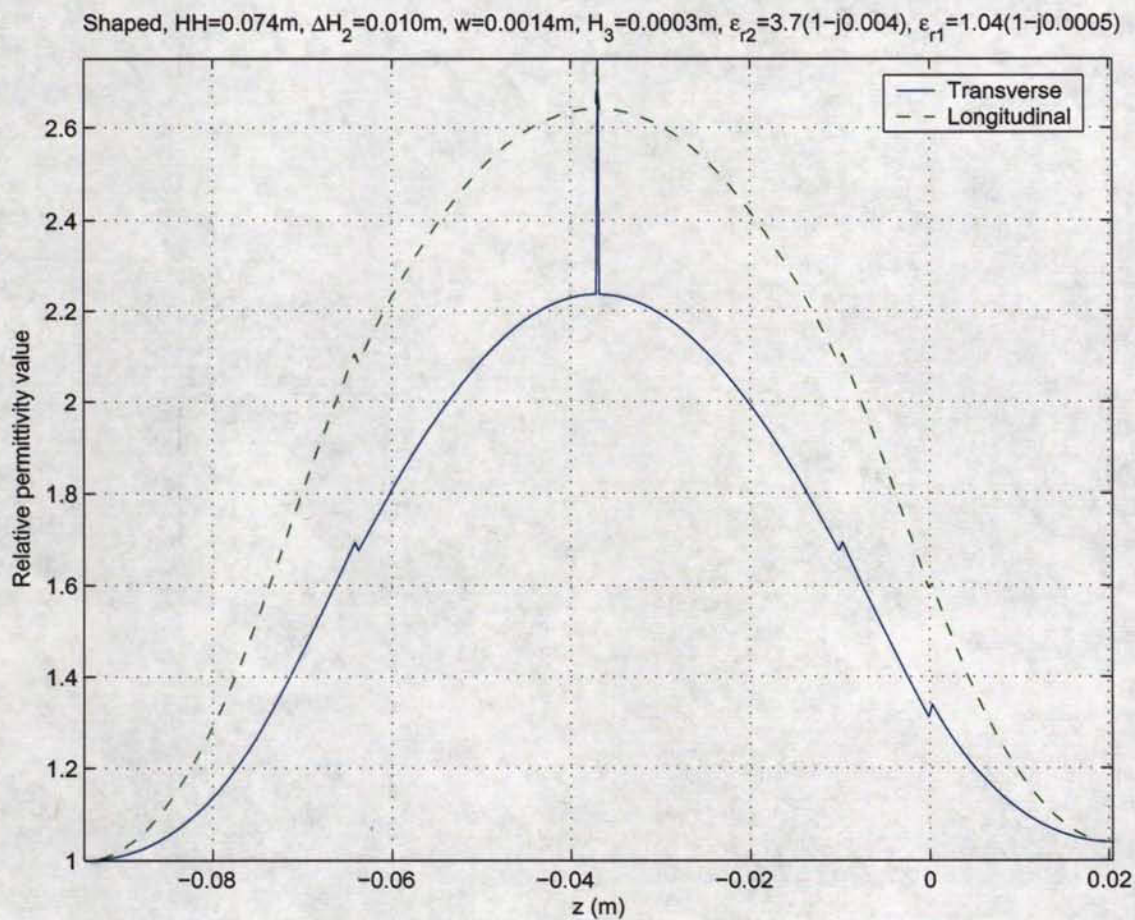
Figure 5.45: This figure shows the intrinsic amplitude propagation constant α_o for the shaped profile with lossy styrofoam present in the region $z > 0$ and $H_3 = 0.0003$ m for the perpendicular polarization. The discretization was $dz \leq 0.0004$ m throughout the plate.

Figure 5.46: This figure shows the intrinsic amplitude propagation constant α_o for the shaped profile with lossy styrofoam present in the region $z > 0$ and $H_3 = 0.0003$ m for the parallel polarization. The discretization was $dz \leq 0.0004$ m throughout the plate.

Shaped, HH=0.074m, ΔH_2=0.010m, w=0.0014m, H_3=0.0003m, ε_{r2}=3.7(1−j0.004), ε_{r1}=1.04(1−j0.0005)
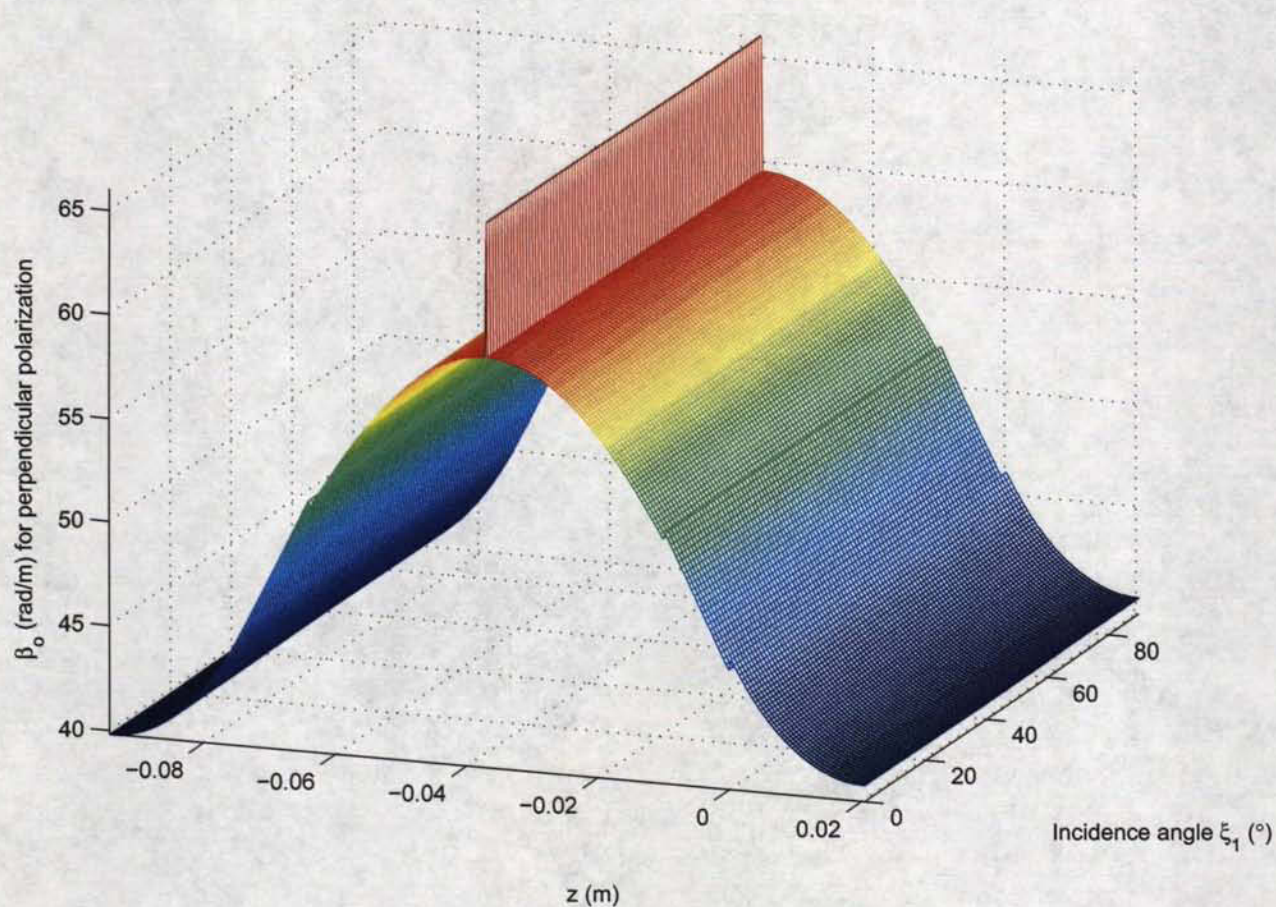
Figure 5.47: This figure shows the intrinsic phase propagation constant β_o for the shaped profile with lossy styrofoam present in the region $z > 0$ and $H_3 = 0.0003$ m for the perpendicular polarization. The discretization was $dz \leq 0.0004$ m throughout the plate.
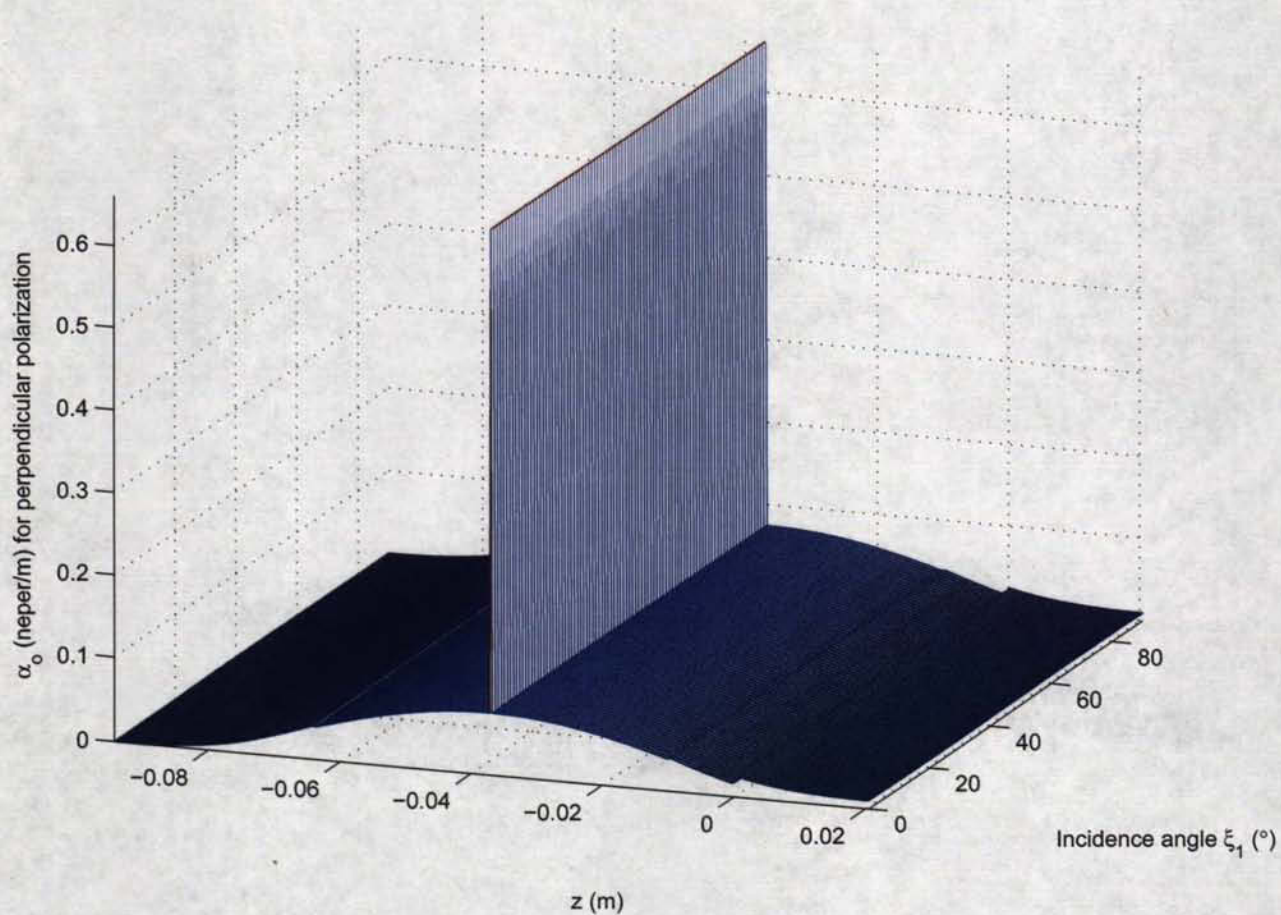
Figure 5.48: This figure shows the intrinsic phase propagation constant β_o for the shaped profile with lossy styrofoam present in the region $z > 0$ and $H_3 = 0.0003$ m for the parallel polarization. The discretization was $dz \leq 0.0004$ m throughout the plate.

Shaped, HH=0.074m, ΔH_2=0.010m, w=0.0014m, H_3=0.0003m, ε_{r2}=3.7(1−j0.004), ε_{r1}=1.04(1−j0.0005)
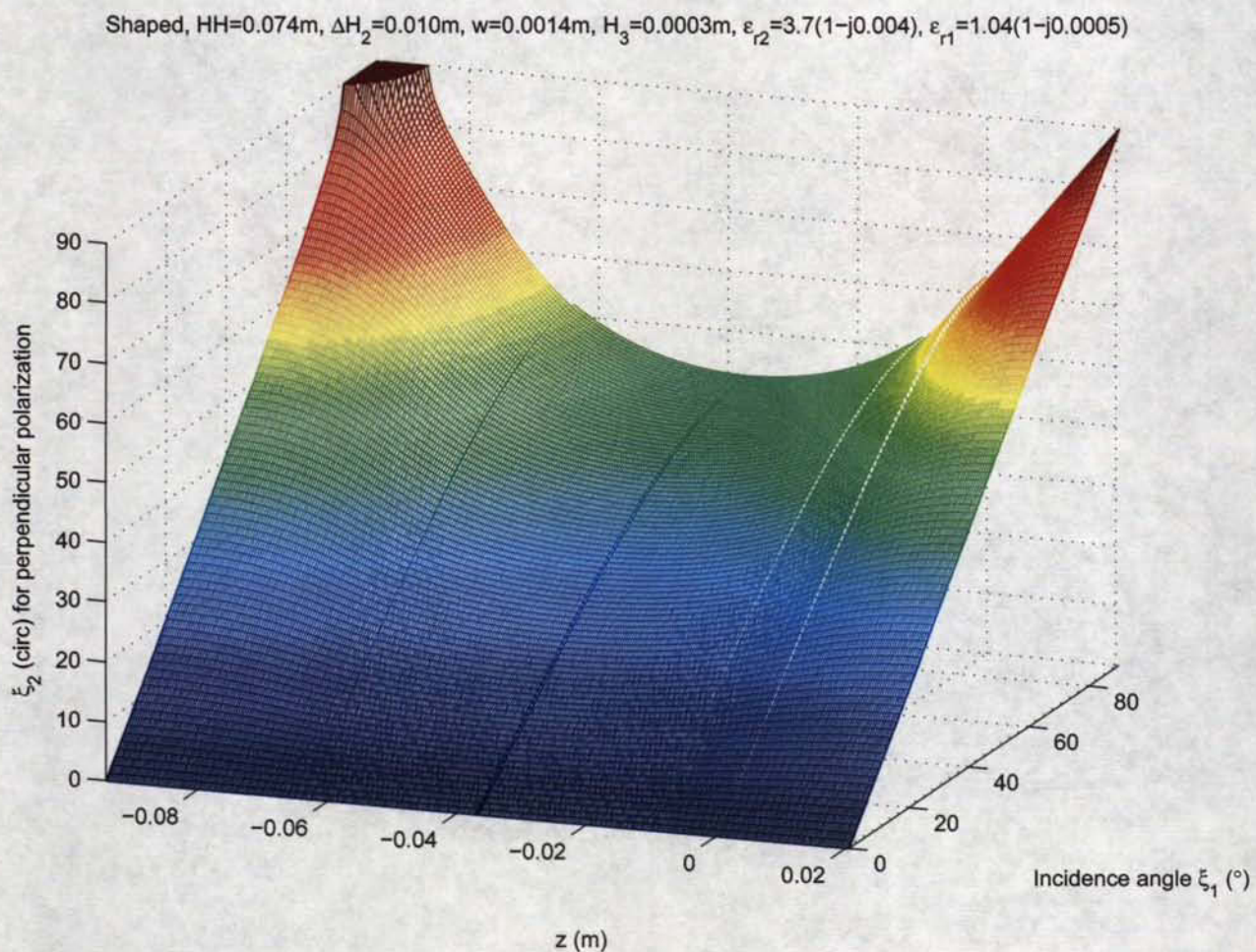
Figure 5.49: This figure shows the value of the angle ξ_2 at all the interfaces through the plate for the shaped profile with lossy styrofoam present in the region $z > 0$ and $H_3 = 0.0003$ m for the perpendicular polarization. The discretization was $dz \leq 0.0004$ m throughout the plate.
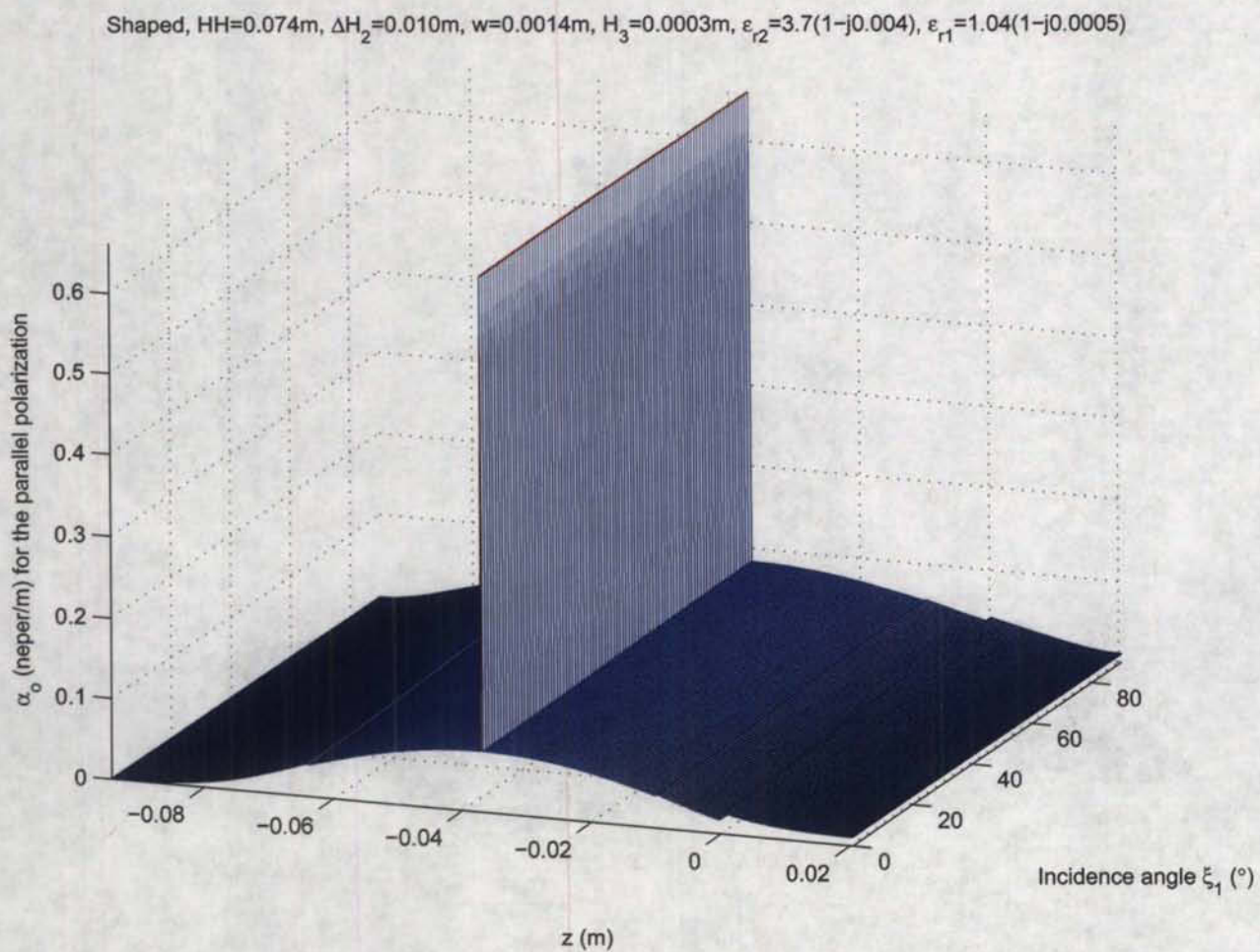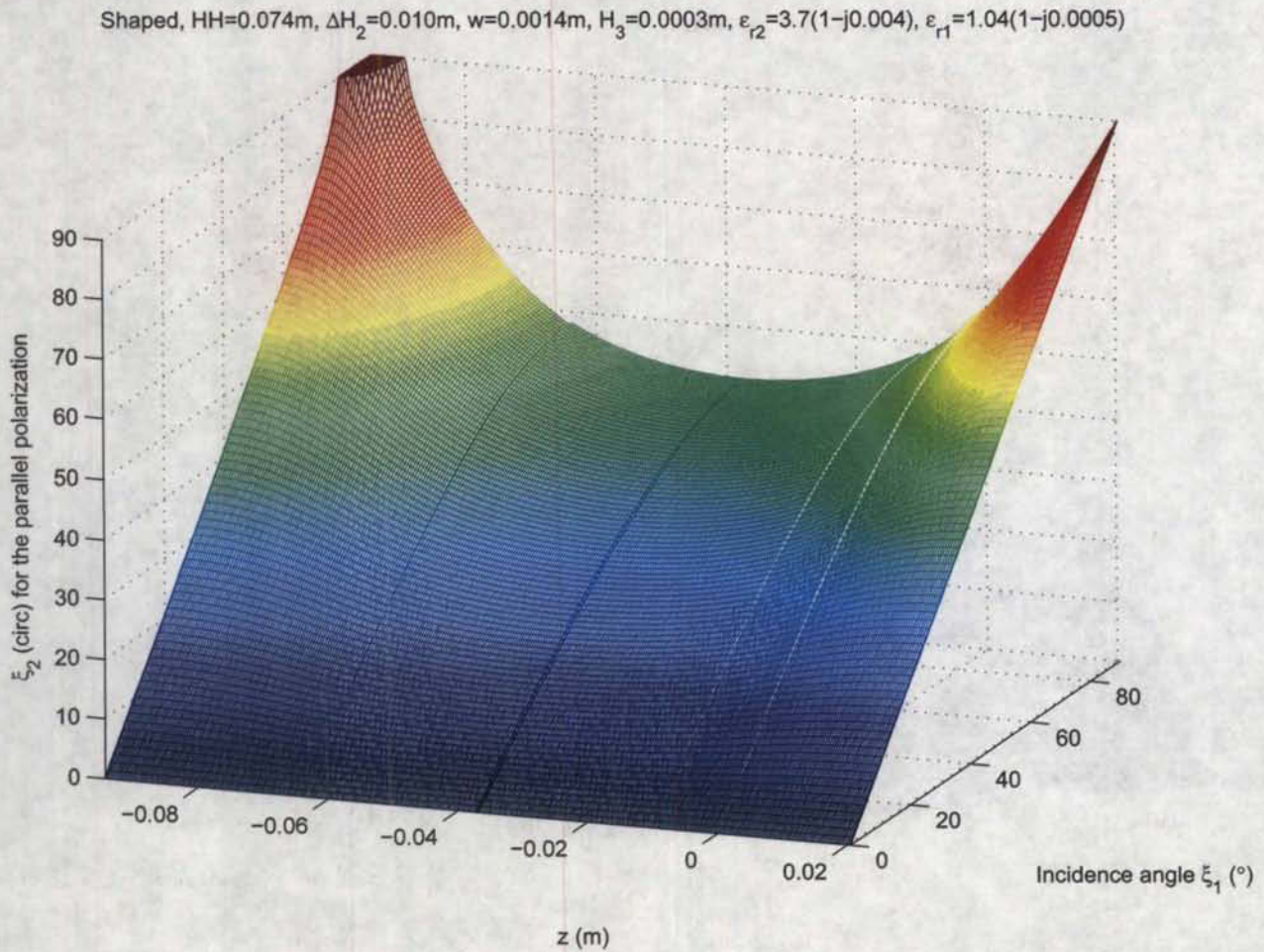
Figure 5.50: This figure shows the value of the angle ξ_2 at all the interfaces through the plate for the shaped profile with lossy styrofoam present in the region $z > 0$ and $H_3 = 0.0003$ m for the parallel polarization. The discretization was $dz \leq 0.0004$ m throughout the plate.

Shaped, HH=0.074m, ΔH_2=0.010m, w=0.0014m, H_3=0.0003m, ε_{r2}=3.7(1−j0.004), ε_{r1}=1.04(1−j0.0005)

Figure 5.51: This figure shows the value of the angle $-\rho_2$ at all the interfaces through the plate for the shaped profile with lossy styrofoam present in the region $z > 0$ and $H_3 = 0.0003$ m for the perpendicular polarization. The discretization was $dz \leq 0.0004$ m throughout the plate. Note that MATLAB could not produce properly the 3D rendition of the plot below the plane $\rho_2 = 0$ at the back section of the plate.

Shaped, HH=0.074m, ΔH_2=0.010m, w=0.0014m, H_3=0.0003m, ε_{r2}=3.7(1−j0.004), ε_{r1}=1.04(1−j0.0005)
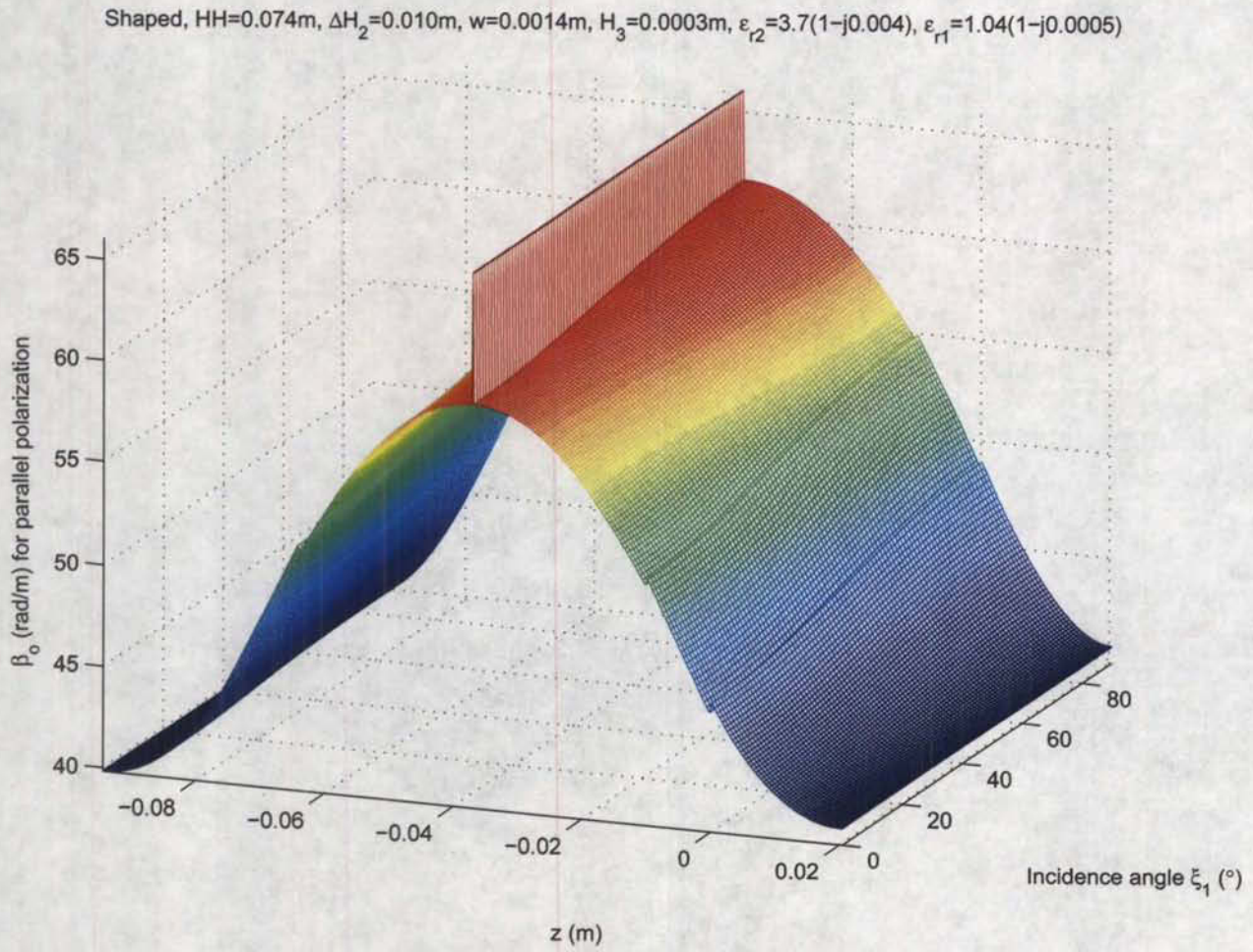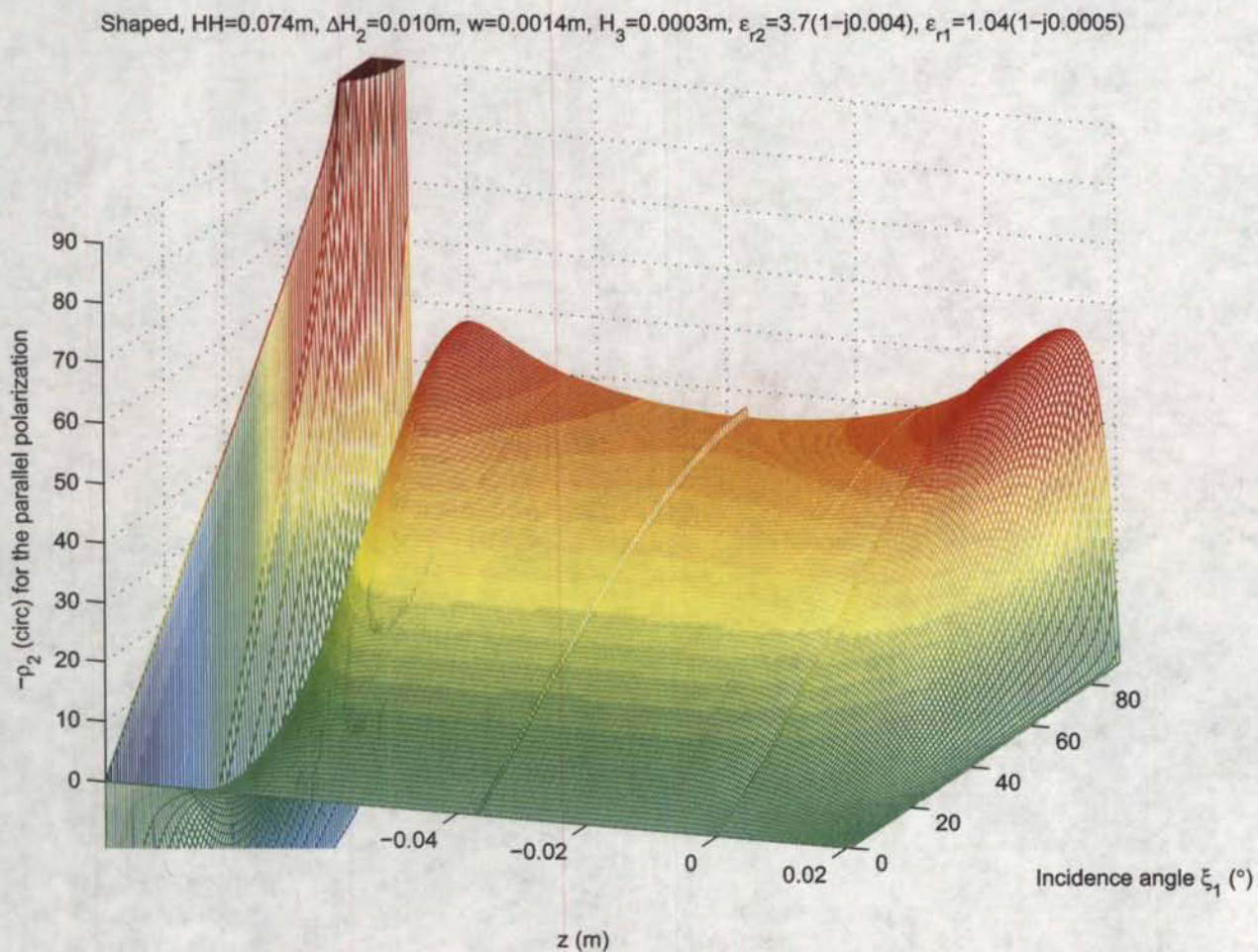
Figure 5.52: This figure shows the value of the angle $-\rho_2$ at all the interfaces through the plate for the shaped profile with lossy styrofoam present in the region $z > 0$ and $H_3 = 0.0003$ m for the parallel polarization. The discretization was $dz \leq 0.0004$ m throughout the plate. Not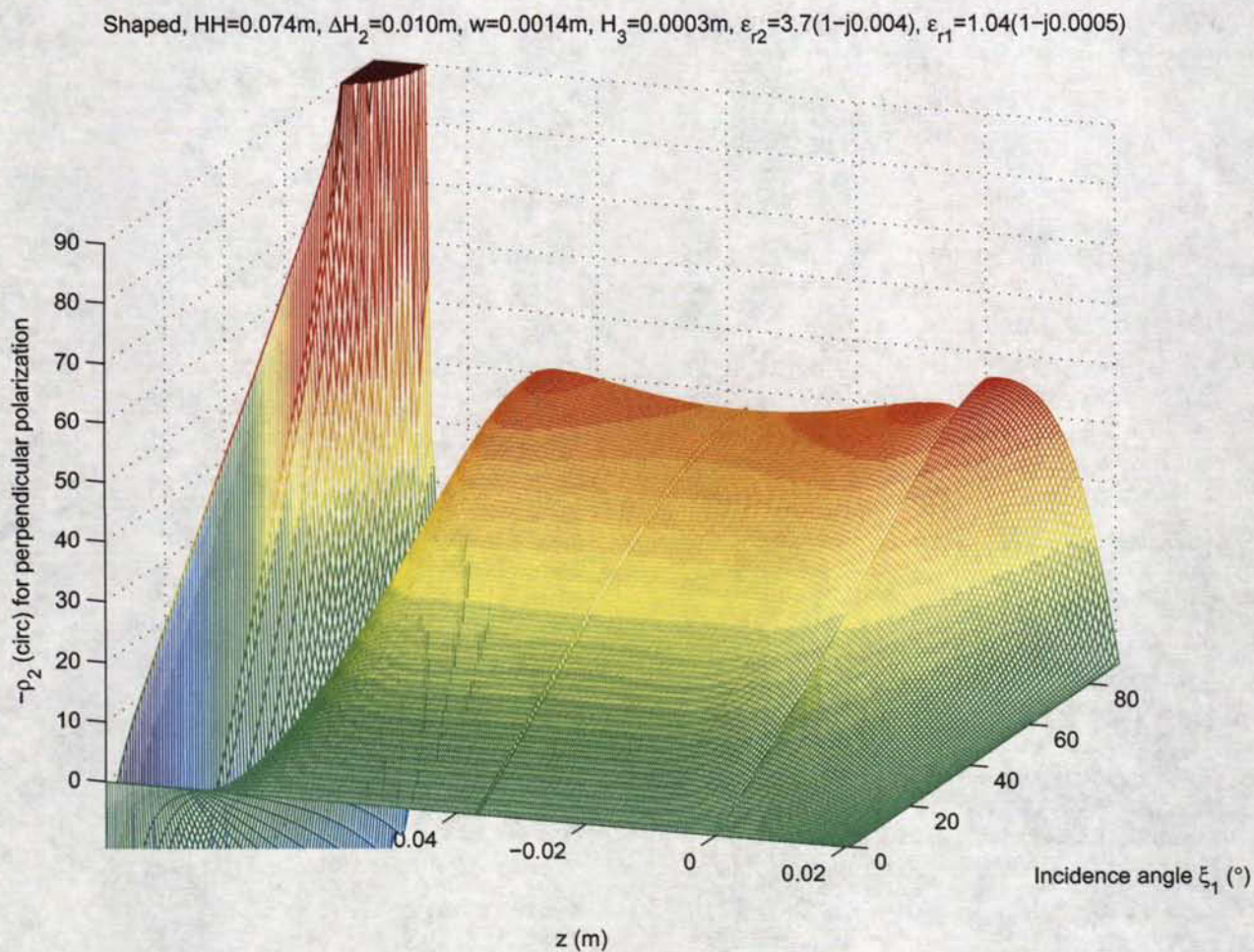e that MATLAB could not produce properly the 3D rendition of the plot below the plane $\rho_2 = 0$ at the back section of the plate.

Chapter 6

Conclusion

This report has presented the analysis technique and the predicted results for a uniaxial composite plate with the optic axis normal to the plate. The analysis technique contains two elements of novelty:

1. a new result for the effective propagation constants α and β within a lossy material;

2. a new approach based on the Adler-Chu-Fano formulation for predicting the behaviour of the extraordinary wave within a uniaxial medium.

A computer program was written in MATLAB to implement the analysis technique. A series of simulations revealed a choice of parameters that provides a reflection level of less than about -22 dB over an angular range of $0°$ to about $50°$. The mounting plate was manufactured and its response measured. Originally, it was planned that the measurement setup, procedure, results and comparison between predicted and measured results would be reported in another document as Part II. The comparison, however, turned out to be rather poor due to limitation in measurement setup[1].

---

[1] Although the boom was extended to its full length, the spacing between the transmitting horn positioned at the end of the boom, and the mounting plate positioned at the centre of the rotating table, is thought to have been insufficient.

Chapter 7

References

This chapter present the lists of references for the whole document, including the appendices.

Bibliography

[1] Allen Taflove and Suzanne C. Hagness, <u>Computational Electrodynamics, the finite difference time-domain method</u>, 3rd Edition, Artech House, 2005, p. 285.

[2] Z.S. Sacks, D.M. Kingsland, R. Lee and J-F. Lee, "A Perfectly Matched Anisotropic Absorber for Use as an Absorbing Boundary Condition", *IEEE Trans. Antennas Propagat.*, Vol. AP-43, No. 12, Dec. 1995, pp. 1460-1463.

[3] K. Walther, "Reflection Factor of Gradual-Transition Absorbers for Electromagnetic and Acoustic Waves", *IRE Trans. Antennas Propagat.*, Vol. AP-8, Nov. 1960, pp. 608-621.

[4] R.B. Adler, L.J. Chu, and R.M Fano, <u>Electromagnetic Energy Transmission and Radiation</u>, New York, Wiley, 1960, chapters 7 and 8.

[5] J.R. Wait, <u>Electromagnetic Wave Theory</u>, Harper & Row Publishers, 1985.

[6] R.D. Radcliff and C.A. Balanis, "Modified Propagation Constants for Nonuniform Plane Wave Transmission Through Conducting Media", *IEEE Trans. Geosci. Remote Sensing*, Vol. GE-20, No. 3, July 1982, pp. 408-411.

[7] H.C. Chen, <u>Theory of Electromagnetic Waves, A Coordinate-Free Approach</u>, McGraw-Hill, 1983.

[8] J.J. Holmes and C.A. Balanis, "Refraction of a Uniform Plane Wave Incident on a Plane Boundary Between Two Lossy Media", *IEEE Trans. Antennas Propagat.*, Vol. AP-26, No. 5, Sept. 1978, pp. 738-741.

[9] Paul Lorrain and Dale Corson, <u>Electromagnetic Fields and Waves</u>, W.H. Freeman and Company, 2nd Ed., 1970.

[10] T. Cwik and R. Mittra, "The Cascade Connection of Planar Periodic Surfaces and Lossy Dielectric Layers to Form an Arbitrary Periodic

Screen", *IEEE Trans. Antennas Propagat.*, Vol. AP-35, No. 12, December 1987, pp. 1397-1405.

[11] T. Cwik and R. Mittra, "Correction to "The Cascade Connection of Planar Periodic Surfaces and Lossy Dielectric Layers to Form an Arbitrary Periodic Screen", *IEEE Trans. Antennas Propagat.*, Vol. AP-36, No. 9, September 1988, pp. 1335.

[12] R. Mittra, C.H. Chan and T. Cwik, "Techniques for Analyzing Frequency Selective Surfaces - A Review", *Proc. IEEE*, Vol. 76, No. 12, December 1988, pp. 1593-1615.

[13] J.E. Roy, Reciprocal Circular Polarization Selective Surfaces, Ph.D. thesis, University of Manitoba, Winnipeg, Canada, 1996.

[14] N.N. Rao, Elements of Engineering Electromagnetics, 3rd. Ed., Prentice-Hall, 1991.

[15] M.N.O. Sadiku, Elements of Electromagnetics, 3rd. Ed., Oxford University Press, 2001.

[16] F.T. Ulaby, Fundamentals of Applied Electromagnetics, 2001 Media Ed., Prentice-Hall, 2001.

[17] N. Ida and J.P.A. Bastos, Electromagnetics and Calculation of Fields, Springer-Verlag, 1992.

[18] W.H. Hayt Jr. and J.A. Buck, Engineering Electromagnetics, 6th Ed., McGraw-Hill, 2001.

[19] Roy N. Adams and Eugene D. Denman, Wave Propagation in Turbulent Media, American Elsevier Pub. Co., New York, 1966.

[20] D.T. Paris and F.K. Hurd, Basic Electromagnetic Theory, McGraw-Hill, New York, 1969, chapter 8.

[21] C.A. Balanis, Advanced Engineering Electromagnetics, John Wiley and Sons, 1989.

[22] D.W. Berreman, "Optics in Stratified and Anisotropic Media: 4x4-Matrix Formulation", *Journal of the Optical Society of America*, Vol. 62, No. 4, 1972, pp. 502-510.

[23] S. Teitler and B.W. Henvis, "Refraction in Stratified, Anisotropic Media", *Journal of the Optical Society of America*, Vol. 60, No. 6, 1970, pp. 830-834.

[24] B.S. Agrawal and E. Bahar, "Propagation of EM Waves in Inhomogeneous Anisotropic Media", *IEEE Trans. Antennas Propagat.*, Vol. AP-28, No. 3, 1980, pp. 422-424.

[25] R.D. Graglia, P.L.E. Uslenghi and R.E. Zich, "Reflection and Transmission For Planar Structures of Bianisotropic Media", *Electromagnetics*, Vol. 11, 1991, pp. 193-208.

[26] M.A. Morgan, D.L. Fisher and E.A. Milne, "Electromagnetic Scattering by Stratified Inhomogeneous Anisotropic Media", *IEEE Trans. Antennas Propagat.*, Vol. AP-35, No. 2, 1987, pp. 191-197.

[27] J.B. Titchener and J.R. Willis, "The Reflection of Electromagnetic Waves from Stratified Anisotropic Media", *IRE Trans. Antennas Propagat.*, Vol. AP-39, No. 1, Jan. 1991, pp. 35-39.

[28] A. Lakhtakia, V.K. Varadan and V.V. Varadan, "Reflection and transmission of plane waves at the planar interface of a general uniaxial medium and free space", *J. Modern Opt.*, Vol. 38, No. 4, 1991, pp. 649-657.

[29] E.F. Kuester and Christopher L. Holloway, Plane-Wave Reflection from Inhomogeneous Uniaxially Anisotropic Absorbing Dielectric Layers, Scientific Report No. 97, Electromagnetic Laboratory, University of Colorado, May 1989.

[30] K. Sarabandi, "Simulation of a Periodic Dielectric Corrugation with an Equivalent Anisotropic Layer", *Intern. J. Infrared and Millimeter Waves*, Vol. 11, No. 11, 1990, pp. 1303-1321.

[31] J.R. Wait, Lectures on Wave Propagation Theory, Oxford: Pergamon, 1982.

[32] L.J. Peter Linnér, "Exact Formulas for Wave Impedance and Propagation Constants of Homogeneous, Lossy Dielectric and/or Magnetic Materials", *IEEE Trans. Antennas Propagat.*, Vol. AP-37, No. 3, March 1989, pp. 410-411.

[33] J.E. Roy and L. Shafai, "Generalized scattering matrix and symmetry principles for infinite planar structures", *Can. J. Phys.*, Vol. 75, 1997, pp. 413-431.

[34] Arun K. Bhattacharyya, Electromagnetic Fields in Multilayered, Structures Theory and Applications, Artech House, 1994, chapter 2.

[35] S. Contu and R. Tascone, "Scattering from passive arrays in plane stratified regions", *Electromagnetics*, Vol. 5, 1985, pp. 285-306.

[36] R. Orta, R. Tascone and R. Zich, "A unified formulation for the analysis of general frequency selective surfaces", *Electromagnetics*, Vol. 5, 1985, pp. 307-329.

[37] Jose Perini and Lawrence S. Cohen, "Design of Broad-Band Radar-Absorbing Materials for Large Angles of Incidence", *IEEE Trans. EMC*, Vol. 35, May 1993, pp. 223-230.

[38] L.B. Felsen, "Propagation and diffraction in uniaxially anisotropic regions: Part 1. Theory", *Proc. IEE*, Vol. 111, No. 3, March 1964, pp. 445-453.

[39] Raymond Redheffer, "On the Relation of Transmission-Line Theory to Scattering and Transfer", Journal of Mathematics and Physics, Vol. 41, pp. 1-41, 1962.

[40] David M. Kerns, Plane-Wave Scattering-Matrix Theory of Antennas and Antenna-Antenna Interactions, National Bureau of Standards, Monograph #162, June 1981.

[41] Thorkild B. Hansen and Arthur D. Yaghjian, Plane-Wave Theory of Time-Domain Fields, Near-Field Scanning Applications, IEEE Press, 1999.

[42] Weng Cho Chu, Waves and Fields in Inhomogeneous Media, IEEE Press, 1995.

[43] R. Carminati, M. Nieto-Vesperinas and J. Greffet, "Reciprocity of evanescent electromagnetic waves", *J. Opt. Soc. A*, Vol. 15, No. 3, March 1998, pp. 706-712.

[44] R.E. Collin, Foundation for Microwave Engineering, McGraw-Hill Book Co., 1966.

[45] Ross A. Speciale, "Renormalization of the Scattering Matrix", Proc. 17th Annual Review of Progress in Applied Computational Electromagnetics (ACES), Naval Postgraduate School, Monterey, CA, March 19-23, 2001, pp. 553-561.

[46] D.G. Bodnar and H.L. Bassett, "Analysis of an Anisotropic Dielectric Radome", *IEEE Trans. Antennas Propagat.*, Vol. AP-23, No. 6, Nov. 1975, pp. 841-846.

[47] R.E. Collin, Field Theory of Guided Waves, McGraw-Hill Book Co., 1960.

[48] A.R. Mickelson, Physical Optics, Van Nostrand Reinhold, Chapter 4, 1992.

[49] C.C. Johnson, Field and Wave Electrodynamics, McGraw-Hill, 1965.

[50] P.C. Clemmow, The Plane Wave Spectrum Representation of Electromagnetic Fields, Pergamon Press, 1966, chapter VIII.

[51] G. Eichmann, "Scaling for Rotationally Symmetric Potential in a Uni-axial Media", *Radio Science*, Vol. 2 (New Series), August 1967, pp. 833-836.

[52] I. V. Lindell,"TE/TM Decomposition of Electromagnetic sources in uniaxial anisotropic media", *Microwave and Optical Techn. Letters*, Vol. 9, No. 2, June 1995, pp. 108-111.

[53] C.M. Krowne, "Green's Function in the Spectral Domain for Biaxial and Uniaxial Anisotropic Planar Dielectric Sturcutres", *IEEE Trans. Antennas Propagat.*, Vol. AP-32, No. 12, 1984, pp. 1273-1281.

[54] A.E. Philippe, "Reflection and Transmission of Radio Waves at a Di-electric Slab with Variable Permittivity', *IEEE Trans. Antennas Prop-agat.*, Vol. AP-21, March 1973, pp. 234-236.

[55] J.H. Richmond, "The WKB Solution for Transmission Through Inho-mogeneous Plane Layers", *IRE Trans. Antennas Propagat.*, July 1962, pp. 472-473.

[56] Tie Jun Cui, Chang Hong Liang and Werner Wiesbeck, "Closed-Form Solutions for One-Dimensional Inhomogeneous Anisotropic Medium in a Special Case - Part I: Direct Scattering Problem", *IEEE Trans. An-tennas Propagat.*, Vol. 45, June 1997, pp. 936-941.

[57] J.H. Richmond, "Scattering by a Dielectric Cylinder of Arbitrary Cross Section Shape", *IEEE Trans. Antennas Propagat.*, Vol. AP-13, May 1965, pp. 334-341.

[58] J.H. Richmond, "TE Wave Scattering by a Dielectric Cylinder of Arbi-trary Cross Section Shape", *IEEE Trans. Antennas Propagat.*, Vol. AP-14, July 1966, pp. 460-464.

[59] T. Morita and S.B. Cohn, "Microwave lens matching by simulated quarter-wave transformer", *IEEE Trans. Antennas Propagat.*, Vol. AP-4, No. 1, Jan. 1956, pp. 33-39.

[60] R.E. Collin, "Reflection and Transmission at a Slotted Dielectric In-terface", *Can. J. Phys.*, Vol. 34, April, 1956, pp. 398-411.

[61] R.E. Collin, "A Simple Artificial Anisotropic Dielectric Medium", *IRE Trans. Microw. Theory Tech.*, April, 1958, pp. 206-209.

[62] C.L. Holloway and E.F. Kuester, "Impedance-Type Boundary Con-ditions for a Periodic Interface Between a Dielectric and a Highly Conducting Medium", *IEEE Trans. Antennas Propagat.*, Vol. AP-48, No. 10, October 2000, pp. 1660-1672.

[63] M.K. Moaveni, "Plane Wave Diffraction by Dielectric Gratings, Finite-Difference Formulation", *IEEE Trans. Antennas Propagat.*, Vol. AP-37, No. 8, 1989, pp. 1026-1031.

[64] M.G. Moharam and T.K. Gaylord, "Three-dimensional vector coupled-wave analysis of planar-grating diffraction", *J. Opt. Soc. Am.*, Vol. 73, No. 9, 1983, pp. 1105-1112.

[65] R. Petit, Electromagnetic Theory of Gratings, Springer-Verlag, 1980.

[66] D.H. Raguin and G.M. Morris, "Antireflection structured surfaces for the infrared spectral region", *Applied Optics*, Vol. 32, No. 7, March 1993, pp. 1154-1167.

[67] E.F. Kuester and C.L. Holloway, "Comparison of Approximations for Effective Parameters of Artificial Dielectrics", *IEEE Trans. Microwaves Theory Tech.*, Vol. 38, 1990, pp. 1752-1755.

[68] E.F. Kuester and C.L. Holloway, "A Low-Frequency Model for Wedge or Pyramid Absorber Arrays", *IEEE Trans. Electromagn. Compat.*, Vol. 36, 1994, pp. 300-313.

[69] C.L. Holloway, R.R. DeLyser, R.F. German, P. McKenna and M. Kanda, "Comparison of Electromagnetic Absorber Used in Anechoic and Semi-Anechoic Chambers for Emissions and Immunity Testing of Digital Devices", *IEEE Trans. Electromagn. Compat.*, Vol. 39, 1997, pp. 33-47.

[70] C.L. Holloway, E.F. Kuester, M. Johanson, R.T. Johnk and D.R. Novotny, "A Model for Predicting the Reflection Coeffifcient for Hollow Pyramidal Absorbers", *IEEE International Symposium on Electromagnetic Compatibility*, Seattle, Washington, August 2-6 1999, pp. 861-866.

[71] R. Janaswamy, "Oblique Scattering from Lossy Periodic Surfaces with Application to Anechoic Chamber Absorbers", *IEEE Trans. Antennas Propagat.*, Vol. AP-40, No. 2, 1992, pp. 162-169.

[72] N. Marly, D. De Zutter and H.F. Pues, "A Surface Integral Equation Approach to the Scattering and Absorption of Doubly Periodic Lossy Structures", *IEEE Trans. Electromagn. Compat.*, Vol. 36, 1994, pp. 14-22.

[73] N. Marly, B Baekelandt, D. De Zutter and H.F. Pues, "Integral Equation Modeling of the Scattering and Absorption of Multilayered Doubly-Periodic Lossy Structures", *IEEE Trans. Antennas Propagat.*, Vol. AP-43, No. 11, 1995, pp. 1281-1287.

[74] W. Kohler, G. Papanicolaou and S. Varadhan, "Boundary and Interface Problems in Regions with Very Rough Boundaries", in Multiple Scattering and Waves in Random Media, P.L. Chow, W.E. Kohler and G.C. Papanicolaou, Eds. Amsterdam, The Netherlands: North-Holland, 1981, pp. 165-197.

[75] M. Born and E. Wolf, Principle of Optics, Pergammon Press, Chapter XIV, 1959.

[76] W. Menzel, "A New Interpretation of the Spectral Domain Immitance Matrix Approach", *IEEE Trans. on MTT*, Vol. 3, No. 9, Sept. 1993, pp. 305-306.

[77] K.E. Oughstun, "Polarization properties of the freely propagating electromagnetic field of arbitrary spatial and temporal form", *J. Opt. Soc. Am. A*, Vol. 9, No. 4, Apr. 1992, pp. 578-584.

[78] M-S Lin and C.H. Chen, "Plane-Wave Shielding Characteristics of Anisotropic Laminated Composites", *IEEE Trans. Electromagn. Compat.*, Vol. 35, No. 1, Febr. 1993, pp. 21-27.

[79] M-S Lin, C-M Lin, R-B Wu and C.H. Chen, "Transient Propagation in Anisotropic Lamminated Composites", *IEEE Trans. Electromagn. Compat.*, Vol. 35, No. 3, Aug. 1993, pp. 357-364.

[80] M.L. Kales, "Part III - Elliptically Polarized Waves and Antennas", *Proc. I.R.E.*, May 1951, pp. 544-549.

[81] I.V. Lindell, Methods for Electromagnetic Field Analysis, Series on Electromagnetic Wave Theory, IEEE press and Oxford University press, 1995, chapter 1.

[82] MATLAB Symbolic Math Toolbox from "The Math Works Inc.", User's guide, version 2, third printing 1997.

[83] R.L. Haupt and M. Cote, "Snell's Law Applied to Finite Surfaces", *IEEE Trans. Antennas Propagat.*, Vol. AP-41, No. 2, Febr. 1994, pp. 227-230.

[84] J.A. Stratton, Electromagnetic Theory, McGraw-Hill, 1941.

[85] R. Peterson and R. Mittra, Computational Methods for Electromagnetics, 1998.

Appendix A

Equivalence between approaches using instantaneous parameters and steady-state parameters

This appendix presents the proof for the mathematical identity of Equation (3.29). The input reflection coefficient computed by the method of multiple reflections is given as (see Reference [44, Equation (5.35), p. 226]):

$$\Gamma_{\text{in}} = \frac{\Gamma_1 + \Gamma_3 e^{-j2\beta_z d}}{1 + \Gamma_1 \Gamma_3 e^{-j2\beta_z d}} \qquad (A.1)$$

where:

$$\Gamma_1 = \frac{Z_2 - Z_1}{Z_2 + Z_1}$$

$$\Gamma_3 = \frac{Z_3 - Z_2}{Z_3 + Z_2}$$

Substituting the last two expressions into the first one produces:

$$\Gamma_{\text{in}} = \frac{(Z_2 - Z_1)(Z_3 + Z_2) + (Z_2 + Z_1)(Z_3 - Z_2)e^{-j2\beta_z d}}{(Z_2 + Z_1)(Z_3 + Z_2) + (Z_2 - Z_1)(Z_3 - Z_2)e^{-j2\beta_z d}}$$

Multiplying the numerator and the denominator by $e^{j\beta_z d}$ produces:

$$\Gamma_{\text{in}} = \frac{(Z_2 - Z_1)(Z_3 + Z_2)e^{j\beta_z d} + (Z_2 + Z_1)(Z_3 - Z_2)e^{-j\beta_z d}}{(Z_2 + Z_1)(Z_3 + Z_2)e^{j\beta_z d} + (Z_2 - Z_1)(Z_3 - Z_2)e^{-j\beta_z d}}$$

Using Euler's expressions for the trigonometric functions written in terms of the complex exponentials, and collecting the terms of equal power produces:

$$\Gamma_{\text{in}} = \frac{(Z_2 Z_3 - Z_1 Z_2)\cos(\beta_z d) + (Z_2^2 - Z_1 Z_3)j\sin(\beta_z d)}{(Z_2 Z_3 + Z_1 Z_2)\cos(\beta_z d) + (Z_2^2 + Z_1 Z_3)j\sin(\beta_z d)}$$

Dividing by $\cos(\beta_z d)$ produces:

$$\Gamma_{\text{in}} = \frac{(Z_2 Z_3 - Z_1 Z_2) + (Z_2^2 - Z_1 Z_3)j\tan(\beta_z d)}{(Z_2 Z_3 + Z_1 Z_2) + (Z_2^2 + Z_1 Z_3)j\tan(\beta_z d)}$$

Using $\tanh(jx) = j\tan(x)$ produces:

$$\Gamma_{\text{in}} = \frac{(Z_2 Z_3 - Z_1 Z_2) + (Z_2^2 - Z_1 Z_3)\tanh(j\beta_z d)}{(Z_2 Z_3 + Z_1 Z_2) + (Z_2^2 + Z_1 Z_3)\tanh(j\beta_z d)} \qquad (A.2)$$

Now, the input reflection coefficient computed by the method of steady-state parameters is given as:

$$\Gamma_{\text{in}} = \frac{Z_{\text{in}} - Z_1}{Z_{\text{in}} + Z_1}$$

where Z_{in} is given as (see Reference [44, Equation (3.91), p. 94]):

$$Z_{\text{in}} = Z_2 \frac{Z_3 + Z_2\tanh(\gamma_z d)}{Z_2 + Z_3\tanh(\gamma_z d)}$$

Substituting the last expression into the second last one and collecting the terms produces:

$$\Gamma_{\text{in}} = \frac{(Z_2 Z_3 - Z_1 Z_2) + (Z_2^2 - Z_1 Z_3)\tanh(\gamma_z d)}{(Z_2 Z_3 + Z_1 Z_2) + (Z_2^2 + Z_1 Z_3)\tanh(\gamma_z d)} \qquad (A.3)$$

When the system becomes lossy, $j\beta_z$ becomes $\gamma_z = \alpha_z + j\beta_z$ and thus, the expression in Equation (A.2) becomes the same as that in Equation (A.3), and this proves the mathematical equality. Note, however, that the transmission coefficient obtained by summing all the instantaneous waves emergent from the system is obtained as:

$$T_{\text{out}} = T_2 e^{-j\beta_z d} T_3 \frac{1}{1 + \Gamma_1 \Gamma_3 e^{-j2\beta_z d}}$$

where:

$$T_2 = \frac{2Z_2}{Z_2 + Z_1}$$

$$T_3 = \frac{2Z_3}{Z_3 + Z_2}$$

Upon substituting and carrying out algebraic manipulations similar to those above, one obtains:

$$T_{\text{out}} = \frac{2Z_2 Z_3 / \cosh(j\beta_z d)}{(Z_2 Z_3 + Z_1 Z_2) + (Z_2^2 + Z_1 Z_3)\tanh(j\beta_z d)}$$

whereas

$$\frac{2Z_{\text{in}}}{Z_{\text{in}} + Z_1} = \frac{2Z_2(Z_3 + Z_2\tanh(\gamma_z d))}{(Z_2 Z_3 + Z_1 Z_2) + (Z_2^2 + Z_1 Z_3)\tanh(\gamma_z d)}$$

hence, the last two results are, in general, different (notwithstanding that $j\beta_z$ becomes $\gamma_z = \alpha_z + j\beta_z$ when the system becomes lossy). Therefore, the steady-state reflection coefficient is obtained as $(Z_{\text{in}} - Z_1)/(Z_{\text{in}} + Z_1)$, but the steady-state transmission coefficient is not obtained as $2Z_{\text{in}}/(Z_{\text{in}} + Z_1)$. See also References [5, Equations 4.172, 4.175] and [19, Equations 7.15, 7.19]. The reason for this difference lies in the fact that with the steady-state approach, the rest of the circuit lying beyond the interface where Z_{in} is computed, is effectively enclosed in a black box that does not give access to the output port where the knowledge of the transmitted wave is desired.

Appendix B

Equivalence between a uniform plane wave with a complex-valued propagation angle and a non-uniform plane wave with real-valued propagation angles

This appendix presents the expressions for computing the complex propagation angle of a uniform plane wave from the knowledge of the real propagation angles of the corresponding non-uniform plane wave. The development presented here is more general than that presented in Reference [4, pp. 330-334]. The non-uniform plane wave is written as $e^{-\vec{\gamma}\cdot\vec{r}}$ where $\vec{\gamma} = \vec{\alpha} + j\vec{\beta}$ with the directions of $\vec{\alpha}$ given by θ_α and ϕ_α, and the directions of $\vec{\beta}$ given by θ_β and ϕ_β, in a spherical coordinate system with $\hat{z}$ parallel to the normal of the interfaces. In contrast, the uniform plane wave is written as $e^{-j\vec{k}\cdot\vec{r}}$ where the directions of $\vec{k}$ is given by $\theta_R + j\theta_I$ and $\phi_R + j\phi_I$ in the same spherical coordinate system. Requiring an equivalence imposes the following:

$$e^{-\vec{\gamma}\cdot\vec{r}} = e^{-j\vec{k}\cdot\vec{r}}$$

where:

$$\vec{\alpha} = \alpha(\sin\theta_\alpha\cos\phi_\alpha\hat{x} + \sin\theta_\alpha\sin\phi_\alpha\hat{y} + \cos\theta_\alpha\hat{z})$$

$$\vec{\beta} = \beta(\sin\theta_\beta\cos\phi_\beta\hat{x} + \sin\theta_\beta\sin\phi_\beta\hat{y} + \cos\theta_\beta\hat{z})$$

$$\vec{k} = k(\sin(\theta_R+j\theta_I)\cos(\phi_R+j\phi_I)\hat{x} + \sin(\theta_R+j\theta_I)\sin(\phi_R+j\phi_I)\hat{y} + \cos(\theta_R+j\theta_I)\hat{z})$$

For the equivalence to hold for any $\vec{r}$ requires that:

$$\alpha\sin\theta_\alpha\cos\phi_\alpha + j\beta\sin\theta_\beta\cos\phi_\beta = jk\sin(\theta_R + j\theta_I)\cos(\phi_R + j\phi_I)$$

$$\alpha\sin\theta_\alpha\sin\phi_\alpha + j\beta\sin\theta_\beta\sin\phi_\beta = jk\sin(\theta_R + j\theta_I)\sin(\phi_R + j\phi_I)$$

$$\alpha\cos\theta_\alpha + j\beta\cos\theta_\beta = jk\cos(\theta_R + j\theta_I)$$

Squaring the last three equations and summing the results produces $\vec{\gamma}\cdot\vec{\gamma} = -k^2$ but $\vec{\gamma}\cdot\vec{\gamma} = \gamma_o^2 = (\alpha_o + j\beta_o)^2$ hence $\gamma_o^2 = -k^2$ and thus $jk = \gamma_o = \alpha_o + j\beta_o$ where α_o and β_o are the intrinsic propagation constants of the medium. Hence, we have:

$$\alpha\sin\theta_\alpha\cos\phi_\alpha + j\beta\sin\theta_\beta\cos\phi_\beta = (\alpha_o + j\beta_o)\sin(\theta_R + j\theta_I)\cos(\phi_R + j\phi_I) \quad \text{(B.1)}$$

$$\alpha\sin\theta_\alpha\sin\phi_\alpha + j\beta\sin\theta_\beta\sin\phi_\beta = (\alpha_o + j\beta_o)\sin(\theta_R + j\theta_I)\sin(\phi_R + j\phi_I) \quad \text{(B.2)}$$

$$\alpha\cos\theta_\alpha + j\beta\cos\theta_\beta = (\alpha_o + j\beta_o)\cos(\theta_R + j\theta_I) \quad \text{(B.3)}$$

Dividing Equation (B.2) by Equation (B.1) produces:

$$\tan(\phi_R + j\phi_I) = \frac{\alpha\sin\theta_\alpha\sin\phi_\alpha + j\beta\sin\theta_\beta\sin\phi_\beta}{\alpha\sin\theta_\alpha\cos\phi_\alpha + j\beta\sin\theta_\beta\cos\phi_\beta}$$

Now the left hand side of the last equation gives:

$$\tan(\phi_R + j\phi_I) = \frac{\tan\phi_R + j\tanh\phi_I}{1 - j\tan\phi_R\tanh\phi_I}$$

Multiplying the numerator and denominator of the right hand side of the last two equations by the conjugate expression of their respective denominator, then carrying out some algebraic manipulations and equating real and imaginary parts on both sides of the resulting equation produces:

$$\frac{\sin\phi_R}{\cosh\phi_I}\frac{1}{\sqrt{\cos^2\phi_R + \sinh^2\phi_I}} = \frac{\alpha^2\sin^2\theta_\alpha\sin\phi_\alpha\cos\phi_\alpha + \beta^2\sin^2\theta_\beta\sin\phi_\beta\cos\phi_\beta}{\alpha^2\sin^2\theta_\alpha\cos^2\phi_\alpha + \beta^2\sin^2\theta_\beta\cos^2\phi_\beta} \equiv \frac{A}{D}$$

$$\text{(B.4)}$$

$$\frac{\sinh\phi_I}{\cos\phi_R}\frac{1}{\sqrt{\cos^2\phi_R + \sinh^2\phi_I}} = \frac{\alpha\beta\sin\theta_\alpha\sin\theta_\beta\sin(\phi_\beta - \phi_\alpha)}{\alpha^2\sin^2\theta_\alpha\cos^2\phi_\alpha + \beta^2\sin^2\theta_\beta\cos^2\phi_\beta} \equiv \frac{B}{D} \quad \text{(B.5)}$$

Hence:

$$\frac{D}{\sqrt{\cos^2\phi_R + \sinh^2\phi_I}} = A\frac{\cosh\phi_I}{\sin\phi_R} = B\frac{\cos\phi_R}{\sinh\phi_I}$$

from which one obtains:

$$\sinh(2\phi_I) = \frac{B}{A}\sin(2\phi_R) \qquad\qquad \text{(B.6)}$$

Squaring Equation (B.5) and carrying out some algebraic manipulations produces:

$$(D^2 - B^2\cos^2\phi_R)\sinh^2\phi_I = B^2\cos^4\phi_R \qquad \text{(B.7)}$$

Now using Equation (B.6) and the knowledge of:

$$2\cosh^2\phi_I - 1 = \cosh(2\phi_I) = \sqrt{1 + \sinh^2(2\phi_I)}$$

and

$$\sinh^2\phi_I = \cosh^2\phi_I - 1$$

to obtain an expression for $\sinh^2\phi_I$ to substitute in Equation (B.7), then collecting the terms of equal power in $\cos^2\phi_R$ produces the following cubic polynomial in the unknown $X = \cos^2\phi_R$:

$$4B^2(U_3X^3 + U_2X^2 + U_1X + U_0) = 0$$

where:

$$U_3 = -B^2(A^2 + B^2)$$
$$U_2 = B^2(A^2 + B^2 + 2D^2)$$
$$U_1 = -D^2(A^2 + 2B^2 + D^2)$$
$$U_0 = D^4$$

For $B \neq 0$, the solution for X can be obtained with MATLAB and is not reproduced here because of its length. Out of the three possible solutions for X, two are complex-valued and must be rejected. From the knowledge of X, one obtains the knowledge of ϕ_R, then substituting in Equation (B.7), one obtains the knowledge of ϕ_I. For $B = 0$, the solution is found simply from Equation (B.5) as $\phi_I = 0$ and then, from Equation (B.4) as $\phi_R = \arctan(\frac{A}{D})$.

For instance, when $B = 0$ due to $\phi_\alpha = \phi_\beta \equiv \phi$, we obtain $\frac{A}{D} = \tan\phi$ and thus, $\phi_R = \phi$ and $\phi_I = 0$, as expected.

Expanding Equation (B.3) and equating real and imaginary parts on both sides of the equation produces the following two equations:

$$\alpha\cos\theta_\alpha = \alpha_o\cos\theta_R\cosh\theta_I + \beta_o\sin\theta_R\sinh\theta_I \tag{B.8}$$

$$\beta\cos\theta_\beta = \beta_o\cos\theta_R\cosh\theta_I - \alpha_o\sin\theta_R\sinh\theta_I \tag{B.9}$$

Squaring Equations (B.8) and (B.9) and adding their results gives:

$$\cos^2\theta_R + \sinh^2\theta_I = \frac{\alpha^2\cos^2\theta_\alpha + \beta^2\cos^2\theta_\beta}{\alpha_o^2 + \beta_o^2} = C$$

from which one obtains:

$$\sinh^2\theta_I = C - \cos^2\theta_R \tag{B.10}$$

$$\cosh^2\theta_I = C + \sin^2\theta_R \tag{B.11}$$

Substituting these results in the square of Equation (B.8), carrying out simple algebraic maniputations and collecting the terms of equal power in $\cos\theta_R$ produces the following quartic polynomial in the unknown $Y = \cos\theta_R$:

$$V_4 Y^4 + V_3 Y^3 + V_2 Y^2 + V_1 Y + V_0 = 0$$

where:
$$V_4 = (\alpha_o^2 + \beta_o^2)^2$$
$$V_3 = -2(C + 1)V_4$$
$$V_2 = (C + 1)^2 V_4 + 2((\alpha_o^2 + \beta_o^2)\beta_o^2 C + (\alpha_o^2 - \beta_o^2)\alpha^2\cos^2\theta_\alpha)$$
$$V_1 = -2(C + 1)((\alpha_o^2 + \beta_o^2)\beta_o^2 C + (\alpha_o^2 - \beta_o^2)\alpha^2\cos^2\theta_\alpha)$$
$$V_0 = (\alpha^2\cos^2\theta_\alpha - \beta_o^2 C)^2$$

The solution for Y can be obtained with MATLAB and is not reproduced here because of its length. Out of the four possible solutions for Y, the third one given by MATLAB was usually (but not always) found to be the correct one. This passing of the correct solution from one root of the polynomial to another one makes the determination of Y ambiguous and is a drawback of the method. However, once Y has been correctly determined, one obtains the knowledge of θ_R, then substituting in Equation (B.10) or (B.11) one obtains the knowledge of θ_I.

Therefore the four variables θ_R, θ_I, ϕ_R and ϕ_I can be determined from the knowledge of α_o, β_o, α, β, θ_α, θ_β, ϕ_α and ϕ_β. We note, however, that the converse operation of finding out the values for θ_α, θ_β, ϕ_α and ϕ_β from the knowledge of α_o, β_o, θ_R, θ_I, ϕ_R and ϕ_I is not possible because the knowledge of $\cos(\rho) = \sin(\theta_\alpha)\sin(\theta_\beta)\cos(\phi_\alpha - \phi_\beta) + \cos(\theta_\alpha)\cos(\theta_\beta)$ is needed to compute α and β. One exception is the special case treated in Section 2.4.1 where $\rho = -\xi$ and thus, α and β are given by Equations (2.36) and (2.35), respectively. In this special case, $\psi = 0$ and thus, $\phi_I = 0$, $\phi_R = \phi_\alpha = \phi_\beta$, and the knowledge of θ_α and θ_β is obtained from Equations (B.8) and (B.9).

Appendix C

Comparison between Holmes's approach and our approach in computing the effective propagation constants

This appendix presents a comparison between Holmes's method and the method presented in Chapter 2 for computing the effective propagation constants of non-uniform plane waves at the planar interface of two isotropic homogeneous possibly lossy media of infinite transverse dimensions.

Holmes' expressions for computing β_2 and α_2 are [6, Equations (18-19)]:

$$\beta_2 = \sqrt{\frac{|\gamma_{1t}|^2 - \mathrm{Re}\left(\gamma_{o2}^2\right) + |\gamma_{1t}^2 - \gamma_{o2}^2|}{2}} \tag{C.1}$$

$$\alpha_2 = \sqrt{\frac{|\gamma_{1t}|^2 + \mathrm{Re}\left(\gamma_{o2}^2\right) + |\gamma_{1t}^2 - \gamma_{o2}^2|}{2}} \tag{C.2}$$

where $\gamma_{1t} = V + jW$ with $V = \alpha_1 \sin(\xi_1 + \rho_1)$ and $W = \beta_1 \sin(\xi_1)$.

Solving for ξ_2 from Equation (2.16) and the knowledge of β_2 leads to two possible solutions:

$$\xi_2 = \begin{cases} \arcsin\left(\frac{W}{\beta_2}\right) \\ \pi - \arcsin\left(\frac{W}{\beta_2}\right) \end{cases} \tag{C.3}$$

Solving for ρ_2 from Equation (2.15) and the knowledge of α_2 and the two possible solutions for ξ_2 leads to four possible solutions:

181

$$\rho_2 = \begin{cases} \arcsin\left(\frac{V}{\alpha_2}\right) - \arcsin\left(\frac{W}{\beta_2}\right) \\ \pi - \arcsin\left(\frac{V}{\alpha_2}\right) - \arcsin\left(\frac{W}{\beta_2}\right) \\ \arcsin\left(\frac{V}{\alpha_2}\right) + \arcsin\left(\frac{W}{\beta_2}\right) - \pi \\ -\arcsin\left(\frac{V}{\alpha_2}\right) + \arcsin\left(\frac{W}{\beta_2}\right) \end{cases} \qquad \text{(C.4)}$$

All computations in this appendix pertain to a case found in Reference [6], i.e. $f = 1$ MHz, $\varepsilon'_{r1} = 4.0$, $\sigma_1 = 0.01$ S/m, $\varepsilon'_{r2} = 10.0$ and $\sigma_2 = 0.001$ S/m. Figures C.1 and C.2 show the results of computing ρ_2 as per Equations (2.44) and (C.4) for the case $\rho_1 = 0°$, respectively. Note that the corresponding curve given by Holmes'method is, in fact, made up of two solutions joint at a cross-over value of $\xi_1 \approx 19°$:

$$\rho_2 = \begin{cases} \arcsin\left(\frac{V}{\alpha_2}\right) - \arcsin\left(\frac{W}{\beta_2}\right) & \text{for } \xi_1 < 19° \\ \pi - \arcsin\left(\frac{V}{\alpha_2}\right) - \arcsin\left(\frac{W}{\beta_2}\right) & \text{for } \xi_1 > 19° \end{cases}$$

In contrast, the solution given by the new procedure presented in Chapter 2 yields the entire curve for all values of ξ_1 in the range $0° \leq \xi_1 \leq 90°$. Figures C.3 and C.4 repeat the comparison for the case of $\rho_1 = +20°$. The cross-over value is now about $\xi_1 \approx 11°$. Figures C.5 and C.6 repeat the comparison for the case of $\rho_1 = -20°$. The cross-over value is now about $\xi_1 \approx 32°$ with the solution for $\xi_1 > 32°$ now being given by $\rho_2 = \left(\arcsin\left(\frac{V}{\alpha_2}\right) + \arcsin\left(\frac{W}{\beta_2}\right) - \pi\right)$. This passing of the correct solution from one possible solution to another one as ξ_1 varies makes Holmes' method difficult to use.

Figure C.1: The four possible solutions for ρ_2 as per the method presented in Chapter 2 as a function of the incidence angle ξ_1 for $\rho_1 = 0°$. The valid solution is given here by the solid line.

Figure C.2: The four possible solutions for ρ_2 as per Equation (C.4) as a function of the incidence angle ξ_1 for $\rho_1 = 0°$. Here, $\xi_I = \arcsin\left(\frac{W}{\beta_2}\right)$ and $\xi_{II} = \pi - \arcsin\left(\frac{W}{\beta_2}\right)$. The valid solution is given here by the solid line for $\xi_1 < 19°$ and the dash line for $\xi_1 > 19°$.
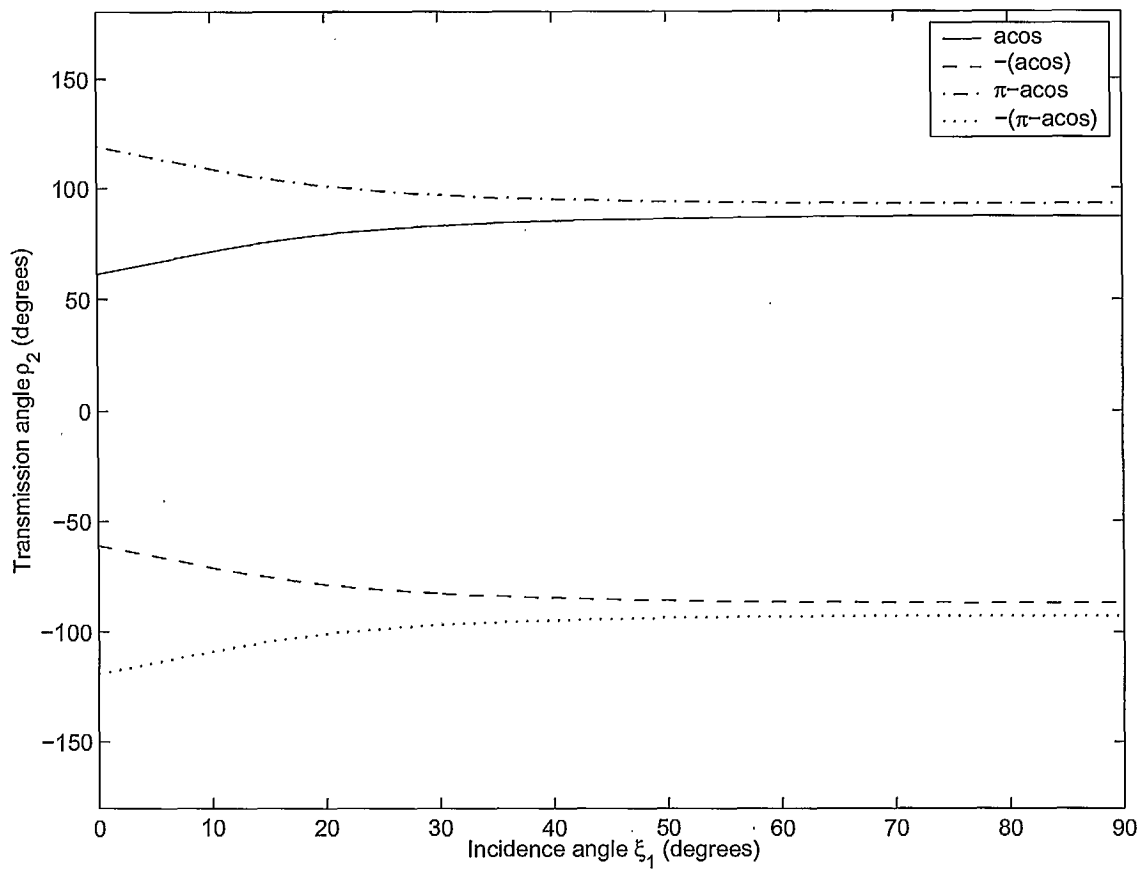
Figure C.3: The four possible solutions for ρ_2 as per the method presented in Chapter 2 as a function of the incidence angle ξ_1 for $\rho_1 = 20°$. The valid solution is given here by the solid line.
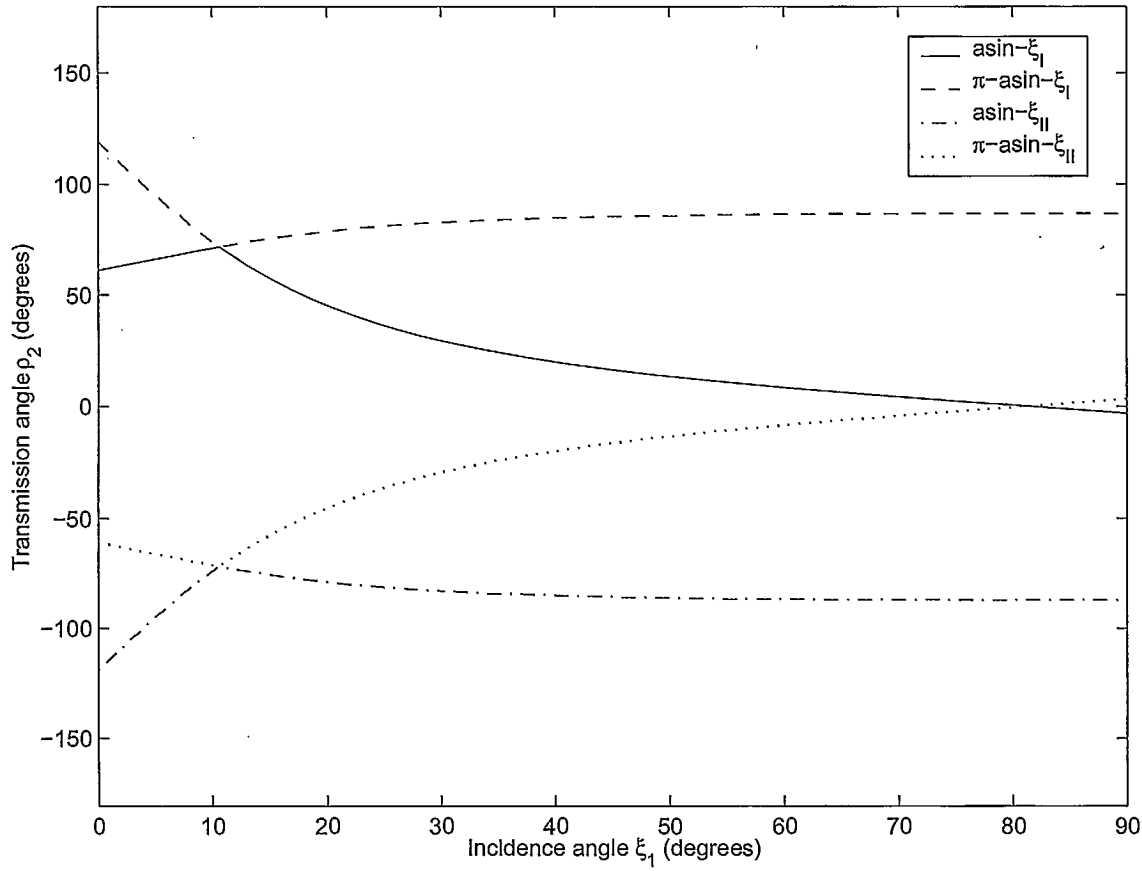
Figure C.4: The four possible solutions for ρ_2 as per Equation (C.4) as a function of the incidence angle ξ_1 for $\rho_1 = 20°$. Here, $\xi_I = \arcsin\left(\frac{W}{\beta_2}\right)$ and $\xi_{II} = \pi - \arcsin\left(\frac{W}{\beta_2}\right)$. The valid solution is given here by the solid line for $\xi_1 < 11°$ and the dash line for $\xi_1 > 11°$.
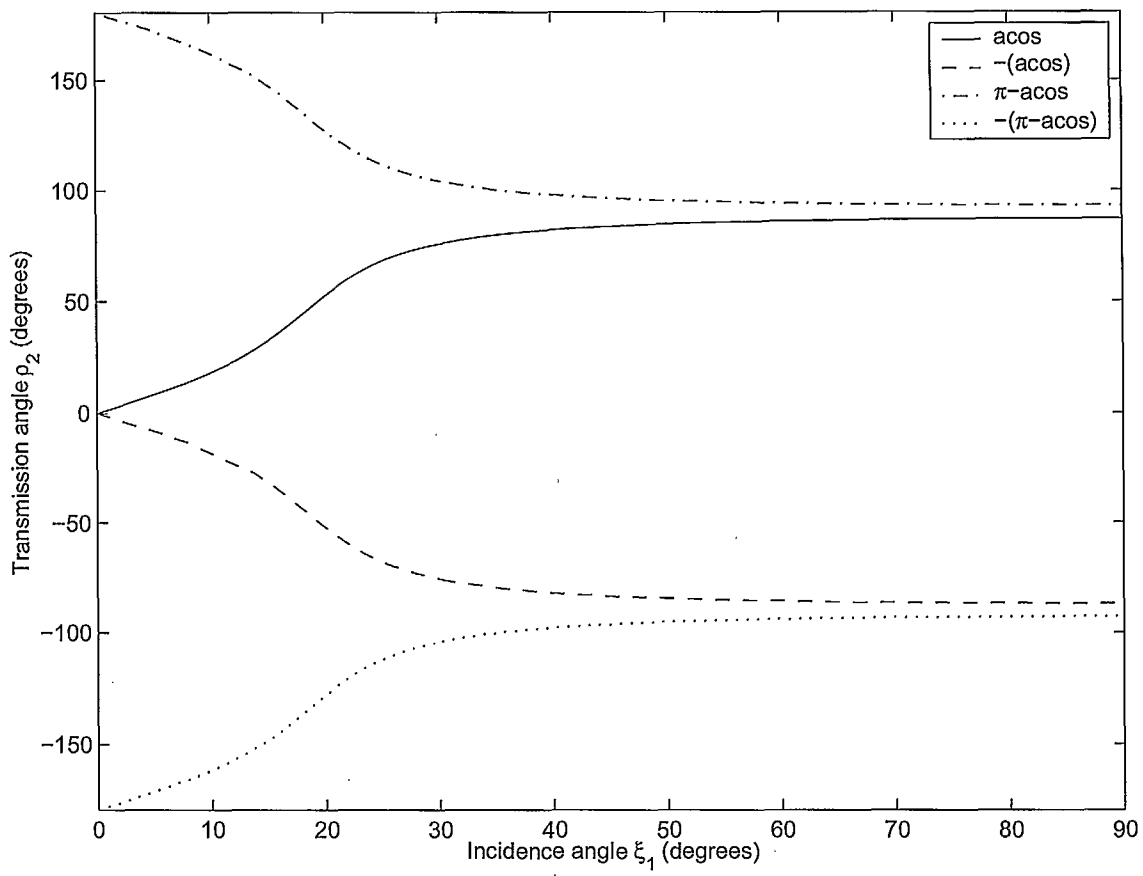
186
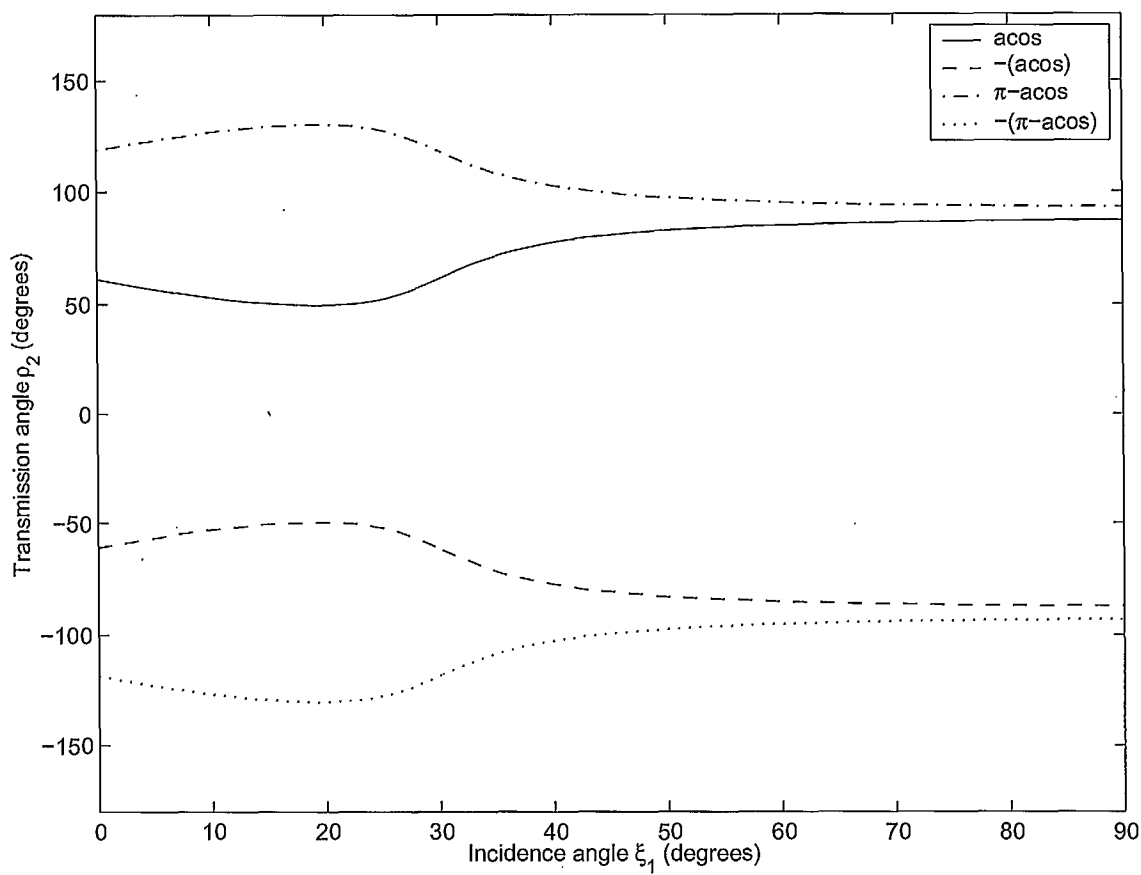
Figure C.5: The four possible solutions for ρ_2 as per the method presented in Chapter 2 as a function of the incidence angle ξ_1 for $\rho_1 = -20°$. The valid solution is given here by the dash line.
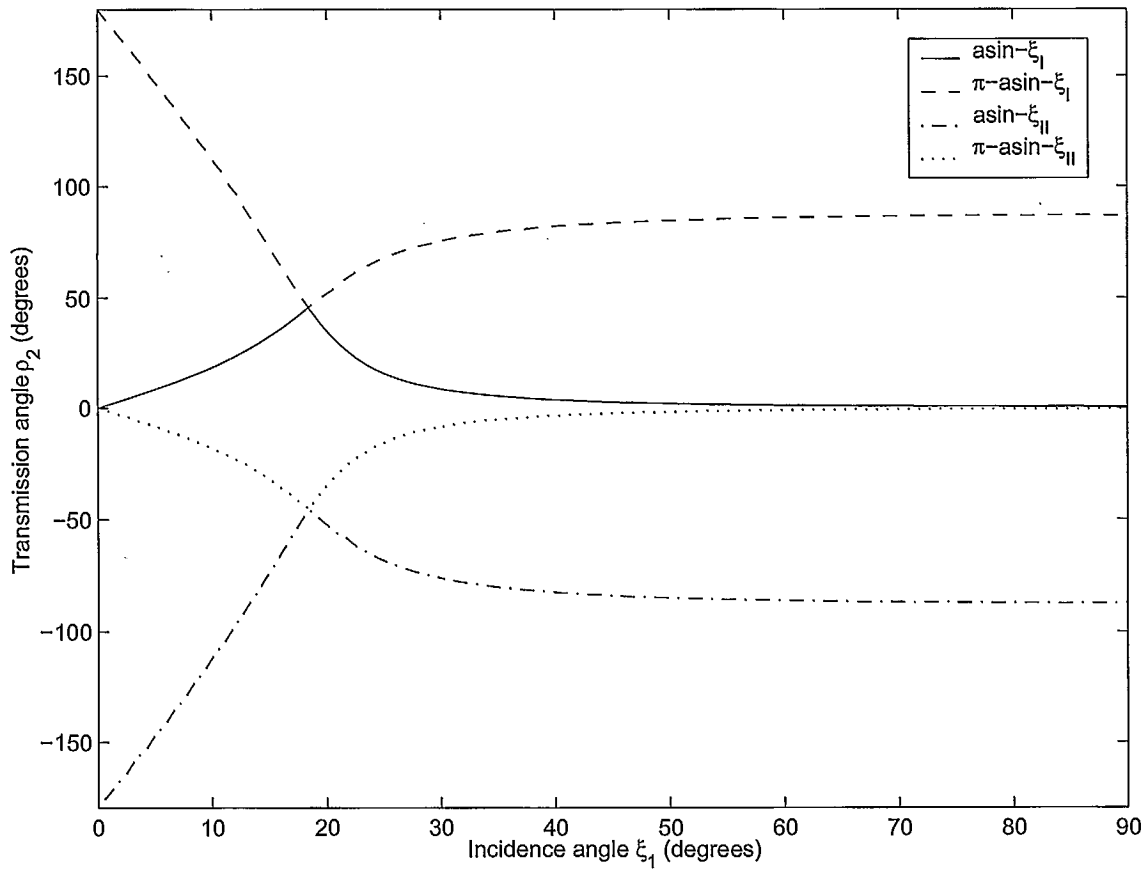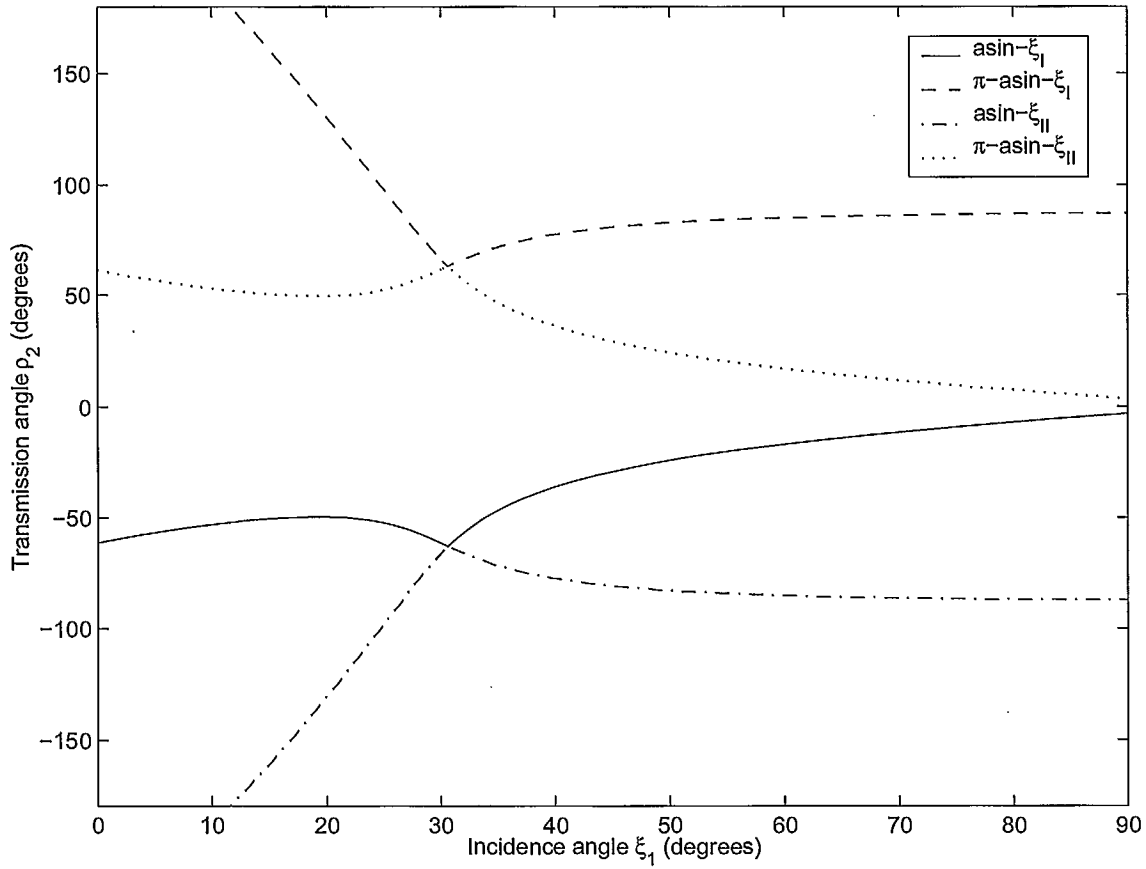
Figure C.6: The four possible solutions for ρ_2 as per Equation (C.4) as a function of the incidence angle ξ_1 for $\rho_1 = -20°$. Here, $\xi_I = \arcsin\left(\frac{W}{\beta_2}\right)$ and $\xi_{II} = \pi - \arcsin\left(\frac{W}{\beta_2}\right)$. The valid solution is given here by the solid line for $\xi_1 < 32°$ and the dash-dot line for $\xi_1 > 32°$.

Appendix D

Effective permittivity

D.1 Uniaxial media

Figure D.1 is a simplified reproduction of Figure 10.27 of Reference [49, p.361]. Throughout this section, it is assumed that the optic axis lies at an arbitrary θ_o value in the incidence plane, which is taken to be the xz plane in Figure D.1. Snell's law for the phase wavefront of the extraordinary wave is written from Equation (10.82) of the above Reference as:

$$\frac{\sin\theta_i}{\sin\theta_t} = \frac{c_i}{c_t} \tag{D.1}$$

where $c_i = 1/\sqrt{\mu_o\varepsilon^i}$ where $\varepsilon^i = \varepsilon_r^i\varepsilon_o$ is the permittivity of the incidence medium, i.e. the isotropic half-space. Equation (10.80) of the above Reference gives c_t as [75, p. 677]:

$$c_t^2 = c_1^2\cos^2\theta + c_3^2\sin^2\theta \tag{D.2}$$

where:

$$c_t = c_o/\sqrt{\varepsilon_r^{\parallel}} \tag{D.3}$$

$$c_1 = c_o/\sqrt{\varepsilon_r^{\text{trans}}} \tag{D.4}$$

$$c_3 = c_o/\sqrt{\varepsilon_r^{\text{long}}} \tag{D.5}$$

where $\varepsilon_r^{\parallel}$ is the effective relative permittivity that the extraordinary waves sees as it propagates through the uniaxial medium, $\theta = (\theta_t + \theta_o)$, $c_o = 1/\sqrt{\mu_o\varepsilon_o}$ and the super-indices "trans" and "long" refer to the directions perpendicular and parallel to the optic axis, respectively. Note that c_1 and c_3 become complex-valued when $\varepsilon_r^{\text{trans}}$ and $\varepsilon_r^{\text{long}}$ become complex-valued, respectively. Born and Wolf in Reference [75, p. 668] point out that c_1, c_2 and c_3 are not components of a vector and are defined only with reference to the three principal dielectric axes.

Pulling all these equations together and using the trigonometric identities $\cos^2\theta = (1 + \cos 2\theta)/2$ and $\sin^2\theta = (1 - \cos 2\theta)/2$ gives:

$$c_i^2\left(1 - \cos 2\theta_t\right) = \sin^2\theta_i\left[(c_1^2 + c_3^2) + (c_1^2 - c_3^2)\cos 2(\theta_t + \theta_o)\right] \tag{D.6}$$

Expanding $\cos 2(\theta_t + \theta_o)$ and regrouping the terms in θ_t leads to:

$$c_i^2 - (c_1^2 + c_3^2)\sin^2\theta_i = a\cos 2\theta_t - b\sin 2\theta_t \tag{D.7}$$

where:

$$a = c_i^2 + (c_1^2 - c_3^2)\sin^2\theta_i\cos 2\theta_o \tag{D.8}$$

$$b = (c_1^2 - c_3^2)\sin^2\theta_i\sin 2\theta_o \tag{D.9}$$

Using the identity:

$$a\cos x - b\sin x = -\sqrt{a^2 + b^2}\sin(x - \arctan a/b) \tag{D.10}$$

leads to:

$$\sin\left(2\theta_t - \arctan B\right) = \frac{\left[(c_1^2 + c_3^2)\sin^2\theta_i - c_i^2\right]}{\sqrt{D}} \tag{D.11}$$

where:

$$B = \frac{a}{b} = \frac{\left[(c_1^2 - c_3^2)\sin^2\theta_i + c_i^2\right] - 2(c_1^2 - c_3^2)\sin^2\theta_i\sin^2\theta_o}{(c_1^2 - c_3^2)\sin^2\theta_i\sin 2\theta_o} \tag{D.12}$$

$$D = a^2 + b^2 = \left[(c_1^2 - c_3^2)\sin^2\theta_i + c_i^2\right]^2 - 4c_i^2(c_1^2 - c_3^2)\sin^2\theta_i\sin^2\theta_o \tag{D.13}$$

Squaring both sides of Equation (D.11) and using the identity $\sin^2 x = (1 - \cos 2x)/2$ and some simple algebraic manipulations gives:

$$\theta_t = \frac{\arccos A}{4} + \frac{\arctan B}{2} \tag{D.14}$$

where:

$$A = 1 - 2\frac{\left[(c_1^2 + c_3^2)\sin^2\theta_i - c_i^2\right]^2}{D} \tag{D.15}$$

Note that θ_t becomes complex-valued when c_1 and c_3 become complex-valued. Substituting the result for θ_t of Equation (D.14) into Equation (D.1) and using the trigonometric[1] identities $\cos(x/2) = \sqrt{1 + \cos x}/\sqrt{2}$ and $\sin(x/2) = \sqrt{1 - \cos x}/\sqrt{2}$ and $\cos(\arctan x) = 1/\sqrt{1 + x^2}$ and $\sin(\arctan x) = x/\sqrt{1 + x^2}$ gives the effective relative permittivity for the extraordinary wave $\varepsilon_r^{\parallel}$ as:

$$\frac{\varepsilon_r^{\parallel}}{\varepsilon_r^i} \equiv \left(\frac{c_i}{c_t}\right)^2 = \frac{2\sin^2\theta_i}{1 - \sqrt{\frac{1+A}{2}}\frac{1}{\sqrt{1+B^2}} + \sqrt{\frac{1-A}{2}}\frac{B}{\sqrt{1+B^2}}} \tag{D.16}$$

Note that:

$$\frac{1}{\sqrt{1 + B^2}} = \frac{(c_1^2 - c_3^2)\sin^2\theta_i\sin 2\theta_o}{\sqrt{D}} \tag{D.17}$$

$$\frac{B}{\sqrt{1 + B^2}} = \frac{(c_1^2 - c_3^2)\sin^2\theta_i\cos 2\theta_o + c_i^2}{\sqrt{D}} \tag{D.18}$$

---

[1]These trigonometric identities need to be modified when the argument is complex-valued. Rigorously, the development presented here applies only to the case of lossless media so that θ_t be real-valued. However, the losses can be taken into account after treating the case of lossless uniaxial media as was done for Equation (4.7).

$$\sqrt{\frac{1+A}{2}} = \sqrt{2\frac{c_i^2\left[(c_1^2+c_3^2)+(c_1^2-c_3^2)\cos 2\theta_o\right]-2c_1^2c_3^2\sin^2\theta_i}{D}}\,\sin\theta_i \quad (D.19)$$

$$\sqrt{\frac{1-A}{2}} = \frac{(c_1^2+c_3^2)\sin^2\theta_i\cos 2\theta_o - c_i^2}{\sqrt{D}} \quad (D.20)$$

Therefore, the product of Equations (D.17) and (D.19) results in 0 whenever $\sin 2\theta_o = 0$. Note also that B tends to infinity whenever $\sin 2\theta_o = 0$ but $B/\sqrt{1+B^2} = +1$ when $\theta_o = 0$, and $B/\sqrt{1+B^2} = -1$ when $\theta_o = \pm 90°$. There results for $\theta_o = 0°$:

$$\frac{\varepsilon_r^{\parallel}}{\varepsilon_r^i} = \frac{(c_1^2-c_3^2)\sin^2\theta_i + c_i^2}{c_1^2} = \frac{\varepsilon_r^{\text{trans}}}{\varepsilon_r^i} + \left(1 - \frac{\varepsilon_r^{\text{trans}}}{\varepsilon_r^{\text{long}}}\right)\sin^2\theta_i \quad (D.21)$$

and for $\theta_o = \pm 90°$:

$$\frac{\varepsilon_r^{\parallel}}{\varepsilon_r^i} = \frac{(c_3^2-c_1^2)\sin^2\theta_i + c_i^2}{c_3^2} = \frac{\varepsilon_r^{\text{long}}}{\varepsilon_r^i} + \left(1 - \frac{\varepsilon_r^{\text{long}}}{\varepsilon_r^{\text{trans}}}\right)\sin^2\theta_i \quad (D.22)$$

When the incidence medium is free space, $\varepsilon_r^i = 1$ and thus, Equation (D.21) reduces to Equation (4.6). Note that both the transverse direction for $\theta_o = 0°$ and the longitudinal direction for $\theta_o = \pm 90°$ correspond to the same direction which is the direction that is both parallel to the interface and in the incidence plane. Similarly, both the longitudinal direction for $\theta_o = 0°$ and the transverse direction for $\theta_o = \pm 90°$ correspond to the same direction which is the direction perpendicular to the interface. Therefore, with respect to the x and z axes of Figure D.1, the effective relative permittivity for the extraordinary wave is given as:

$$\frac{\varepsilon_r^{\parallel}}{\varepsilon_r^i} = \frac{\varepsilon_{rx}}{\varepsilon_r^i} + \left(1 - \frac{\varepsilon_{rx}}{\varepsilon_{rz}}\right)\sin^2\theta_i \quad (D.23)$$

when[2] $\theta_o = 0°$ or $\theta_o = \pm 90°$. Such a coincidence between these two cases of θ_o is also pointed out in Reference [7, p. 251].

---

[2]Note: Equation (D.23) does not generalize to the case of an intermediate value of θ_o, i.e. $0° < \theta_o < 90°$. This can be seen by working out a numerical example for an intermediate value of θ_o in Equation (D.16).

For the TE^z polarization, the effective relative permittivity $\varepsilon_r^\perp = \varepsilon_{ry}$. In contrast, for the TM^z polarization, the effective relative permittivity $\varepsilon_r^\|$ is not, in general, the same as that which $\vec{D}$ sees "in the interface", i.e. ε_{rx}. Consequently, there results the surprising observation that different permittivities are used in the numerator and denominator of Equation (3.5) for the wave impedance Z_W in the transmission uniaxial medium. The permittivity in the denominator is that which appears in Equations (3.6), (3.7) (4.17), (4.21), i.e. ε_{rx}, whereas the numerator is computed from the effective relative permittivity $\varepsilon_r^\|$ given by Equation (D.23) or Equation (4.6).
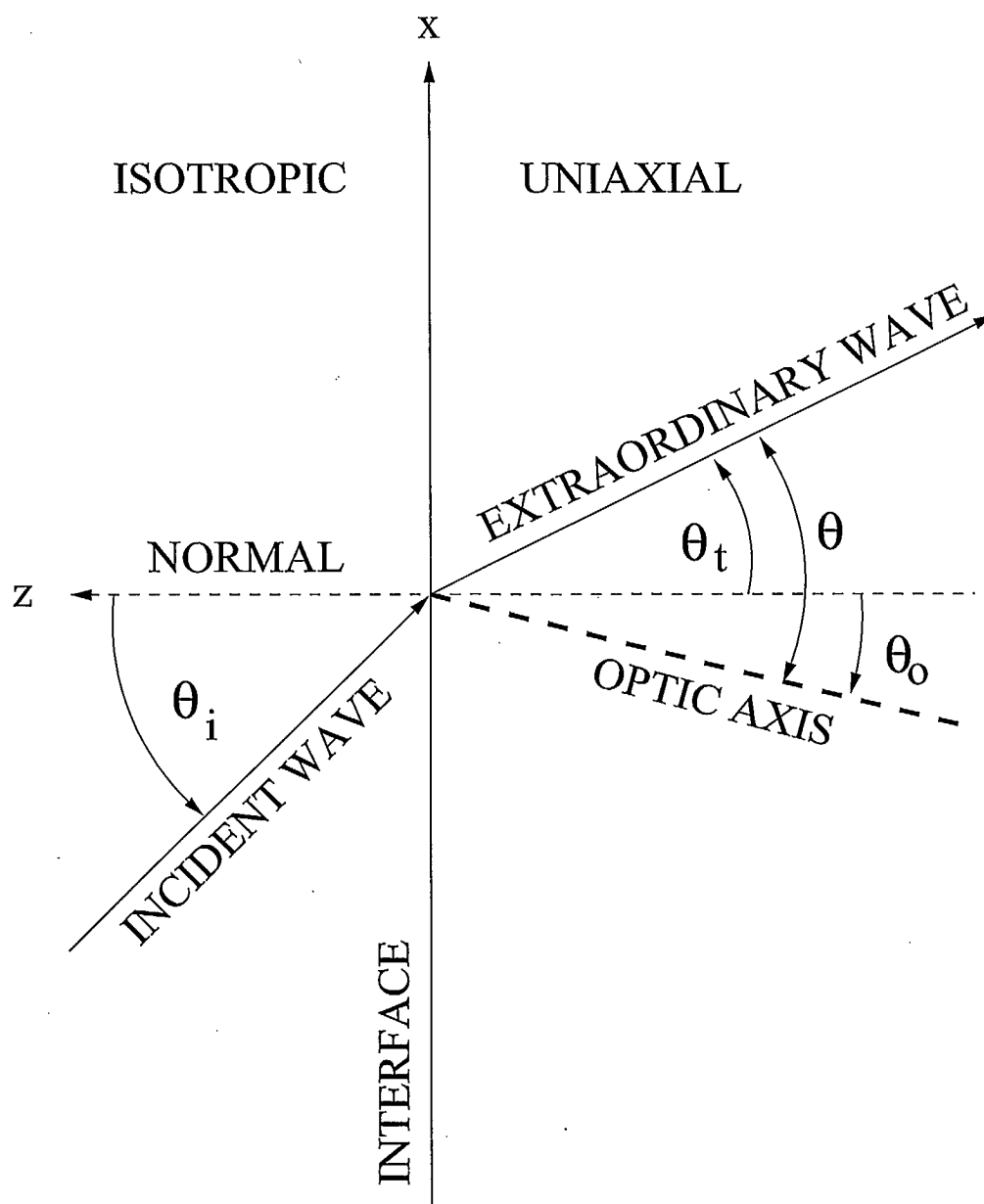
Figure D.1: Simplified reproduction of Figure 10.27 of Reference [49, p.361]. It depicts the wave phenomenon at the interface between an isotropic half-space on the left and a uniaxial half-space on the right. The optic axis lies in the incidence plane.

D.2 Generalization to biaxial media

Treating the general case of biaxial media is important for its own sake as well as for mitigating certain limitations. For instance, anisotropy can be readily handled by the FDTD method only if the three axes of anisotropy are aligned with the Yee lattice of the FDTD method. For another example, the uniaxial property is obtained in this report for the case of inclusions in the shape of circular cylinders; if the inclusions were to be elliptical cylinders instead of circular cylinders, the medium would become biaxial since the permittivity would not be the same in all transverse directions. For yet another example, suppose that the medium were uniaxial due to the inclusion of circular cylinders but the axes of the cylinders would be at an oblique angle with respect to the normal of the interface instead of being parallel to the normal of the interface. By discretizing the structure in thin layers parallel to the interface, the circular cylindrical inclusion would become elliptical inclusions in each layer. In the stacking process, the present analysis does not take into account how the dielectric material within each layer aligns from one layer to the next because each layer is modelled as a homogeneous layer (see Reference [66]). Each layer with the elliptical cylindrical inclusions could be shifted to reshape the circular cylindrical inclusions whose axes are oblique, into elliptical cylindrical inclusions whose axes would be normal to the interface. Hence, a uniaxial medium with oblique optic axis could be modeled as a biaxial medium whose three axes of anisotropy would be aligned with the Yee lattice, provided that one would know how to obtain the two transverse intrinsic permittivity values corresponding to elliptical inclusions. Being able to treat analytically the case of the uniaxial medium with oblique cylinders would allow to validate whether the choice of the two transverse (to the interfaces) permittivity values for elliptical cylindrical inclusions were correct in a FDTD simulation.

Figure D.2 shows the Cartesian coordinates (u, v, w) used to specify the direction of the three principal dielectric axes corresponding to ε_{ru}, ε_{rv} and ε_{rw} with the corresponding principal velocities c_u, c_v and c_w, and the Cartesian coordinates (x, y, z) used to specify the interface and the refraction angle θ_t in the transmission medium. The orientation of the uvw coordinate system is known in the xyz coordinate system in terms of the angles θ_w, ϕ_w and ϕ_u. We assume here that the principal axes for the permittivity coincide with the principal axes for the conductivity.

Equation (D.2) is generalized for propagation in a biaxial medium as (see Reference [84, p. 341]):

$$c_t^2 = c_u^2 \left(\underbrace{\hat{D}_t \cdot \hat{u}}_{\cos \delta_u} \right)^2 + c_v^2 \left(\underbrace{\hat{D}_t \cdot \hat{v}}_{\cos \delta_v} \right)^2 + c_w^2 \left(\underbrace{\hat{D}_t \cdot \hat{w}}_{\cos \delta_w} \right)^2 \qquad (D.24)$$

where:

$$c_t = c_o / \sqrt{\varepsilon_r^{\parallel}} \qquad (D.25)$$

$$c_l = c_o / \sqrt{\varepsilon_r^l} \qquad (D.26)$$

where $l = \{u, v, w\}$, and $c_o = 1/\sqrt{\mu_o \varepsilon_o}$ and $(\delta_u, \delta_v, \delta_w)$ are the direction angles for $\vec{D}_t$ in the uvw coordinate system. Also $\varepsilon_r^{\parallel}$ is the effective relative permittivity that the eigenwave sees as it propagates through the biaxial medium. Note that c_l becomes complex-valued when ε_r^l becomes complex-valued. Note carefully that c_u is the intrinsic velocity when the polarization vector $\vec{D}$ points in the $\hat{u}$ direction, and similarly for c_v and c_w. Consequently, $\gamma_l \neq j\omega\sqrt{\mu_o \varepsilon_l}$ where γ_l is the value of γ when the phase wavefront propagation vector $\vec{\beta}$ points in the $\hat{l}$ direction.

From spherical trigonometry, we have:

$$\cos \delta_u = \sin \theta_u \sin \theta_D \cos (\phi_u - \phi_D) + \cos \theta_u \cos \theta_D \qquad (D.27)$$

$$\cos \delta_v = \sin \theta_v \sin \theta_D \cos (\phi_v - \phi_D) + \cos \theta_v \cos \theta_D \qquad (D.28)$$

$$\cos \delta_w = \sin \theta_w \sin \theta_D \cos (\phi_w - \phi_D) + \cos \theta_w \cos \theta_D \qquad (D.29)$$

where θ_D and ϕ_D are the spherical coordinate angles for $\vec{D}$ in the xyz coordinate system. When the medium is uniaxial with its optic axis $\hat{w}$ lying in the xz incidence plane (i.e. $\hat{v} = -\hat{y}$) on one side of the z axis while $\vec{k}_t \equiv j\vec{\beta}_t$ lies on the opposite side as shown in Figure D.1, we have $\phi_u = 0°$, $\phi_v = 270°$, $\phi_w = 180°$, $\theta_u = 90° + \theta_o$, $\theta_v = 90°$, $\theta_w = 180° - \theta_o$.

Now if the polarization of the wave propagating in the uniaxial medium is such that its $\vec{D}$ field lies in the incidence xz plane, i.e. $D_y = 0$, then the propagating wave is the extraordinary wave and we have $\phi_D = 0°$, and $\theta_D = \theta_t - 90° = (180° - \theta_t') - 90° = 90° - \theta_t'$ where θ_t' corresponds to θ_t in Figure D.1, and we obtain:

196

$$\cos \delta_u = \cos \theta_o \cos \theta'_t - \sin \theta_o \sin \theta'_t = \cos \left(\theta'_t + \theta_o \right)$$

$$\cos \delta_v = 0$$

$$\cos \delta_w = - \sin \theta_o \cos \theta'_t - \cos \theta_o \sin \theta'_t = - \sin \left(\theta'_t + \theta_o \right)$$

and Equation (D.24) reduces to Equation (D.2). If the polarization is changed such that $\hat{D} = \hat{y}$, then the propagating wave is the ordinary wave and we have $\phi_D = 90°$, and $\theta_D = 90°$ and we obtain:

$$\cos \delta_u = 0$$

$$\cos \delta_v = -1$$

$$\cos \delta_w = 0$$

and thus, Equation (D.24) reduces to $c_t = c_2$ and since the medium is uniaxial with the optic axis along $\hat{w}$, then $c_1 = c_2$ and thus $c_t = c_1 = c_2$ as expected. For the general case where the uvw coordinate system is arbitrarily oriented with respect to the xyz coordinate system, we obtain from coordinate transformation:

$$\sin \theta_u = \pm \frac{\cos \theta_w}{D} \tag{D.30}$$

$$\cos \theta_u = \pm \frac{\sin \theta_w \cos \left(\phi_u - \phi_w \right)}{D} \tag{D.31}$$

$$\sin \theta_v = \pm \frac{E}{D} \tag{D.32}$$

$$\cos \theta_v = \pm \frac{\sin \left(2\theta_w \right) \sin \left(\phi_u - \phi_w \right)}{2D} \tag{D.33}$$

197

$$\sin \phi_v = \pm \frac{\cos^2 \theta_w \cos \phi_u + \sin^2 \theta_w \cos \phi_w \cos (\phi_u - \phi_w)}{E} \qquad (D.34)$$

$$\cos \phi_v = \pm \frac{\cos^2 \theta_w \sin \phi_u + \sin^2 \theta_w \sin \phi_w \cos (\phi_u - \phi_w)}{E} \qquad (D.35)$$

$$D = \sqrt{1 - \sin^2 \theta_w \sin^2 (\phi_u - \phi_w)} \qquad (D.36)$$

$$E = \sqrt{1 - (1 - \cos^4 \theta_w) \sin^2 (\phi_u - \phi_w)} \qquad (D.37)$$

For the above case with $\phi_u = 0°$, $\phi_v = 270°$, $\phi_w = 180°$, $\theta_u = 90° + \theta_o$, $\theta_v = 90°$, $\theta_w = 180° - \theta_o$, we obtain $D = 1$, $E = 1$ and:

$$\sin \theta_u = \pm(-\cos \theta_o) \Longrightarrow \cos \theta_o \quad \text{for the lower sign}$$

$$\cos \theta_u = \pm(-\sin \theta_o) \Longrightarrow -\sin \theta_o \quad \text{for the upper sign}$$

$$\sin \theta_v = \pm 1 \Longrightarrow +1 \quad \text{for the upper sign}$$

$$\cos \theta_v = 0 \Longrightarrow \quad \text{still ambiguous}$$

$$\sin \phi_v = \pm 1 \Longrightarrow -1 \quad \text{for the lower sign}$$

$$\cos \phi_v = 0 \Longrightarrow \quad \text{still ambiguous}$$

For the case where the uvw system is rotated by 90° about the $\hat{w}$ axis such that $\hat{u}$ and $\hat{v}$ become $\hat{v}$ and $-\hat{u}$, respectively, we obtain $\phi_u = 270°$, $\phi_v = 180°$, $\phi_w = 180°$, $\theta_u = 90°$, $\theta_v = \theta_o - 90°$, $\theta_w = 180° - \theta_o$, $D = \cos \theta_o$, $E = \cos^2 \theta_o$ and:

$$\sin \theta_u = \pm(-1) \Longrightarrow +1 \quad \text{for the lower sign}$$

$$\cos\theta_u = 0$$

$$\sin\theta_v = \pm(\cos\theta_o) \implies -\cos\theta_o \quad \text{for the lower sign}$$

$$\cos\theta_v = \pm(-\sin\theta_o) \implies \sin\theta_o \quad \text{for the lower sign}$$

$$\sin\phi_v = 0$$

$$\cos\phi_v = \pm(-1) \implies -1 \quad \text{for the upper sign}$$

Comparing the choice of signs for these two known examples shows that the correct choice can vary whenever any one of the three axes changes octan. There are too many cases to identify the correct choice of signs for them all here but suffice to say that the sign ambiguity can be resolved for any orientation of the uvw axes by solving the three simpler neighbouring cases where two of the uvw axes lie in a plane of the xyz system.

From Equations (D.1) and (D.24), we obtain:

$$c_t^2 = \left(\frac{c_i}{\sin\theta_i}\right)^2 \sin^2\theta_t = c_u^2\cos^2\delta_u + c_v^2\cos^2\delta_v + c_w^2\cos^2\delta_w \qquad \text{(D.38)}$$

Now, squaring Equations (D.27-D.29) and using $l = \{u, v, w\}$, we obtain:

$$
\begin{aligned}
\cos^2\delta_l =\ & \left[1 - \sin^2\theta_l\sin^2(\phi_l - \phi_D)\right] \\
& + \left[\cos 2\theta_l + \sin^2\theta_l\sin^2(\phi_l - \phi_D)\right]\cos 2\theta_D \\
& + \left[0.5\sin 2\theta_l\cos(\phi_l - \phi_D)\right]\sin 2\theta_D
\end{aligned}
$$

Substituting this last equation into Equation (D.38) produces:

$$
\begin{aligned}
\left(\frac{c_i}{\sin\theta_i}\right)^2\sin^2\theta_t =\ & \left[\sum c_l^2 - \sum c_l^2\sin^2\theta_l\sin^2(\phi_l - \phi_D)\right] \\
& + \left[\sum c_l^2\left(\cos 2\theta_l + \sin^2\theta_l\sin^2(\phi_l - \phi_D)\right)\right]\cos 2\theta_D \\
& + \left[0.5\sum c_l^2\sin 2\theta_l\cos(\phi_l - \phi_D)\right]\sin 2\theta_D
\end{aligned}
$$
$$\text{(D.39)}$$

where, for convenience, the summation index is understood to be $l = \{u, v, w\}$. From geometry[3] and Figure D.3, we have:

$$\phi_D = \phi_t + 90° - \xi \tag{D.40}$$

and:

$$\xi = \arctan\left(\cos\theta_t \tan\zeta\right) \tag{D.41}$$

where the polarization angle ζ determines the polarization of the transmitted wave. This real-valued angle is measured positive from the axis $+\hat{\phi}_t$ in the winding direction toward the axis $+\hat{\theta}_t$ through a 90° rotation while looking into the $+\hat{\beta}_t$ direction. The angle ζ ranges from 0° to 360°. For $\zeta = 0°$, $\hat{D} = +\hat{y} = +\hat{\phi}_t$, and for $\zeta = 180°$, $\hat{D} = -\hat{y} = -\hat{\phi}_t$, and the wave is an ordinary wave. For $\zeta = 90°$, $\hat{D} = +\hat{\theta}_t$, and for $\zeta = 270°$, $\hat{D} = -\hat{\theta}_t$, and the wave is an extraordinary wave.

Note that from Snell's law of refraction for the phase wavefront (see Equation (2.23)[4]), we have $\phi_t = \phi_i$ if $\vec{k}_i$ is given in the outwards convention[5].

Hence, we obtain:

$$\cos\phi_D = \frac{\cos\theta_t \tan\zeta \cos\phi_t - \sin\phi_t}{\sqrt{1 + \cos^2\theta_t \tan^2\zeta}} \tag{D.42}$$

$$\sin\phi_D = \frac{\cos\theta_t \tan\zeta \sin\phi_t + \cos\phi_t}{\sqrt{1 + \cos^2\theta_t \tan^2\zeta}} \tag{D.43}$$

$$\sin 2\phi_D = \frac{2\cos\theta_t \tan\zeta \cos 2\phi_t - \sin 2\phi_t \left(1 - \cos^2\theta_t \tan^2\zeta\right)}{1 + \cos^2\theta_t \tan^2\zeta} \tag{D.44}$$

$$\cos 2\phi_D = -\frac{2\cos\theta_t \tan\zeta \sin 2\phi_t + \cos 2\phi_t \left(1 - \cos^2\theta_t \tan^2\zeta\right)}{1 + \cos^2\theta_t \tan^2\zeta} \tag{D.45}$$

---

[3]J.E. Roy,"Generalization of the Ludwig-3 Definition for Linear Copolarization and Cross Polarization", i*IEEE Trans. Antennas Propagat.*, Vol. AP-49, No. 6, June 2001, pp. 1006-1010.

[4]Note that ξ in Equation (2.23) does not mean the same thing as ξ in Equation (D.41).

[5]In the outwards convention, the spherical coordinate angles θ_i and ϕ_i that specify the direction of $\vec{k}_i$ are those for $\vec{k}_i$ pointing outwards from the origin of the xyz coordinate system.

$$\sin^2\left(\phi_l - \phi_D\right) = \frac{\left(\cos\theta_t \tan\zeta \sin\left(\phi_l - \phi_t\right) - \cos\left(\phi_l - \phi_t\right)\right)^2}{1 + \cos^2\theta_t \tan^2\zeta} \qquad (D.46)$$

$$\cos\left(\phi_l - \phi_D\right) = \frac{\cos\theta_t \tan\zeta \cos\left(\phi_l - \phi_t\right) + \sin\left(\phi_l - \phi_t\right)}{\sqrt{1 + \cos^2\theta_t \tan^2\zeta}} \qquad (D.47)$$

From spherical trigonometry, we have:

$$\cos\zeta = \sin\theta_D \cos\xi \qquad (D.48)$$

Substituting Equation (D.41) and rearranging, we obtain:

$$\cos 2\theta_D = 1 - 2\left(1 + \cos^2\theta_t \tan^2\zeta\right)\cos^2\zeta \qquad (D.49)$$

$$\sin 2\theta_D = \left(\sqrt{1 + \cos^2\theta_t \tan^2\zeta}\right)\sin 2\zeta \sin\theta_t \qquad (D.50)$$

Substituting Equations (D.42-D.50) into the expanded version of Equation (D.39) and regrouping terms in θ_t produces:

$$
\begin{aligned}
0 = & \underbrace{\left[\left(\sum c_l^2 \left(1 - \sin^2\theta_l \cos^2\left(\phi_l - \phi_t\right) - \cos 2\zeta \left(\cos^2\theta_l - \sin^2\theta_l \sin^2\left(\phi_l - \phi_t\right)\right)\right)\right) - \left(\frac{c_i}{\sin\theta_i}\right)^2\right]}_{E} \\
& + \underbrace{\left[\left(\cos 2\zeta - 1\right)\left(\sum c_l^2 \left(\cos^2\theta_l - \sin^2\theta_l \cos^2\left(\phi_l - \phi_t\right)\right)\right) + \left(\frac{c_i}{\sin\theta_i}\right)^2\right]}_{D}\cos^2\theta_t \\
& + \underbrace{\left[\left(-\sin 2\zeta\right)\sum c_l^2 \left(\sin^2\theta_l\right)\sin 2(\phi_l - \phi_t)\right]}_{B}\cos\theta_t \\
& + \underbrace{\left[\left(0.5\sin 2\zeta\right)\sum c_l^2 \left(\sin 2\theta_l\right)\sin\left(\phi_l - \phi_t\right)\right]}_{A}\sin\theta_t \\
& + \underbrace{\left[0.5\left(\cos 2\zeta + 1\right)\sum c_l^2 \left(\sin 2\theta_l\right)\cos\left(\phi_l - \phi_t\right)\right]}_{C}\sin\theta_t \cos\theta_t
\end{aligned}
$$
$$(D.51)$$

where A, B, C, D, E and θ_t are complex-valued. Note that the ambiguity of Equations (D.30-D.35) affect terms A, B, and C. The corresponding generic equation is:

$$(A_1+jB_1)\sin Q+(A_2+jB_2)\cos Q+(A_3+jB_3)\sin Q\cos Q+(A_4+jB_4)\cos^2 Q+(A_5+jB_5)=0$$
$$(D.52)$$

where $Q=(\alpha+j\beta)$ and all other variables A_1, B_1, A_2, B_2, A_3, B_3, A_4, B_4, A_5, B_5, α, β are real-valued. The solution of this equation is obtained as follows. The trigonometric functions are exressed in terms of the exponentials $e^{j\alpha}$ and e^{β} by using Euler's identities. There results:

$$\cos(\alpha+j\beta)=\frac{1}{2}\left(e^{j(\alpha+j\beta)}+e^{-j(\alpha+j\beta)}\right)=\frac{1}{2}\left(\frac{e^{2\alpha}+e^{2\beta}}{e^{j\alpha}e^{\beta}}\right) \qquad (D.53)$$

$$\sin(\alpha+j\beta)=\frac{-j}{2}\left(e^{j(\alpha+j\beta)}-e^{-j(\alpha+j\beta)}\right)=\frac{-j}{2}\left(\frac{e^{2\alpha}-e^{2\beta}}{e^{j\alpha}e^{\beta}}\right) \qquad (D.54)$$

Substituting Equations (D.53-D.54) into Equation (D.52) and collecting the terms of equal power of e^{β} gives the following quartic polynomial in the parameter e^{β} with complex-valued coefficients:

$$(a_4+jb_4)e^{4\beta}+(a_3+jb_3)e^{3\beta}+(a_2+jb_2)e^{2\beta}+(a_1+jb_1)e^{\beta}+(a_0+jb_0)=0 \quad (D.55)$$

where:

$$a_4+jb_4=(A_4-B_3)+j(B_4+A_3)$$

$$a_3+jb_3=2e^{j\alpha}[(A_2-B_1))+j(B_2+A_1)]$$

$$a_2+jb_2=2e^{j2\alpha}(A_4+jB_4)$$

$$a_1+jb_1=\left[2e^{j3\alpha}(A_2+B_1)+4e^{j\alpha}A_5\right]+j\left[2e^{j3\alpha}(B_2-A_1)+4e^{j\alpha}B_5\right]$$

$$a_0+jb_o=e^{j4\alpha}[(A_4+B_3)+j(B_4-A_3)]$$

Splitting this complex-valued equation into its real and imaginary parts gives two real-valued equations to be solved simultaneously:

$$a_4 e^{4\beta} + a_3 e^{3\beta} + a_2 e^{2\beta} + a_1 e^{\beta} + a_0 = 0 \qquad (D.56)$$

where:

$$a_4 = A_4 - B_3$$

$$a_3 = 2\left[(A_2 - B_1)\cos\alpha - (B_2 + A_1)\sin\alpha\right]$$

$$a_2 = 2\left[A_4 \cos 2\alpha - B_4 \sin 2\alpha\right]$$

$$a_1 = 2\left[(A_2 + B_1)\cos 3\alpha + (A_1 - B_2)\sin 3\alpha + 2A_5 \cos\alpha - 2B_5 \sin\alpha\right]$$

$$a_0 = \left[(A_4 + B_3)\cos 4\alpha + (A_3 - B_4)\sin 4\alpha\right]$$

and:

$$b_4 e^{4\beta} + b_3 e^{3\beta} + b_2 e^{2\beta} + b_1 e^{\beta} + b_0 = 0 \qquad (D.57)$$

where:

$$b_4 = B_4 + A_3$$

$$b_3 = 2\left[(A_1 + B_2)\cos\alpha + (A_2 - B_1)\sin\alpha\right]$$

$$b_2 = 2\left[B_4 \cos 2\alpha + A_4 \sin 2\alpha\right]$$

$$b_1 = 2\left[(B_2 - A_1)\cos 3\alpha + (B_1 + A_2)\sin 3\alpha + 2B_5 \cos\alpha + 2A_5 \sin\alpha\right]$$

$$b_0 = [(B_4 - A_3) \cdot \cos 4\alpha + (B_3 + A_4) \sin 4\alpha]$$

Using once more Equations (D.53) and (D.54) with $\beta = 0$ and adjusting all terms to an equal denominator and getting rid of this denominator by moving it to the Right-Hand-Side of the equality sign transforms the quartic polynomial in the parameter e^β of Equation (D.56) into:

$$X_4 e^{4\beta} + X_3 e^{3\beta} + X_2 e^{2\beta} + X_1 e^\beta + X_0 = 0 \qquad (D.58)$$

where:

$$X_4 = 16 e^{j4\alpha} (A_4 - B_3)$$

$$X_3 = 16 e^{j5\alpha} [(A_2 - B_1) + j(A_1 + B_2)] + 16 e^{j3\alpha} [(A_2 - B_1) - j(A_1 + B_2)]$$

$$X_2 = 8 e^{j6\alpha} [(A_4 + B_4)] + 16 e^{j4\alpha} [A_4 - B_4] + 8 e^{j2\alpha} [A_4 + B_4]$$

$$
\begin{aligned}
X_1 = \ & 4 e^{j7\alpha} [(A_2 + B_1) + j(A_1 - B_2)] \\
& + 4 e^{j5\alpha} [(3(B_1 + A_2) + 8A_5) - j(3(A_1 - B_2) - 8B_5)] \\
& + 4 e^{j3\alpha} [(3(B_1 + A_2) + 8A_5) + j(3(A_1 - B_2) - 8B_5)] \\
& + 4 e^{j\alpha} [(B_1 + A_2) - j(A_1 - B_2)]
\end{aligned}
$$

$$
\begin{aligned}
X_0 = \ & e^{j8\alpha} [B_3 + A_4 + A_3 - B_4] + e^{j6\alpha} [4(B_3 + A_4 - A_3 + B_4)] \\
& + e^{j4\alpha} [6(B_3 + A_4 + A_3 - B_4)] + e^{j2\alpha} [4(B_3 + A_4 - A_3 + B_4)] \\
& + [B_3 + A_4 + A_3 - B_4]
\end{aligned}
$$

and the quartic polynomial in the parameter e^β of Equation (D.57) into:

$$Y_4 e^{4\beta} + Y_3 e^{3\beta} + Y_2 e^{2\beta} + Y_1 e^\beta + Y_0 = 0 \qquad (D.59)$$

where:

$$Y_4 = 16 e^{j4\alpha} (B_4 + A_3)$$

204

$$Y_3 = 16e^{j5\alpha}\left[(A_1 + B_2) - j(A_2 - B_1)\right] + 16e^{j3\alpha}\left[(A_1 + B_2) + j(A_2 - B_1)\right]$$

$$Y_2 = 8e^{j6\alpha}\left[(B_4 - A_4)\right] + 16e^{j4\alpha}\left[B_4 + A_4\right] + 8e^{j2\alpha}\left[B_4 - A_4\right]$$

$$\begin{aligned}
Y_1 = \ & 4e^{j7\alpha}\left[(B_2 - A_1) + j(B_1 + A_2)\right] \\
& +4e^{j5\alpha}\left[(3(B_2 - A_1) + 8B_5) - j(3(B_1 + A_2) + 8A_5)\right] \\
& +4e^{j3\alpha}\left[(3(B_2 - A_1) + 8B_5) + j(3(B_1 + A_2) + 8A_5)\right] \\
& +4e^{j\alpha}\left[(B_2 - A_1) - j(B_1 + A_2)\right]
\end{aligned}$$

$$\begin{aligned}
Y_0 = \ & e^{j8\alpha}\left[B_4 - A_3 + B_3 + A_4\right] + e^{j6\alpha}\left[4(B_4 - A_3 - B_3 - A_4)\right] \\
& +e^{j4\alpha}\left[6(B_4 - A_3 + B_3 + A_4)\right] + e^{j2\alpha}\left[4(B_4 - A_3 - B_3 - A_4)\right] \\
& +\left[B_4 - A_3 + B_3 + A_4\right]
\end{aligned}$$

Since the same real-valued solution for e^β must satisfy simultaneously both polynomials of the fourth degree in the parameter e^β of Equations (D.58) and (D.59), the two sets of four possible solutions for both polynomials are equated[6] among themselves, resulting in 16 functions of various powers (including fractional powers) in the parameter $e^{j\alpha}$. Although the correct solution for e^β is real-valued, not all 16 functions are necessarily real-valued because some of the false solutions for e^β might be complex-valued. Furthermore, the presence of fractional powers makes it impossible to write the functions in a clean polynomial form where the terms of equal powers of $e^{j\alpha}$ are collected. In any case, the degree of the polynomial is larger than 4 and thus, the solution for each function must be solved numerically using a root-searching algorithm, e.g. the subroutine ZANLY[7] of the IMSL Fortran library. The possible solutions for $e^{j\alpha}$ are then substituted into the quartic polynomial of Equation (D.58) or (D.59) to obtain the possible solutions for e^β. Once the correct value of e^β and the correct value of $e^{j\alpha}$ are identified, the value of $\sin\theta_t$ can be computed from Equation (D.54) and substituted into Equation (D.1) to find the value of the effective permittivity $\varepsilon_r^{\text{eff}}$ as:

---

[6]Simply creating a single equation by adding or subtracting (and more generally, taking a linear combination of) the two Equations (D.58) and (D.59) is not satisfactory because for the equality to hold for any and all linear combinations would require either that the solution be the trivial solution, i.e. each coefficient is zero-valued regardless of the value of e^β, or the solution has β tending to $-\infty$ so that e^β tends to zero.

[7]ZANLY could be used to solve directly Equation (D.52) since ZANLY can handle a complex function of a complex variable. However, it was felt that more accurate results might be obtained by solving the problem analytically as much as possible. In our solution approach, only $e^{j\alpha}$ is determined by numerical means whereas e^β is determined from the exact solution of a quartic polynomial.

$$\frac{\varepsilon_r{}^{\text{eff}}}{\varepsilon_r^i} \equiv \left(\frac{c_i}{c_t}\right)^2 = \left(\frac{\sin\theta_i}{\sin\theta_t}\right)^2. \tag{D.60}$$

Note that up to this point, the computation of the propagation constants $\vec{\alpha}$ and $\vec{\beta}$ imposed no restriction on the incidence plane, the polarization angle ζ, or the orientation of the three principal dielectric axes of the anisotropic medium, provided that the propagation constant of the amplitude wavefront $\vec{\alpha}$ be normal[8] to the interfaces. But how do we know the value of ζ in the transmission medium? If the TE/TM decomposition were still valid then, assuming that the incidence plane lied in the xz plane (i.e. $\phi_i = \{0°, 180°\}$), the polarization angle ζ in the transmission medium would be known as $\zeta = \{90°, 270°\}$ for the TM^z polarization, and $\zeta = \{0°, 180°\}$ for the TE^z polarization.

The above approach to compute $\varepsilon_r{}^{\text{eff}}$ for a biaxial medium has the same clear physical interpretation as did the uniaxial case in Section D.1. However, a simpler (albeit less physical and more mathematical) approach is to use the dispersion equation Equation (E.11) and the interpretation that $\gamma^2 = -k_o^2\varepsilon_r{}^{\text{eff}}$.

---

[8]The case where the propagation constant of the amplitude wavefront $\vec{\alpha}$ would not be normal to the interfaces is beyond the scope of this generalization.

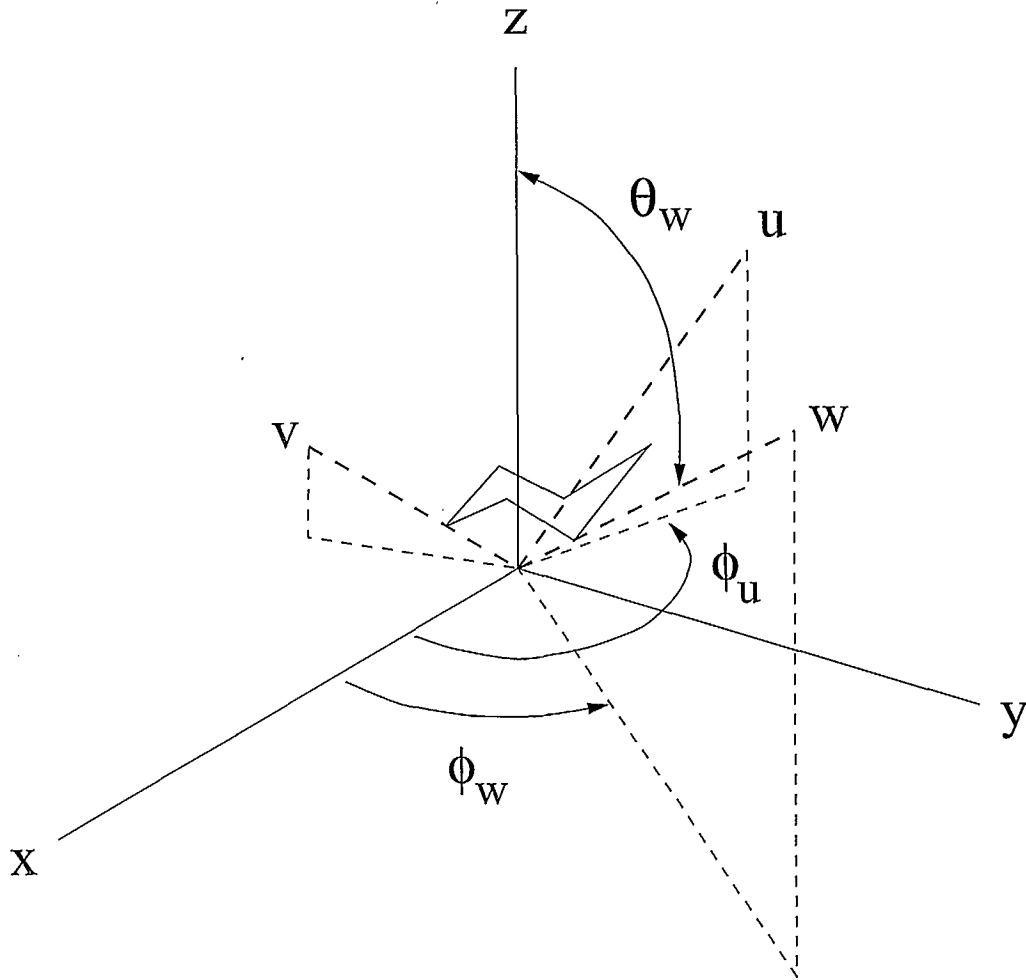Figure D.2: Generalized case of an anisotropic medium with its three principal dielectric axes u, v, w being arbitrarily oriented with respect to the reference xyz coordinate system.
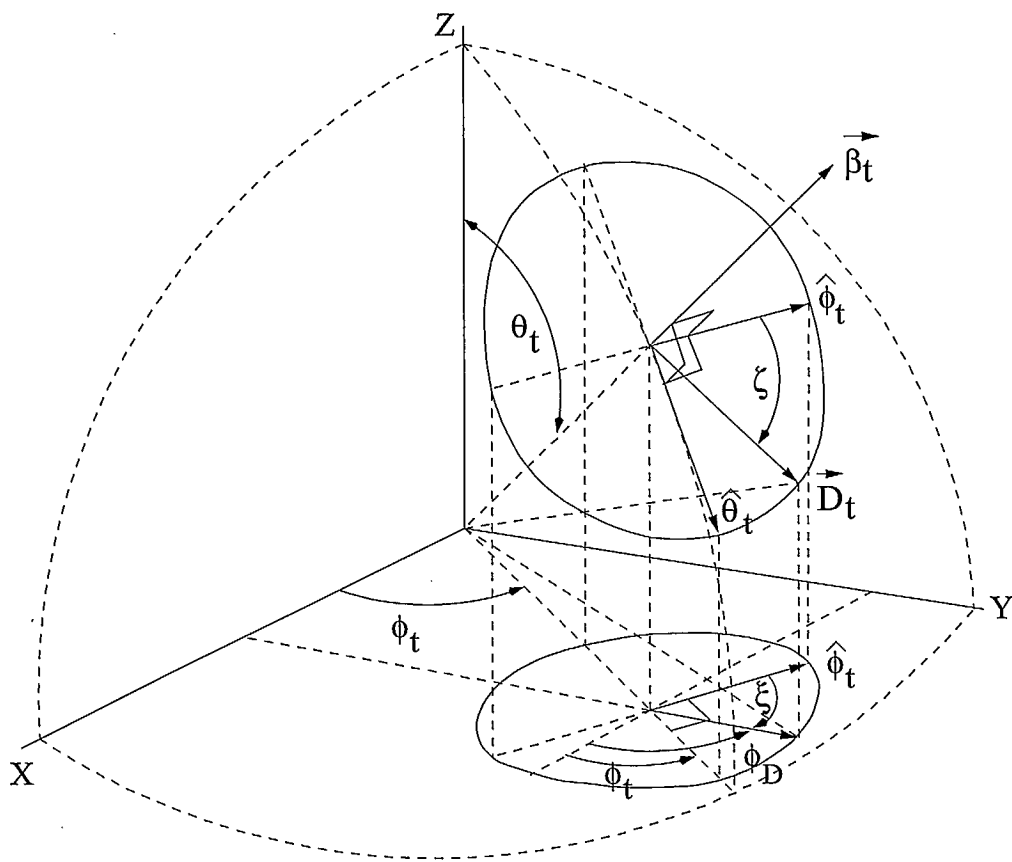
Figure D.3: Definition of the angles ξ and ζ.

Appendix E

Dispersion equation for the lossy biaxial medium

This appendix presents the dispersion equation for the lossy biaxial non-magnetic medium. The time-harmonic factor $e^{j\omega t}$ is implicit throughout the development. A non-uniform plane wave is written as $e^{-\vec{\gamma}\cdot\vec{r}}$ where $\vec{\gamma} = (\vec{\alpha} + j\vec{\beta})$. Hence, the time derivative leads to a scalar multiplication by $j\omega$ whereas the space derivative leads to vector multiplication by $-\vec{\gamma}$. The electrical conductivity is taken into account by the complex permittivity tensor which is assumed to take the diagonal form:

$$\overset{\leftrightarrow}{\varepsilon} = \begin{pmatrix} \varepsilon_u & 0 & 0 \\ 0 & \varepsilon_v & 0 \\ 0 & 0 & \varepsilon_w \end{pmatrix} \tag{E.1}$$

where:

$$\varepsilon_l = \varepsilon_o \left(\varepsilon'_{rl} - j\frac{\sigma_l}{\omega\varepsilon_o} \right)$$

with $l = \{u, v, w\}$. Hence, the principal conductivity axes are assumed to coincide with the principal dielectric axes which are given by the axes u, v and w. Although $\hat{D} \neq \hat{E}$ in general, $\hat{D} = \hat{E}$ in the direction of the three principal dielectric axes [75, p. 664] since $D_l = \varepsilon_l E_l$. Maxwell's equations become:

$$\vec{\gamma} \times \vec{E} = -j\omega\mu_o \vec{H} \tag{E.2}$$

$$\vec{\gamma} \times \vec{H} = +j\omega \overleftrightarrow{\varepsilon} \cdot \vec{E} \qquad (E.3)$$

$$\vec{\gamma} \cdot \vec{D} = 0 \qquad (E.4)$$

$$\vec{\gamma} \cdot \vec{H} = 0 \qquad (E.5)$$

Substituting Equation (E.3) into Equation (E.2) and using the vector calculus identity:

$$\vec{\gamma} \times (\vec{\gamma} \times \vec{E}) = \underbrace{(\vec{\gamma} \cdot \vec{\gamma})}_{\gamma^2} \vec{E} - \underbrace{\vec{\gamma}(\vec{\gamma} \cdot \vec{E})}_{\vec{\gamma}\vec{\gamma} \cdot \vec{E}}$$

where $\vec{\gamma}\vec{\gamma}$ is a dyadic, produces the Helmoltz vector equation:

$$\left(\vec{\gamma}\vec{\gamma} - \gamma^2 \overleftrightarrow{I} - \omega^2 \mu_o \overleftrightarrow{\varepsilon} \right) \cdot \vec{E} = 0 \qquad (E.6)$$

where $\overleftrightarrow{I}$ is the unit diagonal tensor, i.e. the identity matrix. This agrees with Reference [7, p. 184, Equation (5.15)] upon using the dyadic identity:

$$\left(\vec{\gamma}\vec{\gamma} - \vec{\gamma}^2 \overleftrightarrow{I} \right) = \left(\vec{\gamma} \times \overleftrightarrow{I} \right)^2$$

given in Reference [7, p. 17, Equation (1.100)]. Developing Equation (E.6) gives:

$$\begin{pmatrix} \gamma_u^2 - \gamma^2 - \omega^2 \mu_o \varepsilon_u & \gamma_u \gamma_v & \gamma_u \gamma_w \\ \gamma_u \gamma_v & \gamma_v^2 - \gamma^2 - \omega^2 \mu_o \varepsilon_v & \gamma_v \gamma_w \\ \gamma_u \gamma_w & \gamma_v \gamma_w & \gamma_w^2 - \gamma^2 - \omega^2 \mu_o \varepsilon_w \end{pmatrix} \begin{pmatrix} E_u \\ E_v \\ E_w \end{pmatrix} = 0 \qquad (E.7)$$

Note that $\gamma_l \neq j\omega\sqrt{\mu_o \varepsilon_l}$ where $l = \{u, v, w\}$ with ε_l referring to the permittivity in the three principal dielectric axes. Note that γ_u is the value of γ when the phase wavefront propagation vector $\vec{\beta}$, not the polarization vector $\vec{D}$, points in the $\hat{u}$ direction, and similarly for γ_v and γ_w.

To avoid the trivial solution requires that the determinant of the matrix be 0. Developing the determinant from the first row of the matrix and then dividing the result by $-\omega^2\mu_o$ gives this quadratic equation in γ^2:

$$a\gamma^4 + b\gamma^2 + c = 0$$

where:

$$a = (\varepsilon_u + \varepsilon_v + \varepsilon_w)$$

$$b = \omega^2\mu_o\left(\varepsilon_v\varepsilon_w + \varepsilon_u\varepsilon_w + \varepsilon_u\varepsilon_v\right) - \left((\varepsilon_v + \varepsilon_w)\gamma_u^2 + (\varepsilon_u + \varepsilon_w)\gamma_v^2 + (\varepsilon_u + \varepsilon_v)\gamma_w^2\right)$$

$$c = \omega^4\mu_o^2\varepsilon_u\varepsilon_v\varepsilon_w - \omega^2\mu_o\left(\varepsilon_v\varepsilon_w\gamma_u^2 + \varepsilon_u\varepsilon_w\gamma_v^2 + \varepsilon_u\varepsilon_v\gamma_w^2\right)$$

Substituting $\gamma_w = (\gamma^2 - \gamma_u^2 - \gamma_v^2)$ where γ_u and γ_v are the independent variables, produces the same quartic equation but with new coefficients:

$$a = \varepsilon_u \tag{E.8}$$

$$b = \omega^2\mu_o\varepsilon_w\left(\varepsilon_u + \varepsilon_v\right) - \left((\varepsilon_w - \varepsilon_u)\gamma_u^2 + (\varepsilon_w - \varepsilon_v)\gamma_v^2\right) \tag{E.9}$$

$$c = \omega^4\mu_o^2\varepsilon_u\varepsilon_v\varepsilon_w - \omega^2\mu_o\left(\varepsilon_v(\varepsilon_w - \varepsilon_u)\gamma_u^2 + \varepsilon_u(\varepsilon_w - \varepsilon_v)\gamma_v^2\right) \tag{E.10}$$

Solving for γ^2 produces the dispersion equation:

$$\gamma^2 = \frac{\left(\begin{array}{c}-\omega^2\mu_o\varepsilon_w(\varepsilon_u + \varepsilon_v) + (\varepsilon_w - \varepsilon_u)\gamma_u^2 + (\varepsilon_w - \varepsilon_v)\gamma_v^2 \\ \pm\sqrt{\left(\omega^2\mu_o\varepsilon_w(\varepsilon_v - \varepsilon_u) + (\varepsilon_w - \varepsilon_u)\gamma_u^2 - (\varepsilon_w - \varepsilon_v)\gamma_v^2\right)^2 + 4(\varepsilon_w - \varepsilon_u)(\varepsilon_w - \varepsilon_v)\gamma_u^2\gamma_v^2}\end{array}\right)}{2\varepsilon_w} \tag{E.11}$$

Developing Equation (E.7) produces these three equations:

$$\left(\gamma_u^2 - \omega^2\mu_o\varepsilon_u - \gamma^2\right)E_u + \gamma_u\gamma_v E_v + \gamma_u\gamma_w E_w = 0 \tag{E.12}$$

$$\left(\gamma_v^2 - \omega^2\mu_o\varepsilon_v - \gamma^2\right)E_v + \gamma_v\gamma_w E_w + \gamma_u\gamma_v E_u = 0 \tag{E.13}$$

211

$$\left(\gamma_w^2 - \omega^2\mu_o\varepsilon_w - \gamma^2\right)E_w + \gamma_u\gamma_w E_u + \gamma_v\gamma_w E_v = 0 \qquad (E.14)$$

Substituting Equation (E.11) into the last three equations produces:

$$\left(\omega^2\mu_o\varepsilon_w(\varepsilon_v - \varepsilon_u) + \varepsilon_w(\gamma_u^2 - \gamma_v^2) + \varepsilon_u\gamma_u^2 + \varepsilon_v\gamma_v^2\right)E_u + \gamma_u\gamma_v E_v + \gamma_u\gamma_w E_w = 0$$
$$(E.15)$$

$$\left(\omega^2\mu_o\varepsilon_w(\varepsilon_u - \varepsilon_v) + \varepsilon_w(\gamma_v^2 - \gamma_u^2) + \varepsilon_u\gamma_u^2 + \varepsilon_v\gamma_v^2\right)E_v + \gamma_v\gamma_w E_w + \gamma_u\gamma_v E_u = 0$$
$$(E.16)$$

$$(\omega^2\mu_o\varepsilon_w((\varepsilon_u - \varepsilon_w) + (\varepsilon_v - \varepsilon_w)) + \varepsilon_w((\gamma_w^2 - \gamma_u^2) + (\gamma_w^2 - \gamma_v^2)) + \varepsilon_u\gamma_u^2 + \varepsilon_v\gamma_v^2)E_w$$
$$+\gamma_u\gamma_w E_u + \gamma_v\gamma_w E_v = 0$$
$$(E.17)$$

Adding Equations (E.15) and (E.16) produces:

$$E_w = -\frac{B(E_u - E_v) + A(E_u + E_v) + 2\varepsilon_u\gamma_u\gamma_v(E_u + E_v)}{2\varepsilon_w\gamma_w(\gamma_u + \gamma_v)} \qquad (E.18)$$

Substituting this last equation into Equation (E.17) produces:

$$E_u = -\frac{(A + C)(A - B + 2\varepsilon_w\gamma_u\gamma_v) - 4\varepsilon_w^2\gamma_w^2(\gamma_u + \gamma_v)\gamma_v}{(A + C)(A + B + 2\varepsilon_w\gamma_u\gamma_v) - 4\varepsilon_w^2\gamma_w^2(\gamma_u + \gamma_v)\gamma_u}E_v \qquad (E.19)$$

where:

$$A = \varepsilon_u\gamma_u^2 + \varepsilon_v\gamma_v^2 \mp \sqrt{(\omega^2\mu_o\varepsilon_w(\varepsilon_v - \varepsilon_u) + (\varepsilon_w - \varepsilon_u)\gamma_u^2 - (\varepsilon_w - \varepsilon_v)\gamma_v^2)^2 + 4(\varepsilon_w - \varepsilon_u)(\varepsilon_w - \varepsilon_v)\gamma_u^2\gamma_v^2}$$

$$B = \omega^2\mu_o\varepsilon_w((\varepsilon_v - \varepsilon_u) + \varepsilon_w(\gamma_u^2 - \gamma_v^2)$$

$$C = \omega^2\mu_o\varepsilon_w((\varepsilon_u - \varepsilon_w) + (\varepsilon_v - \varepsilon_w)) + \varepsilon_w((\gamma_w^2 - \gamma_u^2) + (\gamma_w^2 - \gamma_v^2))$$

Finally, substituting Equation (E.19) back into Equation (E.18) produces:

$$E_w = 2\varepsilon_w \gamma_w \frac{(A - B + 2\varepsilon_w \gamma_u \gamma_v) - 2\gamma_v B}{(A + C)\,(A + B + 2\varepsilon_w \gamma_u \gamma_v) - 4\varepsilon_w^2 \gamma_w^2 (\gamma_u + \gamma_v)\gamma_u} E_v \qquad \text{(E.20)}$$

Both Equations (E.19) and (E.20) are written in terms of E_v as the independent variable.

Since the transverse (to the interface) variation of the fields are dictated by the incident plane wave, we have $\gamma_x^t = jk_x^i$ and $\gamma_y^t = jk_y^i$ where k_x^i and k_y^i are real-valued. In turn, $\gamma_u = jk_u$ and $\gamma_v = jk_v$ in Equation (E.11) can be obtained from γ_x^t and γ_y^t by coordinate rotation. Although k_x^i and k_y^i are real-valued, i.e. γ_x^t and γ_y^t are pure imaginary values, it does not follow from coordinate rotation that γ_u and γ_v are pure imaginary values. Note that the values of γ_x and γ_y are the values of γ when the propagation vector $\vec{\beta}$ points in the x or y direction, respectively, the same way that γ_l with $l = \{u, v, w\}$ is the value of γ when the progagation vector $\vec{\beta}$ points in the direction $\hat{l}$. There obtains:

$$\gamma_u = (\sin\theta_u \cos\phi_u)\gamma_x^t + (\sin\theta_u \sin\phi_u)\gamma_y^t + (\cos\theta_u)\gamma_z^t \qquad \text{(E.21)}$$

$$\gamma_v = (\sin\theta_v \cos\phi_v)\gamma_x^t + (\sin\theta_v \sin\phi_v)\gamma_y^t + (\cos\theta_v)\gamma_z^t \qquad \text{(E.22)}$$

where $\gamma_x^t = jk_x^i$, $\gamma_y^t = jk_y^i$, $(\gamma_z^t)^2 = \gamma^2 - (\gamma_x^t)^2 - (\gamma_y^t)^2 = \gamma^2 + (k_x^i)^2 + (k_y^i)^2$, $\sin\theta_u$ is given by Equation (D.30), $\cos\theta_u$ is given by Equation (D.31), $\sin\theta_v$ is given by Equation (D.32), and $\cos\theta_v$ is given by Equation (D.33). Substituting these expressions into Equations (E.21-E.22), squaring the results, substituting the results into Equation (E.11) and regrouping the terms in γ^2 produce the following quartic[1] in the variable γ^2:

$$\left. \begin{array}{l} (\gamma^2)^4 \left[G_4^2 \right] \\ + (\gamma^2)^3 \left[2G_4 G_2 + Q^2 \right] \\ + (\gamma^2)^2 \left[G_2^2 + 2G_4 G_0 + 2\omega^2 \mu_o QS + Q^2((k_x^i)^2 + (k_y^i)^2) \right] \\ + (\gamma^2) \left[2G_2 G_0 + 2\omega^2 \mu_o QS((k_x^i)^2 + (k_y^i)^2) + \omega^4 \mu_o^2 S^2 \right] \\ + \left[G_o^2 + \omega^4 \mu_o^2 S^2 (k_x^i)^2 + ((k_y^i)^2) \right] \end{array} \right\} = 0 \qquad \text{(E.23)}$$

where:

---

[1] This is somewhat reminiscent of the Booker quartic equation in Reference [7, pp. 205-208].

$$G_4 = \varepsilon_w - \left((\varepsilon_w - \varepsilon_u)\cos^2\theta_u + (\varepsilon_w - \varepsilon_v)\cos^2\theta_v \right)$$

$$G_2 = \omega^2\mu_o\varepsilon_w(\varepsilon_u + \varepsilon_v) - P - \omega^2\mu_o\left(\varepsilon_v(\varepsilon_w - \varepsilon_u)\cos^2\theta_u + \varepsilon_u(\varepsilon_w - \varepsilon_v)\cos^2\theta_v \right)$$

$$G_o = \omega^4\mu_o^2\varepsilon_u\varepsilon_v\varepsilon_w - \omega^2\mu_o R$$

$$
\begin{aligned}
P = &\left((k_x^i)^2 + (k_y^i)^2 \right)\left((\varepsilon_w - \varepsilon_u)\cos^2\theta_u + (\varepsilon_w - \varepsilon_v)\cos^2\theta_v \right) \\
&-(k_x^i)^2\left((\varepsilon_w - \varepsilon_u)\sin^2\theta_u\cos^2\phi_u + (\varepsilon_w - \varepsilon_v)\sin^2\theta_v\cos^2\phi_v \right) \\
&-(k_y^i)^2\left((\varepsilon_w - \varepsilon_u)\sin^2\theta_u\sin^2\phi_u + (\varepsilon_w - \varepsilon_v)\sin^2\theta_v\sin^2\phi_v \right) \\
&+(k_y^i)(k_y^i)\left((\varepsilon_w - \varepsilon_u)\sin^2\theta_u\sin 2\phi_u + (\varepsilon_w - \varepsilon_v)\sin^2\theta_v\sin 2\phi_v \right)
\end{aligned}
$$

$$
\begin{aligned}
Q = &(k_x^i)\left((\varepsilon_w - \varepsilon_u)\sin 2\theta_u\cos\phi_u + (\varepsilon_w - \varepsilon_v)\sin 2\theta_v\cos\phi_v \right) \\
&+(k_y^i)\left((\varepsilon_w - \varepsilon_u)\sin 2\theta_u\sin\phi_u + (\varepsilon_w - \varepsilon_v)\sin 2\theta_v\sin\phi_v \right)
\end{aligned}
$$

$$
\begin{aligned}
R = &\left((k_x^i)^2 + (k_y^i)^2 \right)\left(\varepsilon_v(\varepsilon_w - \varepsilon_u)\cos^2\theta_u + \varepsilon_u(\varepsilon_w - \varepsilon_v)\cos^2\theta_v \right) \\
&-(k_x^i)^2\left(\varepsilon_v(\varepsilon_w - \varepsilon_u)\sin^2\theta_u\cos^2\phi_u + \varepsilon_u(\varepsilon_w - \varepsilon_v)\sin^2\theta_v\cos^2\phi_v \right) \\
&-(k_y^i)^2\left(\varepsilon_v(\varepsilon_w - \varepsilon_u)\sin^2\theta_u\sin^2\phi_u + \varepsilon_u(\varepsilon_w - \varepsilon_v)\sin^2\theta_v\sin^2\phi_v \right) \\
&+(k_y^i)(k_y^i)\left(\varepsilon_v(\varepsilon_w - \varepsilon_u)\sin^2\theta_u\sin 2\phi_u + \varepsilon_u(\varepsilon_w - \varepsilon_v)\sin^2\theta_v\sin 2\phi_v \right)
\end{aligned}
$$

$$
\begin{aligned}
S = &(k_x^i)\left(\varepsilon_v(\varepsilon_w - \varepsilon_u)\sin 2\theta_u\cos\phi_u + \varepsilon_u(\varepsilon_w - \varepsilon_v)\sin 2\theta_v\cos\phi_v \right) \\
&+(k_y^i)\left(\varepsilon_v(\varepsilon_w - \varepsilon_u)\sin 2\theta_u\sin\phi_u + \varepsilon_u(\varepsilon_w - \varepsilon_v)\sin 2\theta_v\sin\phi_v \right)
\end{aligned}
$$

The closed-form solution of the quartic in Equation (E.23) can be obtained by using the MATLAB symbolic math toolbox. This method turns out to be simpler and more precise (because it is fully analytical) than the previous one presented in Section D.2. However, the sign ambiguities introduced by coordinate transformation still remain due to the presence of odd powers of $\sin 2\theta_u$, $\cos 2\theta_u$, $\sin 2\theta_v$, $\cos 2\theta_v$, $\sin\phi_v$, $\cos\phi_v$, $\sin 2\phi_v$ and $\cos 2\phi_v$.

From Equation (E.23) and the interpretation that $\gamma^2 = -k_o^2\varepsilon_r^{\text{eff}}$, the intrinsic propagation constants α_o and β_o for each one of the two eigenwaves

can be determined[2] from Equations (4.2-4.3), respectively. The corresponding effective propagation constants α and β can then be computed by the the procedure presented in Chapter 2.

In summary, one important feature of the analytical technique presented in this report is that computing the effective propagation constants with the Adler-Chu-Fano formulation offers a general method to compute the effective propagation constants in multilayered slabs of biaxial media. The solution method would proceed as follows:

- compute the value $\varepsilon_r{}^{\text{eff}} = -(\gamma^2/k_o^2)$ with γ^2 given by the solution of Equation (E.23) for the desired eigenwave.

- compute the intrinsic propagation constants α_o and β_o from Equations (2.5-2.6) with $\varepsilon_r{}^{\|}$ replaced by $\varepsilon_r{}^{\text{eff}}$;

- compute the effective propagation constants α and β and the real-valued propagation angles ξ and ρ by the method presented in Chapter 2;

- compute the Fresnel equations[3] , if still applicable, written in terms of ε_r^i being the permittivity that $\vec{D}$ sees "in the interface" for the incidence medium, and ε_r^t being the permittivity that $\vec{D}$ sees "in the interface" for the transmission medium. The permittivity that $\vec{D}$ sees "in the interface" for the TM^z polarization would be ε_{rx} given by:

$$\frac{\varepsilon_{rx}}{\varepsilon_r^i} \equiv \left(\frac{c_i}{c_x}\right)^2 . \tag{E.24}$$

where c_x would be computed from Equations (D.24-D.29) with $\phi_D = 0°$ and $\theta_D = 90°$ since D_x is the projection of $\vec{D}$ onto the xy plane.

If Fresnel equations are not applicaple, then the scattering coefficients for the incidence from the free-space side must be derived from amplitude-matching the tangential field components at the interface.

- compute the scattering coefficients of the entire multilayered structure by using $\mathcal{C}$ matrices with the cascade approach of Chapter 3.

---

[2]Equations (4.2-4.3) were written for the extraordinary wave in a uniaxial medium. For the more general case of a biaxial medium, $\varepsilon_r^{\|}$ needs to be replaced by $\varepsilon_r^{\text{eff}}$ corresponding to the eigenwave of interest.

[3]Since Fresnel equations require the knowledge of only $\gamma_z = \sqrt{\gamma^2 + (k_x^i)^2 + (k_y^i)^2}$, Fresnel equations could be computed without having first to find the values of intrinsic α_o, β_o, the values of effective α and β and the values of the propagation angles ρ and ξ.

E.1   Validation

These expressions are first validated for the lossy uniaxial medium with its optic axis parallel to either $\hat{u}$, $\hat{v}$ or $\hat{w}$. The expressions are then validated for the lossy biaxial case with its two optic axes arbitrarily oriented. The subscripts $\perp$ and $\parallel$ will refer to the directions perpendicular and parallel to the single optic axis of the uniaxial medium, respectively. The superscripts ' and " will refer to the ordinary and the extraordinary waves of the uniaxial medium, respectively, or the two eigenwaves of the biaxial medium. The Reference that will be cited in this section is the following:

Rodolfo Echarri and Maria T. Garea, "Behaviour of the Poynting vector in uniaxial absorbent media", Pure Appl. Opt. 3, pp. 931-941, 1994.

Since the expressions are very long, the Matlab symbolic math toolbox was used to carry out the calculations. We will see that for all three uniaxial cases, we always obtain[4]:

$$(\gamma')^2 = -\omega^2 \mu_o \varepsilon_\perp$$

$$(\gamma'')^2 = -\omega^2 \mu_o \varepsilon_\parallel + \gamma_{\text{optic}}^2 \left(1 - \frac{\varepsilon_\parallel}{\varepsilon_\perp} \right)$$

where $\gamma_{\text{optic}} = j\omega\sqrt{\mu_o \varepsilon_\parallel}$ is the value of γ when the polarization vector $\vec{D}$, not the propagation vector $\vec{\beta}$, points in the direction of the optic axis. Consequently, one obtains:

$$(\gamma'')^2 = -\omega^2 \mu_o \varepsilon_\parallel \left(2 - \frac{\varepsilon_\parallel}{\varepsilon_\perp} \right)$$

E.1.1   Lossy uniaxial medium with optic axis along $\hat{w}$

$$\text{For} \quad \begin{cases} \varepsilon_u = \varepsilon_v = \varepsilon_\perp \\ \varepsilon_w = \varepsilon_\parallel \end{cases} \tag{E.25}$$

and using the lower sign in Equation (E.11), there obtains:

---

[4]It is only a coincidence that the equation for $(\gamma'')^2 = -\omega^2 \mu_o \varepsilon^{\text{eff}}$ resembles Equation (D.22) where $\varepsilon_\parallel \equiv \varepsilon^{\text{long}}$ and $\varepsilon_\perp \equiv \varepsilon^{\text{trans}}$. The equation, here, applies to an unbounded medium whereas Equation (D.22) applies to the case of an interface with the optic axis parallel to the interface.

$$(\gamma')^2 = -\omega^2 \mu_o \varepsilon_v = -\omega^2 \mu_o \varepsilon_\perp$$

$$E'_u = -\left(\frac{\gamma_v}{\gamma_u}\right) E_v$$

$$E'_w = 0$$

These last two equations agree with Equation (11) of Echarri and Garea.

$$\vec{D}' \cdot \vec{\gamma}' = 0$$

Using the upper sign in Equation (E.11), there obtains:

$$(\gamma'')^2 = -\omega^2 \mu_o \varepsilon_w - \gamma_w^2 \left(\frac{\varepsilon_w - \varepsilon_v}{\varepsilon_v}\right) = -\omega^2 \mu_o \varepsilon_\parallel + \gamma_w^2 \left(1 - \frac{\varepsilon_\parallel}{\varepsilon_\perp}\right)$$

$$E''_u = \left(\frac{\gamma_u}{\gamma_v}\right) E_v$$

$$E''_w = -\left(\frac{\varepsilon_v}{\varepsilon_w}\right) \left(\frac{\gamma^2 - \gamma_w^2}{\gamma_v \gamma_w}\right) E_v$$

These last two equations agree with Equation (12) of Echarri and Garea.

$$\vec{D}'' \cdot \vec{\gamma}'' = 0$$

And finally:

$$\vec{D}' \cdot \vec{D}'' = 0$$

E.1.2 Lossy uniaxial medium with optic axis along $\hat{u}$

$$\text{For} \quad \begin{cases} \varepsilon_v & = & \varepsilon_w & = & \varepsilon_\perp \\ \varepsilon_u & = & \varepsilon_\parallel \end{cases} \qquad\qquad (E.26)$$

and using the lower sign in Equation (E.11), there obtains:

$$(\gamma')^2 = -\omega^2 \mu_o \varepsilon_w = -\omega^2 \mu_o \varepsilon_\perp$$

$$E_u' = 0$$

$$E_w' = -\left(\frac{\gamma_v}{\gamma_w}\right) E_v$$

$$\vec{D}' \cdot \vec{\gamma}' = 0$$

and using the upper sign in Equation (E.11), there obtains:

$$(\gamma'')^2 = -\omega^2 \mu_o \varepsilon_u + \gamma_u^2 \left(\frac{\varepsilon_w - \varepsilon_u}{\varepsilon_w}\right) = -\omega^2 \mu_o \varepsilon_\parallel + \gamma_u^2 \left(1 - \frac{\varepsilon_\parallel}{\varepsilon_\perp}\right)$$

$$E_u'' = -\left(\frac{\varepsilon_w}{\varepsilon_u}\right) \left(\frac{\gamma^2 - \gamma_u^2}{\gamma_u \gamma_v}\right) E_v$$

$$E_w'' = \left(\frac{\gamma_w}{\gamma_v}\right) E_v$$

$$\vec{D}'' \cdot \vec{\gamma}'' = 0$$

And finally:

$$\vec{D}' \cdot \vec{D}'' = E_v^2 \varepsilon_w^2 \left(1 - \sqrt{\frac{\omega^2 \mu_o \varepsilon_u + (\varepsilon_u/\varepsilon_w)\gamma_u^2 + \gamma_v^2}{\omega^2 \mu_o \varepsilon_w + \gamma_u^2 + \gamma_v^2}}\right)$$

which can be reduced to:

$$\vec{D}' \cdot \vec{D}'' = \left(1 - \frac{\gamma_w''}{\gamma_w'}\right) \varepsilon_w^2 E_v^2$$

This last equation would clearly produce 0 if $\hat{w}$ lied in a planar interface (i.e. if the normal of the interface lied in the uv plane). This would be so because the transverse variations of the fields at a planar interface are dictated by the incident plane wave, i.e. $\gamma_w'' = \gamma_w' = \gamma_w^i$. However, the presence of this condition would not be, in fact, a limitation because the optic axis $\hat{u}$ could still be oriented in an arbitrary direction even if $\hat{w}$ were restricted to lie in the interface. Still, it would be peculiar to have to rely on the presence of a planar interface to insure that the result be null. This suggests that we should have $\gamma_w'' = \gamma_w'$ even without invoking the presence of an interface.

This peculiar reliance on $\gamma_w'' = \gamma_w'$ to make $\vec{D}' \cdot \vec{D}'' = 0$ appears only because $\gamma_w^2 = (\gamma^2 - \gamma_u^2 - \gamma_v^2)$ was used as part of the development of Equation (E.11). This implies that γ_u, γ_v and γ were assumed to be the independent variables in this development. In an unbounded medium, however, γ_w would usually be taken as an independent variable, and it is γ that would become the dependent variable, i.e. for a given propagating direction, the value of γ would depend on γ_u, γ_v, γ_w and the polarization of the wave.

E.1.3   Lossy uniaxial medium with optic axis along $\hat{v}$

$$\text{For} \quad \begin{cases} \varepsilon_u = \varepsilon_w = \varepsilon_\perp \\ \varepsilon_v = \varepsilon_\parallel \end{cases} \tag{E.27}$$

and using the upper sign in Equation (E.11), there obtains:

$$(\gamma')^2 = -\omega^2 \mu_o \varepsilon_w = -\omega^2 \mu_o \varepsilon_\perp$$

and using the lower sign in Equation (E.11), there obtains:

$$(\gamma'')^2 = -\omega^2 \mu_o \varepsilon_v - \gamma_v^2 \left(\frac{\varepsilon_w - \varepsilon_v}{\varepsilon_w}\right) = -\omega^2 \mu_o \varepsilon_\parallel + \gamma_v^2 \left(1 - \frac{\varepsilon_\parallel}{\varepsilon_\perp}\right)$$

Because E is zero in the direction of the optic axis as shown by the two preceding cases, then $E_v = 0$ here. Therefore, E_u and E_w cannot be expressible in terms of E_v since $E_u \neq 0$ and $E_w \neq 0$. Consequently, the present formulation, which is expressed in terms of E_v, cannot be used to show that $(\vec{D} \cdot \vec{\gamma}) = 0$ and $(\vec{D}' \cdot \vec{D}'') = 0$.

E.1.4 Lossy biaxial medium

Since the expressions are very long, the results from using the Matlab symbolic math toolbox are reproduced here:

```
syms om mu real
syms Gu Gv eu ev ew AA BB CC Ev unreal

BB=(om^2)*mu*ew*(ev-eu)+ew*((Gu^2)-(Gv^2));
RAD=simple(sqrt((((om^2)*mu*ew*(ev-eu)+(ew-eu)*(Gu^2)-...
(ew-ev)*(Gv^2))^2)+4*(ew-eu)*(ew-ev)*(Gu^2)*(Gv^2)));
%pretty(simple(RAD))

% For the first eigenvalue of the propagation constant G and
% the corresponding eigenpolarization D.
G2=simple((-(om^2)*mu*ew*(eu+ev)+(ew-eu)*(Gu^2)+(ew-ev)*(Gv^2)+RAD)/(2*ew));
pretty(G2)
```

$$
\begin{aligned}
&\tfrac{1}{2}\,(-\text{om}^2\,\text{mu ew (eu + ev)} + (\text{ew} - \text{eu})\,\text{Gu}^2 + (\text{ew} - \text{ev})\,\text{Gv}^2 + (\\
&\quad \text{om}^4\,\text{mu}^2\,\text{ew}^2\,\text{ev}^2 + \text{om}^4\,\text{mu}^2\,\text{ew}^2\,\text{eu}^2 - 2\,\text{Gu}^2\,\text{ew Gv}^2\,\text{ev}\\
&\quad - 2\,\text{Gu}^2\,\text{eu Gv}^2\,\text{ew} + 2\,\text{Gu}^2\,\text{eu Gv}^2\,\text{ev} - 2\,\text{Gu}^4\,\text{ew eu} + 2\,\text{Gu}^2\,\text{ew}^2\,\text{Gv}^2\\
&\quad - 2\,\text{Gv}^4\,\text{ew ev} + \text{Gu}^4\,\text{ew}^2 + \text{Gu}^4\,\text{eu}^2 + \text{Gv}^4\,\text{ew}^2 + \text{Gv}^4\,\text{ev}^2\\
&\quad - 2\,\text{om}^4\,\text{mu}^2\,\text{ew}^2\,\text{ev eu} + 2\,\text{om}^2\,\text{mu}^2\,\text{ew}^2\,\text{ev Gu}^2\\
&\quad - 2\,\text{om}^2\,\text{mu}^2\,\text{ew ev Gu}^2\,\text{eu} - 2\,\text{om}^2\,\text{mu}^2\,\text{ew}^2\,\text{ev Gv}^2\\
&\quad + 2\,\text{om}^2\,\text{mu}^2\,\text{ew ev}^2\,\text{Gv}^2 - 2\,\text{om}^2\,\text{mu}^2\,\text{ew}^2\,\text{eu Gu}^2\\
&\quad + 2\,\text{om}^2\,\text{mu}^2\,\text{ew eu}^2\,\text{Gu}^2 + 2\,\text{om}^2\,\text{mu}^2\,\text{ew}^2\,\text{eu Gv}^2\\
&\quad - 2\,\text{om}^2\,\text{mu}^2\,\text{ew eu Gv}^2\,\text{ev})^{1/2})/\text{ew}
\end{aligned}
$$

```
Gw=sqrt(G2-((Gu^2)+(Gv^2)));
AA=eu*(Gu^2)+ev*(Gv^2)-RAD;
CC=(om^2)*mu*ew*(eu+ev-2*ew)+ew*(2*(Gw^2)-(Gu^2)-(Gv^2));
Eu=simple(-Ev*((AA+CC)*(AA-BB+2*ew*Gu*Gv)-4*(ew^2)*(Gw^2)*(Gu+Gv)*Gv)/...
((AA+CC)*(AA+BB+2*ew*Gu*Gv)-4*(ew^2)*(Gw^2)*(Gu+Gv)*Gu));
pretty(Eu)
```

$$
\begin{aligned}
- Ev\ (Gu^4\ ew\ &- eu\ Gu^4\ - ev\ Gv^2\ Gu^2\ - 2\ om^2\ mu\ ew\ Gu^2\ eu \\
&+ om^2\ mu\ ew\ Gv^2\ ev\ - om^4\ mu^2\ ew^2\ eu\ + om^4\ mu^2\ ew^2\ ev \\
&+ om^2\ mu^2\ ew^2\ Gu^2\ - om^2\ mu^2\ ew^2\ Gv^2\ + om^2\ mu^2\ ew^2\ \%1^{1/2} \\
&+ Gu^2\ Gv^2\ ew\ - Gu^3\ ew\ Gv\ - Gv^3\ ew\ Gu\ + Gv^3\ ev\ Gu\ + Gv^3\ Gu\ eu \\
&- Gv\ \%1^{1/2}\ Gu^2\ + Gu\ \%1^{1/2}\ - 2\ om^2\ mu\ ew\ Gu\ Gv\ + Gu^2\ om^2\ mu\ ew\ ev \\
&+ Gv^2\ om^2\ mu\ ew\ eu\ Gu\ + Gv\ om^2\ mu\ ew\ ev\ Gu)\ /\ (-ev\ Gv^4 \\
/ \\
&+ om^2\ mu\ ew\ Gu^2\ eu\ - 2\ om^2\ mu\ ew\ Gv^2\ ev\ + om^4\ mu^2\ ew^2\ eu \\
&- om^4\ mu^2\ ew^2\ ev\ - om^2\ mu^2\ ew^2\ Gu^2\ + om^2\ mu^2\ ew^2\ Gv^2 \\
&+ om^2\ mu^2\ ew^2\ \%1^{1/2}\ + Gu^2\ Gv^2\ ew\ - Gu^3\ ew\ Gv\ - Gv^3\ ew\ Gu\ + Gv^3\ ev\ Gu \\
&+ Gv^3\ Gu\ eu\ - Gv\ \%1^{1/2}\ Gu^2\ + Gv\ \%1^{1/2}\ + Gv^4\ ew\ - Gv^2\ eu\ Gu \\
&- 2\ om^2\ mu\ ew\ Gu\ Gv\ + Gv^2\ om^2\ mu\ ew\ eu\ + Gv\ om^2\ mu\ ew\ eu\ Gu \\
&+ Gv\ om^2\ mu\ ew\ ev\ Gu)
\end{aligned}
$$

$$\%1 := om^4\ mu^2\ ew^2\ ev^2 + om^4\ mu^2\ ew^2\ eu^2 - 2\ Gu^2\ ew\ Gv\ ev$$

$$- 2\ Gu^2\ eu\ Gv\ ew + 2\ Gu^2\ eu\ Gv\ ev - 2\ Gu^4\ ew\ eu + 2\ Gu^2\ ew^2\ Gv^2$$

$$- 2\ Gv^4\ ew\ ev + Gu^4\ ew^2 + Gu^4\ eu^2 + Gv^4\ ew^2 + Gv^4\ ev^2$$

$$- 2\ om^4\ mu^2\ ew^2\ ev\ eu + 2\ om^2\ mu^2\ ew^2\ ev\ Gu$$

$$- 2\ om^2\ mu^2\ ew\ ev\ Gu^2\ eu - 2\ om^2\ mu^2\ ew^2\ ev\ Gv$$

$$+ 2\ om^2\ mu^2\ ew\ ev^2\ Gv^2 - 2\ om^2\ mu^2\ ew^2\ eu\ Gu$$

$$+ 2\ om^2\ mu^2\ ew\ eu^2\ Gu^2 + 2\ om^2\ mu^2\ ew^2\ eu\ Gv$$

$$- 2\ om^2\ mu^2\ ew\ eu\ Gv^2\ ev$$

```
Ew=simple(Ev*2*ew*Gw*((AA-BB+2*ew*Gu*Gv)*(Gu-Gv)-2*BB*Gv)/...
((AA+CC)*(AA+BB+2*ew*Gu*Gv)-4*(ew^2)*(Gw^2)*(Gu+Gv)*Gu));
pretty(Ew)
```

$$Ev\ ew \left(\frac{-om^2\ mu\ ew\ (eu + ev) + (ew - eu)\ Gu^2 + (ew - ev)\ Gv^2 + \%1}{ew} - 4\ Gu^2 \right.$$

$$- 4\ Gv^2 \left| \left((Gu^2\ eu + Gv^2\ ev - \%1 - om^2\ mu\ ew\ (ev - eu) \right. \right.^{1/2}$$

$$\left. - ew\ (Gu^2 - Gv^2) + 2\ ew\ Gu\ Gv)\ (Gu - Gv) \right.$$

```
                                                        //
          2                           2     2      / || 2
  - (2 om    mu   ew (ev - eu) + 2 ew (Gu   - Gv )) Gv)  / ||Gu   eu
                                                    /   \\

                                                    /
        2                 2                         |
  + Gv   ev - %1 + om    mu   ew (eu + ev - 2 ew) + ew |
                                                    \

        2                               2               2
  -om    mu   ew (eu + ev) + (ew - eu) Gu  + (ew - ev) Gv  + %1        2
  ---------------------------------------------------------------- - 3 Gu
                                ew


          \\
        2||    2       2            2
  - 3 Gv || (Gu   eu + Gv   ev - %1 + om    mu   ew (ev - eu)
        //

                                              /
        2     2                     2 |
  + ew (Gu   - Gv ) + 2 ew Gu Gv) - 4 ew  |
                                          \

        2                               2               2
      -om    mu   ew (eu + ev) + (ew - eu) Gu  + (ew - ev) Gv  + %1        2
  1/2 ---------------------------------------------------------------- - Gu
                                ew


        \              \
        2|              |
  - Gv  | (Gu + Gv) Gu|
        /              /
```

$$
\begin{aligned}
\%1 := \big(\, & om^4\,mu^2\,ew^2\,ev^2 + om^4\,mu^2\,ew^2\,eu^2 - 2\,Gu^2\,ew\,Gv^2\,ev \\[4pt]
& - 2\,Gu^2\,eu\,Gv^2\,ew + 2\,Gu^2\,eu\,Gv^2\,ev - 2\,Gu^4\,ew\,eu + 2\,Gu^2\,ew^2\,Gv^2 \\[4pt]
& - 2\,Gv^4\,ew\,ev + Gu^4\,ew^2 + Gu^4\,eu^2 + Gv^4\,ew^2 + Gv^4\,ev^2 \\[4pt]
& - 2\,om^4\,mu^2\,ew^2\,ev\,eu + 2\,om^2\,mu^2\,ew^2\,ev\,Gu \\[4pt]
& - 2\,om^2\,mu^2\,ew\,ev\,Gu^2\,eu - 2\,om^2\,mu^2\,ew\,ev\,Gv^2 \\[4pt]
& + 2\,om^2\,mu^2\,ew\,ev^2\,Gv^2 - 2\,om^2\,mu^2\,ew\,eu\,Gu^2 \\[4pt]
& + 2\,om^2\,mu^2\,ew\,eu^2\,Gu^2 + 2\,om^2\,mu^2\,ew\,eu\,Gv^2 \\[4pt]
& - 2\,om^2\,mu^2\,ew\,eu\,Gv^2\,ev\,\big)^{1/2}
\end{aligned}
$$

```
% The first eigenpolarization DTOP.
DTOPu=eu*Eu;
DTOPv=ev*Ev;
DTOPw=ew*Ew;
% To test that the first eigenpolarization is perpendicular (in the complex sense)
% to the propagation vector.
GTOP=simple(Gu*eu*Eu+Gv*ev*Ev+Gw*ew*Ew);
pretty(GTOP)
```

$$0$$

```
% For the second eigenvalue of the propagation constant G
% and the corresponding eigenpolarization D.
G2=simple((-(om^2)*mu*ew*(eu+ev)+(ew-eu)*(Gu^2)+(ew-ev)*(Gv^2)-RAD)/(2*ew));
pretty(G2)
```

$$
\begin{aligned}
&1/2\ (-om^2\ mu\ ew\ (eu + ev) + (ew - eu)\ Gu^2 + (ew - ev)\ Gv^2 - (\\[4pt]
&\quad om^4\ mu^2\ ew^2\ ev^2 + om^4\ mu^2\ ew^2\ eu^2 - 2\ Gu^2\ ew^2\ Gv^2\ ev^2\\[4pt]
&\quad - 2\ Gu^2\ eu^2\ Gv^2\ ew^2 + 2\ Gu^2\ eu^2\ Gv^2\ ev^2 - 2\ Gu^4\ ew^2\ eu^2 + 2\ Gu^2\ ew^2\ Gv^2\\[4pt]
&\quad - 2\ Gv^4\ ew^2\ ev^2 + Gu^4\ ew^4 + Gu^4\ eu^4 + Gv^4\ ew^4 + Gv^4\ ev^4\\[4pt]
&\quad - 2\ om^4\ mu^2\ ew^2\ ev^2\ eu + 2\ om^2\ mu\ ew^2\ ev\ Gu^2\\[4pt]
&\quad - 2\ om^2\ mu\ ew\ ev\ Gu^2\ eu^2 - 2\ om^2\ mu\ ew^2\ ev\ Gv^2\\[4pt]
&\quad + 2\ om^2\ mu\ ew^2\ ev\ Gv^2 - 2\ om^2\ mu\ ew^2\ eu\ Gu^2\\[4pt]
&\quad + 2\ om^2\ mu\ ew^2\ eu^2\ Gu^2 + 2\ om^2\ mu\ ew^2\ eu\ Gv^2\\[4pt]
&\quad - 2\ om^2\ mu\ ew\ eu\ Gv^2\ ev^2)^{1/2}\ )/ew
\end{aligned}
$$

```
Gw=sqrt(G2-((Gu^2)+(Gv^2)));
AA=eu*(Gu^2)+ev*(Gv^2)+RAD;
CC=(om^2)*mu*ew*(eu+ev-2*ew)+ew*(2*(Gw^2)-(Gu^2)-(Gv^2));
Eu=simple(-Ev*((AA+CC)*(AA-BB+2*ew*Gu*Gv)-4*(ew^2)*(Gw^2)*(Gu+Gv)*Gv)/...
((AA+CC)*(AA+BB+2*ew*Gu*Gv)-4*(ew^2)*(Gw^2)*(Gu+Gv)*Gu));
pretty(Eu)
```

$$
\begin{aligned}
E_v \, (&-G_v \, \%1^{1/2} \;\; G_u^2 + G_u^2 \, G_v^2 \, e_v + 2\,om^2 \, mu \, ew \, G_u^2 \, eu - om^2 \, mu \, ew \, G_v^2 \, ev \\[4pt]
&+ om^4 \, mu^2 \, ew^2 \, eu - om^4 \, mu^2 \, ew^2 \, ev - om^2 \, mu^2 \, ew^2 \, G_u^2 \\[4pt]
&+ om^2 \, mu^2 \, ew^2 \, G_v^2 + om^2 \, mu^2 \, ew \, \%1^{1/2} - G_u^2 \, G_v \, ew^2 + G_u \, ew \, G_v^3 \\[4pt]
&+ G_v^3 \, ew \, G_u - G_v^3 \, ev \, G_u - G_v \, G_u^2 \, eu - G_u^2 \, om^2 \, mu \, ew \, ev + G_u^4 \, eu \\[4pt]
&- G_u^4 \, ew + G_u^2 \, \%1^{1/2} + 2\,om^2 \, mu \, ew^2 \, G_u \, G_v - G_v^2 \, om^2 \, mu \, ew \, eu \, G_u \\[4pt]
&- G_v^2 \, om^2 \, mu \, ew \, ev \, G_u) \;\; / \;\; (G_v \, \%1^{1/2} \;\; G_u - ev \, G_v^4 \\[4pt]
&+ om^2 \, mu \, ew \, G_u^2 \, eu - 2\,om^2 \, mu \, ew \, G_v^2 \, ev + om^4 \, mu^2 \, ew^2 \, eu \\[4pt]
&- om^4 \, mu^2 \, ew^2 \, ev - om^2 \, mu^2 \, ew^2 \, G_u^2 + om^2 \, mu^2 \, ew^2 \, G_v^2 \\[4pt]
&- om^2 \, mu^2 \, ew \, \%1^{1/2} + G_u^2 \, G_v^2 \, ew - G_u^3 \, ew \, G_v - G_v^3 \, ew \, G_u + G_v^3 \, ev \, G_u \\[4pt]
&+ G_v^3 \, G_u \, eu - G_v^2 \, \%1^{1/2} + G_v^4 \, ew - G_v^2 \, eu \, G_u^2 - 2\,om^2 \, mu^2 \, ew \, G_u \, G_v \\[4pt]
&+ G_v^2 \, om^2 \, mu^2 \, ew \, eu + G_v \, om^2 \, mu \, ew \, eu \, G_u + G_v \, om^2 \, mu \, ew \, ev \, G_u)
\end{aligned}
$$

226

```
      4    2    2   2       4    2    2   2       2      2
%1 := om   mu   ew  ev  + om   mu   ew   eu  - 2 Gu   ew Gv  ev


       2       2        2       2         4          2   2   2
- 2 Gu   eu Gv  ew + 2 Gu   eu Gv  ev - 2 Gu   ew eu  + 2 Gu   ew  Gv


       4          4   2     4   2     4   2     4   2
- 2 Gv   ew ev + Gu   ew  + Gu   eu  + Gv   ew  + Gv   ev


       4    2   2           2       2      2
- 2 om   mu   ew  ev eu + 2 om   mu   ew   ev Gu


       2           2         2       2      2
- 2 om   mu   ew ev Gu   eu - 2 om   mu   ew   ev Gv


       2           2   2       2       2      2
+ 2 om   mu   ew ev  Gv  - 2 om   mu   ew   eu Gu


       2           2   2       2       2      2
+ 2 om   mu   ew eu  Gu  + 2 om   mu   ew   eu Gv


       2               2
- 2 om   mu   ew eu Gv   ev
```

```
Ew=simple(Ev*2*ew*Gw*((AA-BB+2*ew*Gu*Gv)*(Gu-Gv)-2*BB*Gv)/...
((AA+CC)*(AA+BB+2*ew*Gu*Gv)-4*(ew^2)*(Gw^2)*(Gu+Gv)*Gu));
pretty(Ew)
```

```
        /       2                                 2              2
        |  -om   mu   ew (eu + ev) + (ew - eu) Gu  + (ew - ev) Gv  - %1              2
Ev ew  |2 -----------------------------------------------------------------.- 4 Gu
        \                                ew


              \1/2
            2|         2       2            2
     - 4 Gv  |    ((Gu   eu + Gv   ev + %1 - om   mu   ew (ev - eu)
              /


              2    2
     - ew (Gu   - Gv ) + 2 ew Gu Gv) (Gu - Gv)
```

```
                                                                    //
         2                                       2       2         / ||  2
   - (2 om    mu   ew (ev - eu) + 2 ew (Gu   - Gv )) Gv)  /   ||Gu   eu
                                                        /    \\
                                                       /
         2                 2                           |
   + Gv   ev + %1 + om    mu   ew (eu + ev - 2 ew) + ew |
                                                        \


       2                                     2                2
   -om    mu   ew (eu + ev) + (ew - eu) Gu   + (ew - ev) Gv   - %1       2
   -------------------------------------------------------------- - 3 Gu
                              ew


          \\
          2||     2         2                 2
   - 3 Gv || (Gu   eu + Gv   ev + %1 + om    mu   ew (ev - eu)
          //


                                                   /
           2       2                          2 |
   + ew (Gu   - Gv ) + 2 ew Gu Gv) - 4 ew  |
                                           \


           2                                 2                2
       -om    mu   ew (eu + ev) + (ew - eu) Gu   + (ew - ev) Gv   - %1       2
   1/2 -------------------------------------------------------------- - Gu
                              ew


          \              \
          2|              |
   - Gv  | (Gu + Gv)  Gu|
         /              /
```

$$\%1 := (om^4 \, mu^2 \, ew^2 \, ev^2 + om^4 \, mu^2 \, ew^2 \, eu^2 - 2\,Gu^2 \, ew \, Gv \, ev$$

$$- 2\,Gu^2 \, eu \, Gv \, ew + 2\,Gu^2 \, eu \, Gv \, ev - 2\,Gu^4 \, ew \, eu + 2\,Gu^2 \, ew^2 \, Gv^2$$

$$- 2\,Gv^4 \, ew \, ev + Gu^4 \, ew^2 + Gu^4 \, eu^2 + Gv^4 \, ew^2 + Gv^4 \, ev^2$$

$$- 2\,om^4 \, mu^2 \, ew^2 \, ev \, eu + 2\,om^2 \, mu^2 \, ew^2 \, ev \, Gu$$

$$- 2\,om^2 \, mu^2 \, ew \, ev \, Gu^2 \, eu - 2\,om^2 \, mu^2 \, ew \, ev \, Gv^2$$

$$+ 2\,om^2 \, mu^2 \, ew \, ev \, Gv^2 - 2\,om^2 \, mu^2 \, ew \, eu \, Gu^2$$

$$+ 2\,om^2 \, mu^2 \, ew \, eu^2 \, Gu^2 + 2\,om^2 \, mu^2 \, ew \, eu \, Gv^2$$

$$- 2\,om^2 \, mu^2 \, ew \, eu \, Gv^2 \, ev)^{1/2}$$

```
% The second eigenpolarization DBTM.
DBTMu=eu*Eu;
DBTMv=ev*Ev;
DBTMw=ew*Ew;
% To test that the second eigenpolarization is perpendicular (in the complex sense)
% to the propagation vector.
GBTM=simple(Gu*eu*Eu+Gv*ev*Ev+Gw*ew*Ew);
pretty(GBTM)
```

0

```
% To test if the two eigenpolarizations are perpendicular to one another.
pretty(simple(DTOPu*DBTMu+DTOPv*DBTMv+DTOPw*DBTMw))

        2   2      2        2   2     2                2      2   2
   (4 Ev  Gv  ew  eu  - 4 Ev  eu  om    mu  ew ev + 4 Ev  ew eu  Gu

             2   2    2         2        2   2   2        2   2      2
        + 4 Ev  eu om    mu  ew  - 4 Ev  eu  Gv  ev - 4 Ev  eu  ev Gu

             2     2   2       2         2   2       2      2          2
        + 4 Ev  eu Gv  ev  + 4 Ev  eu ev  Gu  + 4 Ev  eu om    mu  ew ev +

        2   2 1/2       2                 2           2      2
      ew  Ev  2    ((-om    mu  ew eu - om    mu  ew ev - Gu  ew - Gu  eu

           2       2         1/2         2
        - Gv  ew - Gv  ev + %1)/ew)    (- (2 om    mu  ew eu

             2            2         2        2        2
        + 2 om    mu  ew ev + 2 Gu  ew + 2 Gu  eu + 2 Gv  ew + 2 Gv  ev + 2 %1

           1/2       2   2   2        2   2   2       2     2   2 1/2
      )/ew)    eu - 4 Ev  ev  Gv  ew - 4 Ev  ev  om    mu  ew  - ew  Ev  2

           2                2         2        2        2        2
      ((-om    mu  ew eu - om    mu  ew ev - Gu  ew - Gu  eu - Gv  ew - Gv  ev

             1/2        2             2             2
        + %1)/ew)    (- (2 om    mu  ew eu + 2 om    mu  ew ev + 2 Gu  ew

             2        2        2         1/2        2   2      2
        + 2 Gu  eu + 2 Gv  ew + 2 Gv  ev + 2 %1)/ew)    ev - 4 Ev  ev  ew Gu

           /        2           2        2        2        2
      )  /  (4 om    mu  ew eu - 4 om    mu  ew  + 4 Gv  eu + 4 Gu  eu
        /

           2           2
        - 4 Gv  ew - 4 Gu  ew)
```

$$
\begin{aligned}
\%1 := (&\mathrm{om}^4\ \mathrm{mu}^2\ \mathrm{ew}^2\ \mathrm{ev}^2 + \mathrm{om}^4\ \mathrm{mu}^2\ \mathrm{ew}^2\ \mathrm{eu}^2 - 2\ \mathrm{Gu}^2\ \mathrm{ew}\ \mathrm{Gv}^2\ \mathrm{ev} \\
&- 2\ \mathrm{Gu}^2\ \mathrm{eu}\ \mathrm{Gv}^2\ \mathrm{ew} + 2\ \mathrm{Gu}^2\ \mathrm{eu}\ \mathrm{Gv}^2\ \mathrm{ev} - 2\ \mathrm{Gu}^4\ \mathrm{ew}\ \mathrm{eu} + 2\ \mathrm{Gu}^2\ \mathrm{ew}^2\ \mathrm{Gv}^2 \\
&- 2\ \mathrm{Gv}^4\ \mathrm{ew}\ \mathrm{ev} + \mathrm{Gu}^4\ \mathrm{ew}^2 + \mathrm{Gu}^4\ \mathrm{eu}^2 + \mathrm{Gv}^4\ \mathrm{ew}^2 + \mathrm{Gv}^4\ \mathrm{ev}^2 \\
&- 2\ \mathrm{om}^4\ \mathrm{mu}^2\ \mathrm{ew}^2\ \mathrm{ev}\ \mathrm{eu} + 2\ \mathrm{om}^2\ \mathrm{mu}^2\ \mathrm{ew}^2\ \mathrm{ev}\ \mathrm{Gu}^2 \\
&- 2\ \mathrm{om}^2\ \mathrm{mu}^2\ \mathrm{ew}\ \mathrm{ev}\ \mathrm{Gu}^2\ \mathrm{eu} - 2\ \mathrm{om}^2\ \mathrm{mu}^2\ \mathrm{ew}^2\ \mathrm{ev}\ \mathrm{Gv}^2 \\
&+ 2\ \mathrm{om}^2\ \mathrm{mu}^2\ \mathrm{ew}\ \mathrm{ev}\ \mathrm{Gv}^2 - 2\ \mathrm{om}^2\ \mathrm{mu}^2\ \mathrm{ew}^2\ \mathrm{eu}\ \mathrm{Gu}^2 \\
&+ 2\ \mathrm{om}^2\ \mathrm{mu}^2\ \mathrm{ew}\ \mathrm{eu}^2\ \mathrm{Gu}^2 + 2\ \mathrm{om}^2\ \mathrm{mu}^2\ \mathrm{ew}\ \mathrm{eu}\ \mathrm{Gv}^2 \\
&- 2\ \mathrm{om}^2\ \mathrm{mu}^2\ \mathrm{ew}\ \mathrm{eu}\ \mathrm{Gv}^2\ \mathrm{ev})^{1/2}
\end{aligned}
$$

After some algebric manipulations, the result becomes:

$$
\vec{D}' \cdot \vec{D}'' = -E_v^2 \left(\frac{\varepsilon_u - \varepsilon_v}{\varepsilon_u - \varepsilon_w} \right) \left(\varepsilon_u \varepsilon_v - \varepsilon_w(\varepsilon_u + \varepsilon_v) + \varepsilon_w^{3/2} \sqrt{ \frac{\omega^2 \mu_o \varepsilon_u \varepsilon_v + \varepsilon_u \gamma_u^2 + \varepsilon_v \gamma_v^2}{\omega^2 \mu_o \varepsilon_w + \gamma_u^2 + \gamma_v^2} } \right) \tag{E.28}
$$

For an isotropic medium, we have $\varepsilon_u = \varepsilon_v = \varepsilon_w \equiv \varepsilon$ and Equation (E.28) becomes:

$$
\vec{D}' \cdot \vec{D}'' = \left(\frac{0}{0} \right) (0) \rightarrow 0
$$

as expected. For a uniaxial medium with the optic axis parallel to $\hat{w}$, i.e. with $\varepsilon_u = \varepsilon_v$, it is clear that Equation (E.28) produces:

$$
\vec{D}' \cdot \vec{D}'' = 0
$$

in agreement with Section E.1.1. For a uniaxial medium with the optic axis parallel to $\hat{u}$, i.e. with $\varepsilon_v = \varepsilon_w$, Equation (E.28) becomes:

$$\vec{D}' \cdot \vec{D}'' = E_v^2 \varepsilon_w^2 \left(1 - \sqrt{\frac{\omega^2 \mu_o \varepsilon_u + (\varepsilon_u/\varepsilon_w)\gamma_u^2 + \gamma_v^2}{\omega^2 \mu_o \varepsilon_w + \gamma_u^2 + \gamma_v^2}} \right)$$

which is the same expression as that shown in Section E.1.2 and produces a null result when the optic axis lies in a planar interface. For a uniaxial medium with the optic axis parallel to $\hat{v}$, i.e. with $\varepsilon_u = \varepsilon_w$, we know that $E_v = 0$ and thus, Equation (E.28) becomes:

$$\vec{D}' \cdot \vec{D}'' = \left(\frac{0^2}{0} \right) \rightarrow 0$$

in agreement with Section E.1.3.

Therefore, we see that Equation (E.28) produces the expected null result for isotropic or uniaxial media. However, for lossy biaxial media, Equation (E.28) produces $(\vec{D}' \cdot \vec{D}'') \neq 0$. In fact, this result remains the same for a lossless biaxial medium whereby the permittivities are real-valued and $\gamma \equiv jk$. Therefore, this result is **NOT** in agreement with the information shown in References [75, p. 672] and [7, p. 196].

Appendix F

Matlab program to obtain the GSM for a free-standing isotropic slab

```
syms RHH REE RHE REH THH TEE THE TEH unreal
syms GzHp GzHm GzEp GzEm unreal
syms d real

%------------------------------------------------------------------------
% Since this formulation uses reciprocity, then GzHp=GzHm, and GzEp=GzEm.
syms GzH GzE Gz unreal
GzHm=GzHp;
GzEm=GzEp;
%------------------------------------------------------------------------


GHp=GzHp/Gz;
GHm=GzHm/Gz;
GEp=GzEp/Gz;
GEm=GzEm/Gz;

CII11(1,1)=-RHH;
CII11(2,2)=-REE;
CII11(1,2)=-RHE;
CII11(2,1)=-REH;
CII22(1,1)=RHH;
CII22(2,2)=REE;
CII22(1,2)=RHE;
```

```
CII22(2,1)=REH;
CII21(1,1)= THH*GHm;
CII21(2,2)= TEE*GEm;
CII21(1,2)=-THE*GHm;
CII21(2,1)=-TEH*GEm;
CII12(1,1)=THH;
CII12(2,2)=TEE;
CII12(1,2)=THE;
CII12(2,1)=TEH;

CII=[CII11 CII12; CII21 CII22];

CI11(1,1)=RHH;
CI11(2,2)=REE;
CI11(1,2)=RHE;
CI11(2,1)=REH;
CI22(1,1)=-RHH;
CI22(2,2)=-REE;
CI22(1,2)=-RHE;
CI22(2,1)=-REH;
CI21(1,1)=THH;
CI21(2,2)=TEE;
CI21(1,2)=THE;
CI21(2,1)=TEH;
CI12(1,1)= THH*GHp;
CI12(2,2)= TEE*GEp;
CI12(1,2)=-THE*GHp;
CI12(2,1)=-TEH*GEp;

CI=[CI11 CI12; CI21 CI22];

Pp(1,1)=exp(-GzHp*d);
Pp(2,2)=exp(-GzEp*d);
Pp(1,2)=0;
Pp(2,1)=0;
Pm(1,1)=exp(-GzHm*d);
Pm(2,2)=exp(-GzEm*d);
Pm(1,2)=0;
Pm(2,1)=0;
HH1=inv(inv(Pp)-CI22 *Pm*CII11);
HH2=inv(inv(Pm)-CII11*Pp*CI22 );
C11=CI11 +CI12 *HH2*CII11*Pp*CI21 ;
C22=CII22+CII21*HH1*CI22 *Pm*CII12;
C12=CI12 *HH2*CII12;
C21=CII21*HH1*CI21 ;
```

234

```
C11=simple(C11);
C12=simple(C12);
C21=simple(C21);
C22=simple(C22);

CC=[C11 C12; C21 C22];


R=simple(C11-C22)

R =

[ 0, 0]
[ 0, 0]


T=simple(C21-C12)

T =

[ 0, 0]
[ 0, 0]
```

```
%RHH_composite=C11(1,1)
pretty(C11(1,1))


                                                    2
   (RHH  Gz  - 2 RHH  Gz  RHE  %2 REH  - RHH  Gz  REE   exp(-2 GzEp  d )

            3                                3        2
      - RHH   Gz  exp(-2 GzHp  d ) + RHH   Gz  %1 REE

                      2       2            2
      + RHH  Gz  RHE   %1 REH   - 2 RHH   Gz  RHE  %1 REH  REE

                              2                    2         2
      - GzHp  exp(-2 GzHp  d ) THH   RHH + GzHp  %1 THH   RHH  REE

                                                  2
      + GzHp  %1 THH  RHH  THE  REH  REE  - GzHp  %1 THH   REH  RHE  REE

                                                     2
      + GzHp  %2 THH  REH  THE  - GzHp  %1 THH   THE  RHE  REH

                                                  2
      - GzHp  %2 TEH  RHE  THH  + GzHp  %1 TEH  THH  RHE   REH

      + GzHp  %1 TEH  RHE  THE  REH  RHH

      - GzHp  %1 TEH  REE  THH  RHE  RHH

      + GzHp  exp(-2 GzEp  d ) TEH  REE  THE

                                    2     /
      - GzHp  %1 TEH  REE  THE  RHH ) /  (Gz  (1 - 2 RHE  %2 REH
                                    /

           2                    2                     2      2
      - REE   exp(-2 GzEp  d ) - RHH   exp(-2 GzHp  d ) + RHH   %1 REE

           2           2
      + RHE    %1 REH   - 2 RHE  %1 REH  RHH  REE ))

   %1 := exp(-2 d  (GzEp  + GzHp ))

   %2 := exp(-d  (GzEp  + GzHp ))


                                    236
```

```
%RHE_composite=C11(1,2)
pretty(C11(1,2))


                  2                              2
   (RHE   Gz  - 2 RHE    Gz  %2 REH  - RHE  Gz  REE   exp(-2 GzEp  d )


                      2                              2      2
        - RHE  Gz  RHH   exp(-2 GzHp  d ) + RHE  Gz  RHH   %1 REE


              3          2          2
        + RHE    Gz  %1 REH   - 2 RHE    Gz  %1 REH  RHH  REE


        - GzHp  exp(-2 GzHp  d ) THE  RHH  THH


                                         2                    2
        + GzHp  %1 THE  RHH  THH  REE  + GzHp  %1 THE   RHH  REH  REE


                                                              2
        - GzHp  %1 THE  REH  THH  RHE  REE  + GzHp  %2 THE   REH


                    2          2
        - GzHp  %1 THE   RHE  REH   - GzHp  %2 TEE  RHE  THH


                                   2
        + GzHp  %1 TEE  THH  RHE   REH  + GzHp  %1 TEE  RHE  THE  REH  RHH


        - GzHp  %1 TEE  REE  THH  RHE  RHH


        + GzHp  exp(-2 GzEp  d ) TEE  REE  THE


                                   2    /
        - GzHp  %1 TEE  REE  THE  RHH ) / (Gz  (1 - 2 RHE  %2 REH
                                        /


            2                     2                   2      2
        - REE   exp(-2 GzEp  d ) - RHH   exp(-2 GzHp  d ) + RHH   %1 REE


            2          2
        + RHE    %1 REH   - 2 RHE  %1 REH  RHH  REE ))

   %1 := exp(-2 d  (GzEp  + GzHp ))

   %2 := exp(-d  (GzEp  + GzHp ))
```

```
%REH_composite=C11(2,1)
pretty(C11(2,1))


                2                               2
  (REH  Gz  - 2 REH   Gz  RHE  %2 - REH  Gz  REE   exp(-2 GzEp  d )

                    2                           2        2
      - REH  Gz  RHH   exp(-2 GzHp  d ) + REH  Gz  RHH   %1 REE

            3        2             2
      + REH   Gz  RHE   %1 - 2 REH   Gz  RHE  %1 RHH  REE

      + GzEp  exp(-2 GzHp  d ) THH  RHH  TEH

                                      2
      - GzEp  %1 THH  RHH  TEH  REE   - GzEp  %1 THH  RHH  TEE  REH  REE

      + GzEp  %1 THH  REH  TEH  RHE  REE  - GzEp  %2 THH  REH  TEE

                                2                 2
      + GzEp  %1 THH  TEE  RHE  REH  + GzEp  %2 TEH   RHE

                2    2
      - GzEp  %1 TEH   RHE   REH - GzEp  %1 TEH  RHE  TEE  REH  RHH

                2
      + GzEp  %1 TEH   REE  RHE  RHH

      - GzEp  exp(-2 GzEp  d ) TEH  REE  TEE

                                2    /
      + GzEp  %1 TEH  REE  TEE  RHH ) / (Gz  (1 - 2 RHE  %2 REH
                                      /

          2                       2                       2        2
      - REE   exp(-2 GzEp  d ) - RHH   exp(-2 GzHp  d ) + RHH   %1 REE

          2    2
      + RHE   %1 REH   - 2 RHE  %1 REH  RHH  REE ))

  %1 := exp(-2 d  (GzEp  + GzHp ))

  %2 := exp(-d  (GzEp  + GzHp ))
```

238

```
%REE_composite=C11(2,2)
pretty(C11(2,2))
```

$$
\begin{aligned}
(\text{REE} \quad & \text{Gz} \quad - 2 \text{ REE} \quad \text{Gz} \quad \text{RHE} \quad \%2 \text{ REH} \quad - \text{ REE}^3 \quad \text{Gz} \quad \exp(-2 \text{ GzEp} \quad d)\\
& - \text{ REE} \quad \text{Gz} \quad \text{RHH}^2 \quad \exp(-2 \text{ GzHp} \quad d) + \text{REE}^3 \quad \text{Gz} \quad \text{RHH}^2 \quad \%1\\
& + \text{ REE} \quad \text{Gz} \quad \text{RHE}^2 \quad \%1 \text{ REH}^2 \quad - 2 \text{ REE}^2 \quad \text{Gz} \quad \text{RHE} \quad \%1 \text{ REH} \quad \text{RHH}\\
& + \text{ GzEp} \quad \exp(-2 \text{ GzHp} \quad d) \text{ THE} \quad \text{RHH} \quad \text{TEH}\\
& - \text{ GzEp} \quad \%1 \text{ THE} \quad \text{RHH} \quad \text{TEH} \quad \text{REE}^2 \quad - \text{ GzEp} \quad \%1 \text{ THE} \quad \text{RHH} \quad \text{TEE} \quad \text{REH} \quad \text{REE}\\
& + \text{ GzEp} \quad \%1 \text{ THE} \quad \text{REH} \quad \text{TEH} \quad \text{RHE} \quad \text{REE} \quad - \text{ GzEp} \quad \%2 \text{ THE} \quad \text{REH} \quad \text{TEE}\\
& + \text{ GzEp} \quad \%1 \text{ THE} \quad \text{TEE} \quad \text{RHE} \quad \text{REH}^2 \quad + \text{ GzEp} \quad \%2 \text{ TEE} \quad \text{RHE} \quad \text{TEH}\\
& - \text{ GzEp} \quad \%1 \text{ TEE} \quad \text{TEH} \quad \text{RHE}^2 \quad \text{REH} \quad - \text{ GzEp} \quad \%1 \text{ TEE}^2 \quad \text{RHE} \quad \text{REH} \quad \text{RHH}\\
& + \text{ GzEp} \quad \%1 \text{ TEE} \quad \text{REE} \quad \text{TEH} \quad \text{RHE} \quad \text{RHH}\\
& - \text{ GzEp} \quad \exp(-2 \text{ GzEp} \quad d) \text{ TEE}^2 \quad \text{REE} \quad + \text{ GzEp} \quad \%1 \text{ TEE}^2 \quad \text{REE} \quad \text{RHH}^2 \quad) \Big/ \\
& \qquad\qquad / \\
(\text{Gz} \quad & (1 - 2 \text{ RHE} \quad \%2 \text{ REH} \quad - \text{ REE}^2 \quad \exp(-2 \text{ GzEp} \quad d)\\
& - \text{ RHH}^2 \quad \exp(-2 \text{ GzHp} \quad d) + \text{ RHH}^2 \quad \%1 \text{ REE}^2 \quad + \text{ RHE}^2 \quad \%1 \text{ REH}^2\\
& - 2 \text{ RHE} \quad \%1 \text{ REH} \quad \text{RHH} \quad \text{REE} \quad))
\end{aligned}
$$

$$\%1 := \exp(-2 \, d \, (\text{GzEp} + \text{GzHp}))$$

$$\%2 := \exp(-d \, (\text{GzEp} + \text{GzHp}))$$

```
%THH_composite=C21(1,1)
pretty(C21(1,1))


              2                        2              2        2
  - GzHp  (-THH  exp(-GzHp  d ) + THH   %2 RHE   REH  + THH    %1 REE

          + THH   THE   REH   %2 RHH  + THH   THE   REH   %1 REE

          - TEH   THH   RHE   %2 RHH  - TEH   THH   RHE   %1 REE

                                                             2
          + TEH   THE   exp(-GzEp  d ) - TEH   THE   %2 RHH

                                        /
          - TEH   THE   %1 RHE   REH ) /  (Gz  (1
                                        /

                                                           2
          - 2 RHE   exp(-d  (GzEp  + GzHp )) REH  - REE   exp(-2 GzEp  d )

              2                       2                                    2
          - RHH   exp(-2 GzHp  d ) + RHH   exp(-2 d  (GzEp  + GzHp )) REE

              2                   2
          + RHE   exp(-2 d  (GzEp  + GzHp )) REH

          - 2 RHE   exp(-2 d  (GzEp  + GzHp )) REH  RHH  REE ))

  %1 := exp(-d  (GzHp  + 2 GzEp ))

  %2 := exp(-d  (GzEp  + 2 GzHp ))
```

240

```
%THE_composite=C21(1,2)
pretty(C21(1,2))

   GzHp  (THE   THH   exp(-GzHp  d ) - THE   THH   %2 RHE   REH


                          2            2                        2
        - THE   THH   %1 REE   - THE    REH   %2 RHH - THE    REH   %1 REE

        + TEE   THH   RHE   %2 RHH  + TEE   THH   RHE   %1 REE


                                                      2
        - THE   TEE   exp(-GzEp  d ) + TEE   THE   %2 RHH


                             /
        + TEE   THE   %1 RHE   REH )  /  (Gz   (1
                             /


                                                     2
        - 2 RHE   exp(-d  (GzEp  + GzHp )) REH  - REE    exp(-2 GzEp  d )

            2                         2                                      2
        - RHH    exp(-2 GzHp  d ) + RHH    exp(-2 d  (GzEp   + GzHp )) REE

          2                        2
       + RHE    exp(-2 d  (GzEp   + GzHp )) REH

        - 2 RHE   exp(-2 d  (GzEp  + GzHp )) REH   RHH   REE ))

  %1 := exp(-d  (GzHp  + 2 GzEp ))

  %2 := exp(-d  (GzEp  + 2 GzHp ))
```

```
%TEH_composite=C21(2,1)
pretty(C21(2,1))
```

$$GzEp \ (-THH \ TEH \ exp(-GzHp \ d \ ) + THH \ TEH \ \%2 \ RHE \ REH$$

$$+ \ THH \ TEH \ \%1 \ REE^2 \ + THH \ TEE \ REH \ \%2 \ RHH$$

$$+ \ THH \ TEE \ REH \ \%1 \ REE^2 \ - \ TEH^2 \ RHE \ \%2 \ RHH \ - \ TEH^2 \ RHE \ \%1 \ REE$$

$$+ \ TEH \ TEE \ exp(-GzEp \ d \ ) - TEH \ TEE \ \%2 \ RHH^2$$

$$- \ TEH \ TEE \ \%1 \ RHE \ REH \ ) \ / \ (Gz \ (1$$

$$- \ 2 \ RHE \ exp(-d \ (GzEp \ + GzHp \ )) \ REH \ - \ REE^2 \ exp(-2 \ GzEp \ d \ )$$

$$- \ RHH^2 \ exp(-2 \ GzHp \ d \ ) + RHH^2 \ exp(-2 \ d \ (GzEp \ + GzHp \ )) \ REE^2$$

$$+ \ RHE^2 \ exp(-2 \ d \ (GzEp \ + GzHp \ )) \ REH^2$$

$$- \ 2 \ RHE \ exp(-2 \ d \ (GzEp \ + GzHp \ )) \ REH \ RHH \ REE \ ))$$

$$\%1 := exp(-d \ (GzHp \ + 2 \ GzEp \ ))$$

$$\%2 := exp(-d \ (GzEp \ + 2 \ GzHp \ ))$$

```
%TEE_composite=C21(2,2)
pretty(C21(2,2))

   - GzEp  (THE   TEH  exp(-GzHp  d ) - THE   TEH   %2 RHE   REH

                        2
        - THE   TEH   %1 REE   - THE   TEE   REH   %2 RHH

        - THE   TEE   REH   %1 REE  + TEE   TEH   RHE   %2 RHH

                                      2                  2        2
        + TEE   TEH   RHE   %1 REE  - TEE   exp(-GzEp  d ) + TEE    %2 RHH

              2                   /
        + TEE   %1 RHE   REH )  /  (Gz  (1
                                  /

                                                      2
        - 2 RHE  exp(-d  (GzEp  + GzHp )) REH  - REE   exp(-2 GzEp  d )

              2                       2                               2
        - RHH   exp(-2 GzHp  d ) + RHH   exp(-2 d  (GzEp  + GzHp )) REE

              2                           2
        + RHE   exp(-2 d  (GzEp  + GzHp )) REH

        - 2 RHE  exp(-2 d  (GzEp  + GzHp )) REH   RHH   REE ))

  %1  :=  exp(-d  (GzHp  + 2 GzEp ))

  %2  :=  exp(-d  (GzEp  + 2 GzHp ))
```

Appendix G

Estimation of the uncertainty in measuring the direct ray due to the presence of the reflected ray from the mounting plate

Figure G.1 depicts the phenomenon of the reflection off the mounting plate, according to the principle of geometrical optics, i.e. each ray is assumed to be a beam of infinitesimal width[1] . For simplicity, both the transmitter and the receiver are taken to be dimensionless as if they were two points in free space. Consequently, we can assume that only one specular reflected ray comes to perturb the measurement of the direct ray. The power radiation pattern for the receiving horn is approximated as a squared cosine function with a single beam of about 60° width between the two -3 dB points, i.e. $P_{dB}(\psi) \approx 9.05 - 20 \log_{10}(\cos(1.5\psi°))$ where $\psi°$ refers to the ψ value in degrees, and 9.05 refers to the gain (in dB) measured at $\psi = 0°$.

The two limit cases are:

1. $\theta = 0° \implies c = 0°$;

2. $\theta = 90° \implies H\tan(c) = \frac{R}{2} \implies c = \arctan\left(\frac{R}{2H}\right)$.

---

[1]When the array is small, the diffraction of a plane wave around the edges of the array causes the actual value of the reflection angle to be slightly off the specular value [83]. This effect was neglected here.

From simple geometrical considerations, one obtains:

$$
\begin{aligned}
L &= \sqrt{R^2 + \frac{H^2}{\cos^2(c)} - \frac{2RH}{\cos(c)}\cos(180° - (\theta + c))} \\
&= \sqrt{R^2 + \frac{H^2}{\cos^2(c)} + \frac{2RH}{\cos(c)}\cos(\theta + c)}
\end{aligned}
$$

and:

$$
\frac{H^2}{\cos^2(c)} = R^2 + L^2 - 2RL\cos(\theta - c)
$$

After substituting for L and carrying out some algebraic manipulations valid for $\cos(c) \neq 0$, one obtains the following polynomial in $X = \cos(\theta + c)$:

$$
\begin{aligned}
&\left[(R^2\cos^2(c) + H^2 + 2RH\cos(c)X)\left(\sin^2(2c) + \cos(4c)X^2\right)\right. \\
&\quad \left. - (R^2\cos^2(c) + H^2X^2 + 2RH\cos(c)X)\right]^2 \\
&- \left[R^2\cos^2(c) + H^2 + 2RH\cos(c)X\right]^2\sin^2(c)(X^2 - X^4) = 0
\end{aligned}
\tag{G.1}
$$

Since the degree of this polynomial exceeds four, its solution cannot be obtained in closed form. However, a numerical solution is possible whereby X can be obtained for a given value of c provided that the correct solution is carefully selected from the multiple values at which the polynomial goes to zero. This selection is made from the knowledge that the solution is monotonic and from the knowledge of the two limit cases presented above. The results for the case $R = 3.35$ m and $H = 0.50$ m are shown in Figures G.2 and G.3. The solution can be readily approximated with a quadratic polynomial $\theta° = -0.0013(c°)^2 + 1.3251c°$ where $\theta°$ and $c°$ refer to the values of θ and c in degrees. A constraint of zero offset was applied to the regression process in order to insure that $\theta = 0°$ when $c = 0°$. This polynomial can be readily inverted to obtain the knowledge of c as a function of θ. One obtains:

$$
c° = -\frac{1.3251}{2(-0.0013)}\left(1 - \sqrt{1 + \frac{4(-0.0013)}{(1.3251)^2}\theta°}\right) = 509.6538\left(1 - \sqrt{1 - 0.0030\,\theta°}\right)
\tag{G.2}
$$

Figure G.4 shows the steps involved in estimating the relative difference in magnitude and phase between the phasor corresponding to the reflected ray and the phasor corresponding to the direct ray. Since the measurement result corresponds to the vectorial addition of these two phasors, the measurement error introduced by the presence of the reflected ray could be estimated if we had the knowledge of the magnitude and phase values of each phasor. However, we only have the knowledge of the result of the vectorial addition since, by definition, the radiation pattern of the transmitter which affects both the direct and the reflected rays is unknown.

In the absence of the knowledge of the phase value of each phasor, the result of the vectorial addition can range from a minimum value $|E|_{min} = |E_D| - |E_R| = |E_D|(1 - \frac{|E_R|}{|E_D|})$ to a maximum value $|E|_{max} = |E_D| + |E_R| = |E_D|(1 + \frac{|E_R|}{|E_D|})$ where $|E|$ refers to the magnitude of the electric field for the desired polarization at the receiving horn, and the subscripts D and R refer to the direct and the reflected rays, respectively. Note that forming the ratio:

$$\frac{|E|_{max}}{|E|_{min}} = \frac{1 + \frac{|E_R|}{|E_D|}}{1 - \frac{|E_R|}{|E_D|}}$$

results in an expression equivalent to that for the VSWR of the transmission line theory.

Now, we have $\frac{|E_R|}{|E_D|} = \nu\sqrt{P(180° - c)/P(\theta)}$ where P is the radiated power value (on a linear scale) that would be measured if there were no reflection, and ν is a fractional constant that takes into account all the additional losses that the reflected ray incurs over the direct ray. These losses are:

- the loss due to the reflection coefficient of the mounting plate, i.e. $\nu_1 = R(c)$;

- the excess propagation loss due to the excess propagation length, i.e.

$$\nu_2 = \frac{R}{\left(\frac{H}{\cos(c)} + L\right)} = \left(\frac{H}{R\cos(c)} + \sqrt{1 + \left(\frac{H}{R\cos(c)}\right)^2 + \frac{2H}{R\cos(c)}\cos(\theta + c)}\right)^{-1}$$

- the loss due to the fact that the reflected ray is incident at $\psi = (\theta - c)$ rather than $\psi = 0$ on the radiation pattern of the horn: $\nu_3 = \cos(1.5(\theta° - c°))$.

thus, $\nu = \nu_1\nu_2\nu_3$. Hence, the knowledge of $P(180° - c)/P(\theta)$ yields the knowledge of $|E_R|/|E_D|$ which represents the fractional error of the measurement. Now, writing

$$\frac{|E_R|}{|E_D|} = \nu\sqrt{\frac{P(180° - c)}{P(\theta)}} = \frac{\nu\sqrt{P(180° - c)}}{\sqrt{P(\theta)}}$$

suggests that one thinks as $|E_D| = \sqrt{P(\theta)}$ and $|E_R| = \nu\sqrt{P(180° - c)}$.

One approximate way to obtain the knowledge of the ratio $P(180° - c)/P(\theta)$ is to assume that $P(\theta)$ and $P(180° - c)$ are known from two separate measurements, i.e. $P(\theta) = \mathcal{P}(\theta_1)$ and $P(180° - c) = \mathcal{P}(\theta_2)$, even though each measurement value, $\mathcal{P}(\theta_1)$ and $\mathcal{P}(\theta_2)$, is corrupted by the presence of a reflected ray. This leads to having:

$$\left(\frac{|E_R|}{|E_D|}\right)_1 = \nu\sqrt{\frac{P(180° - c)}{P(\theta)}} \approx \nu\sqrt{\frac{\mathcal{P}(\theta_2)}{\mathcal{P}(\theta_1)}} = \frac{(|\mathcal{E}_D|)_2}{(|\mathcal{E}_D|)_1} = \frac{\left(\left|E_D(1+\frac{E_R}{E_D})\right|\right)_2}{\left(\left|E_D(1+\frac{E_R}{E_D})\right|\right)_1}$$
$$(\text{G}.3)$$

However, since θ_2 exceeds 90°, the mounting plate would lie between the transmitter and the receiving horn. This situation must be avoided by merely re-mounting the transmitter onto the plate after giving the transmitter an additional half-turn rotation about the single point representing the transmitter. This single point is the origin of the reference coordinate system with respect to which the radiation pattern of the transmitter is being measured. This point lies at the intersection of the rotation axis for the azimuth positioner and the rotation axis for the roll positioner. From Figure G.5, it becomes apparent that the reflection angle value for the second measurement e is generally different from that for the first measurement c. The value for e is obtained from Equation (G.2) with θ replaced by c. From the knowledge of the values for c and e, we compute the corresponding value for ν and the corresponding fractional error for the second measurement. Therefore, one obtains:

$$\left(\frac{|E_R|}{|E_D|}\right)_1 \doteq (\nu)_1\sqrt{\frac{P(180° - c)}{P(\theta)}} \tag{G.4}$$

$$\left(\frac{|E_R|}{|E_D|}\right)_2 = (\nu)_2\sqrt{\frac{P(e)}{P(c)}} \tag{G.5}$$

where $P(c)$ for the second measurement corresponds to $P(180° - c)$ for the first measurement as a result of the half-turn rotation of the transmitter for the second measurement. Now, the suggestion that one thinks as $|E_D| = \sqrt{P(\theta)}$ and $|E_R| = \nu\sqrt{P(180° - c)}$ leads to the concept that $(|E_R|)_1 = (\nu)_1\sqrt{P(180° - c)} = (\nu)_1\sqrt{P(c)} = (\nu)_1(|E_D|)_2$. Repeating the process for estimating $(|E_R|)_2$ from a third measurement leads to $(|E_R|)_2 = (\nu)_2(|E_D|)_3$. If this process is carried out repeatedly, it leads to $(|E_R|)_k = (\nu)_k(|E_D|)_{k+1}$. With every successive iteration, the reflection angle value becomes smaller

until it reaches zero in which case the direct and the reflected rays can no longer be separated. The process would also stop if $(\nu)_k$ became so small that $(|E_R|)_k$ was truly small enough to be neglected. However, instead of repeating the process many times without guarantee that the process would terminate successfully, one can proceed as follows. Substitute the value of $P(c)$ in Equation (G.5) for the value of $P(180° - c)$ in Equation (G.4) to obtain:

$$\left(\frac{|E_R|}{|E_D|}\right)_2 = (\nu)_1(\nu)_2\sqrt{\frac{P(e)}{P(\theta)}}\left(\frac{|E_D|}{|E_R|}\right)_1 \tag{G.6}$$

Then, substitute $\sqrt{P(e)} = (|E_D|)_3$ and $\sqrt{P(\theta)} = (|E_D|)_1$ in Equation (G.6) to obtain:

$$\left(\frac{|E_R|}{|E_D|}\right)_2 = (\nu)_1(\nu)_2\frac{(|E_D|)_3}{(|E_D|)_1}\left(\frac{|E_D|}{|E_R|}\right)_1 \tag{G.7}$$

and let us estimate the effect that the error on each measurement has onto the desired quantity $(\frac{|E_R|}{|E_D|})_1$ by making allowance for these errors as yet unknown. From Equation (G.3), one obtains:

$$\begin{aligned}\left(\frac{|E_R|}{|E_D|}\right)_1 &\approx \frac{\left(\left|E_D(1+\frac{E_R}{E_D})\right|\right)_2}{\left(\left|E_D(1+\frac{E_R}{E_D})\right|\right)_1} \\ &\approx \frac{(|E_D|)_2}{(|E_D|)_1}\frac{\left(|1+\frac{E_R}{E_D}|\right)_2}{\left(|1+\frac{E_R}{E_D}|\right)_1}\end{aligned} \tag{G.8}$$

Assuming that we do not have the knowledge of the phase values for E_R and E_D, the magnitude for $\left(|1+\frac{E_R}{E_D}|\right)_1$ can range from $1 - \left(\frac{|E_R|}{|E_D|}\right)_1$ to $1 + \left(\frac{|E_R|}{|E_D|}\right)_1$ and similarly, the magnitude for $\left(|1+\frac{E_R}{E_D}|\right)_2$ can range from $1 - \left(\frac{|E_R|}{|E_D|}\right)_2$ to $1 + \left(\frac{|E_R|}{|E_D|}\right)_2$. Therefore, the maximum error for $(\frac{|E_R|}{|E_D|})_1$ in Equation (G.8) is that which maximizes the numerator while also minimizing the denominator. Similarly, the minimum error for $(\frac{|E_R|}{|E_D|})_1$ in Equation (G.8) is that which minimizes the numerator while also maximizing the denominator. For the case of the maximum error, one obtains:

$$\left(\frac{|E_R|}{|E_D|}\right)_1 \approx \frac{(|E_D|)_2}{(|E_D|)_1} \frac{1+\left(\frac{|E_R|}{|E_D|}\right)_2}{1-\left(\frac{|E_R|}{|E_D|}\right)_1}$$

$$\approx \frac{\frac{(|E_D|)_2}{(|E_D|)_1}+(\nu)_1(\nu)_2\frac{(|E_D|)_2(|E_D|)_3}{(|E_D|)_1^2}\left(\frac{|E_D|}{|E_R|}\right)_1}{1-\left(\frac{|E_R|}{|E_D|}\right)_1}$$

(G.9)

where Equation (G.7) was used under the assumption that the reflected and the directed rays could still be separated on the third measurement. Collecting the terms leads to the following polynomial in the variable $V = \left(\frac{|E_R|}{|E_D|}\right)_1$:

$$-V^3 + V^2 - \frac{(|E_D|)_2}{(|E_D|)_1}V - (\nu)_1(\nu)_2\frac{(|E_D|)_2(|E_D|)_3}{(|E_D|)_1^2} \approx 0 \qquad \text{(G.10)}$$

the solution of which is given by:

$$V = \frac{1}{6}\frac{-U^2 + 2U + 12t - 4}{U} \qquad \text{(G.11)}$$

where:

$$t = \frac{(|E_D|)_2}{(|E_D|)_1}$$

$$u = \frac{(|E_D|)_3}{(|E_D|)_1}$$

$$U = \left(+108(\nu)_1(\nu)_2tu - 12\sqrt{3}\,tP + 36t - 8\right)^{1/3}$$

$$P = \sqrt{27(\nu)_1^2(\nu)_2^2tu^2 + 18(\nu)_1(\nu)_2tu + 4t^2 - t - 4(\nu)_1(\nu)_2u}$$

Similarly, for the case of the minimum error, one obtains:

$$\left(\frac{|E_R|}{|E_D|}\right)_1 \approx \frac{(|E_D|)_2}{(|E_D|)_1} \frac{1-\left(\frac{|E_R|}{|E_D|}\right)_2}{1+\left(\frac{|E_R|}{|E_D|}\right)_1}$$

$$\approx \frac{\frac{(|E_D|)_2}{(|E_D|)_1}-(\nu)_1(\nu)_2\frac{(|E_D|)_2(|E_D|)_3}{(|E_D|)_1^2}\left(\frac{|E_D|}{|E_R|}\right)_1}{1+\left(\frac{|E_R|}{|E_D|}\right)_1}$$

(G.12)

which leads to the following polynomial:

$$+V^3 + V^2 - \frac{(|E_D|)_2}{(|E_D|)_1}V + (\nu)_1(\nu)_2\frac{(|E_D|)_2(|E_D|)_3}{(|E_D|)_1^2} \approx 0 \qquad \text{(G.13)}$$

the solution of which is given by:

$$V = \frac{1}{6}\,\frac{W^2 - 2W + 12t + 4}{W} \qquad \text{(G.14)}$$

where:

$$W = \left(-108(\nu)_1(\nu)_2 tu + 12\sqrt{3}\,tQ - 36t - 8\right)^{1/3}$$

$$Q = \sqrt{27(\nu)_1^2(\nu)_2^2 tu^2 + 18(\nu)_1(\nu)_2 tu - 4t^2 - t + 4(\nu)_1(\nu)_2 u}$$

Although $t = \frac{(|E_D|)_2}{(|E_D|)_1}$ and $u = \frac{(|E_D|)_3}{(|E_D|)_1}$ are still unknown, we can approximate them as $\frac{(|\mathcal{E}_D|)_2}{(|\mathcal{E}_D|)_1}$ and $\frac{(|\mathcal{E}_D|)_3}{(|\mathcal{E}_D|)_1}$, respectively, in a way similar to what we did in Equation (G.3). The advantage in computing $\left(\frac{|E_R|}{|E_D|}\right)_1$ from Equations (G.11) and (G.14) rather than Equation (G.3) is two-fold:

1. Equations (G.11) and (G.14) with t and u approximated as $\frac{(|\mathcal{E}_D|)_2}{(|\mathcal{E}_D|)_1}$ and $\frac{(|\mathcal{E}_D|)_3}{(|\mathcal{E}_D|)_1}$, respectively, yield an approximate knowledge of the upper and the lower bounds for the fractional error, respectively;

2. the level of approximation involved in taking $t = \frac{(|E_D|)_2}{(|E_D|)_1} \approx \frac{(|\mathcal{E}_D|)_2}{(|\mathcal{E}_D|)_1}$ in Equations (G.11) and (G.14) is smaller than that involved in computing directly $\left(\frac{|E_R|}{|E_D|}\right)_1 \approx \frac{(|\mathcal{E}_D|)_2}{(|\mathcal{E}_D|)_1}$ since V depends on $\frac{(|\mathcal{E}_D|)_2}{(|\mathcal{E}_D|)_1}$ or $\frac{(|\mathcal{E}_D|)_2(|\mathcal{E}_D|)_3}{(|\mathcal{E}_D|)_1^2}$ in the power 2/3 or less, whereas $\left(\frac{|E_R|}{|E_D|}\right)_1 \approx \frac{(|\mathcal{E}_D|)_2}{(|\mathcal{E}_D|)_1}$ depends on $\frac{(|\mathcal{E}_D|)_2}{(|\mathcal{E}_D|)_1}$ in the power 3/3.

From now on, we will assume that Equations (G.11) and (G.14) have t and u approximated as $\frac{(|\mathcal{E}_D|)_2}{(|\mathcal{E}_D|)_1}$ and $\frac{(|\mathcal{E}_D|)_3}{(|\mathcal{E}_D|)_1}$, respectively. Therefore, one can estimate the fractional error on each measurement $\left(\frac{|E_R|}{|E_D|}\right)_k$ in terms of an upper and a lower bound given by Equations (G.11) and (G.14), respectively, from the knowledge of three measurements $(\mathcal{E}_D)_k$, $(\mathcal{E}_D)_{k+1}$ and $(\mathcal{E}_D)_{k+2}$ corresponding, respectively, to angles θ, $(180° - c)$ and e defined with respect to the radiation pattern of the transmitter. This process could be generalized to include more than three measurements but the corresponding polynomial might become unwieldy and thus, this generalization will not be attempted here.

The true value corresponding to a measurement can thus range from a minimum value $|E|_{min} = |E_D| \left[1 - \left(\frac{|E_R|}{|E_D|} \right)_{max} \right]$ to a maximum value $|E|_{max} = |E_D| \left[1 + \left(\frac{|E_R|}{|E_D|} \right)_{max} \right]$. However, this estimate is with respect to the true value $|E_D|$ rather than with respect to the measured value $|\mathcal{E}_D|$. Since we do not know the true value, we must assume the worst case situation whereby the true and the measured values are separated by the maximum uncertainty $\left(\frac{|E_R|}{|E_D|} \right)_{max}$. Therefore, the true value $|E_D|$ lies in the range of $|\mathcal{E}_D| \pm \left(\frac{|E_R|}{|E_D|} \right)_{max}$ with $\left(\frac{|E_R|}{|E_D|} \right)_{max}$ given by Equation (G.11) where t and u are approximated as $\frac{(|\mathcal{E}_D|)_2}{(|\mathcal{E}_D|)_1}$ and $\frac{(|\mathcal{E}_D|)_3}{(|\mathcal{E}_D|)_1}$, respectively. A more liberal estimation of the error could use the geometrical mean of $\left(\frac{|E_R|}{|E_D|} \right)_{min}$ and $\left(\frac{|E_R|}{|E_D|} \right)_{max}$ instead of just the maximum value $\left(\frac{|E_R|}{|E_D|} \right)_{max}$. The corresponding true value $|E_D|$ would then lie in the range of $|\mathcal{E}_D| \pm \sqrt{ \left(\frac{|E_R|}{|E_D|} \right)_{min} \left(\frac{|E_R|}{|E_D|} \right)_{max} }$ with $\left(\frac{|E_R|}{|E_D|} \right)_{min}$ and $\left(\frac{|E_R|}{|E_D|} \right)_{max}$ given by Equations (G.14) and (G.11), respectively, where t and u are again approximated as $\frac{(|\mathcal{E}_D|)_2}{(|\mathcal{E}_D|)_1}$ and $\frac{(|\mathcal{E}_D|)_3}{(|\mathcal{E}_D|)_1}$, respectively.
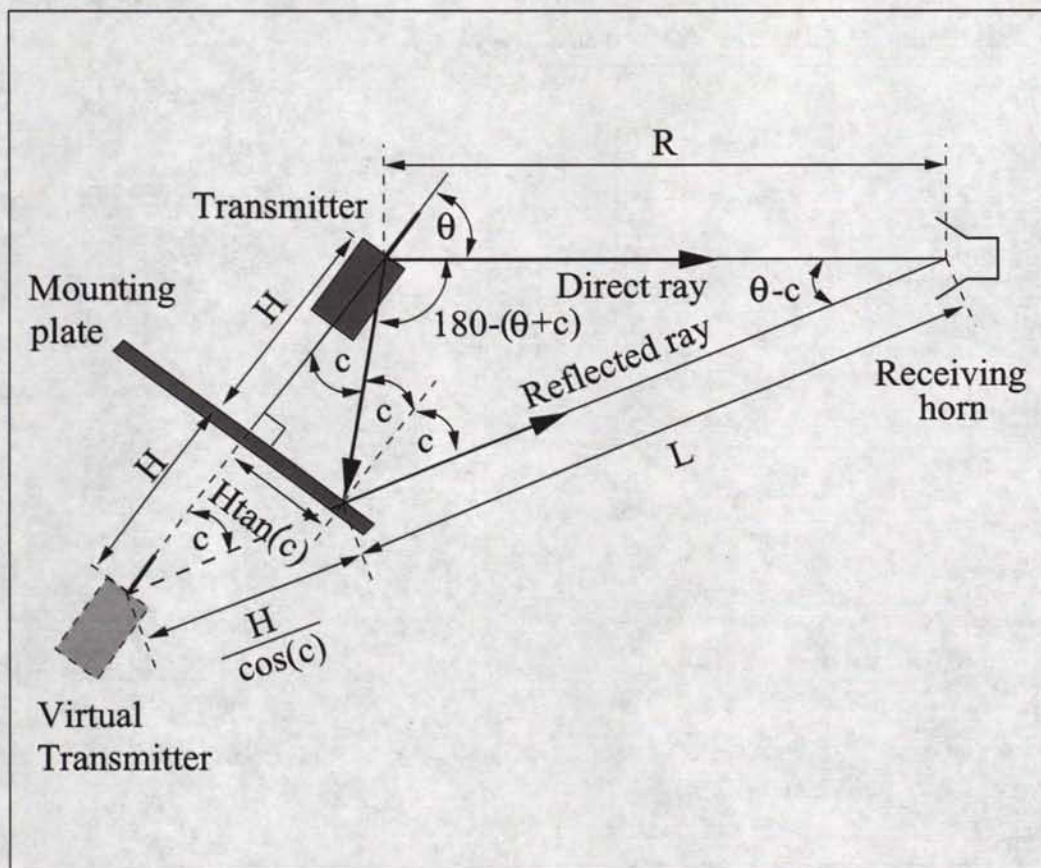
Figure G.1: The phenomenon of reflection off the mounting plate, according to the principle of geometrical optics. For simplicity, the transmitter and the receiver are taken to be dimensionless so that we can assume that only one specular reflected ray comes to perturb the measurement of the direct ray.
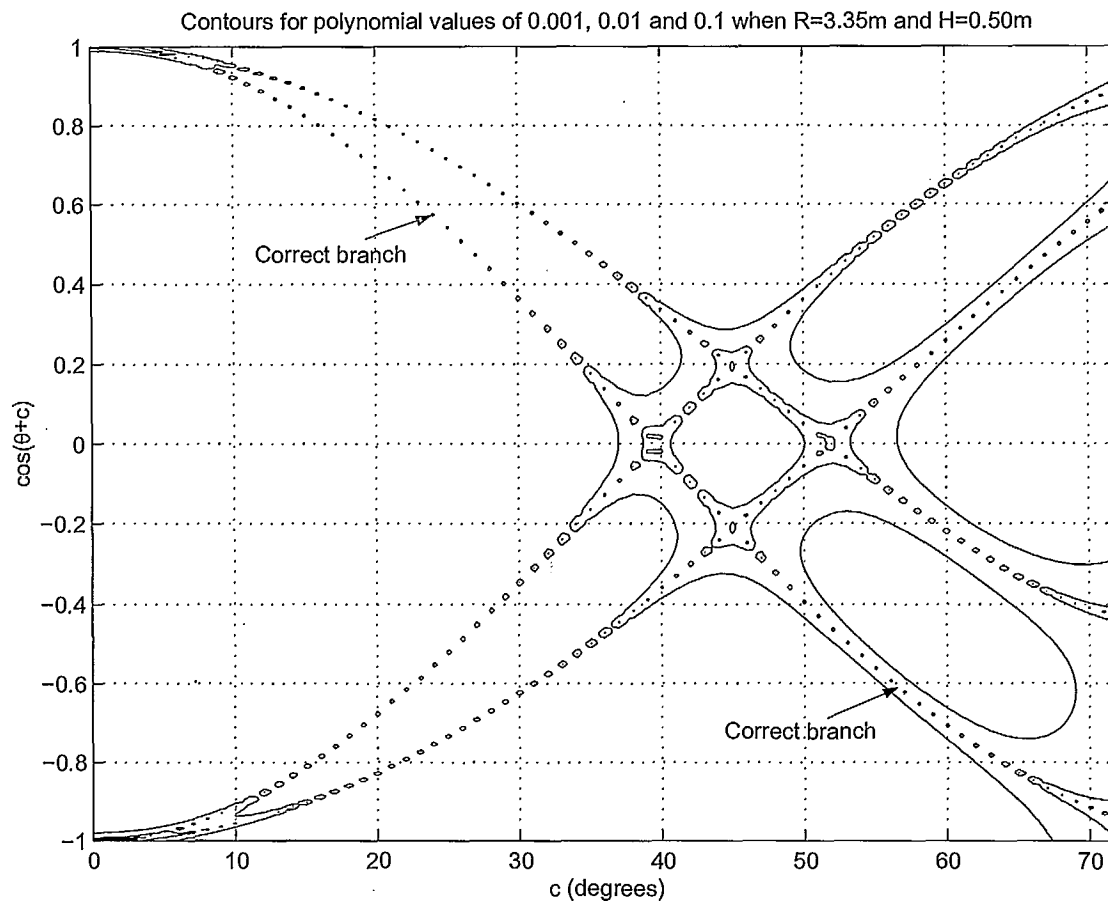
Figure G.2: The contour levels from the polynomial evaluation in Equation (G.1) for values of 0.001, 0.01 and 0.1 for the case $R = 3.35$ m and $H = 0.50$ m. The correct solution is the branch that satisfies the two limit cases: $\theta = 0°$ for $c = 0°$ and $\theta = 90°$ for $c \approx 73.4°$, corresponding to $\cos(\theta + c) = +1$ and $\cos(\theta + c) \approx -0.96$, respectively.
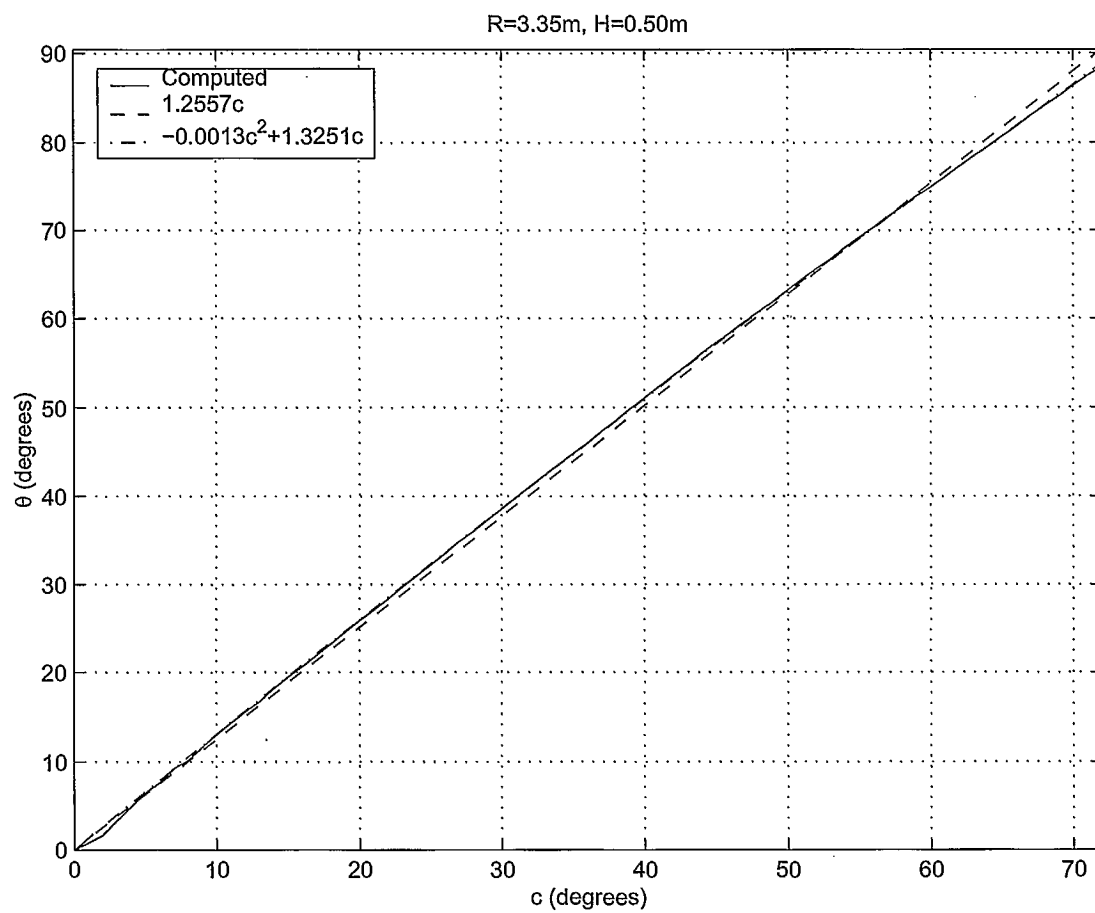
Figure G.3: The plot of θ as a function of c for the correct branch of Figure G.2. The plot shows also the results from a linear or a quadratic regression with a zero offset constraint.
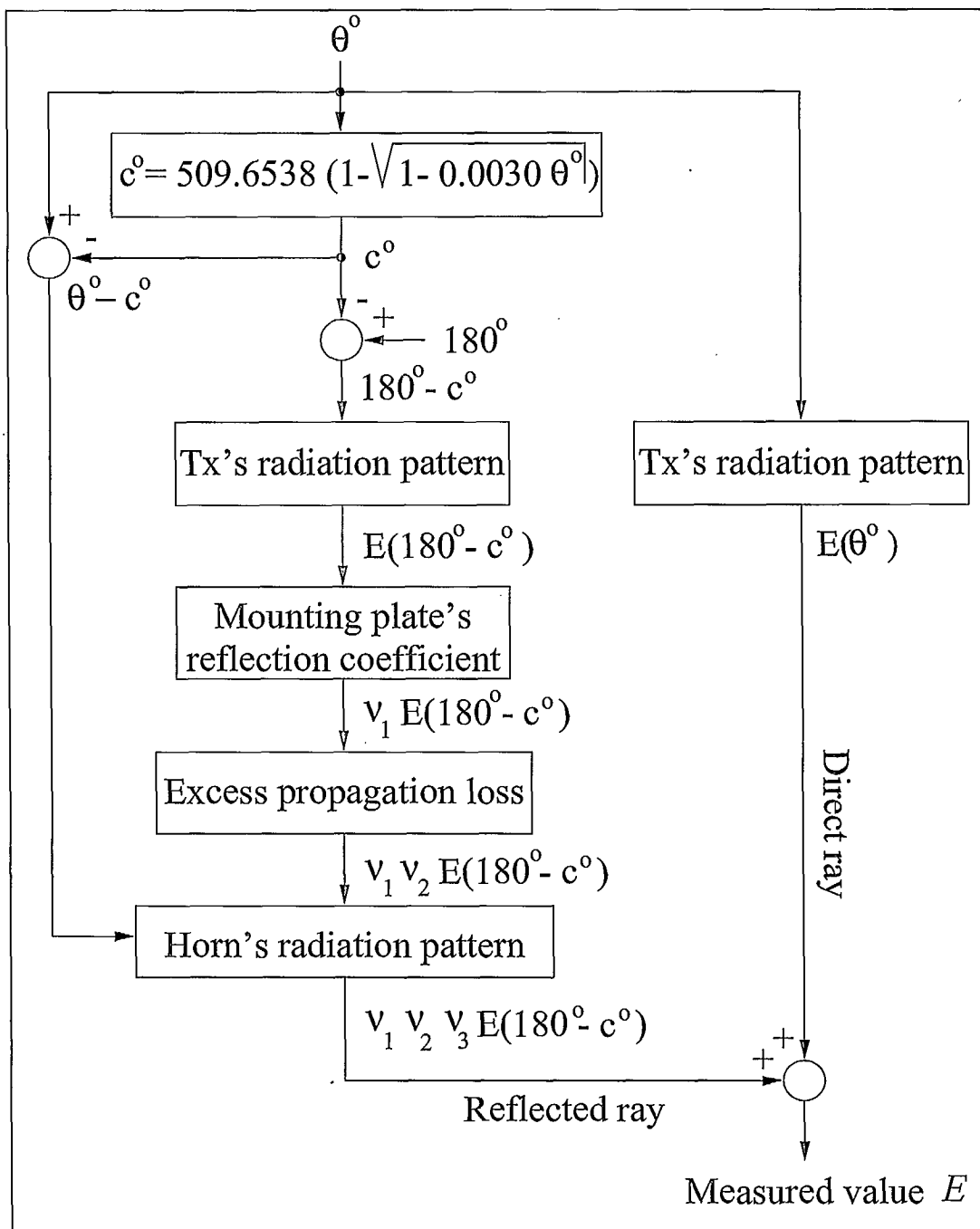
Figure G.4: The diagram showing the steps for estimating the effect of the specular reflected ray onto the measurement of the direct ray for the case $R = 3.35$ m and $H = 0.50$ m.
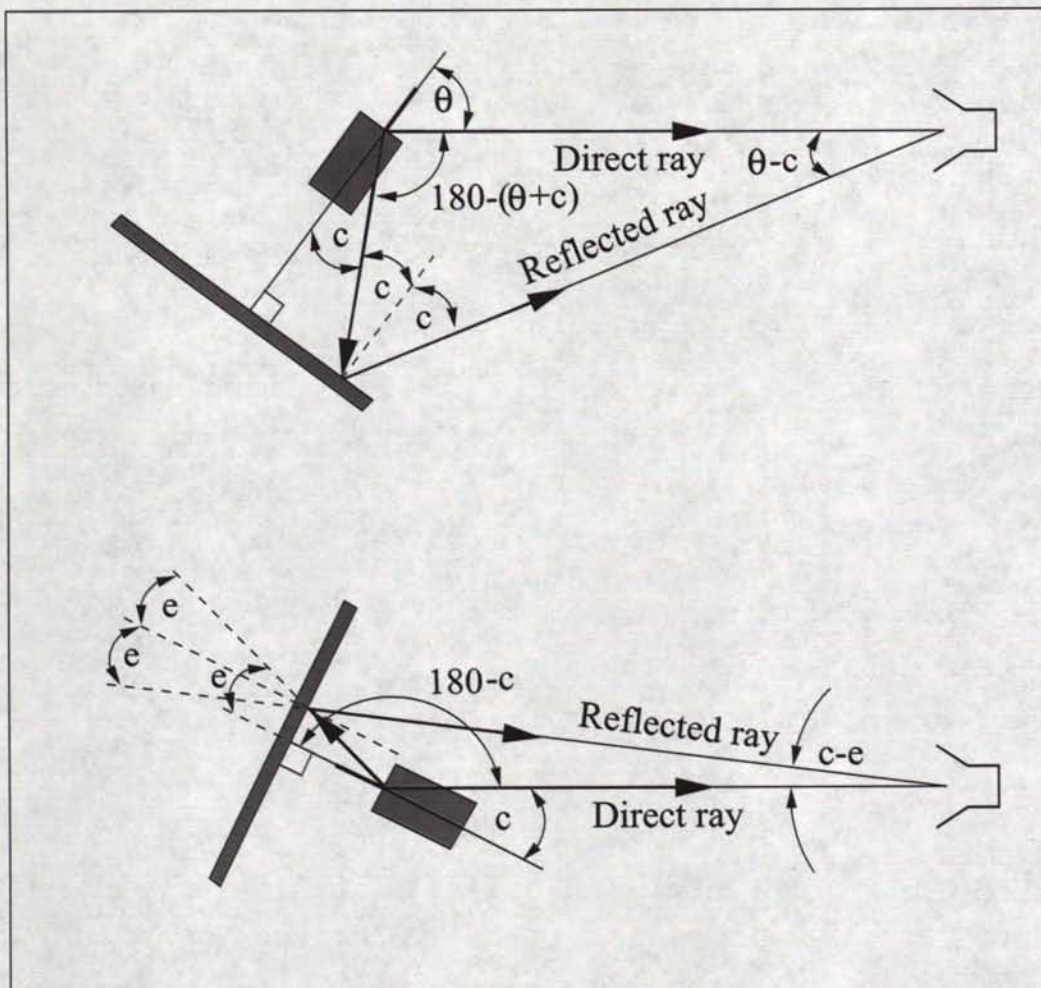
Figure G.5: Comparison between the setup geometry for measuring $P(\theta_1) = P(\theta)$ and $P(\theta_2) = P(180° - c)$.